

**PLANAR CHIRAL LEWIS ACIDS AND LEWIS PAIRS  
BASED ON FERROCENE**

by

JIAWEI CHEN

A Dissertation submitted to the

Graduate School-Newark

Rutgers, The State University of New Jersey

in partial fulfillment of requirements

for the degree of

Doctor of Philosophy

Graduate Program in Chemistry

written under the guidance of Professor Frieder Jäkle

and approved by

---

---

---

---

Newark, New Jersey

May, 2014

© 2014

Jiawei Chen

**ALL RIGHTS RESERVED**

## **ABSTRACT OF THE DISSERTATION**

# **PLANAR CHIRAL LEWIS ACIDS AND LEWIS PAIRS BASED ON FERROCENE**

by Jiawei Chen

Dissertation Advisor: Professor Frieder Jäkle

Organoboranes have been widely used for catalytic transformations, polymerizations, small molecule activation, anion and glycol sensing and construction of electronic materials. These remarkable applications commonly benefit from the electron-deficient nature of tricoordinate boron, i.e., its empty p-orbital can accommodate a lone pair of electrons or participate in conjugation of extended  $\pi$ -systems. Therefore, approaches to enhance the Lewis acidity of the boron center are desirable, and different strategies have been introduced with this aim, including (1) installation of electron withdrawing pendant groups such as pentafluorophenyl groups; (2) generation of cationic borenium species and (3) incorporation of tricoordinate boron into anti-aromatic systems such as borole derivatives. Recently, much effort has been directed to the preparation of the so-called “Frustrated Lewis Pair” (FLP) and the application of their unquenched reactivity for catalytic transformations. However, chiral versions of highly Lewis acidic organoboranes remain scarce. On the other hand, planar chiral ferrocenes have proven to provide rigid frameworks for transition metal ligands such as

phosphines and amines, which have been successfully applied to the asymmetric hydrogenation of alkenes, ketones and other processes.

This dissertation describes our efforts towards the stereoselective synthesis of ferrocene-based multifunctional organoboranes with unique geometric features and electrochemical properties: (1) the 1,2-disubstituted ferrocene backbone provides a rigid planar chiral environment; (2) the reversible oxidation of the ferrocene unit can be exploited for redox active Lewis acids, Lewis pairs and ambiphilic ligands. We demonstrate that a series of highly Lewis acidic derivatives can be synthesized via installation of electronic deficient pentafluorophenyl groups and generation of a borenium cation. The planar chiral borenium cation species serves as a catalyst for the asymmetric hydrosilylation of ketones. Next, we concentrated our attention on the construction of planar chiral borane-pyridine systems: the interactions between the borane and pyridine units can be tuned by introduction of different steric and electronic effects. The coordination of a planar chiral diferrocenylphosphaborin ligand to transition metals is also investigated. We discovered that the F<sup>-</sup> binding to the boryl moiety leads to an enhancement of the electron donating properties as a phosphine ligand by monitoring the  $\nu(\text{CO})$  frequency of the corresponding Vaska-type rhodium complex.

## Acknowledgements

I wish to express my sincere appreciation to my supervisor and mentor, Prof Frieder Jäkle, for his invaluable help and guidance throughout my Ph.D. study. He has been supportive and has given me the freedom to work in my own way and pursue various projects. His example is an inspiration for me about how scientific research should be conducted with enthusiasm, rigor and perseverance.

I would like to thank the rest of my thesis committee: Prof. Alan Goldman, Prof. Elena Galoppini and Prof. Roger Lalancette, for their encouragement, insightful comments and corrections to my thesis.

I am thankful to Prof. Roger Lalancette again for his patient help with single-crystal X-ray crystallography. It has always been fun and exciting to solve an X-ray structure. I am grateful to Prof. John Sheridan for his invaluable support. I thank Dr. Lazaros Kakalis for helping me with some of the NMR measurements and Dr. Roman Brukh for the assistance Maldi-MS and GC measurements. I also thank Dr. Pakkarisamy Thilagar, Dr. Ramez Boshra, Dr. Kshitij Parab, Dr. Ami Doshi, Dr. Chengzhong Cui, Dr. Haiyan Li, Dr. Pangkuan Chen, Dr. Xiaodong Yin for their help with my research. I am indebted to my friend Dr. Fei Cheng for the helpful discussions and encouragement.

I would also like to thank my parents, elder sister and other members of my family. They were always supporting me and encouraging me with their best wishes and continuous love.

Finally, I would like to dedicate this thesis to my wife, Qihong Zhang, and my daughter, Scarlett Chen, for their endless support, patience and understanding. Without them I could not have made it here.

## Table of Contents

Abstract of the dissertation	ii	
Acknowledgements	iv	
Table of Contents	vi	
List of Figures	ix	
List of Schemes	xiv	
List of Tables	xvi	
<b>Chapter 1</b>	<b>General Introduction: The Development of Boron-Containing and Ferrocene-Containing Catalysts</b>	<b>1</b>
1.1	General Goals	1
1.2	Borane Lewis Acids as Catalysts	1
1.2.1	<i>Achiral Borane Lewis Acids</i>	1
1.2.2	<i>Chiral Borane Lewis Acids</i>	5
1.3	Ferrocenes as Frameworks for Catalyst Support	7
1.3.1	<i>Achiral Ferrocene Frameworks</i>	8
1.3.2	<i>Planar Chiral Ferrocene Frameworks</i>	9
1.4	Prior Work on Ferrocene-based Lewis Acids and Lewis Pairs	14
1.5	Notes and References	18
<b>Chapter 2</b>	<b>Characterization of Planar Chiral Lewis Acids Derived from Naphthylferrocenes</b>	<b>21</b>
2.1	Introduction	21
2.2	Results and Discussion	22
2.3	Conclusions	34

2.4	Experimental Section	35
2.5	Supporting Information	43
2.6	Notes and References	50
<b>Chapter 3</b>	<b>Stereoselective Borylation of Planar Chiral Pyridylferrocenes</b>	<b>53</b>
3.1	Introduction of Directed Metalation	53
3.2	Results and Discussion	55
3.3	Mechanistic Study of Borylation	61
3.4	Conclusions	67
3.5	Experimental Section	67
3.6	Supporting Information	80
3.7	Notes and References	94
<b>Chapter 4</b>	<b>Synthesis and Characterization of Planar Chiral Lewis Pairs Derived from Pyridylferrocenes</b>	<b>98</b>
4.1	Introduction	98
4.2	Synthesis and Characterization	99
4.3	Conclusions	113
4.4	Experimental Section	115
4.5	Supporting Information	126
4.6	Notes and References	136
<b>Chapter 5</b>	<b>Catalytic Application of Planar Chiral Ferrocenyl Lewis Acids: Studies of Lewis Acidity, Substrate Binding and Asymmetric Process</b>	<b>138</b>
5.1	Introduction	138
5.2	Synthesis and Characterization	140

5.3	Lewis Acidity Determination and Substrate Binding	142
5.4	Asymmetric Catalytic Process	146
5.5	Experimental Section	148
5.6	Supporting Information	153
5.7	Notes and References	164
<b>Chapter 6</b>	<b>Planar Chiral Diferrocene Systems</b>	<b>167</b>
6.1	Introduction	167
6.2	Results and Discussions	171
6.3	Conclusions	191
6.4	Experimental Section	191
6.5	Supporting Information	205
6.6	Notes and References	216
	Overall Conclusion	218
	List of Publications	221
	Curriculum Vitae	222

## List of Figures

Figure 1-1.	Structure of tris(pentafluorophenyl)borane and its applications in hydrosilylation, hydrostannylation and polymerization reactions	3
Figure 1-2.	Representative chiral boranes for asymmetric transformations	6
Figure 1-3.	A commercially available Dppf ligand and a monodentate phosphinoferrocene	8
Figure 1-4.	Assignment of the stereochemistry of enantiomeric 1,2-heterodisubstituted ferrocenes according to Schlögl	10
Figure 1-5.	Planar chirality determination applying CIP protocol	11
Figure 1-6.	Definition of different structural parameters in this thesis	11
Figure 1-7.	Chiral resolution of <i>rac</i> - <b>O</b> by preparative chiral HPLC	12
Figure 1-8.	Products of direct borylation of ferrocene with different equivalents of BBr <sub>3</sub>	15
Figure 1-9.	Representative ferrocenes with strong Lewis acid and Lewis base substituents	16
Figure 2-1.	Examples of enantiomerically pure planar chiral ferrocenylboranes	22
Figure 2-2.	X-ray crystal structure plots of <b>1</b> and <b>2</b>	24
Figure 2-3.	Low temperature <sup>19</sup> F NMR spectrum of <b>5</b>	27
Figure 2-4.	<sup>19</sup> F- <sup>19</sup> F 2D gCOSY NMR spectrum of <b>5</b>	27
Figure 2-5.	Variable temperature <sup>19</sup> F NMR spectra of <b>5</b>	29
Figure 2-6.	Variable temperature <sup>19</sup> F NMR spectra of <b>4</b>	30
Figure 2-7.	X-ray crystal structure plots of <b>4</b> and <b>5</b>	32

Figure 2-8.	UV/Vis absorption spectra of <b>3</b> , <b>4</b> and <b>5</b>	33
Figure 2-9.	Cyclic voltammogram of compound <b>5</b>	34
Figure 2-10.	Ortep plot of <b>1</b>	43
Figure 2-11.	Ortep plot of <b>2</b>	44
Figure 2-12.	Ortep plot of <b>4</b>	44
Figure 2-13.	Ortep plots of two independent molecules of <b>5</b>	45
Figure 2-14.	Supramolecular Structure of <b>5</b>	46
Figure 2-15.	Intermolecular interactions in <b>4</b>	47
Figure 3-1.	Examples of <i>ortho</i> -lithiation of chiral ferrocenes and the product of borylation of 1,1'-bis(trimethylstannyl)ferrocene (racemate)	53
Figure 3-2.	Ortep plot of (p <i>S</i> )- <b>2Sn</b>	57
Figure 3-3.	<sup>1</sup> H NMR spectra (Cp region) of single crystals of (p <i>R</i> )- <b>3</b>	60
Figure 3-4.	Excerpt of the <sup>1</sup> H- <sup>1</sup> H NOESY NMR spectrum for (p <i>R</i> )- <b>3</b>	60
Figure 3-5.	Ortep plots of (p <i>R</i> )- <b>3</b> and (p <i>S</i> )- <b>3</b>	61
Figure 3-6.	Proposed reaction pathway in the formation of (p <i>R</i> )- <b>3</b> from (p <i>S</i> )- <b>2Sn</b>	62
Figure 3-7.	Ortep plot of (p <i>R</i> , <i>S</i> <sub>s</sub> )- <b>1</b>	82
Figure 3-8.	Crystal structure plot of [(p <i>S</i> )- <b>4</b> ] <sup>+</sup> [Al(OC(CF <sub>3</sub> ) <sub>3</sub> ) <sub>4</sub> ] <sup>-</sup>	82
Figure 3-9.	Multinuclear NMR spectral data	83
Figure 3-10.	Excerpt of the 2D-NOESY spectrum of compound (p <i>R</i> )- <b>3</b> in C <sub>6</sub> D <sub>6</sub>	91
Figure 3-11.	High resolution MALDI-MS data of [(p <i>S</i> )- <b>4</b> ] <sup>+</sup> [B(C <sub>6</sub> F <sub>5</sub> ) <sub>3</sub> Me] <sup>-</sup>	92
Figure 3-12.	HPLC trace and corresponding UV-visible spectrum of (p <i>S</i> )- <b>2Sn</b>	93
Figure 3-13.	HPLC traces and corresponding UV-visible spectra of <b>3</b>	94
Figure 4-1.	Examples of FLPs and planar chiral ferrocenes	99

Figure 4-2.	Ortep plots of (p <i>R</i> )- <b>4-Pf</b> , (p <i>R</i> )- <b>4-Mes</b> , (p <i>S</i> )- <b>5-Pf</b> and (p <i>S</i> )- <b>5-Mes</b>	105
Figure 4-3.	Sections of the <sup>19</sup> F- <sup>19</sup> F EXSY NMR spectrum of <b>5-Pf</b> and illustration of the equilibrium between ‘closed’ and ‘open’ forms of <b>5-Pf</b>	107
Figure 4-4.	Ortep plots for the ring-opened products <b>6</b> and <b>7</b>	109
Figure 4-5.	Difference Fourier electron density contour map of compound <b>7</b>	110
Figure 4- 6.	Cyclic voltammograms of compounds <b>4-Pf</b> , <b>4-Mes</b> , <b>5-Pf</b> and <b>5-Mes</b>	111
Figure 4-7.	Ortep plot for compound <b>4-Pf</b> <sup>+</sup>	113
Figure 4-8.	Ortep plot for compound <b>5-Cl</b>	128
Figure 4-9.	MALDI-MS data of compound <b>4-Mes</b>	129
Figure 4-10.	Comparison of UV-Vis absorption spectra in CHCl <sub>3</sub>	130
Figure 4-11.	Chiral HPLC trace and UV-Vis spectrum of <b>4-Pf</b> (40% ee)	131
Figure 4-12.	Chiral HPLC trace and UV-Vis spectrum of (p <i>R</i> )- <b>4-Pf</b>	131
Figure 4-13.	Chiral HPLC trace and UV-Vis spectrum of (p <i>R</i> )- <b>4-Mes</b>	132
Figure 4-14.	Chiral HPLC trace and UV-Vis spectrum of (p <i>S</i> )- <b>5-Pf</b>	132
Figure 4-15.	Chiral HPLC trace and UV-Vis spectrum of (p <i>S</i> )- <b>5-Mes</b>	132
Figure 4-16.	Chiral HPLC trace and UV-Vis spectrum of (p <i>S</i> )- <b>6</b>	133
Figure 4-17.	Chiral HPLC trace and UV-Vis spectrum of (p <i>S</i> )- <b>7</b>	133
Figure 4-18.	<sup>19</sup> F- <sup>19</sup> F EXSY spectrum of <b>4-Pf</b> at 80 °C in d <sub>8</sub> -toluene	134
Figure 4-19.	<sup>19</sup> F- <sup>19</sup> F EXSY spectrum of <b>5-Pf</b> at 80 °C in d <sub>8</sub> -toluene	135
Figure 5-1.	Examples of highly Lewis acidic organoboranes	139
Figure 5-2.	Expansion of the Cp region of the <sup>1</sup> H NMR spectra for a) (p <i>R</i> )- <b>2</b> ( <i>exo</i> and <i>endo</i> -isomers), b) (p <i>R</i> )- <b>2</b> + B(C <sub>6</sub> F <sub>5</sub> ) <sub>3</sub> and c) (p <i>R</i> )- <b>3</b> <sup>+</sup> (CDCl <sub>3</sub> ) and photographs illustrating the associated color change	141

Figure 5-3.	Ortep plot of (p <i>R</i> )- <b>3</b> <sup>+</sup>	142
Figure 5-4.	Competitive binding of (p <i>R</i> )- <b>3</b> <sup>+</sup> and B(C <sub>6</sub> F <sub>5</sub> ) <sub>3</sub> to Et <sub>3</sub> PO examined by <sup>31</sup> P NMR spectroscopy	143
Figure 5-5.	Competitive binding of (p <i>R</i> )- <b>3</b> <sup>+</sup> and B(C <sub>6</sub> F <sub>5</sub> ) <sub>3</sub> to Et <sub>3</sub> PO examined by <sup>11</sup> B NMR spectroscopy	144
Figure 5-6.	VT <sup>1</sup> H NMR spectra for a mixture of (p <i>R</i> )- <b>3</b> <sup>+</sup> and Et <sub>3</sub> SiH in CDCl <sub>3</sub>	145
Figure 5-7.	Ortep plots of Substrate binding of (p <i>R</i> )- <b>3</b> <sup>+</sup> with acetone, acetophenone and hydride	146
Figure 5-8.	Data corresponding to determination of enantiomeric excess of catalysis products	155
Figure 5-9.	Chiral HPLC analysis for compound (p <i>R</i> )- <b>2</b>	155
Figure 5-10.	Complete <sup>1</sup> H NMR spectra of (p <i>R</i> )- <b>2</b> , (p <i>R</i> )- <b>2</b> + B(C <sub>6</sub> F <sub>5</sub> ) <sub>3</sub> , and (p <i>R</i> )- <b>3</b> <sup>+</sup> in CDCl <sub>3</sub>	156
Figure 5-11.	2D-NOESY spectra of compound (p <i>R</i> )- <b>2</b> in C <sub>6</sub> D <sub>6</sub>	157
Figure 5-12.	Comparison of UV-Vis spectra of (p <i>S</i> )- <b>1</b> , (p <i>R</i> )- <b>2</b> and (p <i>R</i> )- <b>3</b> <sup>+</sup>	158
Figure 5-13.	High-resolution MALDI-MS spectra of compound (p <i>R</i> )- <b>2</b>	159
Figure 5-14.	Competitive binding of (p <i>R</i> )- <b>3</b> <sup>+</sup> and B(C <sub>6</sub> F <sub>5</sub> ) <sub>3</sub> to acetophenone	160
Figure 5-15.	Ortep plot of the second independent molecule of (p <i>R</i> )- <b>3</b> <sup>+</sup>	161
Figure 5-16.	Ortep plots of two independent molecules of (p <i>R</i> )- <b>3</b> <sup>+</sup> (acetophenone)	162
Figure 6-1.	Representative examples of element-bridged diferrocenes	168
Figure 6-2.	Examples of amphiphilic ligands, the different coordination modes and the targeted diferrocenylphosphaborin compound <b>T2</b>	171
Figure 6-3.	Comparison of NMR data for cycles <b>2-SnSn</b> , <b>2-SnSi</b> and <b>2-BSi</b>	174

Figure 6-4.	Ortep plots of <b>2-SnSi</b> and <b>2-BSi</b>	175
Figure 6-5.	Cycle voltammetry and square-wave voltammetry data for <b>2-SnSn</b> , <b>2-SnSi</b> , <b>2-BSi</b>	177
Figure 6-6.	Solid state structure of a doubly oxidized species derived from <b>2-BSi</b>	178
Figure 6-7.	Ortep plots of <b>3a-SnP</b> and <b>3b-SnP</b>	180
Figure 6-8.	Ortep plots of <b>4-BP</b> and <b>5-BP</b>	182
Figure 6-9.	Square-wave voltammetry data for <b>3b-SnP</b> , <b>4-BP</b> and <b>5-BP</b>	185
Figure 6-10.	<sup>1</sup> H and <sup>31</sup> P NMR spectra for complex <b>(5-BP)<sub>2</sub>Rh(CO)Cl</b>	187
Figure 6-11.	Cyclic voltammetry and square-wave voltammetry data for complex <b>(5-BP)<sub>2</sub>Rh(CO)Cl</b>	188
Figure 6-12.	IR spectra for complex <b>(5-BP)<sub>2</sub>Rh(CO)Cl</b> and after addition of F <sup>-</sup>	190
Figure 6-13.	Multinuclear NMR spectral data	205
Figure 6-14.	UV/Vis absorption spectra of cycles <b>2-SnSn</b> , <b>2-SnSi</b> and <b>2-BSi</b>	208
Figure 6-15.	Maldi-MS data of compounds <b>2-SnSn</b> and <b>2-SnSi</b>	209
Figure 6-16.	Maldi-MS data of compound <b>3b-SnP</b>	210
Figure 6-17.	Maldi-MS data of compound <b>3a-SnP</b>	210
Figure 6-18.	Maldi-MS data of compound <b>4-BP</b>	211
Figure 6-19.	Ortep plot of <b>1-Sn</b>	212
Figure 6-20.	Disorder in the solid state of <b>2-SnSi</b>	213
Figure 6-21.	Chiral HPLC traces and the corresponding UV-Vis spectra of <b>2-SnSi</b> , <b>2-BSi</b> , <b>3a-SnP</b> , <b>3b-SnP</b> and <b>4-BP</b>	214

## List of Schemes

Scheme 1-1.	The first example of dihydrogen activation by an intramolecular FLP	4
Scheme 1-2.	The interchange between classical Lewis pair and FLP and its reaction with dihydrogen	4
Scheme 1-3.	Activation of carbonyl groups by a Lewis acidic borenium cation intermediate	7
Scheme 1-4.	An example of a planar chiral ferrocene-based Ir catalyst used for the asymmetric hydrogenation of an imine	9
Scheme 1-5.	Synthesis of <i>rac</i> - <b>O</b>	12
Scheme 1-6.	Synthesis of Joshiphos ligands and stepwise modification of Kagan's sulfinate	14
Scheme 1-7.	Reaction between ferrocene and Piers' borane to give <b>S</b>	15
Scheme 1-8.	Synthesis of <i>rac</i> - <b>W</b> and its chiral resolution by N-methylpseudoephedrine	17
Scheme 2-1.	Synthesis of the enantiomerically pure organometallic naphthylferrocene derivatives <b>1</b> and <b>2</b>	23
Scheme 2-2.	Synthesis of highly Lewis acidic planar chiral ferrocenylboranes	25
Scheme 3-1.	Synthesis of planar chiral pyridylferrocenes ( <i>pS</i> )- <b>2Sn</b> and ( <i>pS</i> )- <b>2Hg</b>	56
Scheme 3-2.	Synthesis and HPLC traces of planar chiral ( <i>pS</i> )- <b>3</b> and ( <i>pR</i> )- <b>3</b>	58
Scheme 3-3.	Reactivity of ( <i>pS</i> )- <b>2Sn</b> toward selected Lewis and Brønsted acids	64
Scheme 3-4.	Reaction of FcLu with PhBCl <sub>2</sub>	66

Scheme 4-1.	Synthesis of planar chiral (p <i>S</i> )- <b>2-Sn</b> and (p <i>S</i> )- <b>3-Hg</b>	100
Scheme 4-2.	Synthesis of planar chiral (p <i>S</i> )- <b>4-Pf</b> , (p <i>S</i> )- <b>4-Mes</b> , (p <i>R</i> )- <b>5-Pf</b> , and (p <i>S</i> )- <b>5-Mes</b>	102
Scheme 4-3.	Reactions of (p <i>S</i> )- <b>5-Pf</b> and (p <i>S</i> )- <b>5-Mes</b> with H <sub>2</sub> O	109
Scheme 4-4.	Preparative oxidation of (p <i>R</i> )- <b>4-Pf</b> and (p <i>S</i> )- <b>5-Mes</b>	113
Scheme 5-1.	Synthesis of (p <i>R</i> )- <b>3<sup>+</sup></b>	140
Scheme 5-2.	Hydrosilylation of ketones catalyzed by (p <i>R</i> )- <b>3<sup>+</sup></b>	147
Scheme 6-1.	Synthesis of planar chiral tin-bridged diferrocene <b>1-Sn</b>	172
Scheme 6-2.	Synthesis of planar chiral cycles <b>2-SnSn</b> and <b>2-SnSi</b>	173
Scheme 6-3.	Synthesis of planar chiral cycle <b>2-BSi</b>	173
Scheme 6-4.	Synthesis of planar chiral cycles <b>3a-SnP</b> and <b>3b-SnP</b>	179
Scheme 6-5.	Synthesis of the ambiphilic ligand <b>5-BP</b>	182
Scheme 6-6.	Synthesis of a Vaska-type rhodium compound	187

## List of Tables

Table 2-1.	Line shape analysis and coalescence temperatures for <b>4</b> and <b>5</b>	28
Table 2-2.	Details of X-ray crystal structure analyses of complexes <b>1</b> , <b>2</b> , <b>4</b> and <b>5</b>	48
Table 2-3.	Coalescence temperatures for compounds <b>4</b> and <b>5</b>	49
Table 2-4.	Line shape analysis results of compounds <b>4</b> and <b>5</b>	49
Table 3-1.	Crystal data and structure refinement details for (p <i>R</i> , <i>S</i> <sub>S</sub> )- <b>1</b> , (p <i>S</i> )- <b>2Sn</b> , (p <i>S</i> )- <b>3</b> , (p <i>R</i> )- <b>3</b> , and [(p <i>S</i> )- <b>4</b> ] <sup>+</sup> [Al(OC(CF <sub>3</sub> ) <sub>3</sub> ) <sub>4</sub> ] <sup>-</sup>	80
Table 4-1.	Crystal data and structure refinement details for <b>4-Pf</b> , <b>5-Pf</b> , <b>4-Mes</b> , <b>5-Mes</b> , <b>4-Pf<sup>+</sup></b> , <b>5-Cl</b> , <b>6</b> and <b>7</b>	126
Table 5-1.	Hydrosilylation of different ketones with silanes in the presence of (p <i>R</i> )- <b>3</b> <sup>+</sup> as catalyst	147
Table 5-2.	Details of X-ray analyses of (p <i>R</i> )- <b>3</b> and (p <i>R</i> )- <b>3</b> <sup>+</sup> (acetophenone)	163
Table 6-1.	X-ray structural parameters of <b>2-SnSi</b> and <b>2-BSi</b>	175
Table 6-2.	Redox potentials of <b>2-SnSn</b> , <b>2-SnSi</b> and <b>2-BSi</b>	178
Table 6-3.	X-ray structural parameters of <b>3a-SnP</b> and <b>3b-SnP</b>	180
Table 6-4.	X-ray structural parameters of <b>4-BP</b> and <b>5-BP</b>	182
Table 6-5.	Redox potentials of <b>3b-SnP</b> , <b>4-BP</b> and <b>5-BP</b>	185
Table 6-6.	Redox potentials of <b>(5-BP)<sub>2</sub>Rh(CO)Cl</b>	188

# Chapter 1 General Introduction: The Development of Boron-Containing and Ferrocene-Containing Catalysts

## 1.1 General Goals

The general goal of my PhD research was to develop new chiral ferrocene compounds featuring highly Lewis acidic borane moieties. The chirality of these Lewis acids is derived from the rigid ferrocene framework. The research initially focused on the synthesis of highly Lewis acidic organoboranes and was then expanded to the area of planar chiral Lewis pairs bearing both Lewis acid (LA) and Lewis base (LB) moieties. These systems are very interesting due to the diverse modes of LA-LB and boron-iron interactions that could greatly impact the properties and enable applications in a variety of research fields.

This chapter provides an overview of the prior research on (a) organoboranes as Lewis acids, (b) the use of ferrocene as a framework for chiral catalyst, and (c) ferrocene-based Lewis acids and Lewis pairs.

## 1.2 Borane Lewis Acids as Catalysts

### 1.2.1 Achiral Borane Lewis Acids

Borane, in the simplest form  $\text{BH}_3$ , is widely recognized by organic chemists for its extensive applications in reduction of unsaturated C-C, C-N, C-O double bonds, as well as C-C triple bonds.<sup>1</sup> Lewis acidic boron halides ( $\text{BX}_3$ ) are utilized in organo-synthetic applications including dealkylation of ethers, condensation reactions, and as catalysts for Friedel-Crafts-type reactions and other acid-related chemistry.<sup>2</sup> In most of the cases,

these processes require the use of stoichiometric amounts of Lewis acid to activate the substrates under anhydrous conditions. Recent years have seen a growing interest in the synthesis of more moisture-tolerant boron-based catalysts by installation of sterically bulky and electronically withdrawing substituents such as pentafluorophenyl groups onto the boron center. Quite a number of reactions such as Mukaiyama aldol reactions, Diels-Alder reactions and others proceed smoothly in the presence of catalytic amounts of tris(pentafluorophenyl)borane [ $\text{B}(\text{C}_6\text{F}_5)_3$ , **A**].<sup>2</sup> Piers and coworkers noted that  $\text{B}(\text{C}_6\text{F}_5)_3$  catalyzes the hydrosilylation reaction of ketones and imines with hydrosilanes through a unique silane activation pathway.<sup>3</sup> Yamamoto and coworkers further explored the hydrostannylation of alkynes, allenes and alkenes by employing the same catalyst.<sup>4</sup> Moreover,  $\text{B}(\text{C}_6\text{F}_5)_3$  also serves as an excellent co-catalyst for Ziegler-Natta type polymerizations. The perfluoroaryl borane is capable of abstracting alkyl or hydride anions, thereby generating activated Ziegler-Natta catalysts based on metallocene and quasimetallocene frameworks. When compared to other Lewis acidic cocatalysts such as trityl ( $\text{Ph}_3\text{C}^+$ ) and MAO (methylaluminoxane), the boron species have the advantage that the steric and electronic properties can be tuned by modifying the perfluoroaryl groups to achieve high activities for polymerization (Figure 1-1).<sup>5</sup>

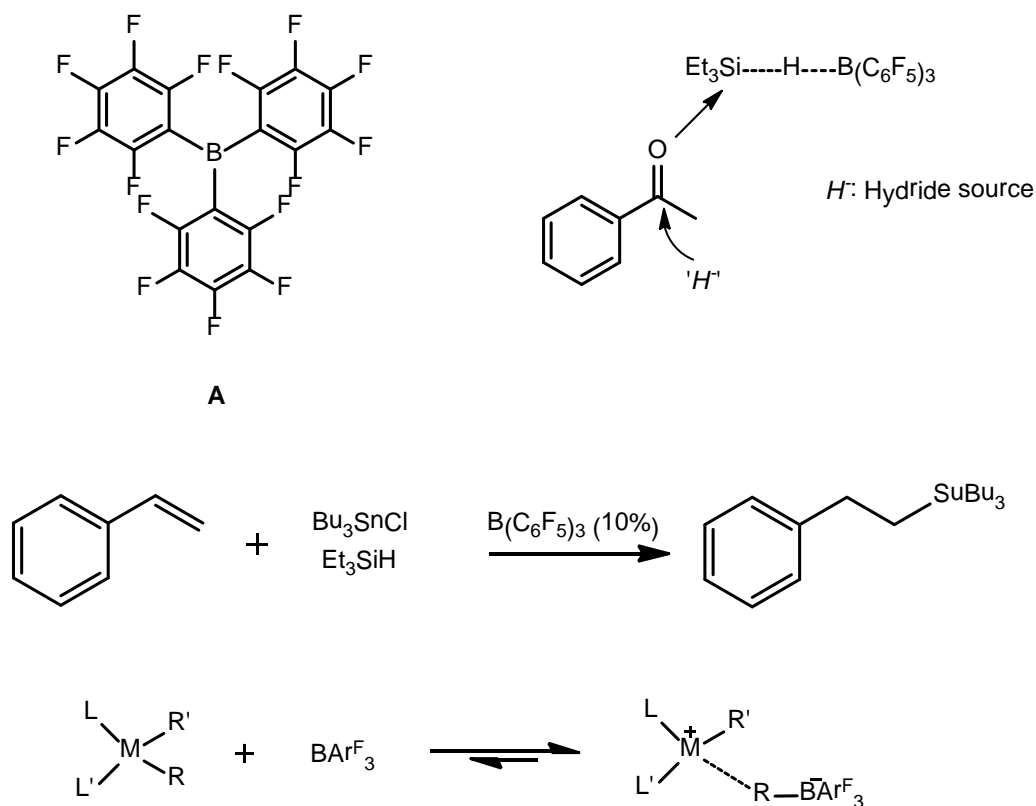
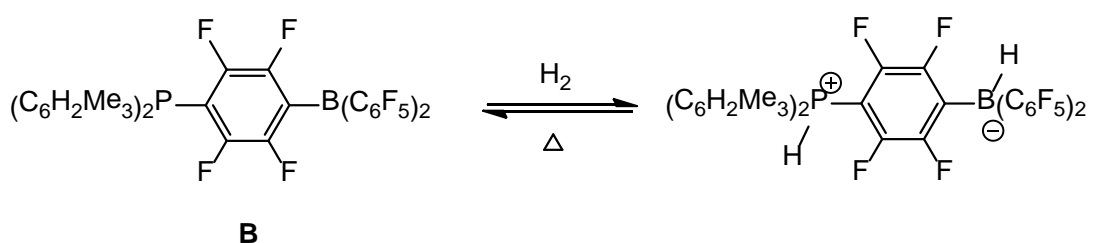


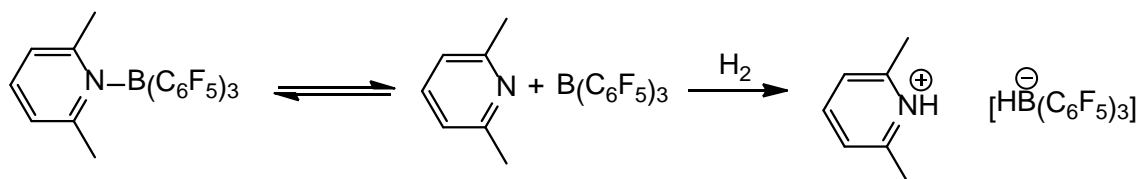
**Figure 1-1.** Structure of tris(pentafluorophenyl)borane and its applications in hydrosilylation, hydrostannylation and polymerization reactions

More recently, the area of so-called “Frustrated Lewis Pairs” (FLPs) has developed dramatically since Stephan’s pioneering research. In 2006, Stephan<sup>6</sup> incorporated a bulky phosphine and highly acidic borane into the same molecule (**B**) and utilized the unquenched reactivity for the heterolytic cleavage of dihydrogen (Scheme 1-1). Sterically demanding Lewis acids (e.g. organoboranes, organoaluminum species, silylium cations) and bulky Lewis bases (e.g. phosphines, amines, pyridines, carbenes) proved to be excellent candidates to compose such types of systems.  $\text{B}(\text{C}_6\text{F}_5)_3$  has been most widely used as the Lewis acid component due to its high Lewis acidity, stability and accessibility.

While initial reports pointed towards the importance of separating Lewis acids and bases by using steric hindrance, more recent studies indicate that there is no strict boundary between conventional Lewis pairs and FLPs. For example, Stephan *et al.* investigated a system consisting of  $B(C_6F_5)_3$  and 2,6-dimethylpyridine.<sup>7</sup> The Lewis adduct exists in thermal equilibrium with the free Lewis acid and base and is therefore capable of activating small molecules such as dihydrogen or THF (Scheme 1-2).



**Scheme 1-1.** The first example of dihydrogen activation by an intramolecular FLP.



**Scheme 1-2.** The interchange between classical Lewis pair and FLP and its reaction with dihydrogen.

In fact, since the first reports of the successful cleavage of dihydrogen by FLPs, a variety of systems have been developed and explored for the activation of alkynes, NO, CO<sub>2</sub>, and other small molecules.<sup>8</sup> More recently, much effort has been focused on the design of FLPs for catalytic processes such as hydrogenation, hydrosilylation and hydroboration of ketones, imines and olefins, as well as the polymerization of olefins.<sup>9</sup>

### 1.2.2 Chiral Borane Lewis Acids

Various chiral organic frameworks containing Lewis acidic borane moieties have been explored as catalysts for asymmetric transformations. Early examples include Brown's pinene-based organohaloboranes<sup>10</sup> (**C**), Hawkins' naphthylcyclohexyl-dichloroboranes<sup>11</sup> (**D**) and organoboron-modified binaphthyl species first studied by Kaufmann (**G**) and later by Yamamoto (**E**) and Piers (**F**).<sup>12</sup> These and related chiral Lewis acidic organoboranes serve as excellent catalysts for enantioselective Diels Alder reactions.<sup>11, 12d, 13</sup> Although the initial examples showed their high effectiveness for stereoselective transformations, the poor stability remained a drawback. To overcome this disadvantage, the halide substituents were replaced with pentafluorophenyl groups. More recently, Oestreich and coworkers reported the synthesis and Lewis acidity study of a binaphthyl-based cyclic borane (**H**) and investigated its applications in hydrosilylation and dehydrogenative coupling reactions.<sup>14</sup> A further communication by Klankermayer demonstrated that camphor can serve as a suitable structural motif (**I**). These chiral boranes were tested as catalysts for metal-free hydrogenation of imines and showed good stereoselectivity. Together with bulky Lewis bases, the camphor-derived chiral systems form FLPs that activate dihydrogen and serve as catalysts for asymmetric hydrosilylation of imines (Figure 1-2).<sup>15</sup>

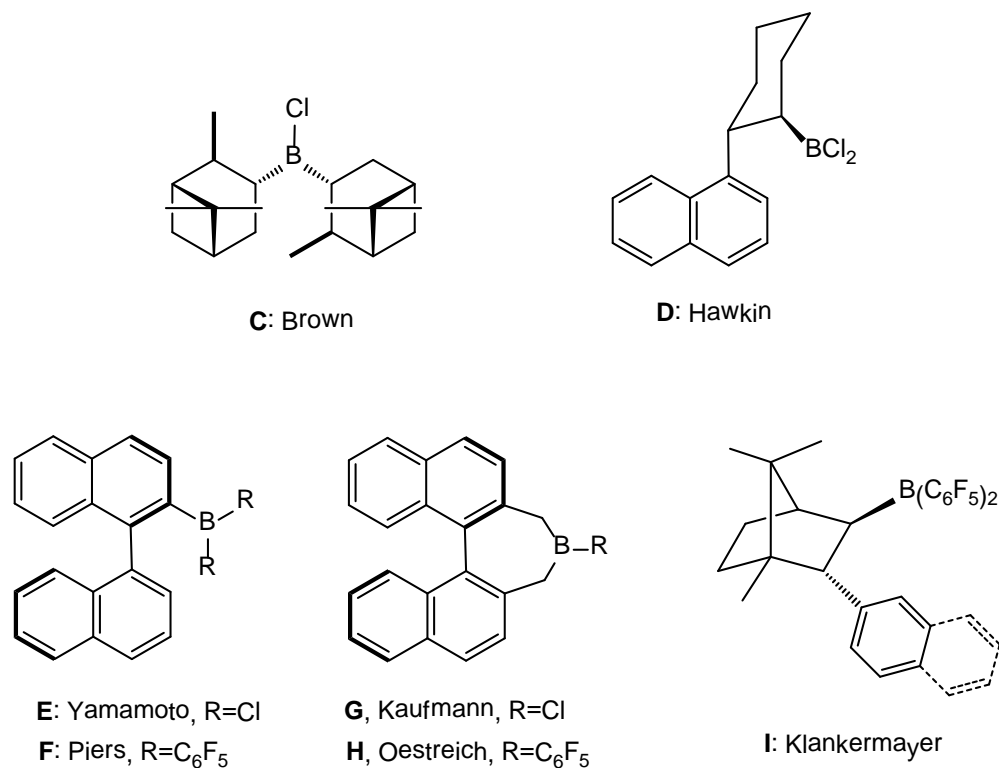
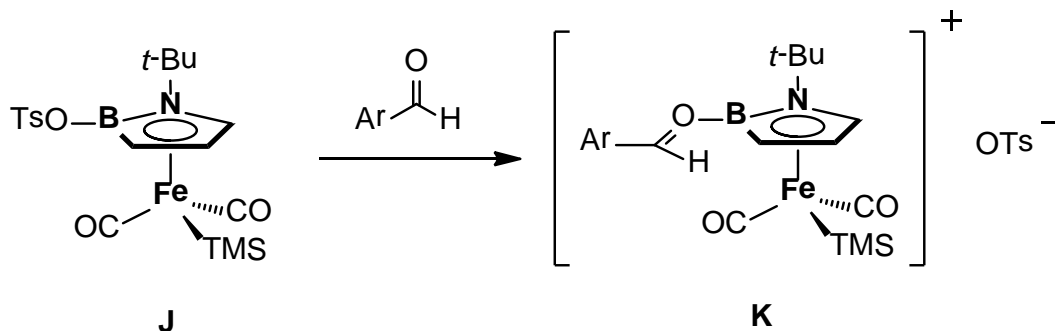


**Figure 1-2.** Representative chiral boranes for asymmetric transformations.

Compared to these purely organic systems, main group Lewis acid catalysts supported by metallocene framework are less developed, not to mention that examples for planar chiral versions remain exceedingly rare. One of the reasons is perhaps that the Lewis acid species tend to be susceptible to oxidative degradation when attached to the electron rich metallocene. This could pose a major problem for purification and chiral resolution. One of the successful examples was reported by Fu and coworkers.<sup>16</sup> They synthesized a planar chiral azaborolyl heterocycle (**J**) which facilitates the asymmetric aldol reaction of silyl ketene acetals with aldehydes with de higher than 95%. Interestingly, the mechanism likely involves a Lewis acidic cationic boron species generated after the dissociation of the tosylate group, which then activates the carbonyl group. However, because of the

high stability of the complexed product, this stereoselective reaction can only proceed with a stoichiometric amount of the Lewis acid (Scheme 1-3).



**Scheme 1-3.** Activation of carbonyl groups by a Lewis acidic borenium cation intermediate.

### 1.3 Ferrocenes as Frameworks for Catalyst Support

The exploration of organometallic chemistry was fueled by the discovery of ferrocene by Pauson and Kealy<sup>17</sup> and the confirmation of its sandwich-type structure by Woodward, Wilkinson and Fischer about 6 decades ago.<sup>18</sup> This organoiron species exhibits a distinct high stability and aromaticity, owing to a new coordination type—the  $\eta^5$  (pentahapto) sandwich structure. Over the past decades, the area of organometallic chemistry has developed dramatically. There are excellent and comprehensive reviews on the topic of ferrocene and its applications in the fields of catalysts, pharmaceuticals, materials chemistry and others.<sup>19</sup> The following brief summary will focus primarily on the most recent progress with planar chiral ferrocene catalysts, closely related to our research topics but not covered in the previous reviews.

### 1.3.1 Achiral Ferrocene Frameworks

Ferrocene is a typical aromatic compound, but it exhibits exciting and unique characteristics when compared to other ordinary aromatics such as benzene, mostly resulting from its negative charge on the Cp (cyclopentadienyl) ring and the sandwich type coordination. For instance, it undergoes electrophilic substitution much faster than the benzene analog; the presence of two Cp rings also provides much more diverse coordination modes when ferrocene is used as a ligand backbone. An example is bis(diphenylphosphino)ferrocene (Dppf, **L**),<sup>19a, 19e</sup> which is a versatile ligand for transition metal catalyzed reactions (Figure 1-3). The free ligand itself and its transition metal complexes have been commercialized and utilized as catalysts for the formation of C-C bonds. The presence of electron rich Cp rings not only renders the phosphine to be a powerful ligand, but flexible rotation allows for different conformations when coordinated to metal centers.

There are only a few examples of achiral ferrocenes in FLP type chemistry. A 1-di-tert-butylphosphino ferrocene derivative (**M**) was synthesized by Stephan and co-workers and FLP type behavior in combination with a strong Lewis acid was demonstrated for the activation of dihydrogen (Figure 1-3).<sup>20</sup>

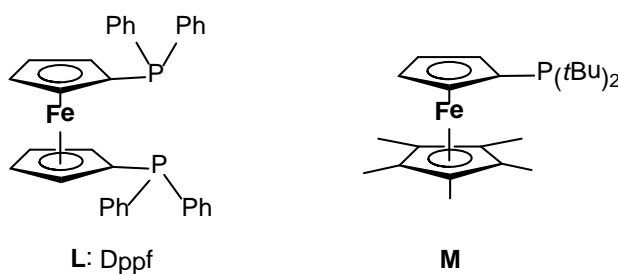
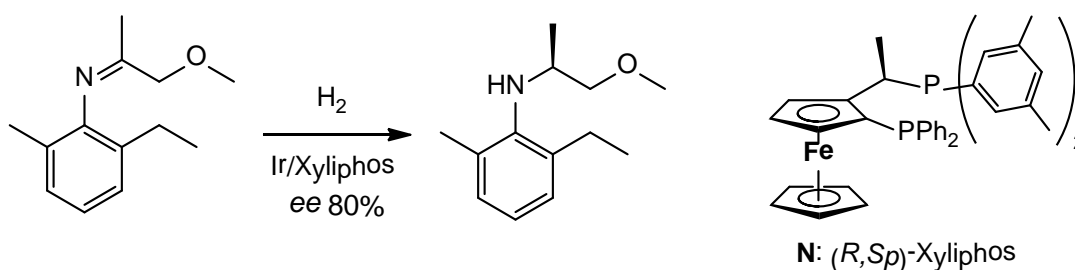


**Figure 1-3.** A commercially available Dppf ligand and a monodentate phosphinoferrocene.

### 1.3.2 Planar Chiral Ferrocene Frameworks

The three dimensional structure of ferrocene results in planar chirality in the case of 1,2- or 1,3- heterodisubstituted species. These planar chiral ferrocene derivatives have been an important tool for asymmetric transformations in academia as well as industry. Perhaps the most successful example is the Josiphos ligand class. By employing an Ir catalyst with (*R,S*)-Xyliphos (**N**) as ligand, the asymmetric hydrogenation of an imine to the corresponding chiral amine is accomplished as showed in Scheme 1-4. The latter is an important intermediate for the synthesis of the herbicide (*S*)-metolachlor. The final product is produced with a volume of 10000 tons per years.<sup>21</sup>



**Scheme 1-4.** An example of a planar chiral ferrocene-based Ir catalyst used for the asymmetric hydrogenation of an imine.

The original nomenclature of planar chirality for ferrocene species is somewhat arbitrary but easy to define and follow. The method according to Schlögl<sup>22</sup> notes that when a molecule is viewed from the top of the substituted Cp ring, the planar chirality is determined by the order going from the substituent with high priority to that with lower priority. For example, if the order is clockwise the molecule has a “*R*” configuration otherwise “*S*”. Stereodescriptors “*R<sub>p</sub>*” and “*S<sub>p</sub>*” are used to denote planar chirality (Figure 1-4). In addition, “*R<sub>X</sub>*” and “*S<sub>X</sub>*” are used to identify noncarbon chirality centers. Literature known compounds will be named consistently using this method in this thesis to minimize confusion.

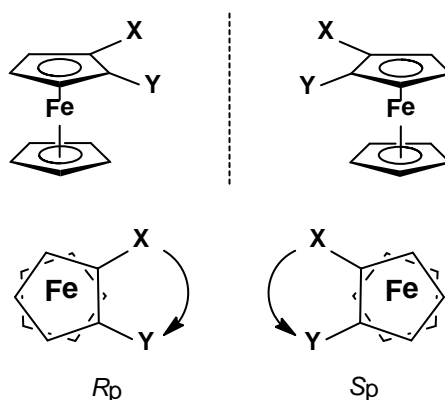


**Figure 1-4.** Assignment of the stereochemistry of enantiomeric 1,2-heterodisubstituted ferrocenes according to Schlägl (priority  $X > Y$ ).

However, in order to avoid ambiguity with phosphorus chirality centers, a more sophisticated nomenclature, the Cahn, Ingold and Prelog (CIP) protocol,<sup>23</sup> could be followed. In this method (Figure 1-5), a pilot atom with the highest priority of the atoms needs to be identified. In the example of of 1,2-disubstituted ferrocenes (*vide infra*) with a boron and tin substituent, C1 (attached to the heavier Sn) is identified as the pilot atom. Next, C1 is considered to be connected to four atoms as a regular tetrahedral carbon, and the substituents are assigned in order of highest priority if there is a choice ( $\text{Sn}^a > \text{Fe}^b > \text{C}^c > \text{C}^d$ ). When viewed from the side of the pilot atom, if the three atoms form a clockwise direction in order of priority, the chirality is assigned as *pR*, otherwise it is assigned as *pS*. This protocol is adopted in our recent publications and also for most of the planar chiral systems described in this thesis.

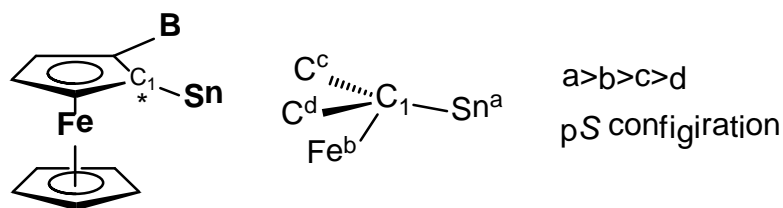


**Figure 1-5.** Planar chirality determination applying CIP protocol.

In addition, some structural parameters are defined herein with the aim to understand the framework-substituent interactions (Figure 1-6): 1) dip angle  $\alpha$  is the bending of the substituent out of the Cp ring, which allows us to investigate the interaction between the iron center and the Lewis acidic pendant group; 2) tilt angle  $\beta$  is the angle of two distorted Cp rings under certain degree of steric hindrance or restriction; 3) bridge angle  $\gamma$  is the bond angle of  $C_{Cp}-X-C_{Cp}$  with the bridging atom X.

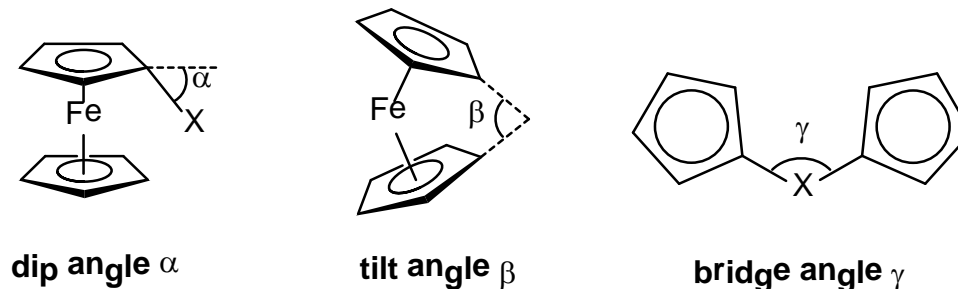


**Figure 1-6.** Definition of different structural parameters which will be discussed in this thesis.

Planar chiral ferrocene derivatives can be obtained starting either from achiral or chiral precursors. In the first synthetic protocol, the functionalization of the ferrocene framework is generally not stereoselective, and further chiral resolution methods are required for the separation into individual enantiomers. Fu et al. noted that reaction of  $FeCl_2$  first with  $Cp^*Li$  and then with a lithiated DMAP-fused Cp ligand species gives a

racemic mixture of *rac-O* (Scheme 1-5). This racemate could be resolved by preparative chiral HPLC and the enantiomerically pure product was employed as chiral catalyst for asymmetric transformations (Figure 1-7). More recently, Fu and co-workers introduced planar chiral versions of azaferrrocene and DMAP derivatives as enantioselective nucleophilic catalysts and successfully applied them in the addition of alcohols to ketenes, rearrangement of O-acylated enolate and acylation of alcohols by anhydrides.<sup>24</sup>

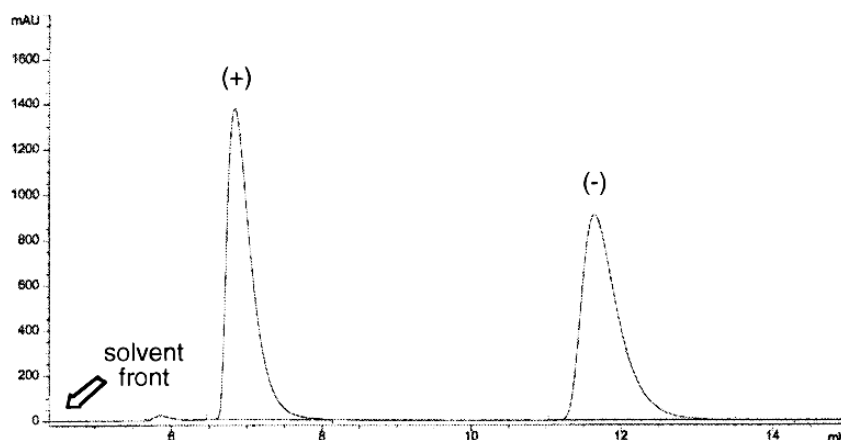
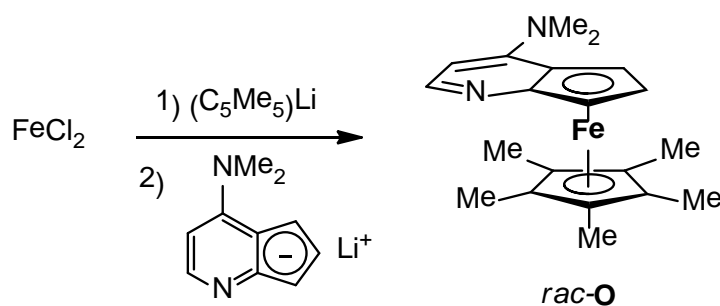
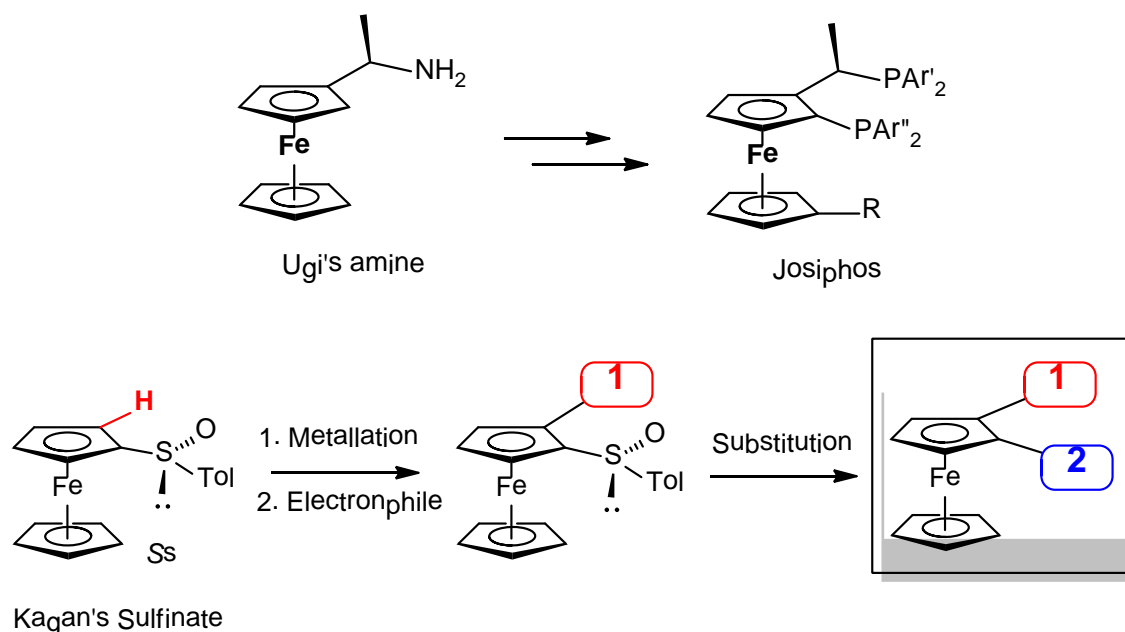


**Figure 1-7.** Chiral resolution of *rac-O* by preparative chiral HPLC.

Chiral resolution of a racemate has the advantage that it does not involve chiral synthesis from the precursor. Moreover, in many cases both of the enantiomers can be utilized, which improves atom economy. However, the limitation of this method is that it

relies heavily on the performance of chiral HPLC columns and the difficulty to find suitable chiral resolving reagents. These problems could be critical if the planar chiral compounds are air and moisture sensitive, which is a common issue with highly Lewis acidic systems. To overcome these drawbacks and develop a more general protocol towards planar chiral ferrocenes, chiral auxiliaries were introduced as substituents to one or both Cp rings. They serve as directing groups for diastereoselective ortho-directed lithiation. Among the very first examples, Ugi and co-workers introduced chiral enantiomers of N,N-dimethyl-1-ferrocenylethylamine (Ugi's amine) as the starting material for diastereoselective ortho-directed metalations, which proved to be a significant breakthrough in ferrocene chemistry.<sup>25</sup> Ugi's amine itself is resolved by complexation with (R)-(+)-tartaric acid. It can be readily deprotonated by n-BuLi in diethyl ether at 27 °C, quenched by addition of an electrophile to form the products with diastereomeric excess values up to 92%. The diastereomer can be purified by simple column chromatography or crystallization. By using this method, planar chiral ferrocenes were first introduced as ligands for catalysts. In the 1990s, a series of planar chiral diphosphine ferrocenes were developed, namely the Josiphos family of ligands. This family of ligands, featuring the general structure shown in Scheme 1-6, has been applied to a variety of reactions including asymmetric reduction of C=C, C=O and C=N unsaturated double bonds. Alternatively, a chiral sulfinate group can be added as an auxiliary. The latter has the advantage that after derivatization of the ortho position, the sulfinate group itself can be readily replaced by lithiation with *tert*-butyl lithium or magnesiation with Grignard species and subsequent treatment with electrophiles (Scheme

1-6).<sup>26</sup> Throughout the thesis, we will follow Kagan's synthesis, which provides excellent control for the stepwise introduction of different substituents.



**Scheme 1-6.** a) Synthesis of Josiphos ligands from Ugi's amine as a chiral precursor. b) Stepwise modification of Kagan's sulfinate for the preparation of bifunctional ferrocenes with a controlled geometry.

#### 1.4 Prior Work on Ferrocene-based Lewis Acids and Lewis Pairs

Different from the ferrocene-based ligands and Lewis base catalysts, ferrocenyl Lewis acids can be obtained by direct electrophilic borylation of ferrocene. Treatment of ferrocene with different amounts of BBr<sub>3</sub> leads to different degree of borylation (Figure 1-8).<sup>27</sup> Ferrocene also reacts readily with HB(C<sub>6</sub>F<sub>5</sub>)<sub>2</sub> at 80 °C to give (**S**) after elimination of a dihydrogen molecule (Scheme 1-7).

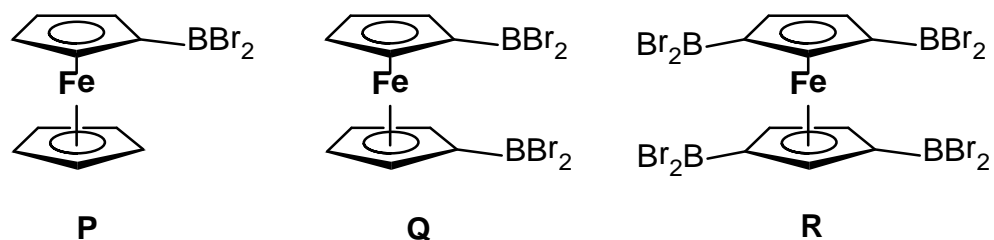
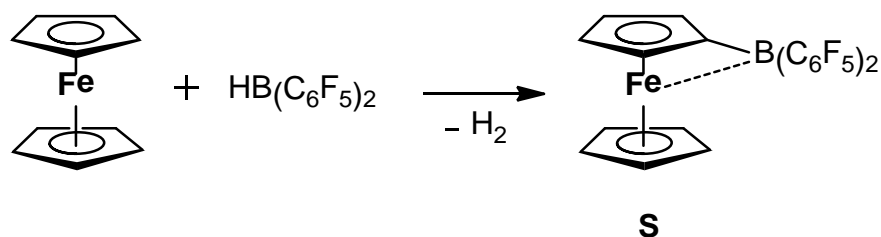


**Figure 1-8.** Products of direct borylation of ferrocene with different equivalents of  $\text{BBr}_3$ .



**Scheme 1-7.** Reaction between ferrocene and Piers' borane to give **S**.

The Lewis acid **S** was initially reported by Piers in 2001 and a detailed the investigation of the Fe-B interaction was provided.<sup>28</sup> Aldridge et al. showed more recently that (**S**), combined with tri-tert-butylphosphine, can be used to detect nitrous oxide with dual sensory signal output. The geometry of the boron changed from trigonal to tetrahedral conformation before and after complexation with nitrous oxide, which is accompanied by colorimetric and electrochemical changes of the ferrocenyl unit.<sup>29</sup> A series of related highly Lewis acidic species was achieved by Oestreich and co-workers by incorporation of tricoordinate silylium cations (**T**). Different substituents, including alkyl and aryl groups, were introduced on the silicon atom to investigate the influence on Lewis acid strength and catalytic performance in Diels Alder reactions.<sup>30</sup>

A more intriguing but less explored direction is to develop systems that bear both Lewis acid and base moieties. One example that was reported by Bourissou is a ferrocene compound with a diphenylphosphino and dimesitylboryl moiety (**U**). The dimesitylboryl group is moderately Lewis acidic, and unlikely to promote FLPs behavior. Nonetheless, it has been applied as an ambiphilic ligand in a Ru-catalyzed hydroformylation.<sup>31</sup> Interestingly, Aldridge succeeded in generating the planar chiral version of this Lewis pair (**V**).<sup>32</sup> Due to the steric hindrance, the interaction between B and P is absent. To our knowledge, small molecule activation or catalytic applications have not been studied with this class of compounds (Figure 1-9).

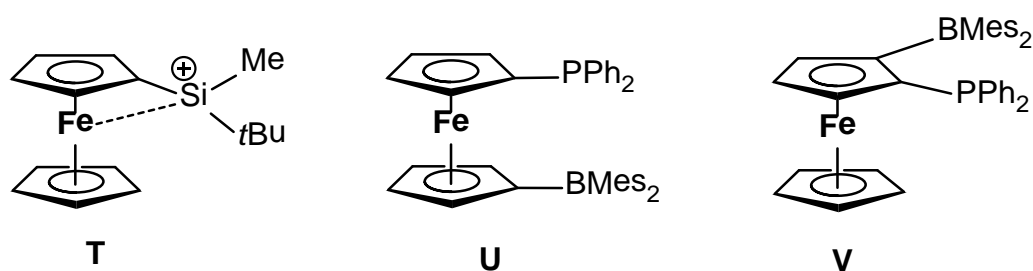
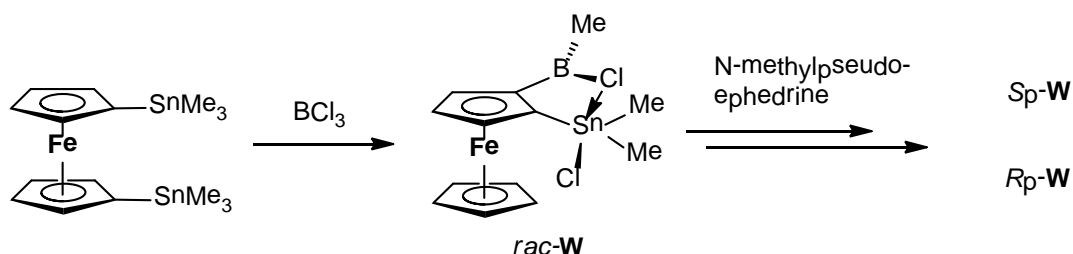


**Figure 1-9.** Representative ferrocenes with strong Lewis acid and Lewis base substituents.

Another unique example is the synthesis and resolution of a planar chiral bifunctional Lewis acid by Jäkle and co-workers.<sup>33</sup> Low temperature borylation of 1,1'-bis(trimethylstannyl)ferrocene with  $\text{BCl}_3$  leads to 1-stannyl-2-borylferrocene (*rac*-**W**) as the major product (Scheme 1-8). This result is remarkable, because for other silylated or stannylated aromatics cleavage of the element-carbon bond in an *ipso*-borodemetalation tends to occur much faster than activation of the C-H bond. The unique reactivity is attributed to the directing effect of the stannyl group, the ability of the iron center to

mediate proton transfer, and the presence of a second stannyl moiety that acts as a good leaving group. The reaction, however, produces a racemate that has to be resolved into the individual enantiomers by the introduction of a chiral resolving reagent [(+)-N-methylpseudoephedrine]. This novel class of bifunctional Lewis acids facilitates the conversion of a ketone into the asymmetric allylated alcohol product with good ee values.



**Scheme 1-8.** Synthesis of *rac-W* and its chiral resolution by N-methylpseudoephedrine.

The research discussed above provides a good starting point for the investigation of ferrocene-based planar chiral Lewis acids and Lewis pair. The survey of the recent literature reveals that a more general protocol for the synthesis of these chiral compounds is lacking. We envisioned that ferrocene would provide a rigid support for Lewis acids and FLP catalyst. Kagan's protocol is ideal to access a variety of planar chiral ferrocenes with different features – not only systems with sterically demanding chiral boranes, but also planar chiral Lewis pairs with distinct steric and electronic properties. This dissertation will describe their stereo-selective synthesis, structural investigation, and asymmetric catalytic applications.

## 1.5 Notes and References

1. Brown, H. C., *Tetrahedron* **1961**, *12*, 117-138.
2. Yamamoto, H., *Lewis Acids in Organic Synthesis*. Wiley VCH: Weinheim, New York, Chichester, Brisbane, Singapore, Toronto, 2000.
3. Parks, D. J.; Piers, W. E., *J. Am. Chem. Soc.* **1996**, *118*, 9440-9441.
4. (a) Gevorgyan, V.; Liu, J.-X.; Yamamoto, Y., *J. Org. Chem.* **1997**, *62*, 2963-2967; (b) Gevorgyan, V.; Liu, J.-X.; Yamamoto, Y., *Chem. Commun.* **1998**, 37-38.
5. Chen, E. Y.-X.; Marks, T. J., *Chem. Rev.* **2000**, *100*, 1391-1434.
6. Welch, G. C.; San Juan, R. R.; Masuda, J. D.; Stephan, D. W., *Science* **2006**, *314*, 1124-1126.
7. Geier, S. J.; Gille, A. L.; Gilbert, T. M.; Stephan, D. W., *Inorg. Chem.* **2009**, *48*, 10466-10474.
8. (a) Kenward, A. L.; Piers, W. E., *Angew. Chem. Int. Ed.* **2008**, *47*, 38-41; (b) Neu, R. C.; Otten, E.; Lough, A.; Stephan, D. W., *Chem. Sci.* **2010**, *2*, 170-176; (c) Zhao, X.; Stephan, D. W., *Chem. Commun.* **2011**, *47*, 1833-1835; (d) Holschumacher, D.; Daniliuc, C. G.; Jones, P. G.; Tamm, M., *Z. Naturforsch. B* **2011**, *66*, 371-377; (e) Marwitz, A. J. V.; Dutton, J. L.; Mercier, L. G.; Piers, W. E., *J. Am. Chem. Soc.* **2011**, *133*, 10026-10029; (f) Theuergarten, E.; Schloesser, J.; Schluens, D.; Freytag, M.; Daniliuc, C. G.; Jones, P. G.; Tamm, M., *Dalton Trans.* **2012**, *41*, 9101-9110; (g) Sajid, M.; Stute, A.; Cardenas, A. J. P.; Culotta, B. J.; Hepperle, J. A. M.; Warren, T. H.; Schirmer, B.; Grimme, S.; Studer, A.; Daniliuc, C. G.; Froehlich, R.; Petersen, J. L.; Kehr, G.; Erker, G., *J. Am. Chem. Soc.* **2012**, *134*, 10156-10168.
9. (a) Zhang, Y.; Miyake, G. M.; Chen, E. Y. X., *Angew. Chem. Int. Ed.* **2010**, *49*, 10158-10162; (b) Heiden, Z. M.; Stephan, D. W., *Chem. Commun.* **2011**, *47*, 5729-5731; (c) Piers, W. E.; Marwitz, A. J. V.; Mercier, L. G., *Inorg. Chem.* **2011**, *50*, 12252-12262; (d) Rosorius, C.; Kehr, G.; Froehlich, R.; Grimme, S.; Erker, G., *Organometallics* **2011**, *30*, 4211-4219; (e) Greb, L.; Ona-Burgos, P.; Schirmer, B.; Grimme, S.; Stephan, D. W.; Paradies, J., *Angew. Chem. Int. Ed.* **2012**, *51*, 10164-10168; (f) Stephan, D. W., *Org. Biomol. Chem.* **2012**, *10*, 5740-5746; (g) Zhang, Y.; Miyake, G. M.; John, M. G.; Falivene, L.; Caporaso, L.; Cavallo, L.; Chen, E. Y. X., *Dalton Trans.* **2012**, *41*, 9119-9134.
10. (a) Brown, H. C.; Ramachandran, P. V., *J. Organomet. Chem.* **1995**, *500*, 1-19; (b) Dhokte, U. P.; Soundararajan, R.; Ramachandran, P. V.; Brown, H. C., *Tetrahedron Lett.* **1996**, *37*, 8345-8348; (c) Dhotke, U. P.; Brown, H. C., *Organometallics* **1998**, *17*, 2891-2896.
11. (a) Hawkins, J. M.; Loren, S.; Nambu, M., *J. Am. Chem. Soc.* **1994**, *116*, 1657-1660; (b) Hawkins, J. M.; Nambu, M.; Loren, S., *Org. Lett.* **2003**, *5*, 4293-4295.
12. (a) Schilling, B.; Kaiser, V.; Kaufmann, D. E., *Chem. Ber.* **1997**, *130*, 923-932; (b) Bir, G.; Ernst, C.; Gross, U. M.; Rehwinkel, C.; Schilling, B.; Thormeier, S.; Kaiser, V.; Kaufmann, D., *Spec. Publ. - R. Soc. Chem.* **1997**, *201*, 193-200; (c) Schilling, B.; Kaufmann, D. E., *Eur. J. Org. Chem.* **1998**, 701-709; (d) Ishihara, K.; Inanaga, K.; Kondo, S.; Funahashi, M.; Yamamoto, H., *Synlett* **1998**, 1053; (e) Morrison, D. J.; Piers, W. E.; Parvez, M., *Synlett* **2004**, 2429-24333.
13. (a) Bir, G.; Kaufmann, D., *Tetrahedron Lett.* **1987**, *28*, 777-80; (b) Kaufmann, D.; Boese, R., *Angew. Chem.* **1990**, *102*, 568-9; (c) Reilly, M.; Oh, T., *Tetrahedron Lett.* **1994**, *35*, 7209-12; (d) Ishihara, K.; Kurihara, H.; Matsumoto, M.; Yamamoto, H., *J. Am.*

- Chem. Soc.* **1998**, *120*, 6920-6930; (e) Ishihara, K.; Yamamoto, H., *Eur. J. Org. Chem.* **1999**, 527-538; (f) Thormeier, S.; Carboni, B.; Kaufmann, D. E., *J. Organomet. Chem.* **2002**, *657*, 136-145.
14. (a) Mewald, M.; Frohlich, R.; Oestreich, M., *Chem. Eur. J.* **2011**, *17*, 9406-9414; (b) Mewald, M.; Oestreich, M., *Chem. Eur. J.* **2012**, *18*, 14079-14084.
15. (a) Chen, D.; Leich, V.; Pan, F.; Klankermayer, J., *Chem. Eur. J.* **2012**, *18*, 5184-5187; (b) Chen, D.; Wang, Y.; Klankermayer, J., *Angew. Chem. Int. Ed.* **2010**, *49*, 9475-9478; (c) Ghattas, G.; Chen, D.; Pan, F.; Klankermayer, J., *Dalton Trans.* **2012**, *41*, 9026-9028.
16. Liu, S. Y.; Hills, I. D.; Fu, G. C., *J. Am. Chem. Soc.* **2005**, *127*, 15352-3.
17. Kealy, T. J.; Pauson, P. L., *Nature* **1951**, *168*, 1039-1040.
18. (a) Wilkinson, G.; Rosenblum, M.; Whiting, M. C.; Woodward, R. B., *J. Am. Chem. Soc.* **1952**, *74*, 2125-2126; (b) Weiss, E.; Fischer, E. O., *Z. Anorg. Allg. Chem.* **1955**, *278*, 219-224.
19. (a) Togni, A.; Hayashi, T., *Ferrocenes: homogeneous catalysis, organic synthesis, material science*. Wiley-VCH: Weinheim, Germany, 1995; (b) Kagan, H. B.; Diter, P.; Gref, A.; Guillaneux, D.; Szymczak, A. M.; Rebiere, F.; Riant, O.; Samuel, O.; Taudien, S., *Pure Appl. Chem.* **1996**, *68*, 29-36; (c) Richards, C. J.; Locke, A. J., *Tetrahedron: Asymmetry* **1998**, *9*, 2377-2407; (d) Atkinson, R. C. J.; Gibson, V. C.; Long, N. J., *Chem. Soc. Rev.* **2004**, *33*, 313-328; (e) Stepnicka, P., *Ferrocenes: ligands, materials and biomolecules*. John Wiley & Sons.: Chichester, U.K., 2008; (f) Togni, A.; Bieler, N.; Burckhardt, U.; Köllner, C.; Pioda, G.; Schneider, R.; Schnyder, A., *Pure Appl. Chem.* **1999**, *71*, 1531; (g) Dai, L. X.; Hou, X. L.; Deng, W. P.; You, S. L.; Zhou, V. G., *Pure Appl. Chem.* **1999**, *71*, 1401-1405; (h) Dai, L.-X.; Tu, T.; You, S.-L.; Deng, W.-P.; Hou, X.-L., *Acc. Chem. Res.* **2003**, *36*, 659-667; (i) Colacot, T. J., *Chem. Rev.* **2003**, *103*, 3101-3118; (j) Barbaro, P.; Bianchini, C.; Giambastiani, G.; Parisel, S. L., *Coord. Chem. Rev.* **2004**, *248*, 2131-2150; (k) Hou, X. L.; You, S. L.; Tu, T.; Deng, W. P.; Wu, X. W.; Li, M.; Yuan, K.; Zhang, T. Z.; Dai, L. X., *Top. Catal.* **2005**, *35*, 87; (l) Arrayas, R. G.; Adrio, J.; Carretero, J. C., *Angew. Chem. Int. Ed.* **2006**, *45*, 7674-7715; (m) Dai, L. X.; Hou, X. L., *Chiral Ferrocenes in Asymmetric Catalysis*. Wiley-VCH: Weinheim, Germany, 2010; (n) Peters, R.; Fischer, D. F.; Jautze, S., *Top. Organomet. Chem.* **2011**, *33*, 139; (o) Schaarschmidt, D.; Lang, H., *Organometallics* **2013**, *32*, 5668-5704.
20. Ramos, A.; Lough, A. J.; Stephan, D. W., *Chem. Commun.* **2009**, 1118-1120.
21. (a) Blaser, H. U.; Brieden, W.; Pugin, B.; Spindler, F.; Studer, M.; Togni, A., *Top. Catal.* **2002**, *19*, 3-16; (b) Blaser, H. U.; Pugin, B.; Spindler, F., *J. Mol. Catal. A Chem.* **2005**, *231*, 1-20.
22. Schlögl, K.; Allinger, N. L.; Eliel, E. L., *Top. Stereochem.* 1967; p 39.
23. Cahn, R. S.; Ingold, C.; Prelog, V., *Angew. Chem.* **1966**, *78*, 413.
24. Fu, G. C., *Acc. Chem. Res.* **2000**, *33*, 412-20.
25. (a) Battelle, L. F.; Bau, R.; Gokel, G. W.; Oyakawa, R. T.; Ugi, I., *Angew. Chem. Int. Ed.* **1972**, *11*, 138; (b) Battelle, L. F.; Bau, R.; Gokel, G. W.; Oyakawa, R. T.; Ugi, I., *J. Am. Chem. Soc.* **1973**, *95*, 482.
26. (a) Guillaneux, D.; Kagan, H. B., *J. Org. Chem.* **1995**, *60*, 2502-2505; (b) Riant, O.; Argouarch, G.; Guillaneux, D.; Samuel, O.; Kagan, H. B., *J. Org. Chem.* **1998**, *63*, 3511-3514.

27. (a) Renk, T.; Ruf, W.; Siebert, W., *J. Organomet. Chem.* **1976**, *120*, 1-25; (b) Ruf, W.; Renk, T.; Siebert, W., *Z. Naturforsch.* **1976**, *31B*, 1028; (c) Appel, A.; Nöth, H.; Schmidt, M., *Chemische Berichte* **1995**, *128*, 621-626; (d) Appel, A.; Jäkle, F.; Priermeier, T.; Schmid, R.; Wagner, M., *Organometallics* **1996**, *15*, 1188-1194.
28. Carpenter, B. E.; Piers, W. E.; Parvez, M.; Yap, G. P. A.; Rettig, S. J., *Can. J. Chem.* **2001**, *79*, 857-867.
29. Kelly, M. J.; Gilbert, J.; Tirfoin, R.; Aldridge, S., *Angew. Chem. Int. Ed.* **2013**, *52*, 14344-14347.
30. (a) Klare, H. F. T.; Bergander, K.; Oestreich, M., *Angew. Chem. Int. Ed.* **2009**, *48*, 9077-9079; (b) Schmidt, R. K.; Muther, K.; Muck-Lichtenfeld, C.; Grimme, S.; Oestreich, M., *J. Am. Chem. Soc.* **2012**, *134*, 4421-4428; (c) Nödling, A. R.; Muther, K.; Rohde, V. H. G.; Hilt, G.; Oestreich, M., *Organometallics* **2013**, *33*, 302-308.
31. Bebbington, M. W. P.; Bontemps, S.; Bouhadir, G.; Hanton, M. J.; Tooze, R. P.; van Rensburg, H.; Bourissou, D., *New J. Chem.* **2010**, *34*, 1556-1559.
32. (a) Morgan, I. R.; Di Paolo, A.; Vidovic, D.; Fallis, I. A.; Aldridge, S., *Chem. Commun.* **2009**, 7288-7290; (b) Siewert, I.; Vidovic, D.; Aldridge, S., *J. Organomet. Chem.* **2011**, *696*, 2528-2532.
33. Boshra, R.; Doshi, A.; Jäkle, F., *Angew. Chem. Int. Ed.* **2008**, *47*, 1134-1137.

## Chapter 2 Synthesis and Characterization of Planar Chiral Lewis Acids Derived from Naphthylferrocenes<sup>a</sup>

### 2.1 Introduction

As discussed in Chapter 1, highly Lewis acidic organoboranes play key roles as reagents and catalysts in organic synthesis.<sup>1</sup> Especially important for organic transformation are chiral derivatives,<sup>2</sup> In an effort at enhancing the Lewis acidity of the boron sites, a backbone-perfluorinated binaphthylborane derivative has also been introduced by Piers and co-workers.<sup>3</sup> Soderquist and co-workers prepared enantiomerically pure 9-borabicyclo[3.3.2]decane derivatives and studied their applications in various organic transformations, including asymmetric allyl-, crotyl-, allenyl-, propargyl-, and hydroboration reactions.<sup>4</sup> Finally, highly Lewis acidic organoboranes are of much interest for transition metal-free hydrogenation reactions. Stephan and co-workers first demonstrated that frustrated Lewis pairs consisting of a combination of a strong Lewis acid and sterically hindered Lewis base are capable of activating dihydrogen and other small molecules.<sup>5</sup> Recent studies have been aimed at utilizing this unusual reaction for stereoselective hydrogenation reactions.<sup>6</sup>

We have focused our attention on ferrocenylborane-based Lewis acids.<sup>7</sup> One motivation has been that preparation of planar chiral derivatives could open up a new entry into enantioselective Lewis acid catalysts.<sup>8</sup> Attractive is also that the Lewis acidity of the borane moiety can be tuned through reversible redox chemistry at the metal centers.<sup>9</sup> Prior efforts by our group involved studies on the binding properties of

---

<sup>a</sup> This chapter is adapted from a journal publication

heteronuclear bidentate 1-stannyl-2-borylferrocene derivatives, which are obtained in their racemic form via a rearrangement reaction from 1,1'-bis(trimethylstannyl) ferrocene and boron halides  $RBCl_2$  ( $R = Cl, Ph, C_6F_5$ ).<sup>7a-c</sup> We have demonstrated that the bidentate Lewis acid 1,2-Fc(BClMe)(SnMe<sub>2</sub>Cl) (**A**) can be resolved into its constituent planar chiral enantiomers and subsequently employed them in the enantioselective allylation of ketones.<sup>10</sup> In this context, we would like to also note that Aldridge and co-workers recently obtained compound (**B**) in enantiomerically pure form via regioselective *ortho*-metalation and subsequent diastereomer separation by recrystallization.<sup>11</sup>

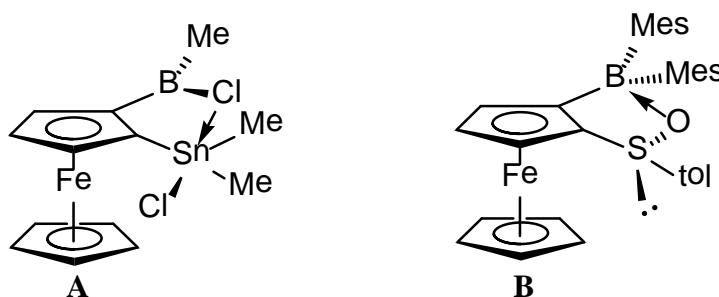


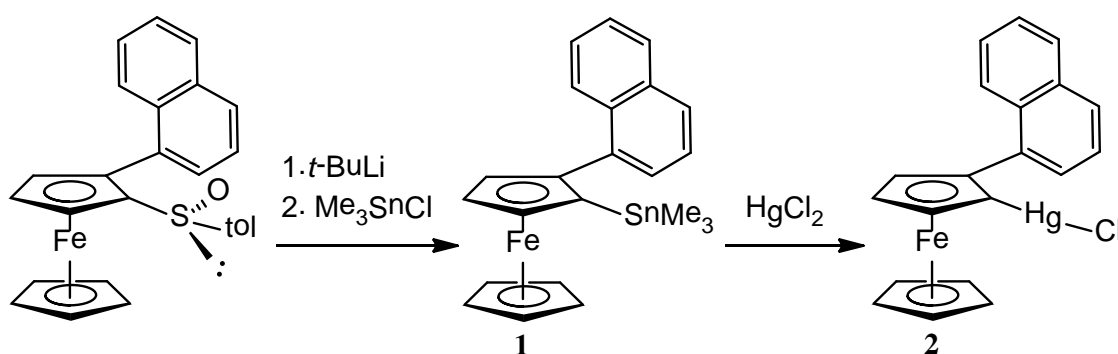
**Figure 2-1.** Examples of enantiomerically pure planar chiral ferrocenylboranes (Mes=2,4,6-trimethylphenyl, Tol=4-methylphenyl).

We describe here a high-yielding enantioselective synthesis route to the planar chiral naphthyl ferrocenylborane 1,2-Fc(Np)(BCl<sub>2</sub>), which in turn serves as a versatile precursor to other chiral organoborane Lewis acids through subsequent transmetalation reactions.

## 2.2 Results and Discussion

(*S<sub>p</sub>*)-2-(1-Naphthyl)-1-(trimethylstannyl)ferrocene (**1**) was prepared in analogy to a literature procedure for the synthesis of (*S<sub>p</sub>*)-2-(1-naphthyl)-1-(tributylstannyl)ferrocene.<sup>12</sup> Reaction of (*S<sub>p</sub>,S<sub>S</sub>*)-2-(1-naphthyl)-1-(*p*-

tolylsulfinyl)ferrocene with *t*-butyllithium followed by quenching with Me<sub>3</sub>SnCl gave **1** in 60% yield after recrystallization from methanol (Scheme 2-1). The <sup>1</sup>H and <sup>13</sup>C NMR spectra of **1** show patterns that are consistent with a 1,2-disubstituted ferrocene derivative, and a signal at  $\delta -7.1$  in the <sup>119</sup>Sn NMR spectrum confirms the attachment of the trimethylstannyl group. The absolute configuration of **1** as the *S<sub>p</sub>* isomer was assigned from the single crystal X-ray structure, which confirms stereoselective replacement of the sulfinato moiety (Figure 2-2a). Two independent molecules are found in the unit cell. The angle between the Cp and the naphthyl group is 72.27(9)° and 83.22(10)°, respectively, and the orientation of the naphthyl group matches that proposed for related compounds<sup>12c</sup> based on NMR studies.



**Scheme 2-1.** Synthesis of the enantiomerically pure organometallic naphthylferrocene derivatives **1** and **2**.

Treatment of aryltin species with HgCl<sub>2</sub> is generally known to lead to highly selective tin-mercury exchange.<sup>7e, 13</sup> Indeed, reaction of **1** with HgCl<sub>2</sub> in acetone led to facile formation of **2** in 84% isolated yield. The <sup>1</sup>H NMR shows three signals at  $\delta$  4.82 (dd), 4.64 (pst), and 4.30 (dd), as expected for a 1,2-disubstituted Cp ring, and a singlet at 4.33 for the free Cp ring. Single crystal X-ray analysis confirmed that the *S<sub>p</sub>* stereochemistry is unchanged relative to that of the Sn precursor (Figure 2-2b). The angle between the Cp

ring and the naphthyl group of  $77.1(1)^\circ$  is similar to that found for **1**. The Hg(1)-C(1) (2.024(5) Å) and Hg(1)-Cl(1) distances (2.312(1) Å) are comparable to those found in chloromercury ferrocene and other related organomercury compounds.<sup>14</sup> The C1-Hg1-Cl1 angle of  $179.0^\circ$  indicates an almost perfect linear coordination geometry at Hg. In the solid state, **2** exhibits an interesting supramolecular structure with infinite helical chains that arise from weak intermolecular Hg1 $\cdots$ Cl1 contacts (3.298(1) Å) as shown in Figure 2-2c.

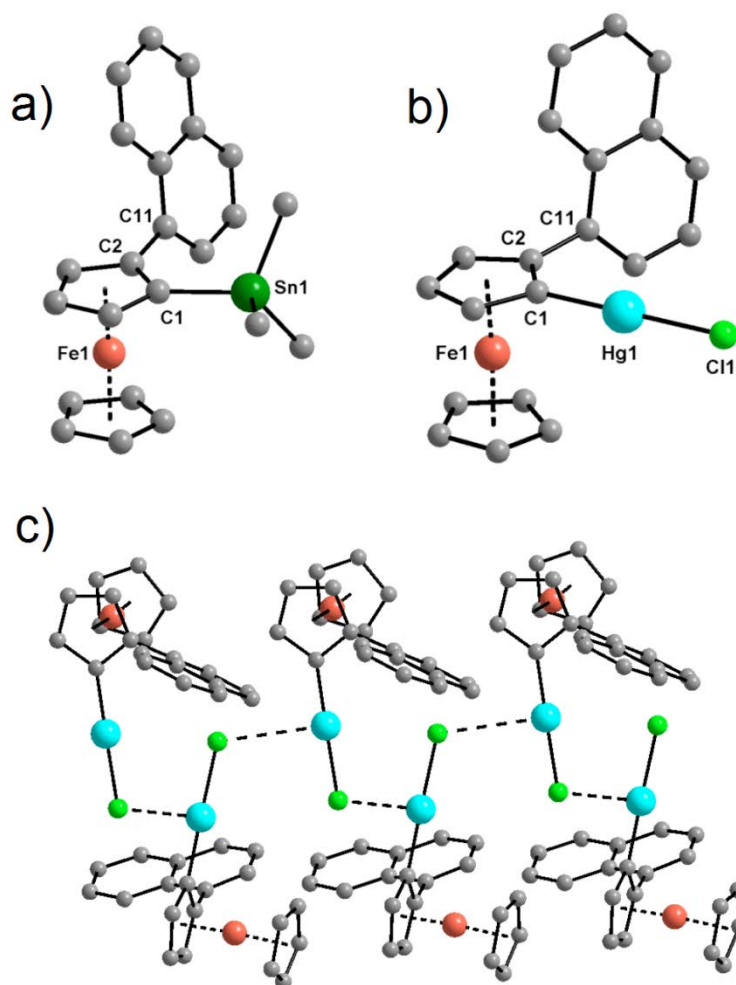
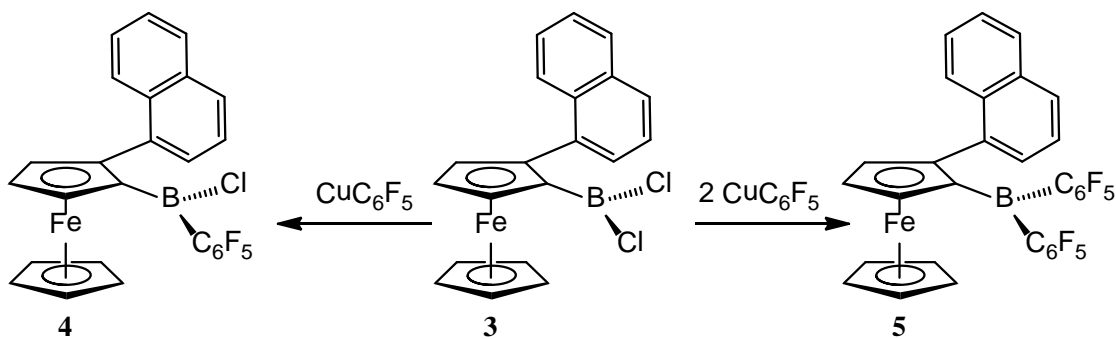


**Figure 2-2.** a) X-ray crystal structure plot of **1**. Hydrogen atoms are omitted for clarity. Selected interatomic distances [Å] and angles [ $^\circ$ ]: Sn1-C1 2.135(3), C2-C11 1.488(4), C1-C2-C11 124.7(3), Sn1-C1-C2 125.6(2). b) X-ray crystal structure plot of **2**. Hydrogen atoms are omitted for clarity. Selected interatomic distances [Å] and angles [ $^\circ$ ]: Hg1-C1,

2.024(5), Hg1-Cl1 2.312(1), C2-C11 1.489(7), C1-Hg1-Cl1 179.0(1), C1-C2-C11 122.4(4), Hg1-C1-C2 123.0(3). c) Illustration of the extended structure of **2** in the solid state.

We then studied the reactivity of these organometallic naphthylferrocene derivatives towards boron halides. Reaction of **1** with  $\text{BBr}_3$  in  $\text{CDCl}_3$  at  $-35\text{ }^\circ\text{C}$  resulted in the formation of a mixture of the 1,1'- and 1,3-disubstituted species according to  $^1\text{H}$  NMR analysis of the crude product mixture (ratio of 57:43) (see Experimental Section). Presumably, rearrangement occurs through interannular proton transfer, as previously reported for the reaction of 1,1'-bis(trimethylstannyl)ferrocene with boron halides.<sup>7b</sup> In contrast, reaction of **2** with one equiv of  $\text{BCl}_3$  at  $-30\text{ }^\circ\text{C}$  in hexanes resulted in clean conversion to the chiral Lewis acid  $R_p$ -1,2-NpFc $\text{BCl}_2$  (**3**) in a good yield of 82%. The formation of **3** was confirmed by  $^1\text{H}$ ,  $^{13}\text{C}$  and  $^{11}\text{B}$  NMR, high resolution MS, and elemental analysis. In the Cp region of the  $^1\text{H}$  NMR spectrum of **3** the pattern of a 1,2-disubstituted ferrocene was retained with three signals at 4.63 (dd), 4.57 (br), and 4.38 (br) for the substituted Cp ring and a singlet at 4.02 for the free Cp ring. The  $^{11}\text{B}$  NMR resonance at  $\delta$  49 is in a similar range as that reported for the achiral analog  $\text{FcBCl}_2$  ( $\delta$  50.5)<sup>15</sup>.



**Scheme 2-2.** Synthesis of highly Lewis acidic planar chiral ferrocenylboranes.

The novel planar chiral diarylchloroborane  $R_p$ -1,2-NpFcBCl(C<sub>6</sub>F<sub>5</sub>) (**4**) and triarylborane species  $R_p$ -1,2-NpFcB(C<sub>6</sub>F<sub>5</sub>)<sub>2</sub> (**5**) were obtained by treatment of **3** with 1 and 2 equiv of pentafluorophenyl copper<sup>16</sup>, respectively (Scheme 2-2). Compounds **4** and **5** were isolated as dark red microcrystalline solids in 80 and 84% yield, respectively. Their structures were confirmed by multinuclear NMR, high resolution MALDI-TOF MS or elemental analysis, and single crystal X-ray analysis. The <sup>11</sup>B NMR shifts of **4** (55 ppm) and **5** (54 ppm) are in a similar range as that reported by Piers for the achiral analog FcB(C<sub>6</sub>F<sub>5</sub>)<sub>2</sub> (53 ppm)<sup>9b</sup>, which is consistent with the presence of a weak Fe→B interaction (see *vide infra*).<sup>17</sup> At room temperature, the <sup>19</sup>F NMR spectrum of **4** shows three slightly broadened resonances at  $\delta$ -130, -154.1, -162.7. In contrast, **5** shows two sets of strongly broadened <sup>19</sup>F NMR peaks, one of which is attributed to the C<sub>6</sub>F<sub>5</sub> ring (A) adjacent to the naphthyl moiety and the other to the C<sub>6</sub>F<sub>5</sub> ring (B) that is pointing away. The apparent signal broadening suggests hindered rotation about the B-C(Cp) and/or the B-C(C<sub>6</sub>F<sub>5</sub>) bonds. We performed variable temperature <sup>19</sup>F NMR studies to further examine the fluxional behavior of compounds **4** and **5**.

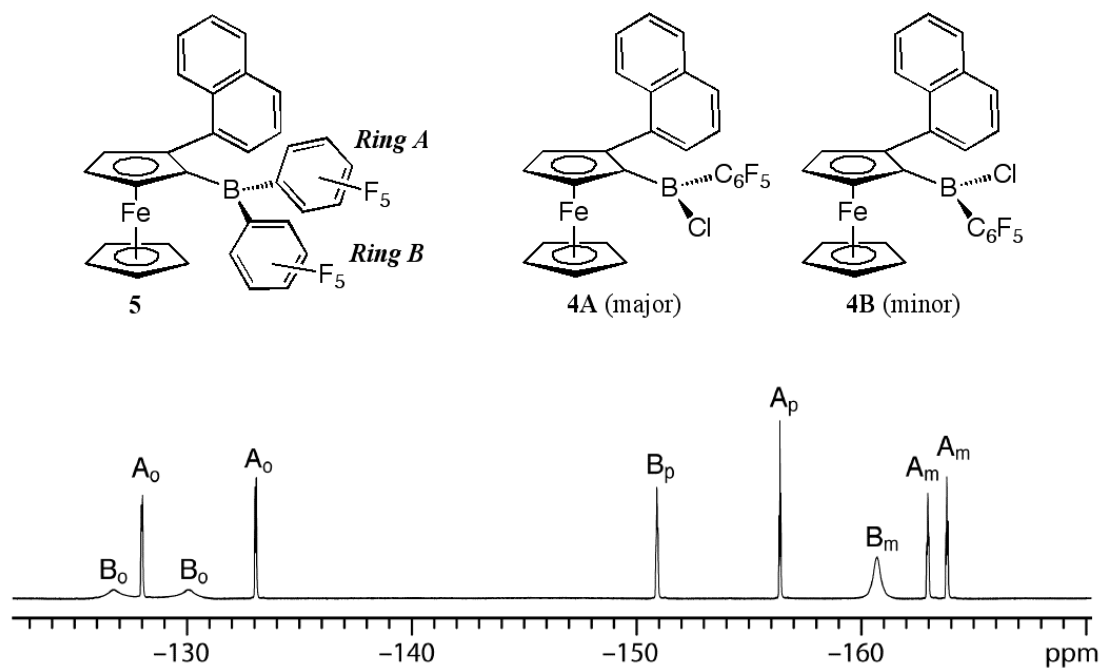


**Figure 2-3.** Low temperature  $^{19}\text{F}$  NMR spectrum of **5** ( $\text{CDCl}_3$ , 470.4 MHz,  $-60\text{ }^\circ\text{C}$ ).

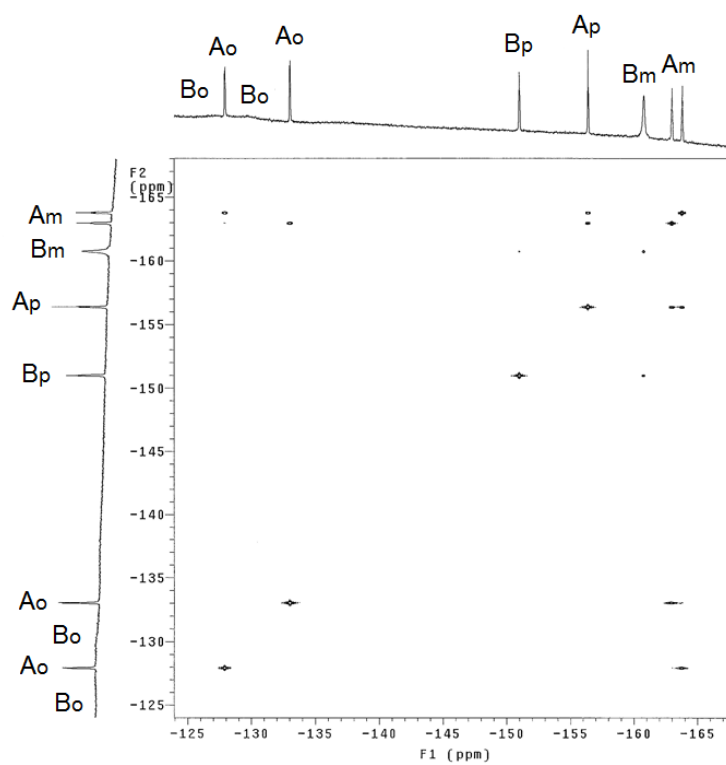


**Figure 2-4.**  $^{19}\text{F}$ - $^{19}\text{F}$  2D gCOSY NMR spectrum of **5** ( $\text{CDCl}_3$ ,  $-50\text{ }^\circ\text{C}$ ).

For compound **5**, two distinct sets of resonances of equal intensity were observed for the C<sub>6</sub>F<sub>5</sub> moieties at -60 °C (Figure 2-3). They were assigned based on 2D <sup>19</sup>F-<sup>19</sup>F NMR spectroscopy (see Figure 2-4). Ring (A) shows five <sup>19</sup>F NMR resonances due to hindered rotation about the C<sub>6</sub>F<sub>5</sub> ring (A), which is a result of the presence of the adjacent naphthyl moiety. In contrast, ring (B) shows only one signal for the *meta*-fluorines and strongly broadened signals for the *ortho*-fluorines, indicating a much lower barrier of rotation. The energy barriers were determined from both line shape analysis<sup>18</sup> and coalescence temperature methods<sup>19</sup> (see Figure 2-5). Analysis of the temperature dependence of the line shape of the *para*-F atoms provides information on the B-C(Cp) barrier, while information on the rotational barrier of the C<sub>6</sub>F<sub>5</sub> ring (A) can be obtained from line shape analysis for the *ortho*- or *meta*-F atoms (Table 2-1). A similar barrier was deduced for exchange of the *meta*-fluorines of ring A ( $\Delta G^\ddagger_{298} = 58.9(1)$  kJ mol<sup>-1</sup>) and the *para*-fluorines of rings A/B ( $\Delta G^\ddagger_{298} = 58.3(6)$  kJ mol<sup>-1</sup>), which indicates that the rotation of ring (A) and interchange between rings (A) and (B) require about the same energy, while rotation of ring (B) is comparatively much more facile ( $\Delta G^\ddagger_{228} = 39.8(6)$  kJ mol<sup>-1</sup> for ring B; cf.  $\Delta G^\ddagger_{228} = 55.5(8)$  kJ mol<sup>-1</sup> for ring A).

**Table 2-1.** Results from line shape analysis and coalescence temperatures for **4** and **5**.

Compd	Probe	$\Delta H^\ddagger_{298}$ <sup>[a]</sup> [kJ mol <sup>-1</sup> ]	$\Delta S^\ddagger_{298}$ <sup>[a]</sup> [J mol <sup>-1</sup> K <sup>-1</sup> ]	$\Delta G^\ddagger_{298}$ <sup>[a]</sup> [kJ mol <sup>-1</sup> ]	$T_c$ <sup>[b]</sup> [K]	$dG^\ddagger_{T_c}$ <sup>[b]</sup> [kJ mol <sup>-1</sup> ]
<b>4</b> A→B	<i>p</i> -F(A)	37.1(6)	-45.5(8)	50.6(4)		
<b>4</b> B→A	<i>p</i> -F(B)	37.0(3)	-36.9(3)	48.0(3)		
<b>4A</b>	<i>m</i> -F(A)	22.1(6)	-110(3)	55.0(4)	265(3)	50.0(6)
<b>4B</b>	<i>o</i> -F(B)	33(1)	-41(2)	45.8(8)	248(3)	44.1(6)
<b>5</b> A→B	<i>p</i> -F(A)	52.5(7)	-19.4(3)	58.3(6)		

<b>5</b> Ring A	<i>m</i> -F(A)	30(1)	-97(4)	58.9(1)	308(3)	58(2)
<b>5</b> Ring B	<i>o</i> -F(B)	[c]	[c]	[c]	228(3)	39.8(6)

[a] Data from line shape analysis using the fitting program DNMR. [b] Data from coalescence temperature method using the approximation  $\Delta G^\ddagger = 19.1 T_c [9.97 + \lg(T_c \Delta \nu^{-1})]$  for estimation of  $\Delta G^\ddagger$  at  $T_c$ .<sup>19</sup> [c] Data were not well resolved.

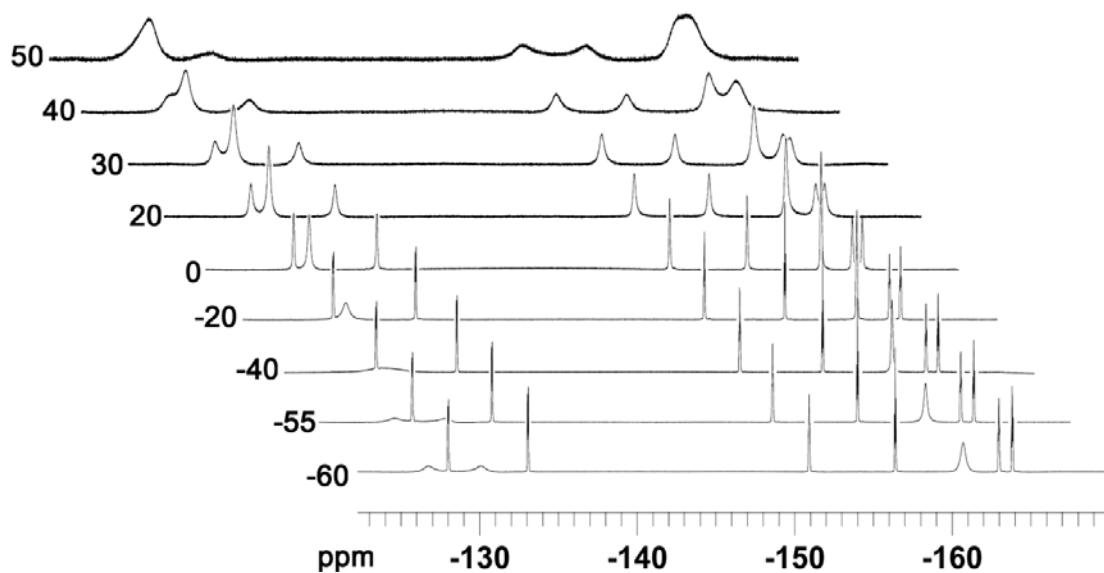


**Figure 2-5.** Variable temperature  $^{19}\text{F}$  NMR spectra of **5** ( $\text{CDCl}_3$ , 470.4 MHz).

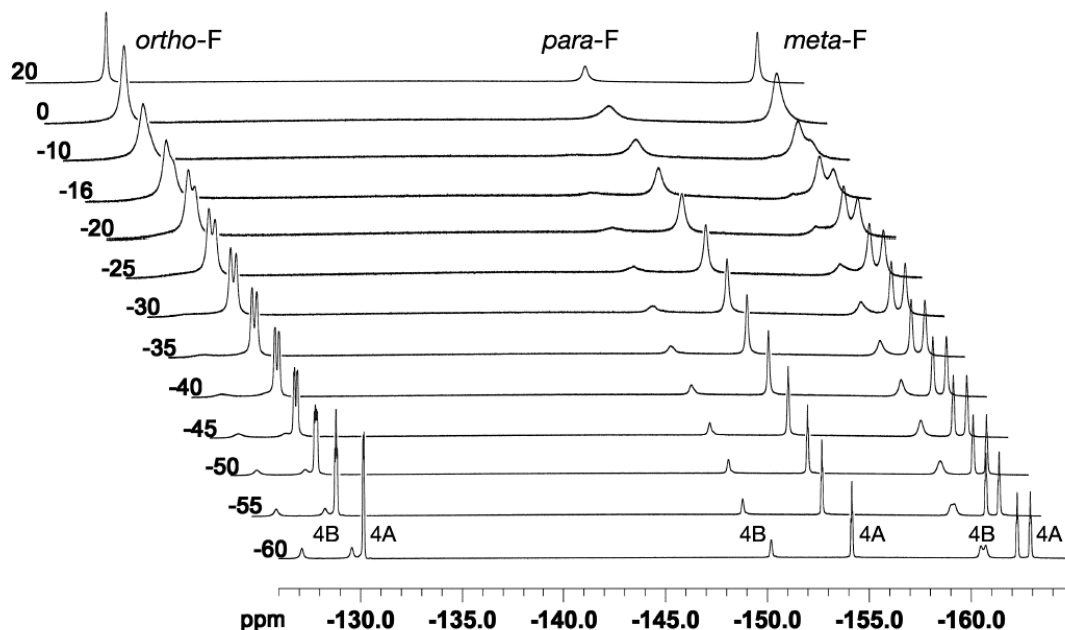


**Figure 2-6.** Variable temperature  $^{19}\text{F}$  NMR spectra of **4** ( $\text{CDCl}_3$ , 470.4 MHz).

Compound **4** also shows two sets of  $^{19}\text{F}$  NMR peaks at  $-60\text{ }^\circ\text{C}$ , but their relative intensity is different (Figure 2-6). Hence, a major and a minor rotational isomer are formed (**4A** and **4B**). Based on a comparison with the NMR data for **5**, we can confidently assign the major isomer to be that with the  $\text{C}_6\text{F}_5$  group pointing toward the naphthyl group. The free energy barriers for interconversion of isomer **4A** into **4B** and vice versa were calculated to be  $\Delta G_{298}^\ddagger = 50.6(4)$  and  $48.0(3)$   $\text{kJ mol}^{-1}$ , respectively, suggesting that the isomer with the pentafluorophenyl group pointing toward the naphthyl group is energetically favourable by about  $2\text{-}3\text{ kJ mol}^{-1}$ .

The solid state structures were examined by single crystal X-ray diffraction. The X-ray analysis of **5** revealed two independent molecules with similar structural features in the asymmetric unit, while only one molecule of **4** was found (Figure 2-7). For **4**, the isomer with the  $\text{C}_6\text{F}_5$  moiety pointing toward the naphthyl group crystallized out, which is

consistent with our findings that this isomer is energetically favourable in solution. The boryl moieties are bent away from the plane of the substituted Cp ring of the ferrocenyl unit in both **4** and **5**, with interplanar angles of Cp//BC<sub>2</sub>Cl = 21.4 for **4** and Cp//BC<sub>3</sub> = 14.8 and 16.0° for the independent molecules of **5**, respectively. This tilting of the boryl group toward the iron atom and the comparatively short B-C bond lengths (for **4**, B-C<sub>Cp</sub> = 1.511(3); for **5**, B-C<sub>Cp</sub> = 1.521(6), 1.501(6) Å) indicate a considerable degree of electronic delocalization between the electron rich ferrocene and the electron deficient boron atom.<sup>17</sup> In comparison, the angle in Piers' structure is ca. 16° and those for the two independent molecules in the asymmetric unit of FcBBr<sub>2</sub> are 17.7 and 18.9°.<sup>20</sup> The observation that the tilting of the boryl group is much more pronounced in **4** than in **5** may suggest increased steric strain in the latter due to the additional C<sub>6</sub>F<sub>5</sub> group, which is preventing even closer contact between Fe and B. Indeed, considerable strain is evident for both molecules from the Cp//Cp tilt angles, which range from 7.0 to 7.6°. Noteworthy is also an intramolecular π-stacking interaction between the naphthyl moiety and the pentafluorophenyl ring (centroid-centroid distances in **4**: 3.792 and 3.579 Å; **5**: 3.512 and 3.701 Å). The interplanar angle between the C<sub>6</sub>F<sub>5</sub> moiety and the naphthyl ring ranges from 7.6° for **5** to 14.7° for **4**. In the solid state, both **4** and **5** reveal an interesting supramolecular 3D network structure as a result of multiple CH⋯π and CF⋯π interactions (see 2.5 Supporting Information, Figures 2-14, 2-15).

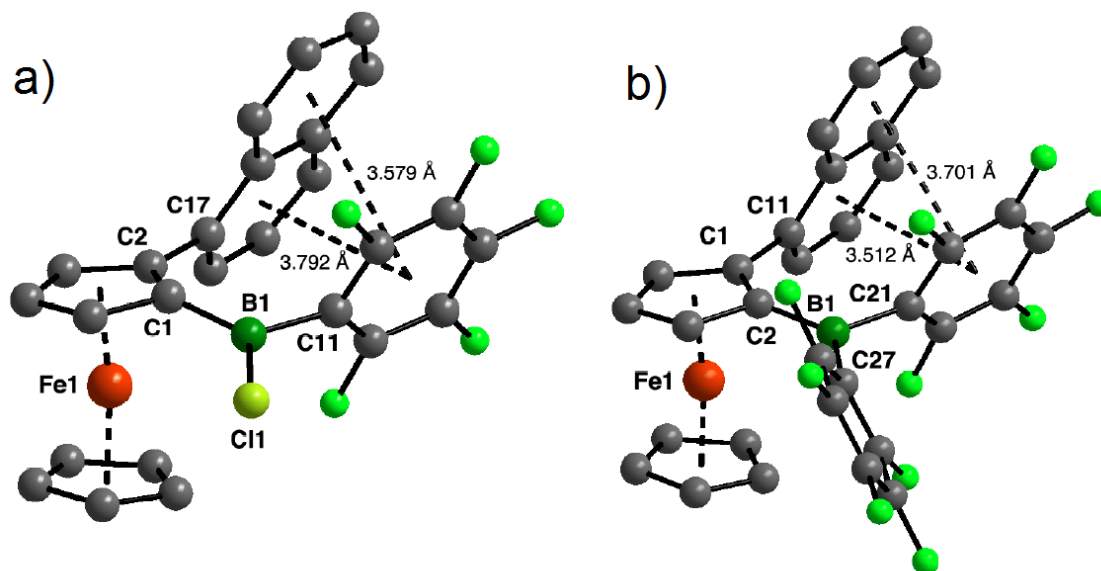


**Figure 2-7.** a) X-ray crystal structure plot of **4**. Hydrogen atoms are omitted for clarity. Selected interatomic distances [Å] and angles [°]: B1-C1 1.511(3), B1-C11 1.587(4), B1-C11 1.787(3), C1-B1-C11 123.9(2), C1-B1-C11 119.5(2), C11-B1-C11 115.95(18), Cp//Cp 7.0, Cp//Np 59.2, C<sub>6</sub>F<sub>5</sub>//Np 14.7. b) X-ray crystal structure plot of one of two independent molecules of **5**. Hydrogen atoms are omitted for clarity. Selected interatomic distances [Å] and angles [°]: B1-C2 1.521(6), B1-C27 1.578(7), B1-C21 1.598(7), C2-B1-C27 123.0(4), C2-B1-C21 122.2(4), C27-B1-C21 114.3(4), Cp//Cp 7.6, Cp//Np 65.1, C<sub>6</sub>F<sub>5</sub>//Np 7.6.

We examined the electronic structures of the ferrocenylborane Lewis acids by UV-visible spectroscopy and cyclic voltammetry measurements. The longest wavelength absorption occurs at lowest energy for the bis(perfluorophenyl)-substituted compound **5** (491 nm,  $\epsilon = 1680$ ), followed by **4** (475 nm,  $\epsilon = 1280$ ) and **3** (455 nm,  $\epsilon = 1120$ ) (Figure 2-8). This band can be attributed to a dd transition of the ferrocene moieties with significant charge transfer character. The particular order may suggest that electronic interactions between the ferrocenyl  $\pi$  orbitals and the empty  $p$ -orbitals on boron are promoted by the electron deficient C<sub>6</sub>F<sub>5</sub> groups more effectively than by the electronegative chlorine atoms.

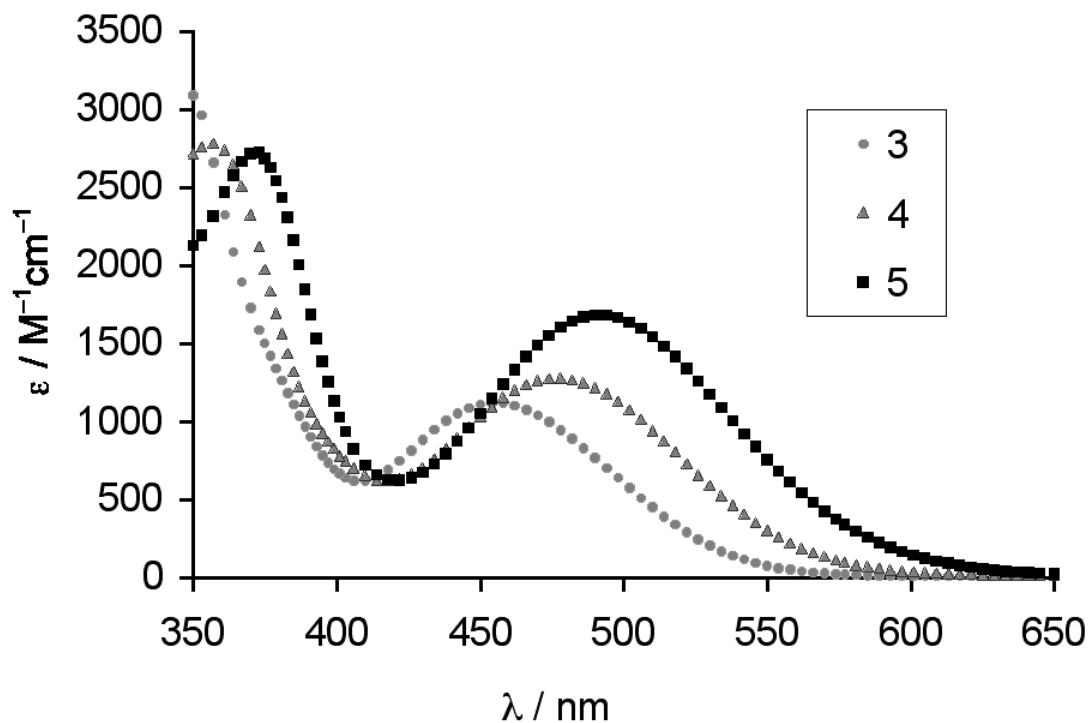


**Figure 2-8.** UV/Vis absorption spectra of chiral ferrocenylboranes **3** (ball), **4** (triangle), and **5** (square).

Finally, we explored the possibility of **5** to undergo reversible oxidation. The cyclic voltammogram of **5** shows a reversible redox process at  $E_{1/2} = +460$  mV vs the Fc/Fc<sup>+</sup> couple (Figure 2-9), which is considerably more anodic than those determined for **1** (+6 mV) and **2** (+127 mV). The higher +ve potential for **5** is in good agreement with data reported by Piers et al. for FcB(C<sub>6</sub>F<sub>5</sub>)<sub>2</sub> (+450 mV in trifluorotoluene/Bu<sub>4</sub>N[B(C<sub>6</sub>F<sub>5</sub>)<sub>4</sub>])<sup>9b</sup> and attributed to the electron withdrawing nature of the B(C<sub>6</sub>F<sub>5</sub>)<sub>2</sub> moiety. Addition of the Lewis base pyridine, which binds to boron and thus renders the boryl group more electron rich, shifts the redox potential of **5** to +90 mV. The fact that **5** undergoes a reversible electrochemical oxidation clearly suggests the possible use of this new class of compounds as redox-active chiral Lewis acid.

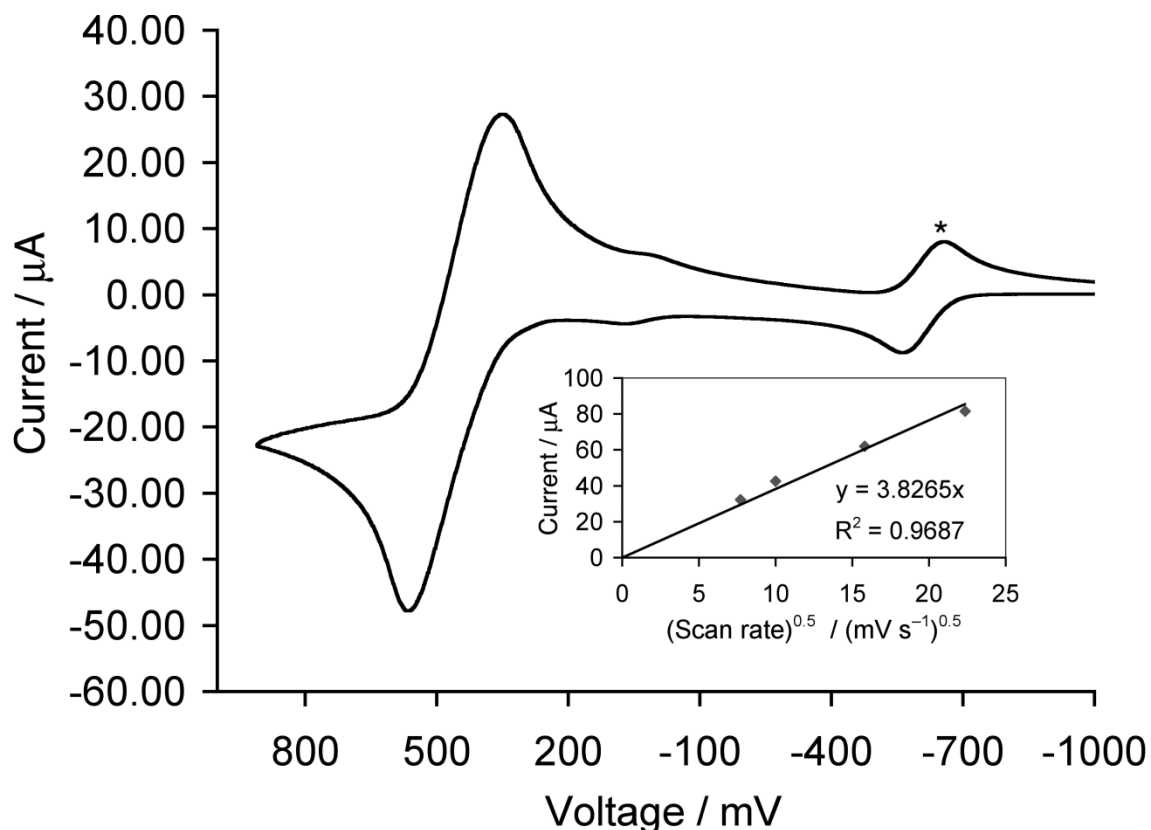


**Figure 2-9.** Cyclic voltammogram of compound **5** ( $\text{CH}_2\text{Cl}_2$ , 0.05 M  $\text{Bu}_4\text{N}[\text{B}(\text{C}_6\text{F}_5)_4]$ , reported versus  $\text{Fc}/\text{Fc}^+$ , which is taken as +610 mV versus  $\text{Cp}^*_2\text{Fe}/\text{Cp}^*_2\text{Fe}^+$  (indicated with an asterisk,  $\text{Cp}^*$ =pentamethylcyclopentadienyl) as an internal reference). The small peak at approximately +50 mV is due to trace amounts of naphthylferrocene that is formed as a result of the reaction of **5** with traces of water (Inset: plot of current versus square root of scan rate).

### 2.3 Conclusions

In conclusion, we describe the first examples of highly Lewis acidic planar chiral ferrocenylborane Lewis acids. Compounds **4** and **5** are structurally closely related to the important class of chiral binaphthyl species, which have found abundant use in catalysis applications. Importantly, the ferrocenyl group not only provides a rigid chiral environment, but the redox-active nature of the central iron atom may allow for tuning and further enhancement of the Lewis acidity. Additional studies in this regard and on the

application of compounds **4** and **5**, as well as related planar chiral Lewis acids, in stereoselective organic synthesis are in progress. To explore the combination of these chiral Lewis acids with sterically hindered Lewis bases in the context of so-called frustrated Lewis pairs will be also of interesting.

## 2.4 Experimental Section

**Materials and General Methods:**  $\text{BCl}_3$  (1M in hexanes), *t*-butyl lithium (1.7M in hexanes), and mercuric chloride were purchased from Acros.  $\text{BBr}_3$  (99+%) was obtained from Aldrich and distilled prior to use. **Caution!** *BBr<sub>3</sub> is toxic and highly corrosive and should be handled appropriately with great care.* Fluorinated grease was used for ground glass joints in all reactions involving boron tribromide.  $(S_P, S_S)$ -2-(1-naphthyl)-1-(*p*-tolylsulfinyl)ferrocene<sup>12a</sup>, pentafluorophenyl copper<sup>21</sup>, and  $(\text{C}_6\text{F}_5)_2\text{BCl}$ <sup>22</sup> were prepared according to literature procedures. All reactions and manipulations were carried out under an atmosphere of prepurified nitrogen using either Schlenk techniques or an inert-atmosphere glovebox (MBraun). THF was distilled from sodium/benzophenone. Hydrocarbon and chlorinated solvents were purified using a solvent purification system (Innovative Technologies; alumina/copper columns for hydrocarbon solvents), and the chlorinated solvents were subsequently degassed via several freeze-pump-thaw cycles. Deuterated chloroform ( $\text{CDCl}_3$  >99.7%) was obtained from Cambridge Isotope Laboratories (CIL). The solvent was stirred for several days over anhydrous  $\text{CaH}_2$ , then degassed via several freeze pump thaw cycles and stored over 3Å molecular sieves. All 499.9 MHz  $^1\text{H}$  NMR, 125.7 MHz  $^{13}\text{C}$  NMR, 470.4 MHz  $^{19}\text{F}$  NMR, 160.4 MHz  $^{11}\text{B}$  NMR, and 186.4 MHz  $^{119}\text{Sn}$  NMR spectra were recorded on a Varian INOVA NMR spectrometer (Varian Inc., Palo Alto, CA) equipped with a 5 mm dual broadband gradient

probe (Nalorac, Varian Inc., Martinez, CA). Solution  $^1\text{H}$  and  $^{13}\text{C}$  NMR spectra were referenced internally to the solvent signals.  $^{19}\text{F}$  NMR spectra were referenced externally to  $\alpha,\alpha',\alpha''$ -trifluorotoluene (0.05% in  $\text{C}_6\text{D}_6$ ;  $\delta = -63.73$ ),  $^{11}\text{B}$  NMR spectra to  $\text{BF}_3\cdot\text{OEt}_2$  ( $\delta = 0$ ) in  $\text{C}_6\text{D}_6$ , and  $^{119}\text{Sn}$  NMR spectra to  $\text{SnMe}_4$  ( $\delta = 0$ ) in  $\text{C}_6\text{D}_6$ . The abbreviation Np is used for 1-naphthyl; splittings of NMR signals are abbreviated as pst (pseudo-triplet), nr (not resolved), br (broad).

GC-MS spectra were acquired on a Hewlett Packard HP 6890 Series GC system equipped with a series 5973 mass selective detector and a series 7683 injector. MALDI-TOF measurements were performed either on an Applied Biosystems 4700 Proteomics Analyzer in reflectron (+) mode with delayed extraction or an Apex Ultra 7.0 Hybrid FT-MS (Bruker Daltonics). Benzo[a]pyrene was used as the matrix (10 mg/mL in toluene). Samples were prepared in toluene (10 mg/mL), a drop of pyridine or picoline was added, the resulting solution was mixed with the matrix in a 1:10 ratio, and then spotted on the wells of a sample plate inside a glove box. UV-visible absorption data were acquired on a Varian Cary 500 UV-vis/NIR spectrophotometer. Solutions were prepared using a microbalance ( $\pm 0.1$  mg) and volumetric glassware and then charged into quartz cuvettes with sealing screw caps (Starna) inside the glovebox. Optical rotation analysis was performed on an Autopol III polarimeter, Rudolph Research Analytical, using a tungsten-halogen light source operating at  $\lambda = 589$  nm. Cyclic voltammetry measurements were carried out on a BAS CV-50W analyzer. The three-electrode system consisted of an Au disk as working electrode, a Pt wire as secondary electrode, and a Ag wire as the pseudo-reference electrode. The voltammograms of **1** and **2** were recorded in  $\text{CH}_2\text{Cl}_2$  containing  $[\text{Bu}_4\text{N}]\text{PF}_6$  (0.1 M) as the supporting electrolyte and that of **5** in  $\text{CH}_2\text{Cl}_2$  containing

[Bu<sub>4</sub>N][B(C<sub>6</sub>F<sub>5</sub>)<sub>4</sub>] (0.05 M). Data were acquired with decamethylferrocene as an internal reference and are reported relative to the ferrocene/ferrocenium couple (+560 mV with 0.1M [Bu<sub>4</sub>N]PF<sub>6</sub> in CH<sub>2</sub>Cl<sub>2</sub> and +610 mV with 0.05 M [Bu<sub>4</sub>N][B(C<sub>6</sub>F<sub>5</sub>)<sub>4</sub>] in CH<sub>2</sub>Cl<sub>2</sub> vs. decamethylferrocene/decamethylferrocenium couple). Elemental analyses were performed by Quantitative Technologies Inc., Whitehouse, NJ.

Yellow needle-like crystals of **1** and yellow rod-like crystals of **2** were obtained from methanol and dichloromethane, respectively; dark red plate-like crystals of **4** and **5** were grown from hexanes at -37 °C. X-ray data for **1**, **2**, **4** and **5** were collected on a Bruker SMART APEX CCD Diffractometer using Cu-K $\alpha$  (1.54178 Å) radiation. Details of X-ray diffraction experiments and crystal structure refinements are provided in Table 2-2. Numerical absorption correction was applied to **4** and **5**, and SADABS<sup>4</sup> absorption correction was applied to **1** and **2**. The structures were solved using direct methods, completed by subsequent difference Fourier syntheses, and refined by full matrix least squares procedures on  $F^2$ . All non-hydrogen atoms were refined with anisotropic displacement coefficients. The H atoms were placed at calculated positions and were refined as riding atoms. All software and source scattering factors are contained in the SHELXTL program package.<sup>5</sup> For **5**, the program Squeeze in Platon was used to remove highly disordered hexanes molecules (8 molecules per unit cell). The Squeeze method found a total electron count of 172.0 and 171.3 in a volume of 799.3 and 799.2 Å<sup>3</sup> in the solvent regions of the unit cell, respectively. The calculated electron count for four hexanes is about 200, which is slightly larger than the experimental values. However, integration of the <sup>1</sup>H NMR spectrum shows that the ratio of **5** to solvent is ca. 14:10,

which indicates that some of the hexanes in the crystal lattice evaporated under high vacuum.

Crystallographic data for the structures of **1**, **2**, **4**, and **5** have been deposited with the Cambridge Crystallographic Data Center as supplementary publication nos. CCDC 765783-765786. Copies of the data can be obtained free of charge on application to CCDC, 12 Union Road, Cambridge CB21EZ, UK (fax: (+44) 1223-336-033; email: [deposit@ccdc.cam.ac.uk](mailto:deposit@ccdc.cam.ac.uk)).

**Synthesis of (*S<sub>p</sub>*)-2-(1-Naphthyl)-1-(trimethylstannyl)ferrocene (1).** A solution of *t*-BuLi (2.45 mL of 1.7M solution in hexanes, 4.17 mmol) was added dropwise via a syringe to a stirred solution of (*S<sub>p</sub>*,*S<sub>s</sub>*)-2-(1-naphthyl)-1-(*p*-tolylsulfinyl)ferrocene (1.71 g, 3.80 mmol) in freshly distilled THF (50 mL) at  $-78$  °C. The solution was stirred for 5 minutes before adding Me<sub>3</sub>SnCl (0.91 g, 4.57 mmol) in THF (30 mL). The solution was stirred at the same temperature for 1 h and subsequently quenched with a small amount of distilled water. Standard workup and flash column chromatography on silica gel with hexanes as the eluent gave a mixture of (*S<sub>p</sub>*)-2-(1-naphthyl)-1-(trimethylstannyl)ferrocene and 1-naphthylferrocene. Recrystallization from methanol gave spectroscopically pure (*S<sub>p</sub>*)-2-(1-naphthyl)-1-(trimethylstannyl)ferrocene. Yield: 1.09 g (60%).  $[\alpha]_D^{20}$  (*c* 0.93, CH<sub>2</sub>Cl<sub>2</sub>) =  $-126^\circ$ . <sup>1</sup>H NMR (499.9 MHz, CDCl<sub>3</sub>, 25 °C)  $\delta$  8.04 (d, *J* = 7.5 Hz, 1H, Np), 7.84 (d, *J* = 8.0 Hz, 2H, Np), 7.80 (d, *J* = 8.5 Hz, 1H, Np), 7.49 (pst, *J* = 7.5 Hz, 1H, Np), 7.44 (pst, *J* = 7.0 Hz, 1H, Np), 7.37 (pst, *J* = 7.5 Hz, 1H, Np), 4.61 (dd, <sup>3/4</sup>*J* = 2.5, 1.0 Hz, <sup>4</sup>*J*(<sup>117/119</sup>Sn,H) = 7.0 Hz, 1H, Cp-3), 4.57 (pst, <sup>3</sup>*J* = 2.5 Hz, 1H, <sup>4</sup>*J*(<sup>117/119</sup>Sn,H) = 6.0 Hz, Cp-4), 4.30 (dd, <sup>3/4</sup>*J* = 2.5, 1.0 Hz, <sup>3</sup>*J*(<sup>117/119</sup>Sn,H) = 10.0 Hz, 1H, Cp-5), 4.29 (s, 5H,

C<sub>5</sub>H<sub>5</sub>),  $-0.07$  (s/d,  $^2J(^{117/119}\text{Sn},\text{H}) = 53/55$  Hz, 9H, SnMe<sub>3</sub>);  $^{13}\text{C}$  NMR (125.7 MHz, CDCl<sub>3</sub>, 25 °C)  $\delta$  137.0, 133.8, 133.4, 129.4, 128.2, 127.4, 126.7, 125.7, 125.7, 125.1 (Np), 96.0 (*ipso*-CpNp), 74.4 (s/d,  $^2J(^{117/119}\text{Sn},\text{C}) = 50$  Hz, Cp-5), 74.3 (s/d,  $^3J(^{117/119}\text{Sn},\text{C}) = 35$  Hz, Cp-4), 73.0 (*ipso*-CpSn), 70.4 (s/d,  $^3J(^{117/119}\text{Sn},\text{C}) = 40$  Hz, Cp-3), 69.4 (C<sub>5</sub>H<sub>5</sub>),  $-8.0$  (s/d,  $^1J(^{117/119}\text{Sn},\text{C}) = 343/360$  Hz, SnMe<sub>3</sub>);  $^{119}\text{Sn}$  NMR (186.4 MHz, CDCl<sub>3</sub>, 25 °C)  $\delta$   $-7.1$ ; GC-MS (m/z, (%)): 476 [M<sup>+</sup>] (76), 461 [M<sup>+</sup>-Me] (100), 431 [M<sup>+</sup>-3Me] (71). UV-Vis (CH<sub>2</sub>Cl<sub>2</sub>,  $2.35 \times 10^{-3}$  M):  $\lambda_{\text{max}} = 448$  nm ( $\varepsilon = 255$ ). CV (CH<sub>2</sub>Cl<sub>2</sub>,  $1.0 \times 10^{-3}$  M):  $E_{1/2} = 6$  mV ( $\Delta E_p = 142$  mV). Elemental analysis for C<sub>23</sub>H<sub>24</sub>FeSn, calcd. C 58.16, H 5.09, found C 58.04, H 5.05%.

**Synthesis of (S<sub>p</sub>)-2-(1-Naphthyl)-1-(chloromercurio)ferrocene (2).** A solution of (S<sub>p</sub>)-2-(1-naphthyl)-1-(trimethylstannyl)ferrocene (175 mg, 0.368 mmol) in acetone (10 mL) was added dropwise to a solution of HgCl<sub>2</sub> (100 mg, 0.368 mmol) in acetone (15 mL). The mixture was stirred for 30 minutes before adding it to water. A yellow solid precipitated, which was collected on a frit and washed first with water and then with hexanes. The product was dried under high vacuum at 60 °C for 6 h. Yield: 169 mg (84%).  $[\alpha]_{\text{D}}^{20}$  (*c* 0.93, CH<sub>2</sub>Cl<sub>2</sub>) =  $-103^\circ$ .  $^1\text{H}$  NMR (499.9 MHz, CDCl<sub>3</sub>, 25 °C)  $\delta$  8.06-8.04 (m, 2H, Np), 7.87 (d,  $J = 7.5$  Hz, 1H, Np), 7.83 (d,  $J = 8.5$  Hz, 1H, Np), 7.52 (pst,  $J = 7.5$  Hz, 1H, Np), 7.47 (pst,  $J = 7.5$  Hz, 1H, Np), 7.43 (pst,  $J = 7.5$  Hz, 1H, Np), 4.82 (dd,  $J = 2.5, 1.0$  Hz, 1H, Cp-3), 4.64 (pst,  $J = 2.5$  Hz, 1H, Cp-4), 4.33 (s, 5H, C<sub>5</sub>H<sub>5</sub>), 4.30 (dd,  $J = 2.5, 1.0$  Hz, 1H, Cp-5).  $^{13}\text{C}$  NMR (125.7 MHz, CDCl<sub>3</sub>, 25 °C)  $\delta$  136.7, 133.8, 133.0, 128.8, 128.6, 128.1, 126.3, 126.2, 125.7, 125.6 (Np), 92.4 (*ipso*-Cp), 90.6 (*ipso*-Cp), 73.1 (Cp), 72.7 (Cp), 70.6 (Cp), 70.2 (C<sub>5</sub>H<sub>5</sub>). UV-Vis (CH<sub>2</sub>Cl<sub>2</sub>,  $2.27 \times 10^{-3}$  M):  $\lambda_{\text{max}}$

= 451 nm ( $\epsilon = 294$ ). CV ( $\text{CH}_2\text{Cl}_2$ ,  $1.0 \times 10^{-3}$  M):  $E_{1/2} = 127$  mV ( $\Delta E_p = 153$  mV). Elemental analysis for  $\text{C}_{20}\text{H}_{15}\text{FeHgCl}$ , calcd. C 43.90, H 2.76, found C 44.19, H 2.65%.

**NMR Scale Reaction of 1 with  $\text{BBr}_3$ .** To a solution of **1** (10.2 mg, 21.5  $\mu\text{mol}$ ) in  $\text{CDCl}_3$  (0.8 mL) was added a solution of  $\text{BBr}_3$  (5.4 mg, 21.6  $\mu\text{mol}$ ) in  $\text{CDCl}_3$  (0.2 mL) at  $-35$  °C. The mixture was stirred for 30 minutes. The ratio of the 1,1'- to 1,3-isomers was determined according to  $^1\text{H}$  NMR integration of the Cp resonances to ca. 57:43. NMR data for the mixture:  $^1\text{H}$  NMR (499.9 MHz,  $\text{CDCl}_3$ , 25 °C) Np region:  $\delta$  8.44 (d,  $J = 7.5$  Hz, Np), 8.35 (d,  $J = 7.0$  Hz, Np), 8.1-7.8 (m, Np), 7.6-7.4 (m, Np), 0.78 (s,  $\text{Me}_3\text{SnBr}$ ); Cp region of 1,1'-isomer  $\delta$  4.86 (pst,  $J = 1.8$  Hz, 2H, Cp-H), 4.76 (pst,  $J = 1.8$  Hz, 2H, Cp-H), 4.62 (pst,  $J = 1.8$  Hz, 2H, Cp-H), 4.49 (pst,  $J = 1.8$  Hz, 2H, Cp-H); Cp region of 1,3-isomer:  $\delta$  5.42 (dd,  $J = 2.5, 1.5$  Hz, 1H, Cp-H4/5), 5.05 (pst,  $J = 1.5$  Hz, 1H, Cp-H2), 4.79 (dd,  $J = 2.5, 1.5$  Hz, 1H, Cp-H4/5), 4.28 (s, 5H,  $\text{C}_5\text{H}_5$ ).  $^{11}\text{B}$  NMR (160.4 MHz,  $\text{C}_6\text{D}_6$ , 25 °C)  $\delta$  47.2.

**Synthesis of 3:** To a suspension of ( $S_p$ )-2-(1-naphthyl)-1-(chloromercurio)ferrocene (**2**) (0.56 g, 0.118 mmol) in hexane (30 mL) at  $-30$  °C was added  $\text{BCl}_3$  (1.24 mL, 1 M solution in hexane) inside a glove box. The reaction mixture was stirred for 2 h. The color of the solution turned orange and a grey solid formed, which was removed by filtration. The filtrate was kept at  $-37$  °C for two days to give an orange crystalline solid. The product was recrystallized once more from warm hexane. A second fraction was obtained upon concentration of the combined mother liquors. Isolated yield: 380 mg (82 %);  $^1\text{H}$  NMR (499.9 MHz,  $\text{C}_6\text{D}_6$ , 25 °C):  $\delta$  7.94 (br d,  $J=7.0$  Hz, 1 H; Np), 7.74 (br d,  $J=6.5$  Hz, 1 H; Np), 7.69–7.65 (m, 2 H; Np), 7.37 (br pst,  $J=6.5$  Hz, 1 H; Np), 7.21 (br pst,  $J=8.0$  Hz, 1 H; Np), 7.14 (br s, 1 H; Np), 4.63 (dd,  $J=2.5, 1.0$  Hz, 1 H; Cp-3/5), 4.57 (br s, 1 H;

Cp-3/5), 4.38 (br pst, 1 H; Cp-4), 4.02 ppm (s, 5 H; free Cp);  $^{13}\text{C}$  NMR (125.69 MHz,  $\text{CDCl}_3$ , 25 °C):  $\delta$ =135.2, 134.1, 133.3, 128.4, 128.3, 128.0, 126.2, 125.9 (2 signals), 125.2 (Np), 97.9, 82.9, 77.3, 75.4, (substituted Cp), 72.6 ppm ( $\text{C}_5\text{H}_5$ ) (the *ipso*-Cp-B signal was not observed);  $^{11}\text{B}$  NMR (160.4 MHz,  $\text{C}_6\text{D}_6$ , 25 °C):  $\delta$ =49.4 ppm ( $w_{1/2}$ =350 Hz); UV/Vis ( $\text{CH}_2\text{Cl}_2$ ,  $1.00\times 10^{-3}$  M):  $\lambda_{\text{max}}$ =455 nm ( $\epsilon$ =1120); MALDI-TOF (+ reflector mode, benzopyrene/pyridine)  $m/z$ : calcd for  $\text{C}_{20}\text{H}_{15}\text{BCl}_2\text{Fe}$ : 391.9993; found: 392.0023; elemental analysis calcd (%) for  $\text{C}_{20}\text{H}_{15}\text{BCl}_2\text{Fe}$ : C 61.14, H 3.85; found C 61.30, H 3.49.

**Synthesis of 4:** A precooled solution of  $[\text{C}_6\text{F}_5\text{Cu}]_4$  (18 mg, 20  $\mu\text{mol}$ ) in toluene (3 mL,  $-37$  °C) was added dropwise to a precooled solution of **3** (31 mg, 79  $\mu\text{mol}$ ) in toluene (5 mL,  $-37$  °C) under stirring. The reaction mixture was stirred for 3 h at RT and then filtered. All volatile components were removed under high vacuum. The crude product was purified by recrystallization from hexane at  $-37$  °C to give a dark red microcrystalline solid. Isolated yield: 39 mg (80 %);  $^1\text{H}$  NMR (499.9 MHz,  $\text{CDCl}_3$ , 25 °C):  $\delta$ =7.71 (d,  $J$ =8.5 Hz, 1 H; Np), 7.66 (d,  $J$ =8.5 Hz, 2 H; Np), 7.47 (br s, 1 H; Np), 7.39 (t,  $J$ =7.1 Hz, 1 H; Np), 7.31 (m,  $J$ =7.5 Hz, 2 H; Np), 5.15 (pst,  $J$ =2.5 Hz, 1 H; Cp), 5.02 (br, 1 H; Cp), 4.9 (br, 1 H; Cp), 4.53 ppm (s, 5 H; free Cp);  $^{13}\text{C}$  NMR (125.69 MHz,  $\text{CDCl}_3$ , 25 °C):  $\delta$ =150–130 (*ortho*-, *meta*-, *para*- $\text{C}_6\text{F}_5$  signals are broad and not resolved), 115.1 (br, *ipso*- $\text{C}_6\text{F}_5$ ), 132.5, 129.1, 127.6, 127.5, 125.8, 125.7, 124.2, 98.1 (*ipso*-Cp-B), 77.7 (Cp), 81.5 (Cp), 75.9 (br, Cp), 71.7 ppm ( $\text{C}_5\text{H}_5$ );  $^{11}\text{B}$  NMR (160.4 MHz,  $\text{C}_6\text{D}_6$ , 25 °C):  $\delta$ =55.3 ppm ( $w_{1/2}$ =500 Hz);  $^{19}\text{F}$  NMR (470.4 MHz,  $\text{CDCl}_3$ , 25 °C):  $\delta$ =-130 (2 F; *ortho*-F), -154.1 (1 F; *para*-F), -162.7 ppm (2 F; *meta*-F); UV/Vis ( $\text{CH}_2\text{Cl}_2$ ,  $1.00\times 10^{-3}$  M):  $\lambda_{\text{max}}$ =475 nm ( $\epsilon$ =1280); elemental analysis calcd (%) for  $\text{C}_{26}\text{H}_{15}\text{BClF}_5\text{Fe}$ : C 59.54, H 2.88; found C 59.41, H 2.88.

**Synthesis of 5:** A solution of  $[\text{C}_6\text{F}_5\text{Cu}]_4$  (117 mg, 127  $\mu\text{mol}$ ) in toluene (5 mL) was added dropwise at RT to a solution of **3** (100 mg, 255  $\mu\text{mol}$ ) in toluene (5 mL) under stirring. The mixture was stirred for 3 h at 80 °C and then cooled to RT and filtered. All volatile components were removed under high vacuum. The crude product was purified by repeated recrystallization from hot hexane to give a dark red microcrystalline solid. Isolated yield: 140 mg (84 %);  $[\alpha]_{\text{D}}^{20}$  ( $c=0.072$ , hexane) =  $-132^\circ$ ;  $^1\text{H}$  NMR (499.9 MHz,  $\text{CDCl}_3$ , 25 °C):  $\delta=7.71$  (d,  $J=6.5$  Hz, 1 H; Np), 7.62 (m, 2 H; Np), 7.53 (d,  $J=8.5$  Hz, 1 H; Np), 7.40–7.25 (m, 3 H; Np), 5.28 (pst,  $J=2.5$  Hz, 1 H; Cp-4), 5.26 (dd,  $J=2.5, 1.0$  Hz, 1 H; Cp-5), 4.61 (s, 5 H; free Cp), 4.17 (br s, 1 H; Cp-3), 2.0–0.8 ppm (ca. 10 H; hexane);  $^{13}\text{C}$  NMR (125.69 MHz,  $\text{CDCl}_3$ , 25 °C):  $\delta=150$ – $130$  (*ortho*-, *meta*-, *para*- $\text{C}_6\text{F}_5$  signals are broad and not resolved), 115.1 (br, *ipso*- $\text{C}_6\text{F}_5$ ), 133.4, 133.3, 132.4, 129.4, 127.8, 127.4, 126.1, 126.0, 125.8, 124.6 (Np), 100.0 (*ipso*-CpC), 83.3 (*ipso*-Cp-B), 77.7 (Cp), 77.5 (Cp), 75.8 (br, Cp), 71.6 ppm ( $\text{C}_5\text{H}_5$ );  $^{11}\text{B}$  NMR (160.4 MHz,  $\text{C}_6\text{D}_6$ , 25 °C):  $\delta=54$  ppm ( $w_{1/2}=900$  Hz);  $^{19}\text{F}$  NMR (470.4 MHz,  $\text{CDCl}_3$ , 25 °C):  $\delta=-127.5$  (br, 1 F; *ortho*- $\text{F}_{\text{A}2}$ ),  $-132.8$  (br, 1 F; *ortho*- $\text{F}_{\text{A}6}$ ),  $-128.7$  (br, 2 F; *ortho*- $\text{F}_{\text{B}3,5}$ ),  $-151.8$  (br, 1 F; *para*- $\text{F}_{\text{A}4}$ ),  $-156.5$  (br, 1 F, *para*- $\text{F}_{\text{B}4}$ ),  $-161.5$  (br, 2 F; *meta*- $\text{F}_{\text{B}3,5}$ ),  $-163.3$  (pst, 1 F; *meta*- $\text{F}_{\text{A}5}$ ),  $-163.8$  ppm (pst, 1 F; *meta*- $\text{F}_{\text{A}3}$ ).  $^{19}\text{F}$  NMR (470.4 MHz,  $\text{CDCl}_3$ ,  $-60^\circ\text{C}$ ):  $\delta=-128.0$  (d,  $J(\text{F},\text{F})=23$  Hz, 1 F; *ortho*- $\text{F}_{\text{A}2}$ ),  $-133.1$  (d,  $J(\text{F},\text{F})=24$  Hz, 1 F; *ortho*- $\text{F}_{\text{A}6}$ ),  $-126.7$ ,  $-130.1$  (very br, *ortho*- $\text{F}_{\text{B}3,5}$ ),  $-150.9$  (t,  $J(\text{F},\text{F})=18$  Hz, 1 F; *para*- $\text{F}_{\text{B}4}$ ),  $-156.4$  (t,  $J(\text{F},\text{F})=21$  Hz, 1 F; *para*- $\text{F}_{\text{A}4}$ ),  $-160.7$  (br, 2 F; *meta*- $\text{F}_{\text{B}3,5}$ ),  $-162.9$  (pst, 1 F; *meta*- $\text{F}_{\text{A}5}$ ),  $-163.8$  ppm (pst, 1 F; *meta*- $\text{F}_{\text{A}3}$ ); UV/Vis ( $\text{CH}_2\text{Cl}_2$ ,  $1.00 \times 10^{-3}$  M):  $\lambda_{\text{max}}=491$  nm ( $\epsilon=1680$ ); CV ( $\text{CH}_2\text{Cl}_2$ ,  $1.9 \times 10^{-3}$  M):  $E_{1/2}=460$  mV ( $\Delta E_{\text{p}}=214$  mV); CV of complex with pyridine ( $\text{CH}_2\text{Cl}_2$ ,

$1.9 \times 10^{-3}$  M):  $E_{1/2} = 93$  mV ( $\Delta E_p = 98$  mV); high-resolution MALDI-TOF (+ mode, benzopyrene/picoline)  $m/z$ : calcd for  $C_{32}H_{15}BF_{10}Fe$ : 656.0457; found: 656.0455.

## 2.5 Supporting Information

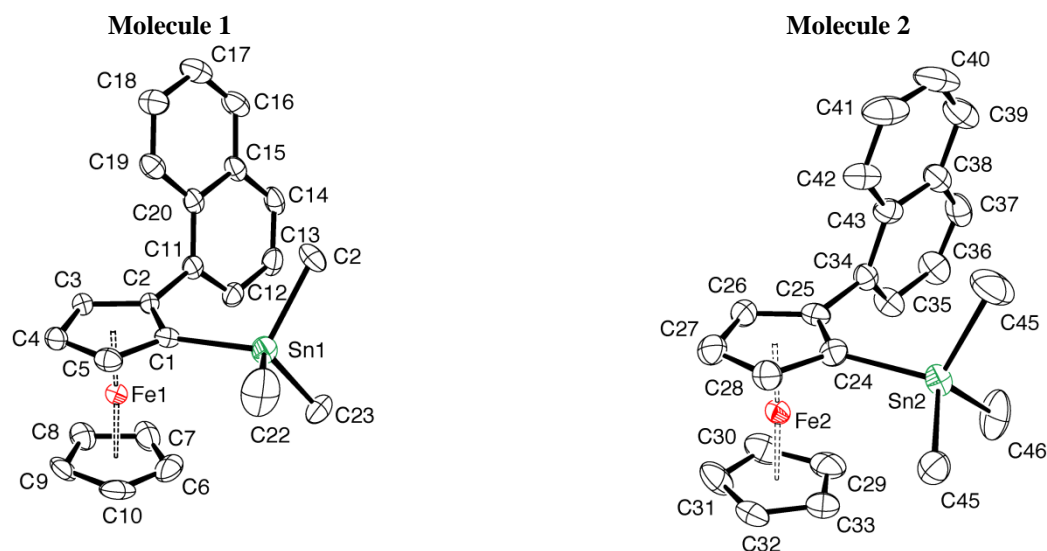


**Figure 2-10.** Ortep plot of **1** with thermal ellipsoids at the 50% probability level; hydrogen atoms are omitted for clarity.

**Molecule 1:** Sn(1)-C(1) 2.135(3), Sn(1)-C(21) 2.144(3), Sn(1)-C(22) 2.138(4), Sn(1)-C(23) 2.148(4), C(2)-C(11) 1.488(4), C(1)-Sn(1)-C(22) 106.51(15), C(1)-Sn(1)-C(21) 109.07(13), C(22)-Sn(1)-C(21) 111.67(19), C(1)-Sn(1)-C(23) 113.37(14), C(22)-Sn(1)-C(23) 110.92(18), C(21)-Sn(1)-C(23) 105.39(15). **Molecule 2:** Sn(2)-C(24) 2.136(3), Sn(2)-C(44) 2.151(4), Sn(2)-C(45) 2.140(4), Sn(2)-C(46) 2.139(4), C(25)-C(34) 1.494(5), C(24)-Sn(2)-C(46) 110.26(15), C(24)-Sn(2)-C(45) 108.56(13), C(46)-Sn(2)-C(45) 108.74(17), C(24)-Sn(2)-C(44) 109.77(16), C(46)-Sn(2)-C(44) 109.8(2), C(45)-Sn(2)-C(44) 109.67(19).

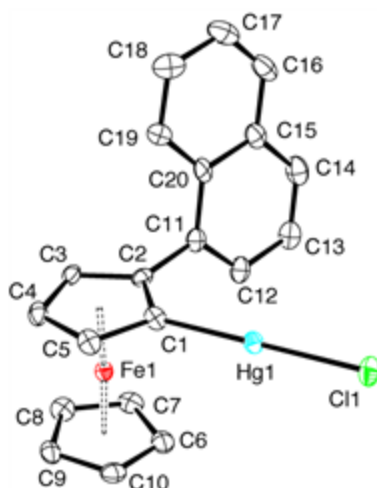


**Figure 2-11.** Ortep plot of **2** with thermal ellipsoids at the 50% probability level; hydrogen atoms are omitted for clarity. Selected interatomic distances (Å) and angles (°): Hg(1)-C(1), 2.024(5), Hg(1)-Cl(1) 2.3120(12), C(2)-C(11) 1.489(7), C(1)-Hg(1)-Cl(1) 179.02(14).

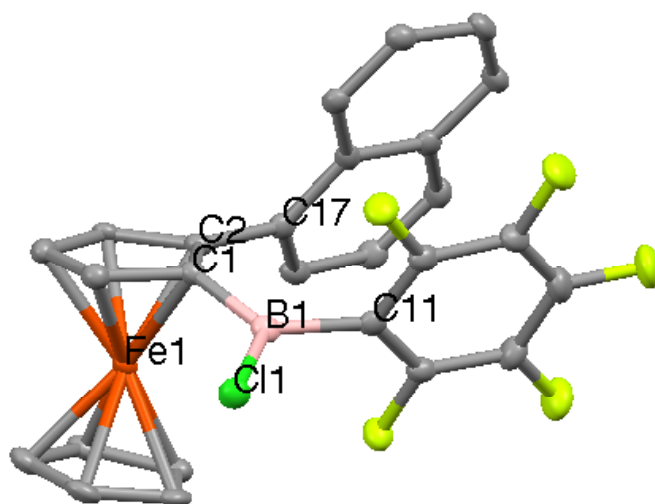


**Figure 2-12.** Ortep plot of **4** with thermal ellipsoids at the 50% probability level; hydrogen atoms are omitted for clarity. Selected interatomic distances (Å) and angles (°): B(1)-C(1) 1.511(3), B(1)-C(11) 1.587(4), B(1)-Cl(1) 1.787(3), C(1)-B(1)-C(11) 123.9(2), C(1)-B(1)-Cl(1) 119.5(2), C(11)-B(1)-Cl(1) 115.95(18); Cp//Cp 7.0, Cp//Np 59.2, C<sub>6</sub>F<sub>5</sub>//Np 14.7.

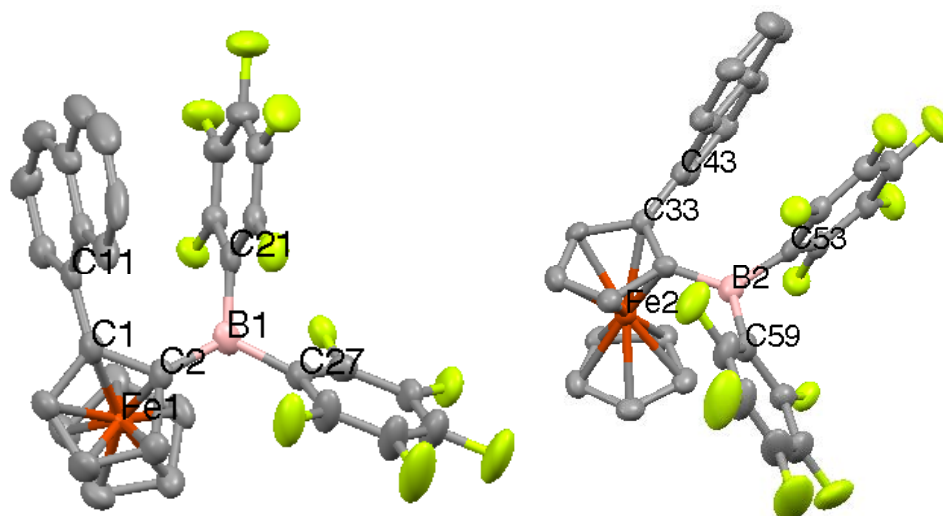


**Figure 2-13.** Ortep plots of two independent molecules of **5** with thermal ellipsoids at the 50% probability level; hydrogen atoms are omitted for clarity. Selected interatomic distances (Å) and angles (°):

Molecule 1: B(1)-C(2) 1.521(6), B(1)-C(21) 1.598(7), B(1)-C(27) 1.578(7), C(1)-C(2) 1.468(6), C(2)-B(1)-C(27) 123.0(4), C(2)-B(1)-C(21) 122.2(4), C(27)-B(1)-C(21) 114.3(4); Cp//Cp 7.6, Cp//Np 65.1, C<sub>6</sub>F<sub>5</sub>//Np 7.6. Molecule 2: B(2)-C(34) 1.501(6), B(2)-C(53) 1.595(6), B(2)-C(59) 1.581(6), C(33)-C(34) 1.484(6), C(34)-B(2)-C(59) 121.5(4), C(34)-B(2)-C(53) 122.2(4), C(59)-B(2)-C(53) 115.6(4); Cp//Cp 7.8, Cp//Np 62.4, C<sub>6</sub>F<sub>5</sub>//Np 12.3.

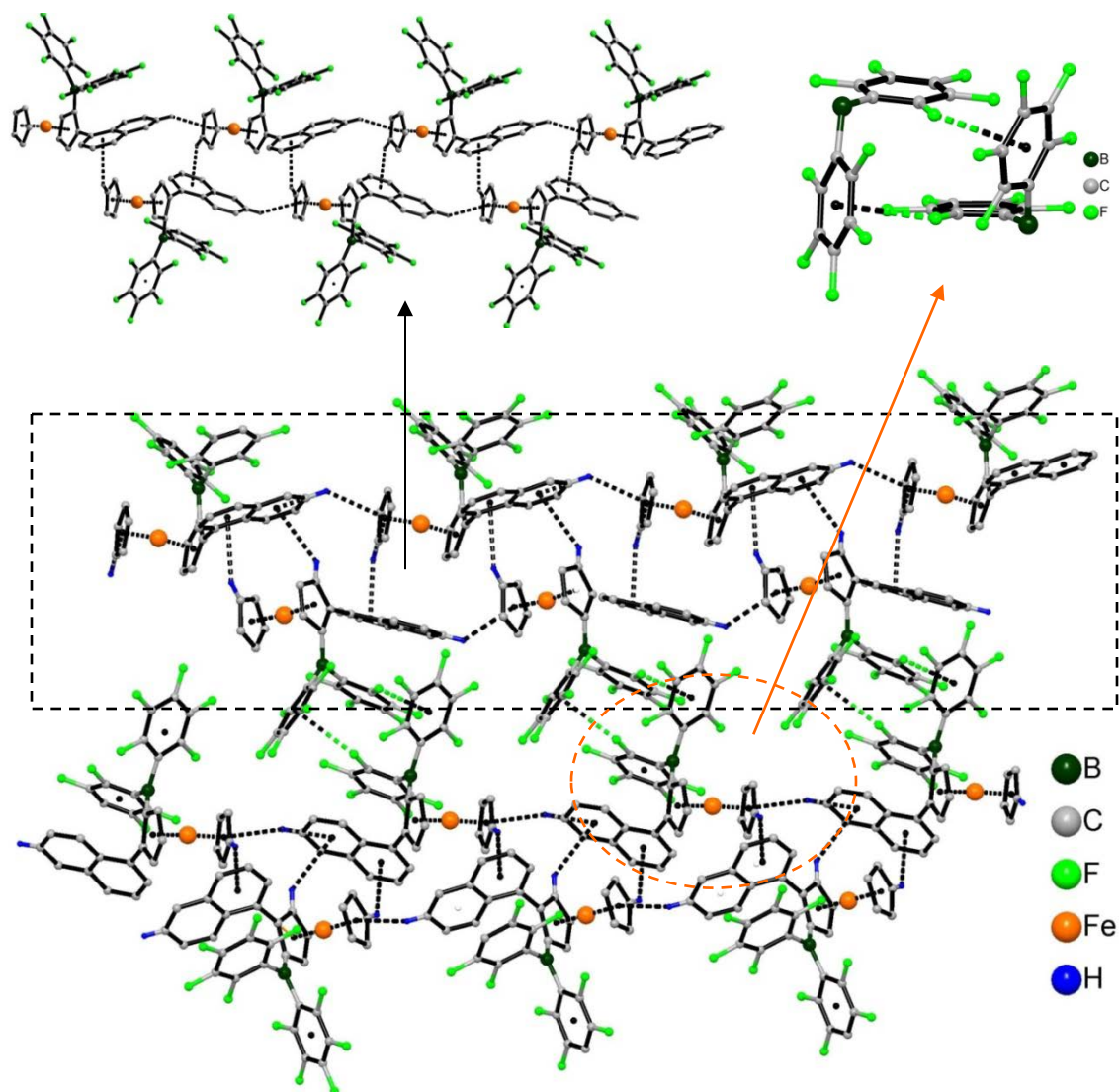


**Figure 2-14.** Supramolecular Structure of **5**.

Two crystallographically independent molecules in the asymmetric unit of **5** generate two different 1D helical chains via intermolecular C-H $\cdots$  $\pi$  (C17-H17 $\cdots$  $\pi_{Cp}$  = 2.968 Å and C49-H49 $\cdots$  $\pi_{Cp}$  = 2.880 Å) interactions between the ferrocene and naphthyl moieties. Further, an intermolecular C-H $\cdots$  $\pi$  interaction (C9-H9 $\cdots$  $\pi_{Np}$  = 2.994 Å and C39-H39 $\cdots$  $\pi_{Np}$  = 2.673 Å) between the aforementioned chains leads to a double helical structure. Each double helical chain interacts with two neighbouring chains via intermolecular C-F $\cdots$  $\pi$  interaction (C15-F15 $\cdots$  $\pi_{Pf}$  = 3.298 Å and C5-F5 $\cdots$  $\pi_{Pf}$  = 3.205 Å). These interactions generate an interesting supramolecular “diboracyclophane” and the propagation of these interactions leads to the formation of a 2D helical layer structure. The C-H $\cdots$ F interactions between the adjacent layers generate a 3D structure

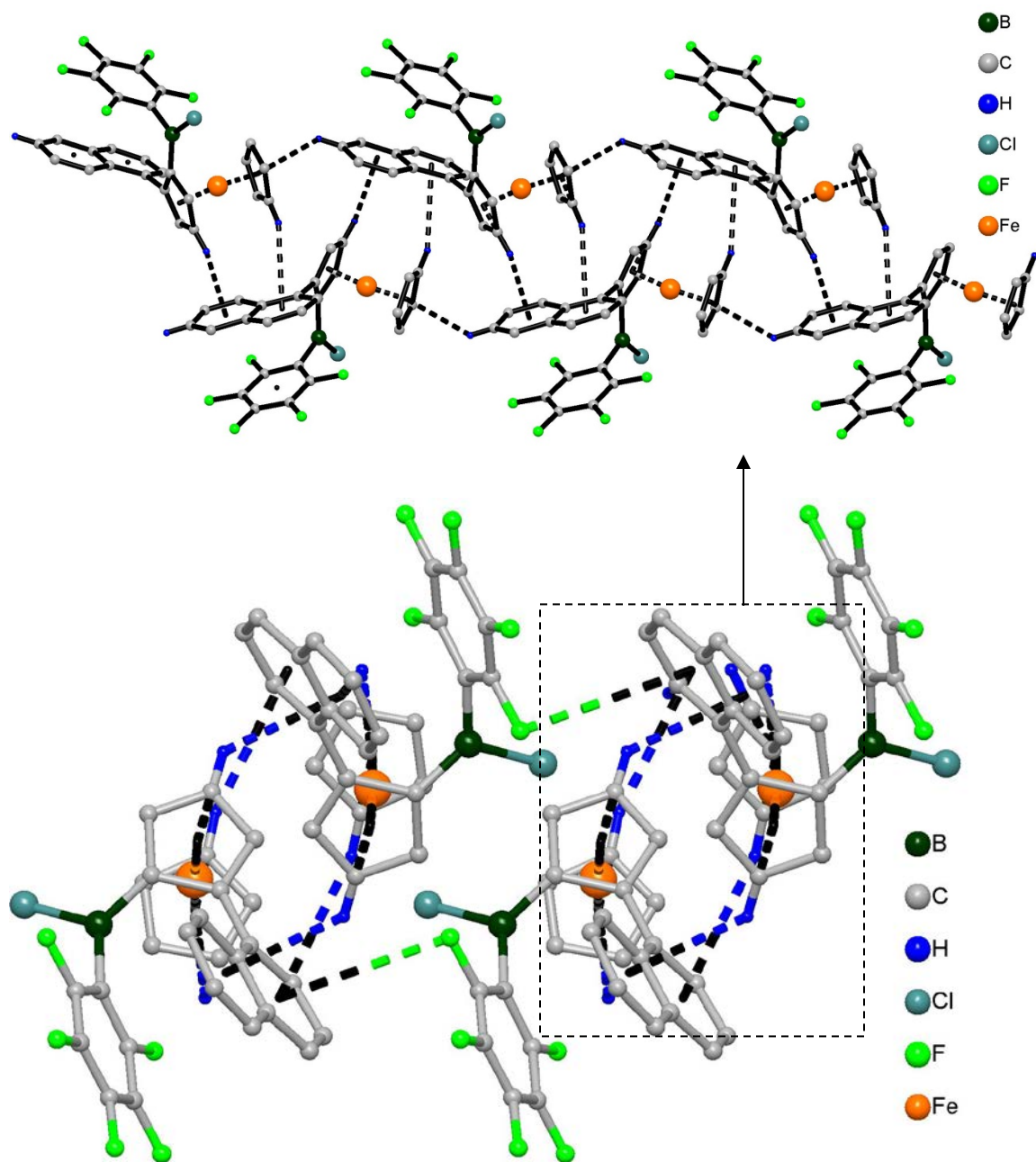


**Figure 2-15.** Intermolecular Interactions in **4**.

A similar supramolecular structure is found as described above for compounds **5**.

**Table 2-2.** Details of X-ray crystal structure analyses of complexes **1**, **2**, **4** and **5**.

Compound	<b>1</b>	<b>2</b>	<b>4</b>	<b>5</b>
empirical formula	C <sub>23</sub> H <sub>24</sub> FeSn	C <sub>20</sub> H <sub>15</sub> ClFeHg	C <sub>26</sub> H <sub>15</sub> BClF <sub>5</sub> Fe	C <sub>32</sub> H <sub>15</sub> BF <sub>10</sub> Fe
MW	474.96	547.21	524.49	656.10
<i>T</i> , K	150(2)	100(2)	100(2)	100(2)
wavelength, Å	1.54178	1.54178	1.54178	0.71073
crystal system	orthorhombic	orthorhombic	Monoclinic	orthorhombic
space group	P2(1)2(1)2(1)	P2(1)2(1)2(1)	P2(1)	P2(1)2(1)2(1)
<i>a</i> , Å	8.7231(2)	7.25690(10)	8.43570(10)	11.7701(14)
<i>b</i> , Å	21.0504(5)	9.7632(2)	11.5784(2)	19.122(2)
<i>c</i> , Å	21.7724(5)	23.4370(5)	10.90310(10)	29.002(3)
<i>V</i> , Å <sup>3</sup>	3997.95(16)	1660.52(5)	1060.94(2)	6527.4(13)
<i>Z</i>	8	4	2	8
$\rho_{\text{calc}}$ , g cm <sup>-3</sup>	1.578	2.189	1.642	1.335
$\mu$ (Mo/Cu K $\alpha$ ), mm <sup>-1</sup>	15.745	24.775	7.374	4.401
Crystal size, mm	0.23 x 0.10 x 0.09	0.07 x 0.06 x 0.06	0.24 x 0.21 x 0.16	0.34 x 0.34 x 0.28
$\theta$ range, deg	2.92-64.58	4.91-64.80	4.07-67.87	3.83-68.13
limiting indices	-8<= <i>h</i> <=9 -24<= <i>k</i> <=20 -25<= <i>l</i> <=16	-8<= <i>h</i> <=8 -11<= <i>k</i> <=11 -24<= <i>l</i> <=26	-10<= <i>h</i> <=10 -13<= <i>k</i> <=13 -13<= <i>l</i> <=12	-14<= <i>h</i> <=14 -22<= <i>k</i> <=22 -32<= <i>l</i> <=34
reflns collected	19883	9462	8093	44303
independent reflns	6222 [ <i>R</i> (int) = 0.0318]	2741 [ <i>R</i> (int) = 0.0291]	3146 [ <i>R</i> (int) = 0.0415]	11627 [ <i>R</i> (int) = 0.1206]
Absorption correction	SADABS	SADABS	Numerical	Numerical
data/restraints/ parameters	6222 / 0 / 458	2741 / 0 / 209	3146 / 1 / 308	11627 / 0 / 794
goodness-of-fit on <i>F</i> <sup>2</sup>	0.891	1.045	1.033	0.983
final <i>R</i> indices [ <i>I</i> > 2 $\sigma$ ( <i>I</i> )] <sup>[a]</sup>	<i>R</i> 1 = 0.0219 <i>wR</i> 2 = 0.0478	<i>R</i> 1 = 0.0179 <i>wR</i> 2 = 0.0382	<i>R</i> 1 = 0.0285 <i>wR</i> 2 = 0.0678	<i>R</i> 1 = 0.0536 <i>wR</i> 2 = 0.1264
<i>R</i> indices (all data) <sup>[a]</sup>	<i>R</i> 1 = 0.0243 <i>wR</i> 2 = 0.0486	<i>R</i> 1 = 0.0191 <i>wR</i> 2 = 0.0386	<i>R</i> 1 = 0.0315 <i>wR</i> 2 = 0.0695	<i>R</i> 1 = 0.0774 <i>wR</i> 2 = 0.1430
Peak <sub>max</sub> /hole <sub>min</sub> (e Å <sup>-3</sup> )	0.734 / -0.284	1.096 / -0.560	0.263 and -0.209	0.454 / -0.413
Absolute structure parameter	0.006(4)	0.033(8)	0.019(4)	0.016(4)

$$[a] R1 = \Sigma||F_o| - |F_c|| / \Sigma|F_o|; wR2 = \{ \Sigma[w(F_o^2 - F_c^2)^2] / \Sigma[w(F_o^2)^2] \}^{1/2}.$$

**Table 2-3.** Coalescence temperatures from analysis of VT NMR data for compounds **4** and **5**.

<b>NpFcBCIPf (4)</b>						
<b>Major</b>	<b>o-F</b>			<b>m-F</b>		
<b>(4A)</b>	T <sub>c</sub> (K)	(ppm)	G <sup>‡</sup> (kJ/mol)	T <sub>c</sub> (K)	(ppm)	G <sup>‡</sup> (kJ/mol)
	257	0.38	49.7±0.7	265	0.72	50.0±0.6
<b>Minor</b>	<b>o-F</b>			<b>m-F</b>		
<b>(4B)</b>	T <sub>c</sub> (K)	(ppm)	G <sup>‡</sup> (kJ/mol)	T <sub>c</sub> (K)	(ppm)	G <sup>‡</sup> (kJ/mol)
	248	2.5	44.1±0.6	220	0.23	43±2

<b>NpFcBPf2 (5)</b>						
<b>o-F</b>			<b>m-F</b>			
<b>(ring B)</b>			<b>(ring A)</b>			
T <sub>c</sub> (K)	(ppm)	G <sup>‡</sup> (kJ/mol)	T <sub>c</sub> (K)	(ppm)	G <sup>‡</sup> (kJ/mol)	
228	3.334	39.8±0.6	308	0.85	58±2	

The approximation  $\Delta G^{\ddagger} = 19.1 T_c [9.97 + \lg(T_c \Delta \nu^{-1})]$  for estimation of  $\Delta G^{\ddagger}$  at T<sub>c</sub> was used; see: M. Hesse, H. Meier, B. Zeeh, Spectroscopic Methods in Organic Chemistry, Thieme, Stuttgart, 1997.

**Table 2-4.** Line shape analysis results from VT NMR data of compounds **4** and **5**.<sup>[a]</sup>

<b>NpFcBCIPf (4)</b>	<b>4A</b>	<b>4B</b>	<b>Isomer 4A</b>	<b>Isomer 4B</b>
	<b>p-F</b>	<b>p-F</b>	<b>m-F</b>	<b>o-F</b>
H <sup>‡</sup> (kJ/mol)	37.1(6)	37.0(3)	22.1(6)	34(1)
S <sup>‡</sup> (J/mol*K)	-45.5(8)	-36.9(3)	-110(3)	-41(2)
G <sub>298</sub> <sup>‡</sup> (kJ/mol)	50.6(4)	48.0(3)	55.0(4)	45.9(8)

<b>NpFcBPf2 (5)</b>	<b>A/B Exchange</b>	<b>Ring A</b>	<b>Ring A</b>
	<b>p-F</b>	<b>o-F</b>	<b>m-F</b>
H <sup>‡</sup> (kJ/mol)	52.5(7)	47.7(13)	30(1)
S <sup>‡</sup> (J/mol*K)	-19.4(3)	-33.4(10)	-97(4)
G <sub>298</sub> <sup>‡</sup> (kJ/mol)	58.3(6)	57.6(10)	58.9(1)
G <sub>222</sub> <sup>‡</sup> (kJ/mol)	56.9(5)	55.3(8)	52.2(1)

[a] Data from line shape analysis using the program DNMR. Error calculations for  $\Delta G^\ddagger$  are based on the covariance relationship between  $\Delta H^\ddagger$  and  $\Delta S^\ddagger$  (see J. Sandström, *Dynamic NMR Spectroscopy*, Academic Press, New York, 1982, p 118).

## 2.6 Notes and References

- (a) Yamamoto, E. H., *Lewis Acids in Organic Synthesis*. Wiley-VCH: New York, 2000; (b) Piers, W. E.; Irvine, G. J.; Williams, V. C., *Eur. J. Inorg. Chem.* **2000**, 2131-2142; (c) Chen, E. Y.-X.; Marks, T. J., *Chem. Rev.* **2000**, *100*, 1391-1434; (d) Piers, W. E., *Adv. Organomet. Chem.* **2005**, *52*, 1-76.
- (a) Ishihara, K., Chiral B(III) Lewis Acids. In *Lewis Acids in Organic Synthesis*, Yamamoto, H., Ed. Wiley VCh: Weinheim, New York, Chichester, Brisbane, Singapore, Toronto, 2000; Vol. 1, pp 135-190; (b) Brown, H. C.; Ramachandran, P. V., *J. Organomet. Chem.* **1995**, *500*, 1-19; (c) Dhokte, U. P.; Soundararajan, R.; Ramachandran, P. V.; Brown, H. C., *Tetrahedron Lett.* **1996**, *37*, 8345-8348; (d) Dhotke, U. P.; Brown, H. C., *Organometallics* **1998**, *17*, 2891-2896; (e) Hawkins, J. M.; Loren, S.; Nambu, M., *J. Am. Chem. Soc.* **1994**, *116*, 1657-1660; (f) Hawkins, J. M.; Nambu, M.; Loren, S., *Org. Lett.* **2003**, *5*, 4293-4295; (g) Schilling, B.; Kaiser, V.; Kaufmann, D. E., *Chem. Ber.* **1997**, *130*, 923-932; (h) Bir, G.; Ernst, C.; Gross, U. M.; Rehwinkel, C.; Schilling, B.; Thormeier, S.; Kaiser, V.; Kaufmann, D., *Spec. Publ. - R. Soc. Chem.* **1997**, *201*, 193-200; (i) Schilling, B.; Kaufmann, D. E., *Eur. J. Org. Chem.* **1998**, 701-709; (j) Ishihara, K.; Inanaga, K.; Kondo, S.; Funahashi, M.; Yamamoto, H., *Synlett* **1998**, 1053; (k) Morrison, D. J.; Piers, W. E.; Parvez, M., *Synlett* **2004**, 2429-2433; (l) Bir, G.; Kaufmann, D., *Tetrahedron Lett.* **1987**, *28*, 777-80; (m) Kaufmann, D.; Boese, R., *Angew. Chem.* **1990**, *102*, 568-9; (n) Reilly, M.; Oh, T., *Tetrahedron Lett.* **1994**, *35*, 7209-12; (o) Ishihara, K.; Kurihara, H.; Matsumoto, M.; Yamamoto, H., *J. Am. Chem. Soc.* **1998**, *120*, 6920-6930; (p) Ishihara, K.; Yamamoto, H., *Eur. J. Org. Chem.* **1999**, 527-538; (q) Thormeier, S.; Carboni, B.; Kaufmann, D. E., *J. Organomet. Chem.* **2002**, *657*, 136-145.
- Morrison, D. J.; Riegel, S. D.; Piers, W. E.; Parvez, M.; McDonald, R., *Chem. Commun.* **2006**, 2875-2877.
- (a) Burgos, C. H.; Canales, E.; Matos, K.; Soderquist, J. A., *J. Am. Chem. Soc.* **2005**, *127*, 8044-8049; (b) Canales, E.; Prasad, K. G.; Soderquist, J. A., *J. Am. Chem. Soc.* **2005**, *127*, 11572-11573; (c) Hernandez, E.; Soderquist, J. A., *Org. Lett.* **2005**, *7*, 5397-5400; (d) Lai, C.; Soderquist, J. A., *Org. Lett.* **2005**, *7*, 799-802; (e) Canales, E.; Hernandez, E.; Soderquist, J. A., *J. Am. Chem. Soc.* **2006**, *128*, 8712-8713; (f) Gonzalez, A. Z.; Canales, E.; Soderquist, J. A., *Org. Lett.* **2006**, *8*, 3331-3334; (g) Hernandez, E.; Canales, E.; Gonzalez, E.; Soderquist, J. A., *Pure Appl. Chem.* **2006**, *78*, 1389-1395; (h) Hernandez, E.; Burgos, C. H.; Alicea, E.; Soderquist, J. A., *Org. Lett.* **2006**, *8*, 4089-4091; (i) Roman, J. G.; Soderquist, J. A., *J. Org. Chem.* **2007**, *72*, 9772-9775; (j) Gonzalez, A. Z.; Roman, J. G.; Gonzalez, E.; Martinez, J.; Medina, J. R.; Matos, K.; Soderquist, J. A., *J. Am. Chem. Soc.* **2008**, *130*, 9218-9219; (k) Gonzalez, J. R.; Gonzalez, A. Z.; Soderquist, J. A., *J. Am. Chem. Soc.* **2009**, *131*, 9924-9925; (l) Munoz-Hernandez, L.; Soderquist, J. A., *Org. Lett.* **2009**, *11*, 2571-2574; (m) Soto-Cairolí, B.; Soderquist, J. A., *Org. Lett.* **2009**, *11*, 401-404.

5. (a) Welch, G. C.; San Juan, R. R.; Masuda, J. D.; Stephan, D. W., *Science* **2006**, *314*, 1124-1126; (b) Stephan, D. W., *Dalton Trans.* **2009**, 3129-3136; (c) Stephan, D. W.; Erker, G., *Angew. Chem. Int. Ed.* **2009**, *49*, 46-76.
6. Chen, D.; Klankermayer, J., *Chem. Commun.* **2008**, 2130-2131.
7. (a) Jäkle, F.; Lough, A. J.; Manners, I., *Chem. Commun.* **1999**, 453-454; (b) Gamboa, J. A.; Sundararaman, A.; Kakalis, L.; Lough, A. J.; Jäkle, F., *Organometallics* **2002**, *21*, 4169-4181; (c) Boshra, R.; Sundararaman, A.; Zakharov, L. N.; Incarvito, C. D.; Rheingold, A. L.; Jäkle, F., *Chem. Eur. J.* **2005**, *11*, 2810; (d) Venkatasubbaiah, K.; Zakharov, L. N.; Kassel, W. S.; Rheingold, A. L.; Jäkle, F., *Angew. Chem. Int. Ed.* **2005**, *44*, 5428-5433; (e) Venkatasubbaiah, K.; Bats, J. W.; Rheingold, A. L.; Jäkle, F., *Organometallics* **2005**, *24*, 6043-6050; (f) Venkatasubbaiah, K.; DiPasquale, A. G.; Rheingold, A. L.; Bolte, M.; Jäkle, F., *Angew. Chem. Int. Ed.* **2006**, *45*, 6838-6841; (g) Boshra, R.; Venkatasubbaiah, K.; Doshi, A.; Lalancette, R. A.; Kakalis, L.; Jäkle, F., *Inorg. Chem.* **2007**, *46*, 10174-10186; (h) Venkatasubbaiah, K.; Pakkirisamy, T.; Lalancette, R. A.; Jäkle, F., *Dalton Trans.* **2008**, 4507-4513; (i) Boshra, R.; Doshi, A.; Jäkle, F., *Organometallics* **2008**, *27*, 1534-1541.
8. (a) Tweddell, J.; Hoic, D. A.; Fu, G. C., *J. Org. Chem.* **1997**, *62*, 8286-8287; (b) Fu, G. C., *J. Org. Chem.* **2004**, *69*, 3245-3249; (c) Liu, S.-Y.; Hills, I. D.; Fu, G. C., *J. Am. Chem. Soc.* **2005**, *127*, 15352-15353.
9. (a) Dusemund, C.; Sandanayake, K. R. A. S.; Shinkai, S., Selective fluoride recognition with ferroceneboronic acid. In *Chem. Commun.*, 1995; pp 333-4; (b) Carpenter, B. E.; Piers, W. E.; Parvez, M.; Yap, G. P. A.; Rettig, S. J., *Can. J. Chem.* **2001**, *79*, 857-867; (c) Carpenter, B. E.; Piers, W. E.; McDonald, R., *Can. J. Chem.* **2001**, *79*, 291-295; (d) Venkatasubbaiah, K.; Nowik, I.; Herber, R. H.; Jäkle, F., *Chem. Commun.* **2007**, 2154-2156; (e) Venkatasubbaiah, K.; Doshi, A.; Nowik, I.; Herber, R. H.; Rheingold, A. L.; Jäkle, F., *Chem. Eur. J.* **2008**, *14*, 444-458; (f) Parab, K.; Jäkle, F., *Macromolecules* **2009**, *42*, 4002-4007; (g) Kaufmann, L.; Vitze, H.; Bolte, M.; Lerner, H. W.; Wagner, M., *Organometallics* **2008**, *27*, 6215-6221; (h) Aldridge, S.; Bresner, C.; Fallis, I. A.; Coles, S. J.; Hursthouse, M. B., *Chem. Commun.* **2002**, 740-741; (i) Bresner, C.; Day, J. K.; Coombs, N. D.; Fallis, I. A.; Aldridge, S.; Coles, S. J.; Hursthouse, M. B., *Dalton Trans.* **2006**, 3660-3667; (j) Day, J. K.; Bresner, C.; Fallis, I. A.; Ooi, L. L.; Watkin, D. J.; Coles, S. J.; Male, L.; Hursthouse, M. B.; Aldridge, S., *Dalton Trans.* **2007**, 3486-3488; (k) Day, J. K.; Bresner, C.; Coombs, N. D.; Fallis, I. A.; Ooi, L. L.; Aldridge, S., *Inorg. Chem.* **2008**, *47*, 793-804; (l) Broomsgrove, A. E. J.; Addy, D. A.; Bresner, C.; Fallis, I. A.; Thompson, A. L.; Aldridge, S., *Chem. Eur. J.* **2008**, *14*, 7525-7529; (m) Broomsgrove, A. E. J.; Addy, D. A.; Di Paolo, A.; Morgan, I. R.; Bresner, C.; Chislett, V.; Fallis, I. A.; Thompson, A. L.; Vidovic, D.; Aldridge, S., *Inorg. Chem.* **2010**, *49*, 157-173.
10. (a) Boshra, R.; Doshi, A.; Jäkle, F., *Angew. Chem. Int. Ed.* **2008**, *47*, 1134-1137; (b) Boshra, R.; Venkatasubbaiah, K.; Doshi, A.; Jäkle, F., *Organometallics* **2009**, *28*, 4141-4149.
11. Morgan, I. R.; Di Paolo, A.; Vidovic, D.; Fallis, I. A.; Aldridge, S., *Chem. Commun.* **2009**, 7288-7290.
12. (a) Riant, O.; Argouarch, G.; Guillaneux, D.; Samuel, O.; Kagan, H. B., *J. Org. Chem.* **1998**, *63*, 3511-3514; (b) Seitzberg, J. G.; Dissing, C.; Sotofte, I.; Norrby, P.-O.;

- Johannsen, M., *J. Org. Chem.* **2005**, *70*, 8332-8337; (c) Pedersen, H. L.; Johannsen, M., *J. Org. Chem.* **2002**, *67*, 7982-7994.
13. (a) Eaborn, C., *J. Organomet. Chem.* **1975**, *100*, 43-57; (b) Rot, N.; de Kanter, F. J. J.; Bickelhaupt, F.; Smeets, W. J. J.; Spek, A. L., *J. Organomet. Chem.* **2000**, *593*, 369-379.
14. (a) Sünkel, K.; Kiebling, T., *J. Organomet. Chem.* **2001**, *637-639*, 796; (b) Huo, S. Q.; Zhu, Y.; Wu, Y. J., *J. Organomet. Chem.* **1995**, *490*, 243; (c) Wu, Y. J.; Cui, X. L.; Liu, Y. H.; Yuan, H. Z.; Mao, X. A., *J. Organomet. Chem.* **1997**, *543*, 63; (d) Lin, K.; Song, M.; Zhu, Y.; Wu, Y., *J. Organomet. Chem.* **2002**, *660*, 139.
15. Renk, T.; Ruf, W.; Siebert, W., *J. Organomet. Chem.* **1976**, *120*, 1-25.
16. Sundararaman, A.; Jäkle, F., *J. Organomet. Chem.* **2003**, *681*, 134-142.
17. Scheibitz, M.; Bolte, M.; Bats, J. W.; Lerner, H.-W.; Nowik, I.; Herber, R. H.; Krapp, A.; Lein, M.; Holthausen, M.; Wagner, M., *Chem. Eur. J.* **2005**, *11*, 584-603.
18. (a) Kaplan, J. I.; Fraenkel, G., In *NMR of Chemically Exchanging Systems*, Academic Press: New York, 1980; pp 71-128; (b) Sandström, J., *Dynamic NMR Spectroscopy*. Academic Press: New York, 1982; pp 77-92.
19. Hesse, M.; Meier, H.; Zeeh, B., *Spectroscopic Methods in Organic Chemistry*. Thieme Verlag: Stuttgart, 1997.
20. Appel, A.; Jäkle, F.; Priermeier, T.; Schmid, R.; Wagner, M., *Organometallics* **1996**, *15*, 1188-1194.
21. (a) Cairncross, A.; Sheppard, W. A.; Wonchoba, E.; Guildford, W. J.; House, C. B.; Coates, R. M., *Org. Synth.* **1980**, *59*, 122-131; (b) Sundararaman, A.; Lalancette, R. A.; Zakharov, L. N.; Rheingold, A. L.; Jäkle, F., *Organometallics* **2003**, *22*, 3526-3532.
22. Parks, D. J.; Piers, W. E.; Yap, G. P. A., *Organometallics* **1998**, *17*, 5492-5503.
23. G. M. Sheldrick, SADABS, Version 2. Multi-Scan Absorption Correction Program, University of Göttingen, Germany, 2001.
24. G. M. Sheldrick, *SHELXTL*, Version 6.14, Bruker AXS Inc., Madison, WI, 2004

## Chapter 3 Stereoselective Borylation of Planar Chiral Pyridylferrocenes<sup>a</sup>

### 3.1 Introduction of Directed Metalation

Directed metalation of aromatic compounds has developed into a powerful synthetic tool over the past two decades.<sup>1</sup> While early studies have primarily focused on lithiations, a variety of other metals (e.g. Mg, Zn, Cd, Mn) have been successfully utilized more recently.<sup>2</sup> Much progress has also been achieved when using mixed metal systems.<sup>3</sup> The *ortho*-metalation of ferrocenes is of particular importance, because it provides an opportunity for stereoselective synthesis of planar chiral derivatives.<sup>4</sup> Planar chiral ferrocenes continue to be critically important ligands in transition metal-catalyzed processes.<sup>5</sup> Typically a chiral substituent on one or both Cp rings is utilized as a directing group. Alternatively, a chiral base can be added as an auxiliary. Early examples include Ugi's chiral aminomethylferrocene derivatives (**A**) and Kagan's *p*-tolylsulfinylferrocene (**B**).<sup>6-8</sup> The latter has the advantage that after derivatization of the *ortho*-position, the sulfinate group itself can be readily replaced by lithiation with *tert*-butyl lithium or magnesiation with Grignard species and subsequent treatment with electrophiles.<sup>9-11</sup>

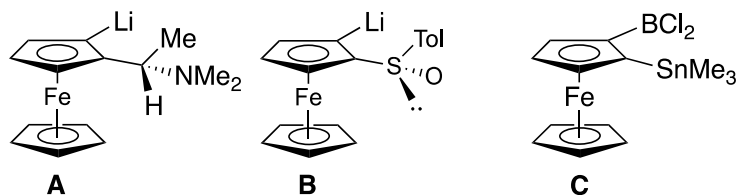


**Figure 3-1.** Examples of *ortho*-lithiation of chiral ferrocenes and the product of borylation of 1,1'-bis(trimethylstannyl)ferrocene (racemate)

<sup>a</sup> This chapter is adapted from a journal publication

The borylation of ferrocenes serves as an important tool in the synthesis of redox-active Lewis acids for anion recognition and Lewis acid catalysis,<sup>11-15</sup> the preparation of redox-active ligands,<sup>6</sup> and the development of new boron-containing electroactive materials<sup>7</sup>. Moreover, ferrocenylboronic acids are interesting building blocks for supramolecular materials<sup>8</sup> and desirable precursors to other ferrocene derivatives by means of Suzuki-Miyaura coupling procedures.<sup>9</sup> Two methods have primarily been used for their synthesis; the direct borylation of ferrocenes with BBr<sub>3</sub> and the metathesis of metalated ferrocenes (FcM, M = Li, Mg, HgX, SnR<sub>3</sub>) with borane species BX<sub>3</sub> (X = F, Cl, Br, OR). While the direct borylation of parent ferrocene is a facile process and multiply borylated species can be obtained with good regioselectivity,<sup>10</sup> the need for use of highly reactive boranes limits the functional group tolerance; moreover, *ortho*-borylation products are very rare due to both steric and electronic deactivation effects. A notable exception is the low temperature borylation of 1,1'-bis(trimethylstannyl)ferrocene with BCl<sub>3</sub>, which leads to 1-stannyl-2-borylferrocene (**C**) as the major product.<sup>11</sup> This result is remarkable, because for other silylated or stannylated aromatics cleavage of the element-carbon bond in an *ipso*-borodemetalation tends to occur much faster than activation of the C-H bond.<sup>12, 13</sup> The unique reactivity is attributed to the directing effect of the stannyl group, the ability of the iron center to mediate proton transfer, and the presence of a second stannyl moiety that acts as a good leaving group.<sup>14</sup> The reaction, however, produces a racemate that has to be resolved into the individual enantiomers.<sup>15</sup>

To develop stereoselective borylation procedures for planar chiral ferrocenes remains a challenging task.<sup>16</sup> Here we demonstrate the selective *ortho*-borylation of planar chiral stannylated and mercurated pyridylferrocenes. We discovered that from a single

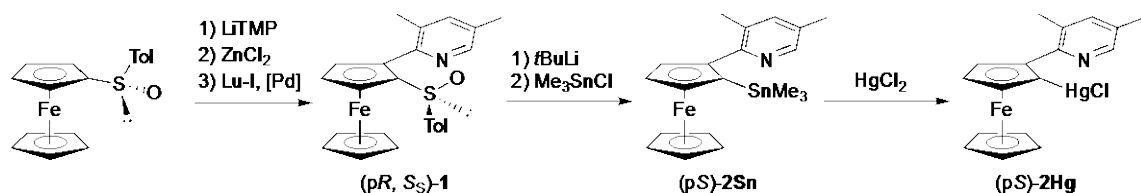
enantiomerically pure 2-pyridyl-1-(*p*-tolylsulfinyl)ferrocene precursor, both (*pR*)- and (*pS*)-2-boryl-1-pyridylferrocene can be generated individually with high stereoselectivity.

### 3.2 Results and Discussion

**Synthesis and Characterization of 2-Pyridyl-1-stannylferrocene (*pS*)-2Sn and 2-Pyridyl-1-mercurioferrocene (*pS*)-2Hg.** The enantiomerically pure planar chiral precursor (*pR*, *S<sub>s</sub>*)-2-(3,5-dimethylpyrid-2-yl)-1-(*p*-tolylsulfinyl)ferrocene ((*pR*, *S<sub>s</sub>*)-**1**)<sup>17</sup> was prepared by Negishi coupling<sup>18</sup> of the corresponding zincated ferrocene species and 2-iodo-3,5-dimethylpyridine in analogy to the synthesis of other 2-aryl-1-sulfinylferrocenes (Scheme 3-1).<sup>9a, 19</sup> The X-ray structure of **1** is displayed in (see 3.6 Supporting Information, Figure 3-7) and confirms the stereochemical assignments. Subsequent reaction of **1** with *tert*-butyl lithium followed by treatment with Me<sub>3</sub>SnCl gave (*pS*)-2-(3,5-dimethylpyrid-2-yl)-1-(trimethylstannyl)ferrocene ((*pS*)-**2Sn**) in 69% yield after crystallization from methanol. The corresponding 1-mercurio-2-pyridylferrocene derivative (*pS*)-**2Hg**, was obtained in essentially quantitative yield by treatment of (*pS*)-**2Sn** with one equivalent of HgCl<sub>2</sub> in acetone. The <sup>1</sup>H and <sup>13</sup>C NMR spectra of (*pS*)-**2Sn** and (*pS*)-**2Hg** show the characteristic pattern of 1,2-disubstituted ferrocenes. The <sup>119</sup>Sn NMR signal for (*pS*)-**2Sn** at  $\delta = -39.9$  ppm is strongly upfield shifted compared to other stannylferrocenes (e.g. 1-trimethylstannyl-2-(1-naphthyl)ferrocene<sup>19c</sup>  $\delta = 7.1$  ppm), which suggests an increase of electron density at the Sn center due to coordination of the adjacent pyridyl group. This is consistent with the X-ray crystal structure of (*pS*)-**2Sn** (Figure 3-2), which reveals a Sn1...N1 distance of 2.805(3) Å that is significantly shorter than the sum of the van der Waal's radii of Sn and

N (3.61 Å<sup>20</sup>). Consequently, the geometry at Sn is distorted toward a trigonal bipyramidal structure as reflected in a large equatorial C1-Sn1-C19 angle of 116.83(18)° (moving towards 120°) and a small C1-Sn1-C20 angle of 102.8(2)° (moving towards 90°). Moreover, the Sn1-C20 bond of 2.165(5) Å is elongated compared to the other Sn-C bonds (2.122(4) - 2.129(5) Å), which is a result of Lewis base binding in the *trans*-position of the Sn center. The pyridyl group is positioned almost co-planar with the substituted Cp ring (Py//Cp = 10°); the slight deviation is likely due to steric repulsion of one of the methyl groups on pyridine and the Cp proton (H3) adjacent to the pyridyl group.

The absolute configuration of (*pS*)-**2Sn** based on the X-ray crystal structure is consistent with the stannyl group assuming the position of the sulfinate moiety in (*pR*)-**1** as shown in Scheme 3-1. Only a single isomer was detected by chiral HPLC analysis and a specific rotation value of  $[\alpha]_D^{20} = -20^\circ$  was determined. The formation of (*pS*)-**2Hg** proceeds with retention of stereochemistry based on a comparison of the optical rotation ( $[\alpha]_D^{20} = -107^\circ$ ) with that of similar compounds<sup>21</sup> that were crystallographically characterized. This is consistent with an *ipso*-mercuriodestannylation, which is the generally accepted mechanism for these types of reaction.<sup>12</sup>



**Scheme 3-1.** Synthesis of planar chiral pyridylferrocenes (*pS*)-**2Sn** and (*pS*)-**2Hg**.

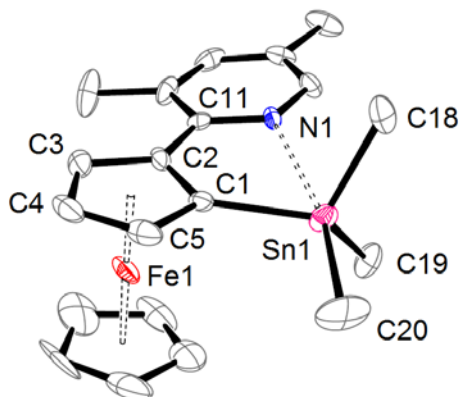
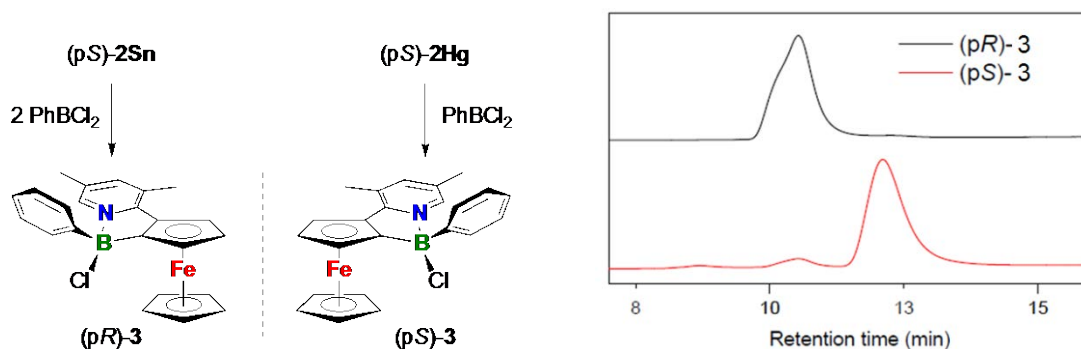


**Figure 3-2.** Ortep plot of (p*S*)-**2Sn** (50% thermal displacement ellipsoids). Hydrogen atoms are omitted for clarity. Selected interatomic distances (Å) and angles (°): Sn1⋯N1 2.805(3), Sn1-C1 2.122(4), Sn1-C18 2.126(5), Sn1-C19 2.129(5), Sn1-C20 2.165(5), C1-Sn1-C18 109.98(17), C1-Sn1-C19 116.83(18), C1-Sn1-C20 102.8(2), C18-Sn1-C19 113.5(2), C18-Sn1-C20 107.3(2), C19-Sn1-C20 105.2(2), N1⋯Sn1-C1 66.65, N1⋯Sn1-C18 81.27, N1⋯Sn1-C19 77.20, N1⋯Sn1-C20 168.6.

**Conversion of (p*S*)-**2Sn** and (p*S*)-**2Hg** to the Boracycles (p*R*)-**3** and (p*S*)-**3**.** The reaction of planar chiral ferrocenyltin species with boron halides generally tends to be unselective because multiple sites on the Cp rings are prone to attack by the electrophile, commonly yielding a mixture of 1,2-, 1,3-, and 1,1'-disubstituted products.<sup>15, 19c, 22</sup> In contrast, transmetalation from Hg to B generally proceeds with high selectivity via cleavage of the (weak) Hg-C bond. We investigated the borylation of both the organotin species (p*S*)-**2Sn** and the organomercury derivative (p*S*)-**2Hg**. (p*S*)-**2Sn** was reacted with an excess of PhBCl<sub>2</sub> in a mixture of toluene and hexanes at -37 °C, while (p*S*)-**2Hg** was treated with one equivalent of PhBCl<sub>2</sub> in toluene at -37 °C. For both reactions the color changed immediately from orange to dark red. The products were isolated in moderate yields as red solids by recrystallization from a mixture of toluene and hexanes at -37 °C. In both cases, the selective formation of a single product with identical NMR spectral data was observed. However, surprisingly, the optical rotation for the product derived

from the mercury precursor (*pS*)-**2Hg** ((*pS*)-**3**;  $[\alpha]_D^{20}$  ( $c = 0.10$ ,  $\text{CH}_2\text{Cl}_2$ ) =  $-2060^\circ$ ) proved to be almost exactly opposite to that derived from the organotin species (*pS*)-**2Sn** ((*pR*)-**3**;  $[\alpha]_D^{20}$  ( $c = 0.10$ ,  $\text{CH}_2\text{Cl}_2$ ) =  $+2110^\circ$ ).<sup>23</sup> Considering also the NMR spectroscopic and X-crystallography results (*vide infra*) we assign the two products to be the enantiomers (*pR*)-**3** and (*pS*)-**3** (Scheme 3-2). Using chiral HPLC, we estimated the enantiomeric excess (ee) to be 99% for (*pR*)-**3** and 90% for (*pS*)-**3**, respectively.<sup>24</sup> The isomer (*pS*)-**3** corresponds to retention of planar chirality, which implies that it is formed as expected through an *ipso*-borodemercuration reaction (boron attacks at C-Hg). In contrast, the observation of (*pR*)-**3** in the reaction of (*pS*)-**2Sn** with  $\text{PhBCl}_2$  is highly unusual and indicates an entirely different mechanistic pathway (*vide infra*).



**Scheme 3-2.** Synthesis of planar chiral 2-boryl-1-pyridylferrocenes (*pS*)-**3** and (*pR*)-**3** (only the B-chiral isomers with the Ph group the exo position are shown) and corresponding chiral HPLC traces.

As enantiomers, (*pR*)-**3** and (*pS*)-**3** show identical NMR spectra, so they are discussed together. An  $^{11}\text{B}$  NMR signal at 6.0 ppm is indicative of a tetracoordinate environment at boron and consistent with formation of the proposed heterocyclic structure due to B-N adduct formation. Upon dissolution of **3** in  $\text{C}_6\text{D}_6$ , initially one set of signals was

observed, but over time a second set gradually started to appear (see Figure 3-3). Equilibration occurred over a period of about 2 days and the final ratio of the (initial) major to the (new) minor component was estimated to about 3.2:1 in  $C_6D_6$ . In  $CDCl_3$  or  $CD_2Cl_2$  equilibration was almost instantaneous and the ratios were slightly lower (2.5:1 and 2.1:1). Coalescence was not observed even at elevated temperature (70 °C), which is consistent with an isomerization that is very slow on the NMR time scale. We attribute the two sets of signals to the formation of two distinct B-chiral isomers, one of which features the phenyl group in the exo position and the other in the endo position (Figure 3-4). The resonances of the substituted Cp ring for the minor and the major isomer appear at similar chemical shifts. However, the signal for the free Cp ring in the minor isomer (3.59 ppm) is strongly upfield shifted, because of the shielding effect of the phenyl group in *endo*-position. Consistent is that the minor isomer is less energetically favorable and thus less abundant due to steric effects between the Ph group and the free Cp ring. The assignments were further confirmed by a 2D NOESY experiment, which clearly revealed an NOE peak between the *o*-Ph protons and the free Cp ring of the minor isomer, but not the major isomer (Figure 3-3). Noteworthy is also that the exo Ph isomer is the only species present in the solid state (*vide infra*), hence it is dominant upon initial dissolution.

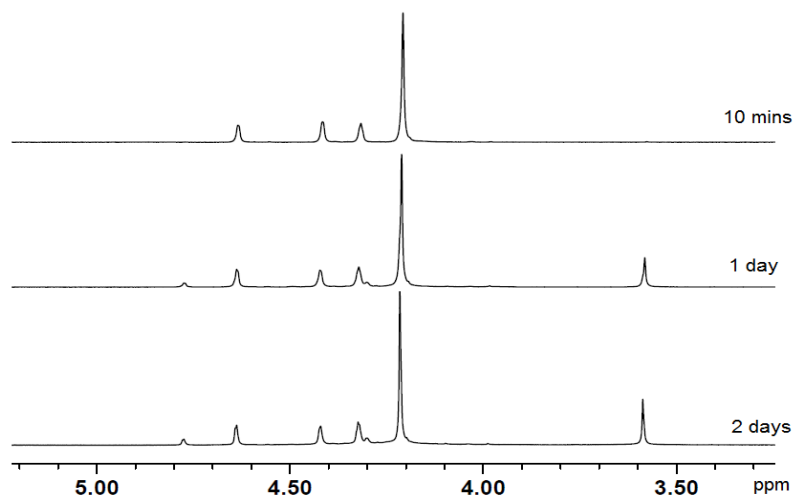


**Figure 3-3.**  $^1\text{H}$  NMR spectra (Cp region) of single crystals of (*pR*)-**3** in  $\text{C}_6\text{D}_6$  after different time intervals.

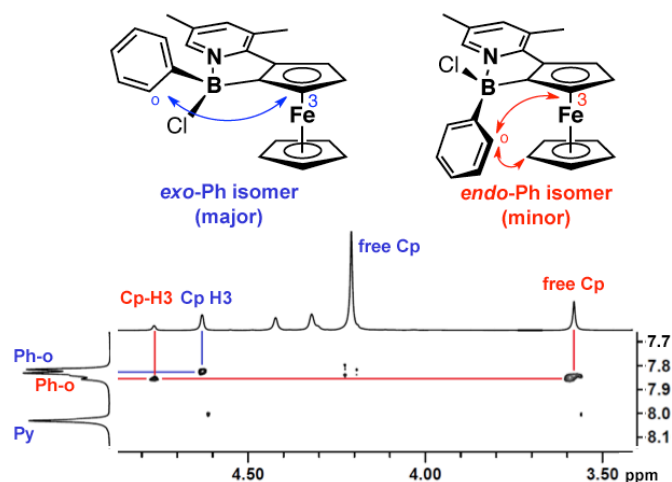


**Figure 3- 4.** Excerpt of the  $^1\text{H}$ - $^1\text{H}$  NOESY NMR spectrum for (*pR*)-**3** and structures of the two different B-chiral isomers observed in  $\text{C}_6\text{D}_6$  solution.

Single crystal X-ray diffraction analyses were performed on both (*pR*)-**3** and (*pS*)-**3**, which proved to be essentially isostructural and gave almost identical unit cell dimensions (Table 3-1). Refinement of the Flack parameter provided the correct stereochemical assignment. In agreement with our NMR analysis, in each case only the major B-chiral isomer with the Ph group in the exo position was observed in the solid

state (Figure 3-5). The B-N bond length of 1.629(3) Å for (*pR*)-**3** [1.618(4) Å for (*pS*)-**3**] is similar to that in Py-B(C<sub>6</sub>F<sub>5</sub>)<sub>3</sub> (1.628(2) Å)<sup>25</sup> and related pyridine-borane adducts. The B-Cl bond length of 1.882(3) Å [1.880(4) Å] is similar to the ones reported for a chlorodibenzoborole-pyridine adduct (1.898(2) and 1.902(2) Å)<sup>26</sup> and significantly longer than in tricoordinate chloroboranes.

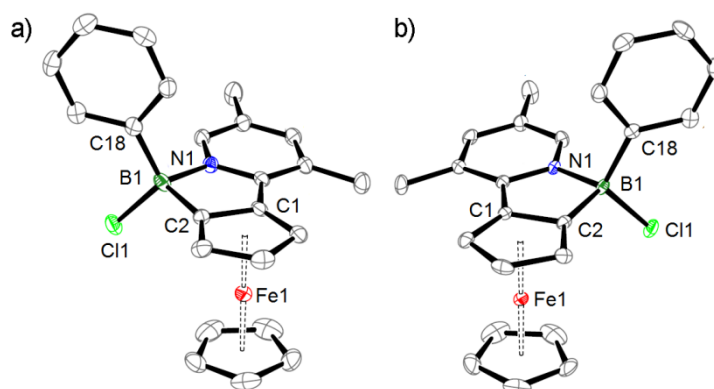


**Figure 3-5.** Ortep plots of a) (*pR*)-**3** and b) (*pS*)-**3** with 50% thermal displacement ellipsoids. Hydrogen atoms and solvent molecules are omitted for clarity. Selected interatomic distances (Å) and angles (°): (*pR*)-**3** [(*pS*)-**3**]: B1-N1 1.629(3) [1.618(4)], B1-Cl1 1.882(3) [1.880(4)], B1-C2 1.603(4) [1.593(5)], B1-C18 1.601(4) [1.613(5)], C2-C1-C11 111.0(2) [110.8(3)], C1-C2-B1 109.16(19) [108.9(2)], C2-B1-N1 96.86(18) [97.5(2)], N1-C11-C1 109.0(2) [109.1(3)].

### 3.3 Mechanistic Study of Borylation

The inversion of stereochemistry in the formation of (*pR*)-**3** from (*pS*)-**2Sn** is a very interesting discovery that warrants further discussion. Given the high regio- and stereoselectivity of the process, the Lewis basic pyridyl group in (*pS*)-**2Sn** appears to act as an *ortho*-directing group that facilitates selective borane attack at the C-H position next to the pyridyl group, followed by a protiodestannylation. A detailed summary of the proposed mechanistic steps is provided in Figure 3-6. Depending on the reaction

conditions, initially, a Me group on Sn may be replaced with a chloro-substituent as indicated by the need for two equivalents of  $\text{PhBCl}_2$ .<sup>27</sup> The first step of the rearrangement mechanism then entails binding of the borane to the Lewis basic pyridyl moiety, followed by electrophilic attack at the *ortho*-carbon in 3-position. In the final step the proton (H3) must be transferred to the carbon atom C1 with subsequent release of  $\text{Me}_3\text{SnCl}$  or  $\text{Me}_2\text{SnCl}_2$ . An intramolecular process is likely considering that the reaction is fast even at low temperature; proton transfer could be mediated by protonation of the pyridine ring or a protonated iron species as indicated in Figure 3-6.<sup>14, 28</sup> Even an intermediate in which the proton adopts a bridging position between Fe and N is conceivable.<sup>28b</sup> To gain further insight into the individual mechanistic steps and to more generally explore the reactivity of the tin species (pS)-**2Sn**, we performed a series of NMR scale experiments with Lewis and Brønsted acids (Scheme 3-3).

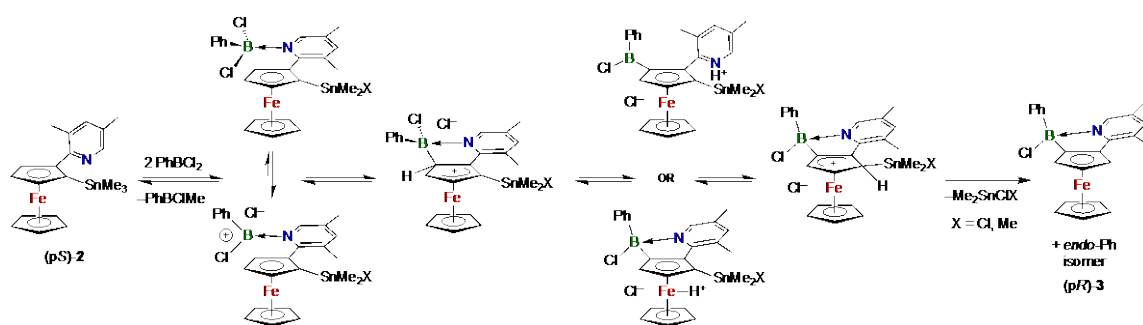


**Figure 3-6.** Proposed reaction pathway in the formation of (pR)-**3** from (pS)-**2Sn** (X = Me, Cl)

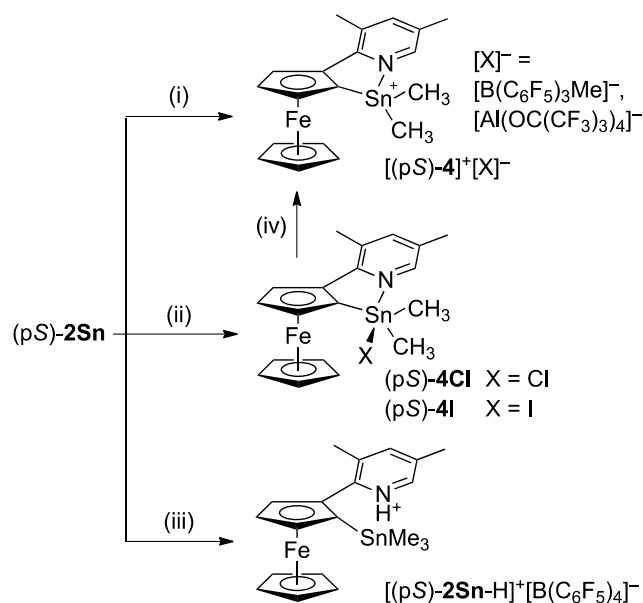
*Step 1: Lewis Acid-Base Adduct Formation and Possible Involvement of a Borenium-Type Intermediate.* The high regio- and stereoselectivity of the borylation process is a strong indication for a directing effect of the pyridyl substituent, which

would require formation of a Lewis acid-base adduct. It is also conceivable that steric strain upon adduct formation with  $\text{PhBCl}_2$  is released by chloride abstraction with formation of a borenium cation, a process that could be facilitated by the presence of excess  $\text{PhBCl}_2$  as a chloride acceptor. Importantly, these types of borenium cations have been shown previously by others<sup>29</sup> to be highly effective intermediates in both intramolecular and intermolecular electrophilic borylation reactions.

Attempts at the direct detection of a Lewis acid-base adduct or a borenium-type species by multinuclear NMR spectroscopy proved unsuccessful because of fast conversion to the final product even at  $-70\text{ }^\circ\text{C}$ . To gather other evidence for such a complex, (pS)-**2Sn** was reacted with  $\text{B}(\text{C}_6\text{F}_5)_3$  as a Lewis acids that was not expected to lead to follow-up reactions with expulsion of the stannyl group as in the case of chloroboranes.<sup>30</sup> Addition of one equivalent of  $\text{B}(\text{C}_6\text{F}_5)_3$  led to a new species with three separate Me signals (1.16, 0.90, 0.56 ppm) of equal integration. The  $^{11}\text{B}$  NMR shifted from ca. 60 ppm for  $\text{B}(\text{C}_6\text{F}_5)_3$  to  $-15.0$  ppm, and the  $^{19}\text{F}$  NMR signal for the *para*-fluorines from  $-148.6$  ppm to  $-164.1$  ppm. These observations suggest that (partial) methyl group abstraction occurred rather than B-N bond formation, with generation of the  $[\text{MeB}(\text{C}_6\text{F}_5)_3]^-$  anion (Scheme 3-3). The presence of the pyridyl-stabilized stannylum cation  $[(\text{pS})\text{-4}]^+$  and the anion  $[\text{MeB}(\text{C}_6\text{F}_5)_3]^-$  was further established by high resolution MALDI-MS analysis in positive and negative mode, respectively.

We note that a similar Me group cleavage reaction also occurred when (pS)-**2Sn** was reacted with one equivalent of  $\text{PhBCl}_2$  in hexanes; the chlorostannylferrocene (pS)-**4Cl** precipitated from the reaction mixture and was isolated as the major product ( $>95\%$ ). We attribute the facile cleavage of the Sn-Me bond to the presence of the pyridyl group in the

trans position, which leads to an elongation of the corresponding Sn-C bond as mentioned earlier in the context of the X-ray structure discussion of (p*S*)-**2Sn**. Indeed treatment of (p*S*)-**2Sn** with iodine also resulted in clean conversion to the iodo derivative (p*S*)-**4I**. Iodide abstraction from (p*S*)-**4I** with Krossing's salt gave [(p*S*)-**4**]<sup>+</sup>[Al(OC(CF<sub>3</sub>)<sub>3</sub>)<sub>4</sub>]<sup>-</sup> (Scheme 3-3). The latter was fully characterized by multinuclear NMR and a single crystal X-ray structure (see 3.6 Supporting Information, Figure 3-8) established the connectivity. The compound also served to further confirm the identity of the cation in [(p*S*)-**4**]<sup>+</sup>[MeB(C<sub>6</sub>F<sub>5</sub>)<sub>3</sub>]<sup>-</sup>.



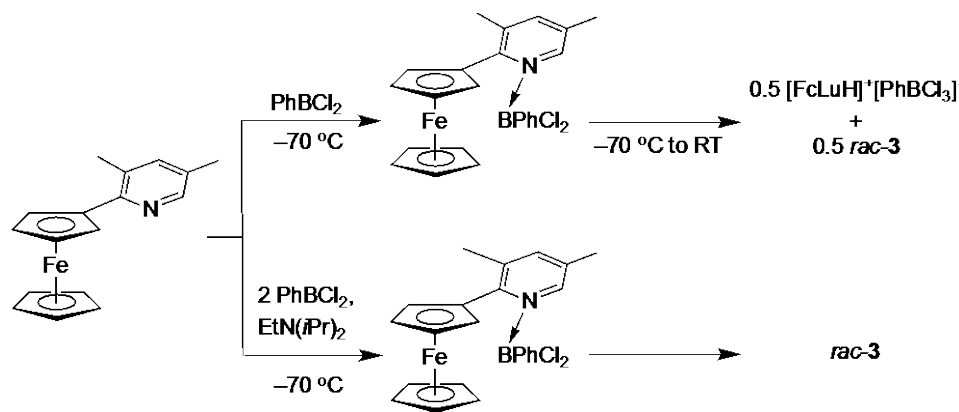
**Scheme 3-3.** Reactivity of (p*S*)-**2Sn** toward selected Lewis and Brønsted acids. (i) B(C<sub>6</sub>F<sub>5</sub>)<sub>3</sub>. (ii) X = Cl: PhBCl<sub>2</sub> in hexanes or Me<sub>2</sub>S·BH<sub>3</sub> in CDCl<sub>3</sub>; X = I: I<sub>2</sub>. (iii) [H(Et<sub>2</sub>O)<sub>2</sub>]<sup>+</sup>[B(C<sub>6</sub>F<sub>5</sub>)<sub>4</sub>]<sup>-</sup>. (iv) [X]<sup>-</sup> = [Al(OC(CF<sub>3</sub>)<sub>3</sub>)<sub>4</sub>]<sup>-</sup>: (p*S*)-**4I** + Li[Al(OC(CF<sub>3</sub>)<sub>3</sub>)<sub>4</sub>].

We reasoned that the presence of the trimethylstannyl group in (p*S*)-**2Sn** as a good leaving group facilitated the low temperature borylation and led to side reactions such as methyl abstraction, which prevented us from observing a Lewis acid-base adduct and/or a

borenium type intermediate. To stabilize the possible intermediates, we decided to use the parent lutidylferrocene (FcLu) as a model compound for our mechanistic studies. As expected, an immediate color change to dark red was observed upon mixing of FcLu and  $B(C_6F_5)_3$  in  $CDCl_3$ . The  $^{11}B$  NMR spectrum revealed a peak at  $-2.1$  ppm, suggesting the formation of a tetracoordinate Lewis acid-base adduct. When we reacted FcLu with 1 equivalent of  $PhBCl_2$  (Scheme 3-4) two major products were observed and identified as *rac-3* and the protonated lutidylferrocene  $[FcLuH]^+[PhBCl_3]^-$  (as a result of HCl release in the formation of *rac-3*). To observe a possible intermediate we carried out an NMR scale reaction of FcLu and  $PhBCl_2$  at  $-70$  °C. Upon addition of 1 equiv of  $PhBCl_2$  at  $-70$  °C formation of a Lewis acid-base adduct was evident from an  $^{11}B$  NMR resonance at 11.7 ppm. As the reaction mixture was allowed to warm up, the adduct converted to the product *rac-3* (ca. 50%), while the other 50% of the starting material was protonated to give  $[FcLuH]^+[PhBCl_3]^-$ . When FcLu,  $EtN(iPr)_2$  and 2 equivs of  $PhBCl_2$  were mixed at  $-70$  °C, we similarly observed adduct formation along with some product *rac-3*. Within a few hours the adduct completely converted to the product even at  $-70$  °C.

Although no evidence of borenium cation formation could be detected based on  $^1H$  and  $^{11}B$  NMR analysis, it is a likely short-lived intermediate giving the fact that the reaction proceeds even at  $-70$  °C in the presence of base and excess  $PhBCl_2$ . By comparison, borylation of unsubstituted ferrocene with  $PhBCl_2$  is very slow under ambient condition. Noteworthy is also that according to recent literature reports<sup>29c</sup> borenium ion-mediated borylation of phenylpyridine occurs only when an excess of  $BBr_3$  is applied in the presence of a bulky base to capture the HBr by-product. In our case, the electron-rich

character of the ferrocene unit allows for reaction even with relatively weakly Lewis acidic compounds such as  $\text{PhBCl}_2$ .



**Scheme 3-4.** Reaction of FcLu with  $\text{PhBCl}_2$ .

**Step 2: Proton Migration.** The second step in the proposed mechanism involves proton migration of Cp-H3 to the C-Sn position, possibly again mediated by the pyridyl group or by the Fe center. To further examine this step, (pS)-**2Sn** was treated with one equivalent of Jutzi's acid,<sup>31</sup>  $[\text{H}(\text{Et}_2\text{O})_2]^+[\text{B}(\text{C}_6\text{F}_5)_4]^-$ . Rapid protonation with formation of the corresponding pyridinium species was observed. The latter exhibits a characteristic triplet at 12.2 ppm with a coupling constant of  $^1J(^{14}\text{N},\text{H}) = 50$  Hz and a chemical shift that is very different from that reported for protonated ferrocene<sup>28b</sup> ( $\delta = -1.5$ ). The corresponding experiment in which the boracycle (pR)-**3** was treated with Jutzi's acid led to a spectrum that contains two major species. A quadrupole-broadened signal is clearly observed at 11.5 ppm, which is indicative of protonation of the pyridyl nitrogen. Based on a comparison of the spectral data with those of an independently prepared sample we identified this species as  $\text{FcLuH}^+$ , which arises from protonolysis of both the B-N and the B-C bond. Based on MALDI-MS evidence, the second species is tentatively assigned to

protonolysis of the dative B-N bond, which would result in a boronium cation that is stabilized by Et<sub>2</sub>O coordination, [FcLu(B(Ph)(OEt<sub>2</sub>)<sub>2</sub>)•HCl]<sup>+</sup>. The observed protonation of the pyridine nitrogen (but not the Fe center) suggests the possible involvement of the pyridine base also in the proton migration step of the rearrangement mechanism.

### 3.4 Conclusions

We have introduced a new stereoselective borylation procedure for the synthesis of planar chiral ferrocenes. The ability to prepare both enantiomers of **3** individually, starting from just one enantiomer of the precursor is very appealing. The inversion of stereochemistry in the formation of (*pR*)-**3** from (*pS*)-**2Sn** is a particularly interesting discovery. Given the high regio- and stereoselectivity of the process, the Lewis basic pyridyl group in (*pS*)-**2Sn** must act as an *ortho*-directing group that facilitates selective borane attack at the C-H position next to the pyridyl group. This ultimately implies that cleavage of the Cp-H<sub>3</sub> bond in (*pS*)-**2Sn** is more facile than the direct cleavage of the Cp-Sn bond. We further propose that formation of a highly reactive borenium cation intermediate enables this unusual reactivity pattern.

The pyridylferrocenylborane heterocycles prepared in here are promising as precursors to new planar chiral borane Lewis acids. We also expect these types of compounds to prove useful as intermediates in the synthesis of chiral pyridylferrocene ligands, by taking advantage of Suzuki-type cross-coupling procedures.<sup>9</sup>

### 3.5 Experimental Section

**Reagents and general methods.** *tert*-Butyl lithium (1.7 M in hexanes), *n*-butyl lithium (1.6 M in hexanes), 2,2,6,6-tetramethylpiperidine, EtN(*i*Pr)<sub>2</sub>, Me<sub>3</sub>SnCl, PhBCl<sub>2</sub>,

$\text{Me}_2\text{S}\cdot\text{BH}_3$  (1.0 M in  $\text{CH}_2\text{Cl}_2$ ), tris(dibenzylideneacetone)dipalladium(0) and tri-*tert*-butylphosphine were purchased from Aldrich and used without further purification. 2,2,6,6-Tetramethylpiperidine and  $\text{EtN}(\text{iPr})_2$  were purchased from Aldrich and distilled from  $\text{CaH}_2$  prior to use. 2-Iodo-3,5-dimethylpyridine,<sup>32</sup> (*S,S*)-*p*-tolylsulfinylferrocene,<sup>33</sup>  $[\text{H}(\text{Et}_2\text{O})_2]^+[\text{B}(\text{C}_6\text{F}_5)_4]^-$ <sup>31</sup>,  $\text{Li}[\text{Al}(\text{OC}(\text{CF}_3)_3)_4]$ <sup>34</sup> were prepared according to literature procedures. 3,5-Dimethylpyrid-2-ylferrocene (FcLu) was prepared from tributylstannylferrocene by treatment with *n*-BuLi, followed by addition of  $\text{ZnBr}_2$  and subsequent Negishi coupling with tris(dibenzylideneacetone)dipalladium(0) / tri-*tert*-butylphosphine as the catalyst system. LiTMP was freshly prepared by addition of *n*-butyl lithium (1.6 M in hexanes) to a THF solution of 2,2,6,6-tetramethylpiperidine at 0 °C. All reactions and manipulations were carried out under an atmosphere of prepurified nitrogen using either Schlenk techniques or an inert-atmosphere glove box (MBraun). 499.9 MHz  $^1\text{H}$ , 125.7 MHz  $^{13}\text{C}$ , 160.4 MHz  $^{11}\text{B}$ , 470.4 MHz  $^{19}\text{F}$ , and 186.4 MHz  $^{119}\text{Sn}$  NMR spectra were recorded on a Varian INOVA NMR spectrometer (Varian Inc., Palo Alto, CA) equipped with a boron-free 5 mm dual broadband gradient probe (Nalorac, Varian Inc., Martinez, CA). Solution  $^1\text{H}$  and  $^{13}\text{C}$  NMR spectra were referenced internally to solvent signals.  $^{11}\text{B}$  NMR spectra were acquired with boron-free quartz NMR tubes and referenced externally to  $\text{BF}_3 \cdot \text{Et}_2\text{O}$  ( $\delta = 0$ ) and  $^{119}\text{Sn}$  NMR data to  $\text{SnMe}_4$  ( $\delta = 0$ ). The following abbreviations are used for signal assignments: Lu = 3,5-dimethylpyrid-2-yl, Fc = ferrocenyl, Cp = cyclopentadienyl. High resolution MALDI-MS (benzo[ $\alpha$ ]pyrene matrix) or ESI-MS (1  $\mu\text{M}$  in toluene) data were obtained on an Apex Ultra 7.0 Hybrid FTMS (Bruker Daltonics). UV/Vis absorption data were acquired on a Varian Cary 500 UV/Vis/NIR spectrophotometer. Optical rotation analyses were

performed on an Autopol III polarimeter, Rudolph Research Analytical, using a tungsten-halogen light source operating at  $\lambda = 589$  nm. Chiral HPLC analyses were performed on a Waters Empower system equipped with a 717plus autosampler, a 1525 binary HPLC pump, and a 2998 photodiode array detector; a CHIRALPAK® IA-3 column was used for separation. Elemental analyses were performed by Intertek Pharmaceutical Services, Whitehouse, NJ.

X-ray diffraction intensities were collected on a Bruker SMART APEX CCD Diffractometer using  $\text{CuK}\alpha$  (1.54178 Å) radiation at 100 K. The structures were refined by full-matrix least squares based on  $F^2$  with all reflections (SHELXTL V5.10; G. Sheldrick, Siemens XRD, Madison, WI). Non-hydrogen atoms were refined with anisotropic displacement coefficients, and hydrogen atoms were treated as idealized contribution. SADABS (Sheldrick, 12 G.M. SADABS (2.01), Bruker/Siemens Area Detector Absorption Correction Program; Bruker AXS: Madison, WI, 1998) absorption correction was applied. Crystallographic data for the structures of (p*R*, *S*<sub>s</sub>)-**1**, (p*S*)-**2Sn**, (p*R*)-**3**, (p*S*)-**3** and [(p*S*)-**4**]<sup>+</sup>[Al(OC(CF<sub>3</sub>)<sub>3</sub>)<sub>4</sub>]<sup>-</sup> have been deposited with the Cambridge Crystallographic Data Center as supplementary publications CCDC 907176 – 907179, and 938810. Copies of the data can be obtained free of charge on application to CCDC, 12 Union Road, Cambridge CB2 1EZ, UK (fax: (+44) 1223-336-033; email: [deposit@ccdc.cam.ac.uk](mailto:deposit@ccdc.cam.ac.uk)).

#### **Synthesis of (p*R*)-2-(3,5-Dimethylpyrid-2-yl)-1-(*p*-tolylsulfinyl)ferrocene (p*R*, *S*<sub>s</sub>)-**

**1.** To a pre-cooled (−78 °C) solution of (*S*<sub>s</sub>)-*p*-tolylsulfinylferrocene (3.00 g, 9.26 mmol) in THF (30 mL) was added a solution of LiTMP (0.5 M in THF, 22.2 mL, 11.1 mmol,

1.20 equiv) dropwise and the mixture was kept stirring for 1 hour. A solution of ZnCl<sub>2</sub> (1.39 g, 10.2 mmol, 1.10 equiv) in THF (20 mL) was then added. After 1 hour at -78 °C the mixture was allowed to warm up and then stirred for 1 hour at 25 °C. Tris(dibenzylideneacetone)dipalladium(0) (0.847 g, 0.926 mmol, 0.10 equiv), tri-*tert*-butylphosphine (0.374 g, 1.85 mmol, 0.20 equiv) and 2-iodo-3,5-dimethylpyridine (4.31 g, 18.5 mmol, 2.00 equiv) were dissolved in a separate flask in THF (20 mL); after stirring for 5 min the solution was added to the pre-made zinc reagent by syringe. The mixture was stirred for 2 days at room temperature. After addition of saturated NH<sub>4</sub>Cl solution (50 mL), the mixture was extracted with CH<sub>2</sub>Cl<sub>2</sub> (3 × 40 mL). The combined organic layers were washed with brine and then water, dried over sodium sulfate and concentrated. The residue was chromatographed on alumina gel with ethyl acetate/hexanes (1: 2) as the eluent, followed by recrystallization from acetone. Yield: 2.4 g (61%).  $[\alpha]_D^{20}$  ( $c = 0.20$ , CH<sub>2</sub>Cl<sub>2</sub>) = -222°. <sup>1</sup>H NMR (499.9 MHz, CDCl<sub>3</sub>, 25 °C):  $\delta = 8.44$  (s, 1H; Lu), 7.86 (d,  $J = 6.0$  Hz, 2H; Tol), 7.37 (d,  $J = 6.0$  Hz, 2H; Tol), 7.25 (s, 1H; Lu), 4.68 (br, 1H; Cp), 4.35 (br, 1H; Cp), 4.13 (s, 5H; free Cp), 4.01 (br, 1H; Cp), 2.47 (s, 3H; Lu-Me), 2.33 (s, 3H; Me), 2.27 (s, 3H; Lu-Me). <sup>13</sup>C NMR (125.69 MHz, CDCl<sub>3</sub>, 25 °C):  $\delta = 151.0$ , 146.9, 141.4, 141.0, 138.4, 131.6, 131.0, 129.1, 125.8 (Lu and Tol), 95.9 (*i*-Cp-S), 88.8 (*i*-Cp-C), 71.6 (Cp), 71.1 (free Cp), 68.5 (Cp), 67.7 (Cp), 21.4, 20.2, 18.0 (Me). High-resolution ESI-MS (pos. mode):  $m/z$  881.1659 ([2M+Na]<sup>+</sup>, 100%, calcd for <sup>12</sup>C<sub>48</sub><sup>1</sup>H<sub>46</sub><sup>14</sup>N<sub>2</sub><sup>23</sup>Na<sup>16</sup>O<sub>2</sub><sup>32</sup>S<sub>2</sub><sup>56</sup>Fe<sub>2</sub> 881.1592). Elemental analysis for C<sub>24</sub>H<sub>23</sub>FeNOS, calcd C 67.13, H 5.40, N 3.26, found C 66.96, H 5.47, N 2.99%.

**Synthesis of (pS)-2Sn.** To a solution of (pR, S<sub>s</sub>)-**1** (1.20 g, 2.80 mmol) in THF (30 mL) that was cooled to -78 °C was added *t*-butyl lithium (1.7 M in hexanes, 2.24 mL, 3.08

mmol, 1.10 equiv) dropwise under stirring. The reaction mixture was kept stirring for 10 min at the same temperature before a solution of Me<sub>3</sub>SnCl (0.67 g, 3.36 mmol, 1.2 equiv) in THF (5 mL) was added via syringe. The resulting solution was stirred for 1 h and the temperature was slowly raised to 25 °C. After addition of water the mixture was extracted with diethyl ether (3 × 5 mL). The combined organic layers were washed with brine solution followed by water, dried over sodium sulfate and concentrated. The residue was subjected to column chromatography on silica gel with hexanes-triethylamine mixture (100:1) as the eluent. The fractions containing the product were concentrated and the residue was taken back up in hot MeOH. Crystallization at -37 °C gave red crystals that proved to be suitable for X-ray diffraction analysis. Yield: 0.87 g (69%).  $[\alpha]_D^{20}$  ( $c = 0.115$ , CHCl<sub>3</sub>) = -20°. <sup>1</sup>H NMR (499.9 MHz, CDCl<sub>3</sub>, 25 °C):  $\delta = 8.03$  (s, 1H; Lu), 7.22 (s, 1H; Lu), 4.90 (nr, 1H; Cp), 4.55 (nr, 1H; Cp), 4.35 (nr, 1H; Cp), 4.05 (s, 5H; free Cp), 2.59 (s, 3H; Lu-Me), 2.26 (s, 3H; Lu-Me), 0.21 (s/d,  $J(^{117/119}\text{Sn,H}) = 45$  Hz, 9H; SnMe<sub>3</sub>). <sup>13</sup>C NMR (125.69 MHz, CDCl<sub>3</sub>, 25 °C):  $\delta = 153.9$ , 145.2, 139.7, 129.5 (Lu), 88.7 (*i*-Cp-C), 75.5 (Cp), 73.0 (*i*-Cp-Sn), 72.6 (s/d,  $J(^{117/119}\text{Sn,C}) = 50$  Hz; Cp), 71.0 (s/d,  $J(^{117/119}\text{Sn,C}) = 38$  Hz; Cp), 68.9 (free Cp), 21.1 (Lu-Me), 17.8 (Lu-Me), -5.8 (s/d,  $J(^{117/119}\text{Sn,C}) = 362/382$  Hz, SnMe<sub>3</sub>). <sup>119</sup>Sn NMR (186.4 MHz, CDCl<sub>3</sub>, 25 °C):  $\delta = -39.9$ . UV-Vis (CHCl<sub>3</sub>):  $\lambda_{\text{max}} = 454$  ( $\epsilon = 570$  M<sup>-1</sup> cm<sup>-1</sup>). High-resolution MALDI-MS (pos. mode, benzo[ $\alpha$ ]pyrene):  $m/z$  440.0124 ([M-Me]<sup>+</sup>, 100%, calcd for <sup>12</sup>C<sub>19</sub><sup>1</sup>H<sub>22</sub><sup>14</sup>N<sup>56</sup>Fe<sup>119</sup>Sn 440.0122). Elemental analysis for C<sub>20</sub>H<sub>25</sub>NFeSn, calcd C 52.89, H 5.55, N 3.09, found C 52.68, H 5.08, N 3.14%.

**Synthesis of (pS)-2Hg.** A solution of (pS)-2Sn (30 mg, 0.066 mmol) in acetone (5 mL) was added dropwise to a solution of HgCl<sub>2</sub> (20 mg, 0.076 mmol, 1.1 equiv) in acetone (5

mL) under stirring. The mixture was allowed to stir for 1 hour and then the solvent was removed under high vacuum. The product, (p*S*)-**2Hg**, was dried under high vacuum for 2 hours at 60 °C and used without further purification.  $[\alpha]_D^{20}$  ( $c = 0.597$ , CHCl<sub>3</sub>) =  $-107^\circ$ . <sup>1</sup>H NMR of (p*S*)-**2Hg** (499.9 MHz, CDCl<sub>3</sub>, 25 °C):  $\delta$  = 8.19 (s, 1H; Lu), 7.28 (s, 1H; Lu), 5.05 (d,  $J = 2.5$  Hz, 1H; Cp), 4.60 (pst,  $J = 2.5$  Hz, 1H; Cp), 4.36 (d,  $J = 2.5$  Hz, 1H; Cp), 4.07 (s, 5H; free Cp), 2.53 (s, 3H; Lu-Me), 2.28 (s, 3H; Lu-Me). <sup>13</sup>C NMR (125.69 MHz, CDCl<sub>3</sub>, 25 °C):  $\delta$  = 153.0, 145.7, 140.7, 130.6, 130.0 (Lu), 87.2 (*i*-Cp-Hg), 85.4 (*i*-Cp-C), 74.6 (Cp), 73.0 (Cp), 70.2 (Cp), 69.7 (free Cp), 21.3 (Lu-Me), 17.8 (Lu-Me). Elemental analysis for C<sub>17</sub>H<sub>16</sub>ClFeHgN, calcd C 38.78, H 3.07, N 2.48, found C 39.20, H 3.07, N 2.48%.

**Synthesis of (p*R*)-3.** A solution of (p*S*)-**2Sn** (100 mg, 0.22 mmol) in a 1:1 mixture of hexanes and toluene (20 mL) was cooled down to  $-37$  °C and then a solution of PhBCl<sub>2</sub> (70 mg, 0.44 mmol, 2.0 equiv) in toluene (2 mL) was added dropwise under stirring. The mixture was stirred over night at room temperature and then the solvents were removed under high vacuum. The residue was taken back up in a mixture of hot hexanes/toluene (1:1). When stored at  $-37$  °C crystals were obtained that contain half an equivalent of toluene; they proved to be suitable for X-ray diffraction analysis. Yield: 55 mg (55%).  $[\alpha]_D^{20}$  ( $c = 0.10$ , CH<sub>2</sub>Cl<sub>2</sub>) =  $+2110^\circ$ . <sup>1</sup>H NMR (499.9 MHz, CDCl<sub>3</sub>, 25 °C): Ratio Major : Minor Isomer = 2.5 : 1;  $\delta$  = 8.23 (s, 1H, Lu; Minor), 8.13 (s, 1H; Lu, Major), 7.58 (s, 1H; Lu, Minor), 7.53 (d,  $J = 7$  Hz, 2H; *o*-Ph, Minor), 7.48 (s, 1H; Lu, Major), 7.37 (pst,  $J = 7$  Hz, 2H; *m*-Ph, Minor), 7.32 (d,  $J = 7$  Hz, 2H; *o*-Ph, Major), 7.26 (nr, 1H, *p*-Ph, Minor), 7.16 (pst,  $J = 7$  Hz, 2H; *m*-Ph, Major), 7.13 (m, 1H, *p*-Ph, Major), 4.77 (dd,  $J = 2.5$  Hz, 1 Hz, 1H; Cp, Major), 4.71 (overlapped, 2H; Cp, Minor), 4.62 (dd,  $J = 2.5$  Hz, 1 Hz, 1 H;

Cp, Major), 4.58 (m, 2H; Cp, Major + Minor), 4.22 (s, 5H; free Cp, Major), 3.65 (s, 5H; free Cp, Minor), 2.52 (s, 3H; Lu-Me, Major), 2.51 (s, 3H; Lu-Me, Minor), 2.38 (s, 3H; Lu-Me, Minor), 2.30 (s, 3H; Lu-Me, Major).  $^1\text{H}$  NMR (499.9 MHz,  $\text{C}_6\text{D}_6$ , 25 °C): Ratio Major : Minor Isomer = 3.2 : 1;  $\delta$  = 8.03 (overlapped s, 1H, Lu-H6, Major and s, 1H; Lu-H6, Minor), 7.85 (d,  $J$  = 7 Hz, 2H; *o*-Ph, Minor), 7.82 (d,  $J$  = 7 Hz, 2H; *o*-Ph, Major), 7.43 (pst,  $J$  = 7 Hz, 2H; *m*-Ph, Minor), 7.27 (overlapped, 1H, *p*-Ph, Minor), 7.27 (pst,  $J$  = 7 Hz, 2H; *m*-Ph, Major), 7.14 (t,  $J$  = 7 Hz, *p*-Ph, Major), 6.47 (s, 1H; Lu-H4, Minor), 6.43 (s, 1H; Lu-H4, Major), 4.77 (nr, 1H; Cp-H3, Minor), 4.64 (nr; Cp-H3, Major), 4.43 (nr, 1 H; Cp-H5, Major), 4.33 (nr, 1H; Cp-H4, Major), 4.31 (nr, 1H; Cp-H4, Minor), 4.22 (s, 5H; free Cp, Major), 4.22 (overlapped, 1H; Cp-H5, Minor), 3.59 (s, 5H; free Cp, Minor), 1.87 (s, 3H; Lu-Me-3, Major), 1.80 (s, 3H; Lu-Me-3, Minor), 1.45 (s, 3H; Lu-Me-5, Minor), 1.34 (s, 3H; Lu-Me-5, Major).  $^{11}\text{B}$  NMR (160.4 MHz,  $\text{CDCl}_3$ , 25° C)  $\delta$  = 6.0 ( $w_{1/2}$  = 210 Hz).  $^{13}\text{C}$  NMR (125.69 MHz,  $\text{CDCl}_3$ , 25 °C)  $\delta$  = 158.3, 157.3, 143.3, 142.8, 142.4, 141.5, 131.5, 131.5, 130.4, 130.3, 129.5, 128.9, 127.3, 127.3, 126.4, 126.2 (Lu + Ph), *i*-Ph-B not observed, 84.0 (*i*-Cp-C, Major), 82.5 (*i*-Cp-C, Minor), 74.7 (Cp, Minor), 74.4 (Cp, Major), 70.3 (*i*-Cp-B, Major), 70.2 (*i*-Cp-B, Minor), 70.1 (free Cp, Major), 69.8 (free Cp, Minor), 64.6 (Cp, Minor), 64.5 (Cp, Major), 18.3 (Lu-Me, Major), 18.3 (Lu-Me, Minor), 18.2 (Lu-Me, Minor), 18.1 (Lu-Me, Major). UV-Vis ( $\text{CH}_2\text{Cl}_2$ ):  $\lambda_{\text{max}}$  = 413 ( $\epsilon$  = 1900  $\text{M}^{-1} \text{cm}^{-1}$ ), 503 ( $\epsilon$  = 2700  $\text{M}^{-1} \text{cm}^{-1}$ ). High-resolution MALDI-MS (pos. mode, benzo[ $\alpha$ ]pyrene):  $m/z$  413.0828 ( $[\text{M}]^+$ , 40%, calcd for  $^{12}\text{C}_{23}^{1}\text{H}_{21}^{11}\text{B}^{14}\text{N}^{35}\text{Cl}^{56}\text{Fe}$  413.0804);  $m/z$  378.1137 ( $[\text{M}-\text{Cl}]^+$ , 100%, calcd for  $^{12}\text{C}_{23}^{1}\text{H}_{21}^{11}\text{B}^{14}\text{N}^{56}\text{Fe}$  378.1115). Elemental analysis for  $(\text{C}_{23}\text{H}_{21}\text{BClFeN})(\text{C}_7\text{H}_8)_{0.2}$ , calcd C 67.85, H 5.27, N 3.24, found C

67.99, H 5.27, N 3.15%; the presence of co-crystallized toluene was confirmed by  $^1\text{H}$  NMR and single crystal X-ray diffraction analysis.

**Synthesis of (pS)-3.** (pS)-2Hg (prepared from 30 mg of (pS)-2Sn as described above) was dissolved in toluene (5 mL) and a solution of  $\text{PhBCl}_2$  (12 mg, 0.076 mmol, 1.1 equiv) in toluene (2 mL) was added at  $-37\text{ }^\circ\text{C}$ . Upon addition the color of the mixture turned dark red. After stirring over night at room temperature the solvent was removed under high vacuum. The residue was re-dissolved in a mixture of hot hexanes and toluene (1:1) and a small amount of a black solid was filtered off. The filtrate was kept at  $-37\text{ }^\circ\text{C}$ ; after repeated filtration to remove small amounts of insoluble impurities, the product formed X-ray quality crystals that contained half an equivalent of toluene. Yield: 11 mg (37%).  $[\alpha]_{\text{D}}^{20}$  ( $c = 0.10$ ,  $\text{CH}_2\text{Cl}_2$ ) =  $-2060^\circ$ .

**Reaction of (pS)-2Sn with one equiv of  $\text{PhBCl}_2$ . Synthesis of (pS)-4Cl.** A solution of (pS)-2Sn (10 mg, 0.022 mmol) in hexanes (2 mL) was cooled down to  $-37\text{ }^\circ\text{C}$  and then a solution of  $\text{PhBCl}_2$  (3.5 mg, 0.022 mmol, 1.0 equiv) in hexanes (1 mL) was added dropwise under stirring. An orange precipitate formed that redissolved upon addition of toluene. The mixture was stirred over night at room temperature and then the solvents were removed under high vacuum. The  $^1\text{H}$  NMR spectrum of the residue revealed the formation of (pS)-4Cl (>95%).  $^1\text{H}$  NMR (499.9 MHz,  $\text{CDCl}_3$ ,  $25\text{ }^\circ\text{C}$ ):  $\delta = 7.82$  (s, 1H; Lu), 7.39 (s, 1H; Lu), 5.03 (d,  $J = 2.0$  Hz, 1H; Cp), 4.92 (dd,  $J = 2.0$  Hz, 1H; Cp), 4.70 (pst,  $J = 2.0$  Hz, 1H; Cp), 4.13 (s, 5H; free Cp), 2.56 (s, 3H; Lu-Me), 2.31 (s, 3H; Lu-Me), 0.92 (s/d,  $J(^{117/119}\text{Sn},\text{H}) = 70$  Hz, 3H; SnMe), 0.69 (s/d,  $J(^{117/119}\text{Sn},\text{H}) = 68$  Hz, 3H; SnMe).  $^{13}\text{C}$  NMR (125.69 MHz,  $\text{CDCl}_3$ ,  $25\text{ }^\circ\text{C}$ ):  $\delta = 154.7$ , 143.4, 142.0, 131.1, 130.5 (Lu), 85.4 (*i*-Cp-C), 76.4 (s/d,  $J(^{117/119}\text{Sn},\text{C}) = 68$  Hz, Cp), 75.0 (*i*-Cp-Sn), 74.6 (s/d,

$J(^{117/119}\text{Sn},\text{C}) = 67$  Hz, Cp), 70.8 (s/d,  $J(^{117/119}\text{Sn},\text{C}) = 48$  Hz, Cp), 69.5 (free Cp), 20.9 (Lu-Me), 17.8 (Lu-Me), 3.3 (nr, SnMe) 1.6 (nr, SnMe).  $^{119}\text{Sn}$  NMR (186.4 MHz,  $\text{CDCl}_3$ , 25 °C):  $\delta = -67.2$ . High-resolution MALDI-MS (pos. mode, benzo[*a*]pyrene): *m/z* 474.9817 ( $[\text{M}]^+$ , 3%, calcd for  $^{12}\text{C}_{19}\text{H}_{22}\text{N}^{35}\text{Cl}^{56}\text{Fe}^{119}\text{Sn}$  474.9804), 459.9589 ( $[\text{M-Me}]^+$ , 20%, calcd for  $^{12}\text{C}_{18}\text{H}_{19}\text{N}^{35}\text{Cl}^{56}\text{Fe}^{119}\text{Sn}$  459.9572), *m/z* 440.0134 ( $[\text{M-Cl}]^+$ , 100%, calcd for  $^{12}\text{C}_{19}\text{H}_{22}\text{N}^{56}\text{Fe}^{119}\text{Sn}$  440.0122).

**Reaction of (pS)-2Sn with one equiv of I<sub>2</sub>. Synthesis of (pS)-4I.** To a solution of (pS)-2Sn (60 mg, 0.132 mmol) in 10 mL of  $\text{CH}_2\text{Cl}_2$  was added a solution of I<sub>2</sub> (34 mg, 0.132 mmol) in 5 mL of  $\text{CH}_2\text{Cl}_2$  at -37 °C. After stirring at room temperature for 0.5 hours the solvent was removed under high vacuum. The residue was washed with cold hexanes and then recrystallized from hot hexanes. Yield: 55 mg (73%).  $^1\text{H}$  NMR (499.9 MHz,  $\text{CDCl}_3$ , 25 °C):  $\delta = 7.84$  (s, 1H; Lu), 7.40 (s, 1H; Lu), 5.07 (nr, 1H; Cp), 5.00 (nr, 1H; Cp), 4.70 (nr, 1H; Cp), 4.15 (s, 5H; free Cp), 2.57 (s, 3H; Lu-Me), 2.32 (s, 3H; Lu-Me), 1.19 (s/d,  $J(^{117/119}\text{Sn},\text{H}) = 68$  Hz, 3H; SnMe), 0.95 (s/d,  $J(^{117/119}\text{Sn},\text{H}) = 66$  Hz, 3H; SnMe).  $^{13}\text{C}$  NMR (125.69 MHz,  $\text{CDCl}_3$ , 25 °C):  $\delta = 154.7$ , 143.3, 142.2, 131.0, 130.7 (Lu), 85.0 (*i*-Cp-C), 77.7 (s/d,  $J(^{117/119}\text{Sn},\text{C}) = 67$  Hz; Cp), 74.0 (s/d,  $J(^{117/119}\text{Sn},\text{C}) = 66$  Hz, Cp), 73.9 (*i*-Cp-Sn), 71.1 (s/d,  $J(^{117/119}\text{Sn},\text{C}) = 45$  Hz; Cp), 69.5 (free Cp), 21.0 (Lu-Me), 17.9 (Lu-Me), 6.5 (s/d,  $J(^{117/119}\text{Sn},\text{C}) = 483/503$  Hz; SnMe), 4.1 (s/d,  $J(^{117/119}\text{Sn},\text{C}) = 543/561$  Hz; SnMe).  $^{119}\text{Sn}$  NMR (186.4 MHz,  $\text{CDCl}_3$ , 25 °C):  $\delta = -115.5$ . High-resolution MALDI-MS (pos. mode, benzo[*a*]pyrene): *m/z* 551.8916 ( $[\text{M-Me}]^+$ , 30%, calcd for  $^{12}\text{C}_{18}\text{H}_{19}\text{N}^{56}\text{Fe}^{119}\text{Sn}^{127}\text{I}$  551.8932), *m/z* 440.0118 ( $[\text{M-I}]^+$ , 100%, calcd for  $^{12}\text{C}_{19}\text{H}_{22}\text{N}^{56}\text{Fe}^{119}\text{Sn}$  440.0122). Elemental analysis for  $\text{C}_{19}\text{H}_{22}\text{FeINSn}$ , calcd C 40.31, H 3.93, N 2.48, found C 40.42, H 3.93, N 2.40%.

**Reaction of (pS)-4I with Krossing's Salt. Synthesis of the Organotin Cation [(pS)-4I]<sup>+</sup>[Al(OC(CF<sub>3</sub>)<sub>3</sub>)<sub>4</sub>]<sup>-</sup>.** To a sample of Li[Al(OC(CF<sub>3</sub>)<sub>3</sub>)<sub>4</sub>] (13.7 mg, 14 μmol) in a 20 mL vial was added a solution of (pS)-4I; 8.0 mg, 14 μmol) in CDCl<sub>3</sub> (1 mL) under vigorous stirring. The mixture was stirred for 0.5 hours and then filtered. <sup>1</sup>H NMR analysis showed complete conversion to the product. X-ray quality single crystals were obtained from CHCl<sub>3</sub> at -37 °C. <sup>1</sup>H NMR (499.9 MHz, CDCl<sub>3</sub>, 25 °C): δ = 7.82 (s, 1H; Lu), 7.76 (s, 1H; Lu), 5.28 (nr, 1H; Cp), 5.00 (nr, 1H; Cp), 4.79 (nr, 1H; Cp), 4.22 (s, 5H; free Cp), 2.64 (s, 3H; Lu-Me), 2.40 (s, 3H; Lu-Me), 1.32 (s/d, *J*(<sup>117/119</sup>Sn,H) = 60 Hz, 3H; SnMe), 1.06 (s/d, *J*(<sup>117/119</sup>Sn,H) = 59 Hz, 3H; SnMe). <sup>13</sup>C NMR (125.69 MHz, CDCl<sub>3</sub>, 25 °C): δ = 157.2, 146.5, 143.1, 134.3, 133.5 (Lu), 121.2 (q, *J*(C,F) = 291 Hz, CF<sub>3</sub>), 85.5 (*i*-Cp-C), 77.5 (Cp), 75.4 (s/d, *J*(<sup>117/119</sup>Sn,C) = 80 Hz, Cp), 72.2 (s/d, *J*(<sup>117/119</sup>Sn,C) = 40 Hz, Cp), 71.3 (*i*-Cp-Sn), 70.6 (free Cp), 20.8 (Lu-Me), 17.5 (Lu-Me), 0.4 (br, SnMe) 0.0 (br, SnMe). <sup>19</sup>F NMR (470.4 MHz, CDCl<sub>3</sub>, 25 °C): δ = -75.4. <sup>119</sup>Sn NMR (470.4 MHz, CDCl<sub>3</sub>, 25 °C): δ = +171 (br). High-resolution MALDI-MS (pos. mode, benzo[α]pyrene): *m/z* 440.0120 ([M]<sup>+</sup>, 100%, calcd for <sup>12</sup>C<sub>19</sub><sup>1</sup>H<sub>22</sub><sup>14</sup>N<sup>56</sup>Fe<sup>119</sup>Sn 440.0122), 409.9656 ([M-2Me]<sup>+</sup>, 35%, calcd for <sup>12</sup>C<sub>17</sub><sup>1</sup>H<sub>16</sub><sup>14</sup>N<sup>56</sup>Fe<sup>119</sup>Sn 409.9652).

**NMR scale reactions of (pS)-2Sn with Lewis and Brønsted acids.** Compound (pS)-2Sn (ca. 10 mg) was dissolved in 0.7 mL of CDCl<sub>3</sub> (or CD<sub>2</sub>Cl<sub>2</sub>) in a J. Young's NMR tube and the solution was cooled to -37 °C. The selected acid was added either neat or as a solution (Me<sub>2</sub>S·BH<sub>3</sub>). NMR data were acquired at room temperature right after mixing the components.

(a) Reaction of (pS)-2Sn with Me<sub>2</sub>S·BH<sub>3</sub>. A ca. 5-fold excess of Me<sub>2</sub>S·BH<sub>3</sub> (1M in CH<sub>2</sub>Cl<sub>2</sub>) was added to a solution of (pS)-2Sn in CDCl<sub>3</sub>. Analysis by <sup>1</sup>H and <sup>11</sup>B NMR

spectroscopy revealed the adduct (pS)-**2**·BH<sub>3</sub> (ca. 20%) in equilibrium with the starting components. For (pS)-**2Sn**·BH<sub>3</sub>: <sup>1</sup>H NMR (499.9 MHz, CDCl<sub>3</sub>, 25 °C): δ = 8.49 (s, 1H; Lu), 7.56 (s, 1H; Lu), 4.69 (br, 1H; Cp), 4.57 (br, 1H; Cp), 4.44 (br, 1H; Cp), 4.20 (s, 5H; free Cp), 3.06 (s, 3H; Lu-Me), 2.32 (s, 3H; Lu-Me), 0.08 (s/d,  $J(^{117}/^{119}\text{Sn},\text{H}) = 63$  Hz, 9H; SnMe<sub>3</sub>). <sup>11</sup>B NMR (160.4 MHz, CDCl<sub>3</sub>, 25 °C) δ = -11.0 (m). Over a period of 48 h (pS)-**2** converted to the chlorostannyl derivative (pS)-**4Cl** as confirmed by comparison of <sup>1</sup>H NMR and high resolution MALDI-MS data with those of an authentic sample prepared from (pS)-**2Sn** and PhBCl<sub>2</sub> as described above.

(b) Reaction of (pS)-**2Sn** with B(C<sub>6</sub>F<sub>5</sub>)<sub>3</sub>. B(C<sub>6</sub>F<sub>5</sub>)<sub>3</sub> was added as a solid to a solution of (pS)-**2Sn** in CDCl<sub>3</sub>. The color of the mixture turned slightly darker. <sup>1</sup>H, <sup>11</sup>B, and <sup>19</sup>F NMR data and MALDI-MS analysis indicated (partial) methyl group abstraction from Sn with formation of the ionic species [(pS)-**4**]<sup>+</sup>[B(C<sub>6</sub>F<sub>5</sub>)<sub>3</sub>Me]<sup>-</sup>. <sup>1</sup>H NMR (499.9 MHz, CDCl<sub>3</sub>, 25 °C): δ = 7.81 (s, 1H; Lu), 7.66 (s, 1H; Lu), 5.19 (br, 1H; Cp), 4.90 (br, 1H; Cp), 4.67 (br, 1H; Cp), 4.17 (s, 5H; free Cp), 2.59 (s, 3H; Lu-Me), 2.32 (s, 3H; Lu-Me), 1.16 (br, 3H; SnMe), 0.90 (br, 3H; SnMe), 0.56 (s, 3H; BMe). <sup>11</sup>B NMR (160.4 MHz, CDCl<sub>3</sub>, 25 °C) δ = -15.0 ( $w_{1/2} = 70$  Hz). <sup>19</sup>F NMR (470.4 MHz, CDCl<sub>3</sub>, 25 °C): δ = -132.6 (d,  $J(\text{F},\text{F}) = 22$  Hz, 6F; *ortho*-F), -164.1 (t,  $J(\text{F},\text{F}) = 20$  Hz, 3F; *para*-F), -166.8 (pst,  $J(\text{F},\text{F}) = 20$  Hz, 6F; *meta*-F). <sup>119</sup>Sn NMR (470.4 MHz, CDCl<sub>3</sub>, 25 °C): δ = +119.2 (br). After addition of another equivalent of B(C<sub>6</sub>F<sub>5</sub>)<sub>3</sub> the <sup>119</sup>Sn NMR shifted to δ = +155.1 (br), suggesting that an equilibrium is established between free acid and product and shifted toward product in the presence of an excess of the Lewis acid. High-resolution MALDI-MS (pos. mode, benzo[*a*]pyrene): m/z 440.0134 ([M]<sup>+</sup>, 100%, calcd for <sup>12</sup>C<sub>19</sub><sup>1</sup>H<sub>22</sub><sup>14</sup>N<sup>56</sup>Fe<sup>119</sup>Sn 440.0120). High-resolution MALDI-MS (neg. mode,

benzo[ $\alpha$ ]pyrene):  $m/z$  527.0061 ( $[M]^-$ , 100%, calcd for  $^{12}\text{C}_{19}^1\text{H}_3^{11}\text{B}^{19}\text{F}_{15}$  527.0083). The identity of  $[(pS)\text{-4}]^+[\text{B}(\text{C}_6\text{F}_5)_3\text{Me}]^-$  was further confirmed by comparison of the NMR and MS data with those of an isolated sample of  $[(pS)\text{-4}]^+[\text{Al}(\text{OC}(\text{CF}_3)_3)_4]^-$ .

(c) Reaction of (pS)-**2Sn** with  $[\text{H}(\text{Et}_2\text{O})_2]^+[\text{B}(\text{C}_6\text{F}_5)_4]^-$ .  $[\text{H}(\text{Et}_2\text{O})_2]^+[\text{B}(\text{C}_6\text{F}_5)_4]^-$  was added to (pS)-**2Sn** in  $\text{CD}_2\text{Cl}_2$ . The color of the mixture turned slightly darker.  $^1\text{H}$  NMR data were acquired immediately, indicating formation of the protonated product  $[(pS)\text{-2Sn-H}]^+[\text{B}(\text{C}_6\text{F}_5)_4]^-$ . However, partial decomposition was observed after a few minutes, preventing isolation.  $^1\text{H}$  NMR (499.9 MHz,  $\text{CD}_2\text{Cl}_2$ , 25 °C):  $\delta = 12.23$  (t,  $^2J(^{14}\text{N},\text{H}) = 50$  Hz, 1H, Lu-H $^+$ ), 8.23 (d,  $^3J(\text{H},\text{H}) = 6.5$  Hz, 1H; *o*-Lu), 8.13 (s, 1H; *p*-Lu), 4.86 (br, 1H; Cp), 4.68 (br, 1H; Cp), 4.59 (br, 1H; Cp), 4.43 (br, 5H; free Cp), 3.50 (br, 8H; ether), 2.59 (s, 3H; Lu-Me), 2.35 (s, 3H; Lu-Me), 1.19 (t,  $J = 7.0$  Hz, 12H; ether), 0.16 (s/d,  $J(^{117/119}\text{Sn},\text{H}) = 55$  Hz, 9H;  $\text{SnMe}_3$ ).

#### NMR scale reactions of FcLu with Lewis and Brønsted acids.

(a) Reaction of FcLu with  $[\text{H}(\text{Et}_2\text{O})_2]^+[\text{B}(\text{C}_6\text{F}_5)_4]^-$ . An equimolar amount of  $[\text{H}(\text{Et}_2\text{O})_2]^+[\text{B}(\text{C}_6\text{F}_5)_4]^-$  was added to a solution of FcLu in  $\text{CD}_2\text{Cl}_2$ . The color of the mixture turned darker red.  $^1\text{H}$  NMR data were acquired immediately, indicating formation of the protonated product  $[\text{FcLuH}]^+[\text{B}(\text{C}_6\text{F}_5)_4]^-$ .  $^1\text{H}$  NMR (499.9 MHz,  $\text{CD}_2\text{Cl}_2$ , 25 °C):  $\delta = 11.49$  (br, 1H; Lu-H $^+$ ), 7.99 (s, 1H; Lu), 7.96 (s, 1H; Lu), 4.85 (nr, 2H; Cp), 4.68 (nr, 2H; Cp), 4.29 (s, 5H; free Cp), 3.49 (br, 8H; ether), 2.72 (s, 3H; Lu-Me), 2.45 (s, 3H; Lu-Me), 1.19 (br, 12H; ether). High-resolution MALDI-MS (pos. mode, benzo[ $\alpha$ ]pyrene):  $m/z$  292.0769 ( $[M]^+$ , 100%, calcd for  $^{12}\text{C}_{17}^1\text{H}_{18}^{14}\text{N}^{56}\text{Fe}$  292.0783). High-resolution MALDI-MS (neg. mode, benzo[ $\alpha$ ]pyrene):  $m/z$  678.9781 ( $[M]^-$ , 100%, calcd for  $^{12}\text{C}_{24}^{11}\text{B}^{19}\text{F}_{20}$  678.9768).

(b) Reaction of FcLu with  $B(C_6F_5)_3$ . An equimolar amount of  $B(C_6F_5)_3$  was added to a solution of FcLu in  $CDCl_3$ . The color of the mixture turned darker red.  $^1H$ ,  $^{11}B$ ,  $^{19}F$  NMR data were acquired immediately, indicating formation of the adduct  $FcLu-B(C_6F_5)_3$ .  $^1H$  NMR (499.9 MHz,  $CDCl_3$ , 25 °C):  $\delta$  = 8.42 (br, 1H; Lu), 7.66 (br, 1H; Lu), 4.46 (br, 2H; Cp), 4.29 (nr, 2H; Cp), 4.12 (s, 5H; free Cp), 3.06 (br, 3H; Lu-Me), 2.33 (s, 3H; Lu-Me).  $^{11}B$  NMR (160.4 MHz,  $CDCl_3$ , 25 °C)  $\delta$  = -2.1 ( $w_{1/2}$  = 800 Hz).  $^{19}F$  NMR (470.4 MHz,  $CDCl_3$ , 25 °C):  $\delta$  = -129.9 (br, 6F; *ortho*-F), -157.3 (br, 3F; *para*-F), -164.2 (br, 6F; *meta*-F).

(c) Low temperature reaction of FcLu with  $PhBCl_2$ . A boron-free NMR tube was immersed in a liquid nitrogen bath and charged first with a solution of  $PhBCl_2$  and then a solution of FcLu (1:1) in  $CD_2Cl_2$ . The tube was warmed up to -100 °C to let the solid melt and mix. The resulting solution was placed in the NMR spectrometer that was preset to -70 °C. Data were required at -70 °C and then at different temperatures upon warming to RT. The NMR data showed evidence of  $[FcLuH]^+[PhBCl_3]^-$  and another species that is assigned as the Lewis acid-base adduct.  $^1H$  NMR for  $FcLu\cdot PhBCl_2$  (499.9 MHz,  $CD_2Cl_2$ , -70 °C):  $\delta$  = 9.30 (br, 1H; Lu), 7.70 (s, 1H; Lu), 7.00 (br, 2H; Ph), 6.89 (br, 3H; Ph), 4.53 (br, 2H; Cp), 4.01 (nr, 2H; Cp), 3.93 (s, 5H; free Cp), 2.88 (s, 3H; Lu-Me), 2.46 (s, 3H; Lu-Me).  $^{11}B$  NMR (160.4 MHz,  $CD_2Cl_2$ , -70 °C)  $\delta$  = 11.7 ( $w_{1/2}$  = 900 Hz).

(d) Low temperature reaction of FcLu with 2 equiv  $PhBCl_2$  in the presence of  $EtN(iPr)_2$ . A boron-free NMR tube was immersed in a liquid nitrogen bath and charged first with a solution of FcLu, then 1 equiv  $EtN(iPr)_2$  and finally 2 equivs of  $PhBCl_2$  in  $CD_2Cl_2$ . The tube was warmed up to -100 °C to let the solid melt and mix. The resulting solution was placed in the NMR spectrometer that was preset to -70 °C and data were

required. Initially compound **3** and the Lewis acid-base adduct were observed as the major species. Signals for the latter gradually disappeared over time giving rise to *rac-3* as the major product.

**NMR scale reaction of (pR)-3 with  $[\text{H}(\text{Et}_2\text{O})_2]^+[\text{B}(\text{C}_6\text{F}_5)_4]^-$ .**  $[\text{H}(\text{Et}_2\text{O})_2]^+[\text{B}(\text{C}_6\text{F}_5)_4]^-$  was added to a solution of (pR)-**3** in  $\text{CD}_2\text{Cl}_2$ . The color of the mixture turned dark purple.  $^1\text{H}$  NMR (Figure 3-9i), 2D COSY and NOESY data were acquired, which revealed formation of the protonated species  $[\text{FcLu-H}]^+$  and one additional ferrocene-containing compound.

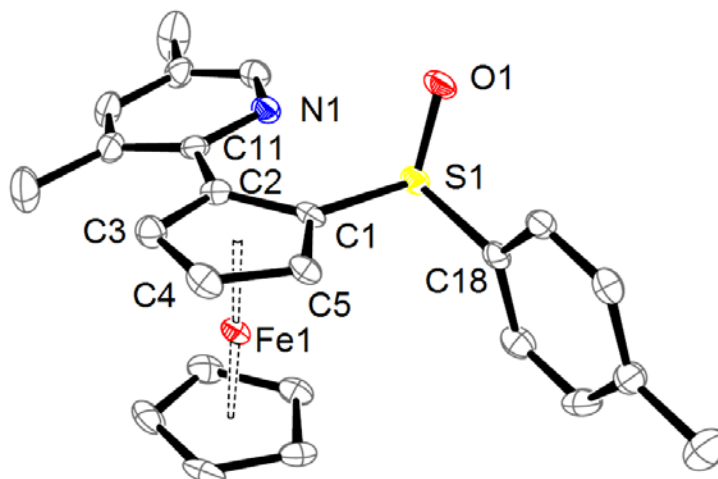
### 3.6 Supporting Information

**Table 3-1.** Crystal data and structure refinement details for (pR, *S<sub>S</sub>*)-**1**, (pS)-**2Sn**, (pS)-**3**, (pR)-**3**, and  $[(\text{pS})\text{-4}]^+[\text{X}]^-$  ( $[\text{X}]^- = [\text{Al}(\text{OC}(\text{CF}_3)_3)_4]^-$ ).

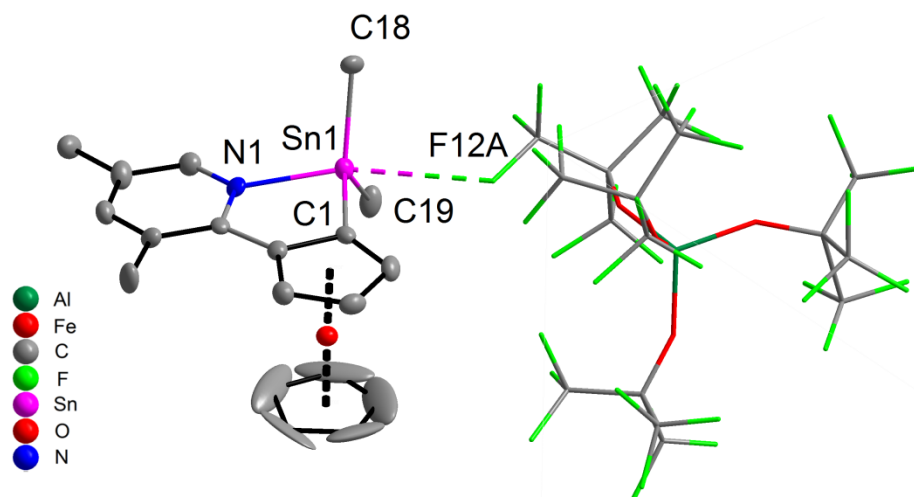
Compound	(pR, <i>S<sub>S</sub></i> )- <b>1</b>	(pS)- <b>2Sn</b>	(pR)- <b>3</b>	(pS)- <b>3</b>	$[(\text{pS})\text{-4}]^+[\text{X}]^-$
empirical formula	$\text{C}_{24}\text{H}_{23}\text{FeNOS}$	$\text{C}_{20}\text{H}_{25}\text{FeNSn}$	$2(\text{C}_{23}\text{H}_{21}\text{BClFeN}) \cdot \text{C}_7\text{H}_8$	$2(\text{C}_{23}\text{H}_{21}\text{BClFeN}) \cdot \text{C}_7\text{H}_8$	$[\text{C}_{19}\text{H}_{22}\text{FeNSn}] [\text{C}_{16}\text{AlF}_{36}\text{O}_4] \cdot \text{CHCl}_3$
MW	429.34	453.95	919.17	919.17	1525.42
<i>T</i> , K	100(2)	100(2)	100(2)	100(2)	100(2)
wavelength, Å	1.54178	1.54178	1.54178	1.54178	1.54178
crystal system	hexagonal	hexagonal	monoclinic	monoclinic	orthorhombic
space group	<i>P</i> 6 <sub>1</sub>	<i>P</i> 6 <sub>1</sub>	<i>C</i> 2	<i>C</i> 2	<i>P</i> 2 <sub>1</sub> 2 <sub>1</sub> 2 <sub>1</sub>
<i>a</i> , Å	9.1420 (1)	10.0515 (2)	21.8325(3)	21.8206(3)	13.1651(4)
<i>b</i> , Å	9.1420 (1)	10.0515 (2)	8.9628(1)	8.9498(1)	14.3393(4)
<i>c</i> , Å	40.0765 (5)	32.8264 (8)	11.3912(2)	11.3981(1)	26.7028(7)
<i>α</i> , deg	90	90	90	90	90
<i>β</i> , deg	90	90	98.691(1)	98.716(1)	90
<i>γ</i> , deg	120	120	90	90	90
<i>V</i> , Å <sup>3</sup>	2900.70 (6)	2872.21 (11)	2203.44(5)	2200.23(4)	5040.9
<i>Z</i>	6	6	2	2	4
$\rho_{\text{calc}}$ , g cm <sup>-3</sup>	1.475	1.575	1.385	1.387	2.010
$\mu$ (Cu K $\alpha$ ), mm <sup>-1</sup>	7.37	16.42	6.75	6.70	9.53
crystal size, mm	0.50×0.21 ×0.19	0.49×0.27 ×0.18	0.36×0.16 ×0.12	0.52×0.16 ×0.11	0.41×0.41 ×0.27
$\theta$ range, deg	3.3-70.9	4.0-70.9	3.9-70.3	3.9-71.3	3.3-69.6

limiting indices	$-10 \leq h \leq 10$	$-11 \leq h \leq 11$	$-24 \leq h \leq 25$	$-25 \leq h \leq 26$	$-15 \leq h \leq 15$
	$-10 \leq k \leq 10$	$-11 \leq k \leq 12$	$-10 \leq k \leq 10$	$-9 \leq k \leq 10$	$-17 \leq k \leq 14$
	$-46 \leq l \leq 41$	$-40 \leq l \leq 38$	$-13 \leq l \leq 13$	$-13 \leq l \leq 13$	$-32 \leq l \leq 32$
reflns collected	28521	26424	10255	10282	40092
independent reflns	3036 [ $R(\text{int}) = 0.035$ ]	3397 [ $R(\text{int}) = 0.053$ ]	3314 [ $R(\text{int}) = 0.030$ ]	3267 [ $R(\text{int}) = 0.043$ ]	8686 [ $R(\text{int}) = 0.0430$ ]
absorption correction	Numerical	Numerical	Numerical	Numerical	Numerical
data/restraints/ parameters	3036 / 1 / 257	3397 / 1 / 214	3314 / 1 / 280	3267 / 1 / 280	8686 / 52 / 752
goodness-of-fit on $F^2$	1.07	1.08	1.00	1.05	1.03
final $R$ indices	$R1 = 0.025$	$R1 = 0.027$	$R1 = 0.028$	$R1 = 0.038$	$R1 = 0.065$
[ $I > 2\sigma(I)$ ] <sup>[a]</sup>	$wR2 = 0.061$	$wR2 = 0.065$	$wR2 = 0.059$	$wR2 = 0.075$	$wR2 = 0.164$
$R$ indices (all data) <sup>[a]</sup>	$R1 = 0.027$	$R1 = 0.028$	$R1 = 0.032$	$R1 = 0.045$	$R1 = 0.068$
	$wR2 = 0.061$	$wR2 = 0.065$	$wR2 = 0.060$	$wR2 = 0.077$	$wR2 = 0.166$
peak <sub>max</sub> /hole <sub>min</sub> (e $\text{\AA}^{-3}$ )	0.23 / -0.24	1.14 / -0.61	0.33 / -0.17	0.33 / -0.40	1.96 / -1.96
absolute structure parameter	0.016(3)	0.044(7)	0.011(3)	0.021(4)	0.091(9)

[a]  $R1 = \sum ||F_o| - |F_c|| / \sum |F_o|$ ;  $wR2 = \{ \sum [w(F_o^2 - F_c^2)^2] / \sum [w(F_o^2)^2] \}^{1/2}$

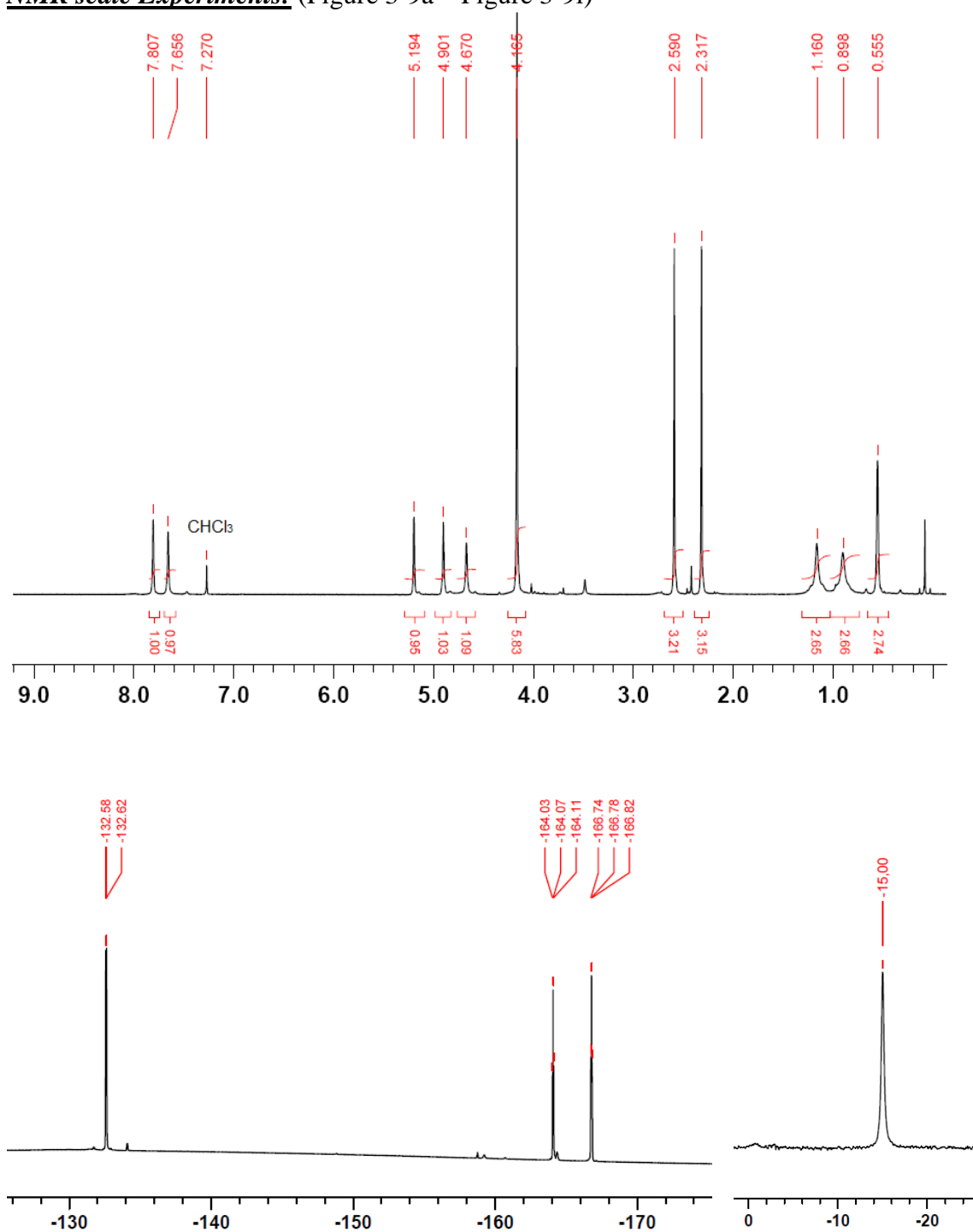


**Figure 3-7.** Ortep plot of (pR,  $S_s$ )-1 (50% thermal displacement ellipsoids). Hydrogen atoms are omitted for clarity. Selected interatomic distances (Å) and angles (°): N1···S1 2.852, S1-O1 1.49678(18), S1-C1 1.797(2), S1-C18 1.808(3), O1-S1-C1 107.05(11), O1-S1-C18 103.94(11), C1-S1-C18 97.14 (11), Cp/Lu 15.03.

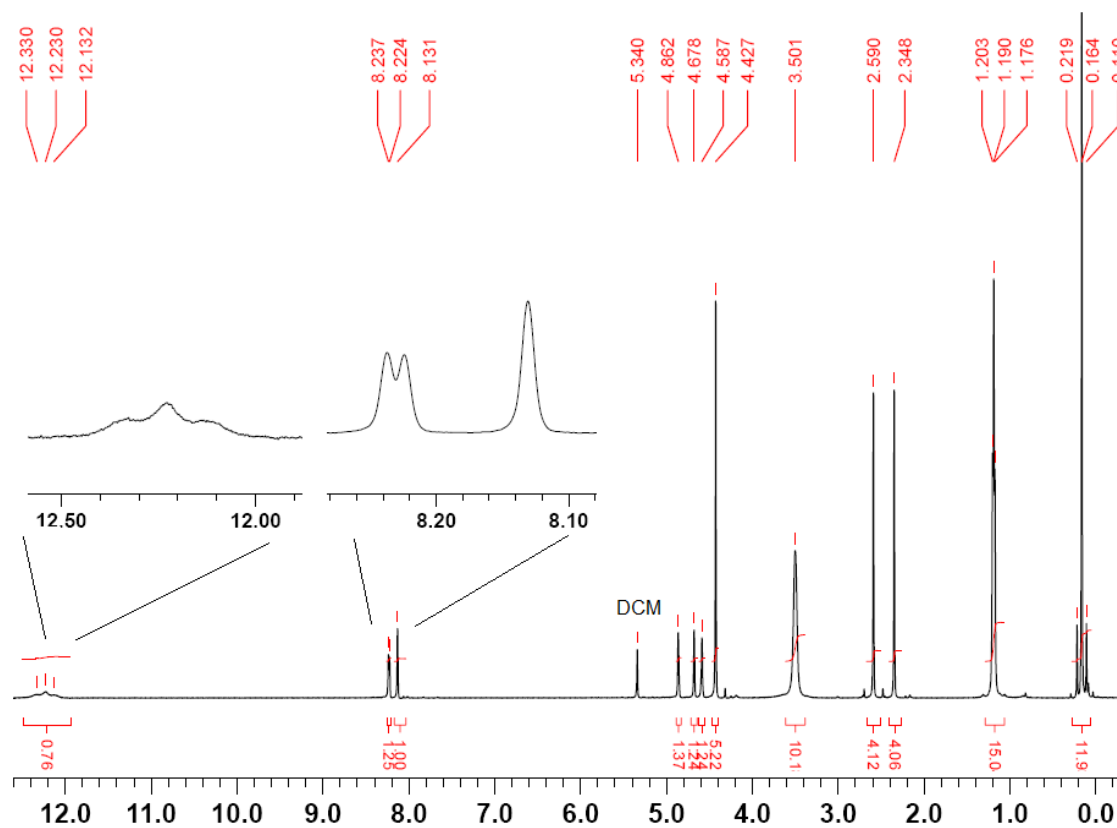


**Figure 3-8.** Crystal structure plot of [(pS)-4]<sup>+</sup>[Al(OC(CF<sub>3</sub>)<sub>3</sub>)<sub>4</sub>]<sup>-</sup>. (50% thermal displacement ellipsoids for the cation). Hydrogen and solvent are omitted for clarity. Due to the disorder of the Crossing anion, which is commonly observed in the solid state, two of the carbon atoms in the anion are found 'Non Positive Definite', and some of the carbon and fluorine atoms display a high ADP max/min ratio. We used ISOR, DELU, and SADI to try to compensate, they still remain disordered. Fortunately, the cation [(pS)-4]<sup>+</sup> could be refined anisotropically without any problem. Selected distances (Å) and angles (°): Sn1-C1 2.097(8), Sn1-C18 2.130(9), Sn1-C19 2.105(10), Sn1-N1 2.202(7), Sn1···F12A 3.063, C1-Sn1-C18 116.5(3), C19-Sn1-C18 118.7(4), C1-Sn1-N1 80.2(3), C19-Sn1-N1 106.4(3), C18-Sn1-N1 102.4(3), N1-Sn1···F12A 155.7.

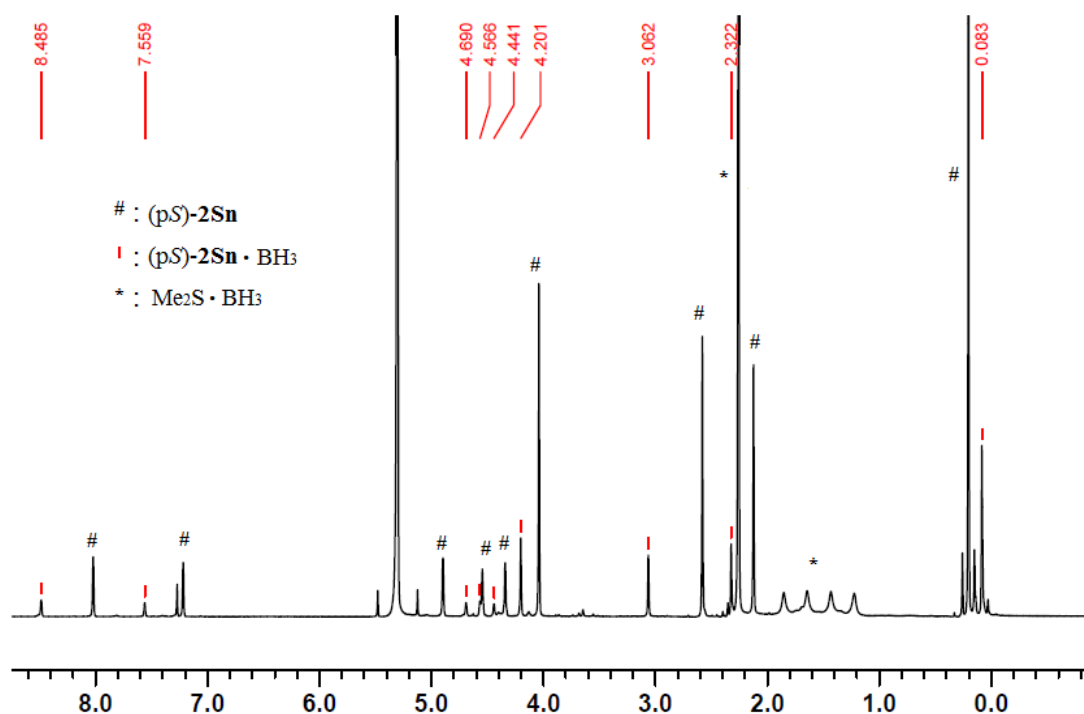
**NMR scale Experiments:** (Figure 3-9a – Figure 3-9i)

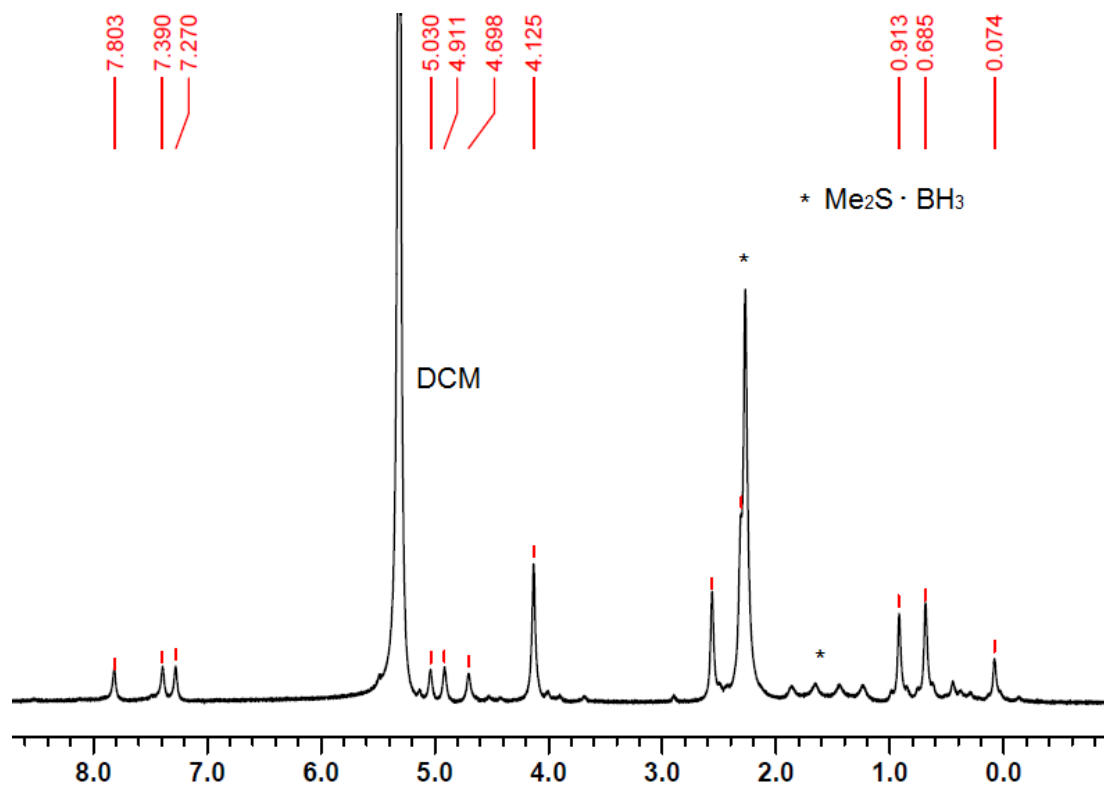


**Figure 3-9a.**  $^1\text{H}$  (top),  $^{19}\text{F}$  (bottom left), and  $^{11}\text{B}$  (bottom right) NMR spectra of the reaction mixture from treatment of (pS)-**2Sn** with  $\text{B}(\text{C}_6\text{F}_5)_3$  in  $\text{CDCl}_3$ .

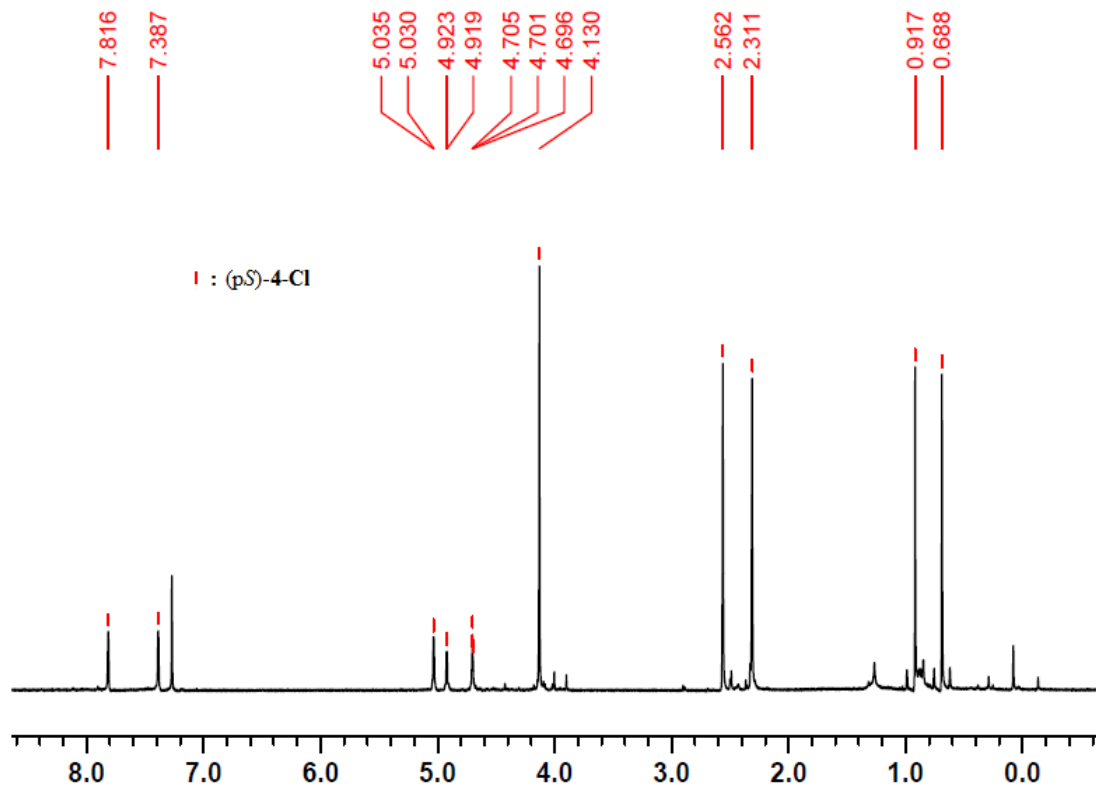


**Figure 3-9b.**  $^1\text{H}$  NMR spectrum of the reaction mixture from treatment of (*pS*)-**2Sn** with  $[\text{H}(\text{Et}_2\text{O})_2]^+[\text{B}(\text{C}_6\text{F}_5)_4]^-$  in  $\text{CD}_2\text{Cl}_2$ .

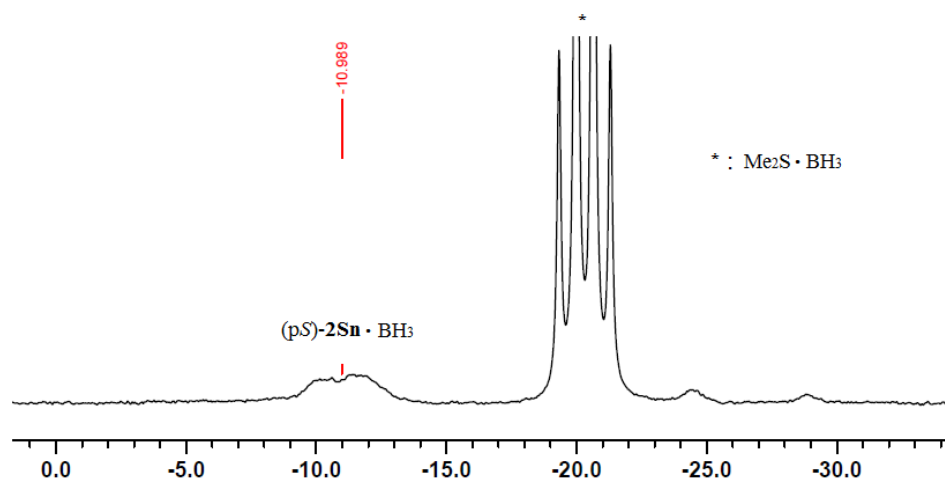




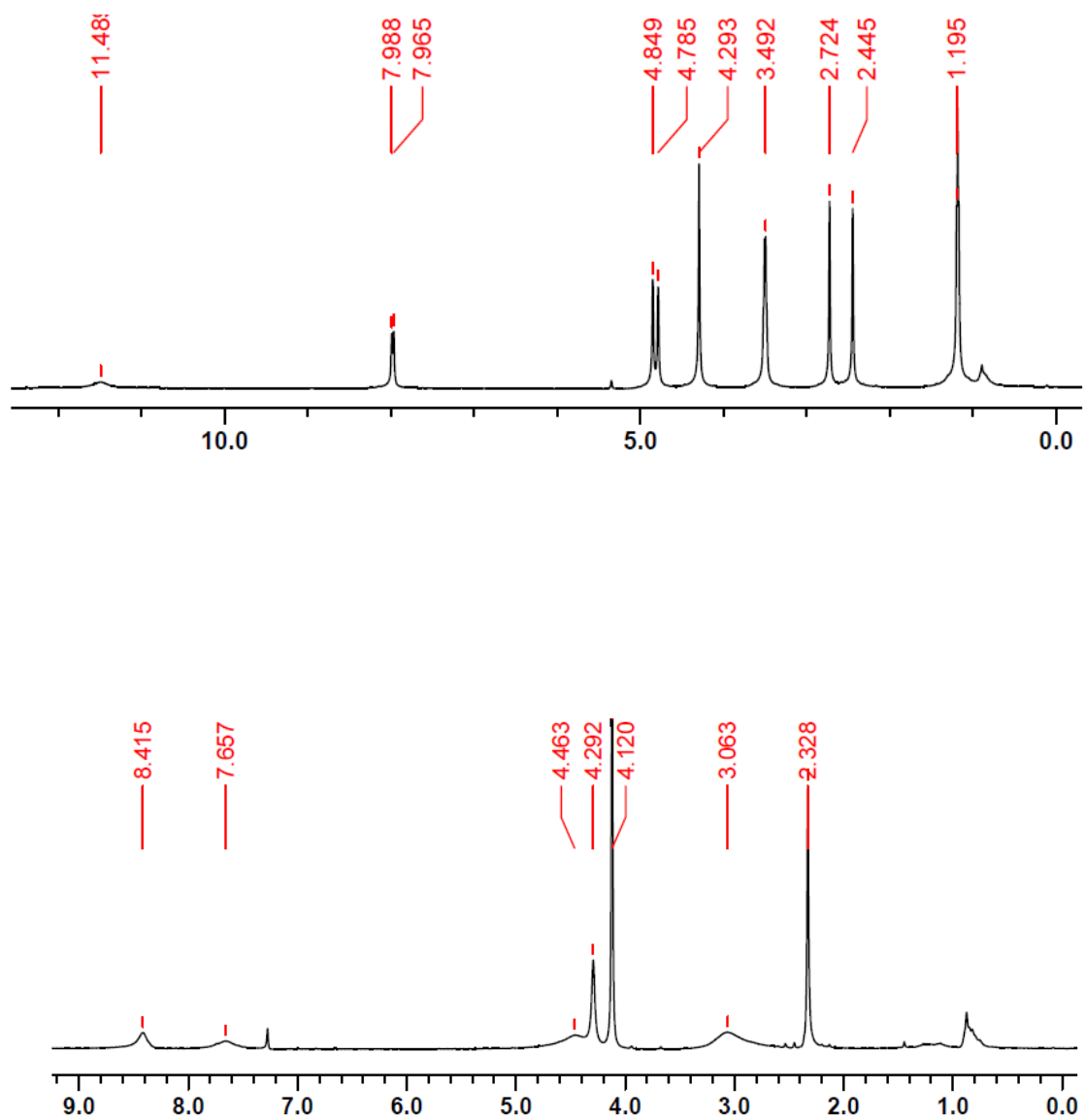
**Figure 3-9c.**  $^1\text{H}$  NMR spectra of the reaction mixture from treatment of (pS)-2Sn with an excess of Me<sub>2</sub>S·BH<sub>3</sub> in CDCl<sub>3</sub> (top) after 5 min; (bottom) after 48 h.



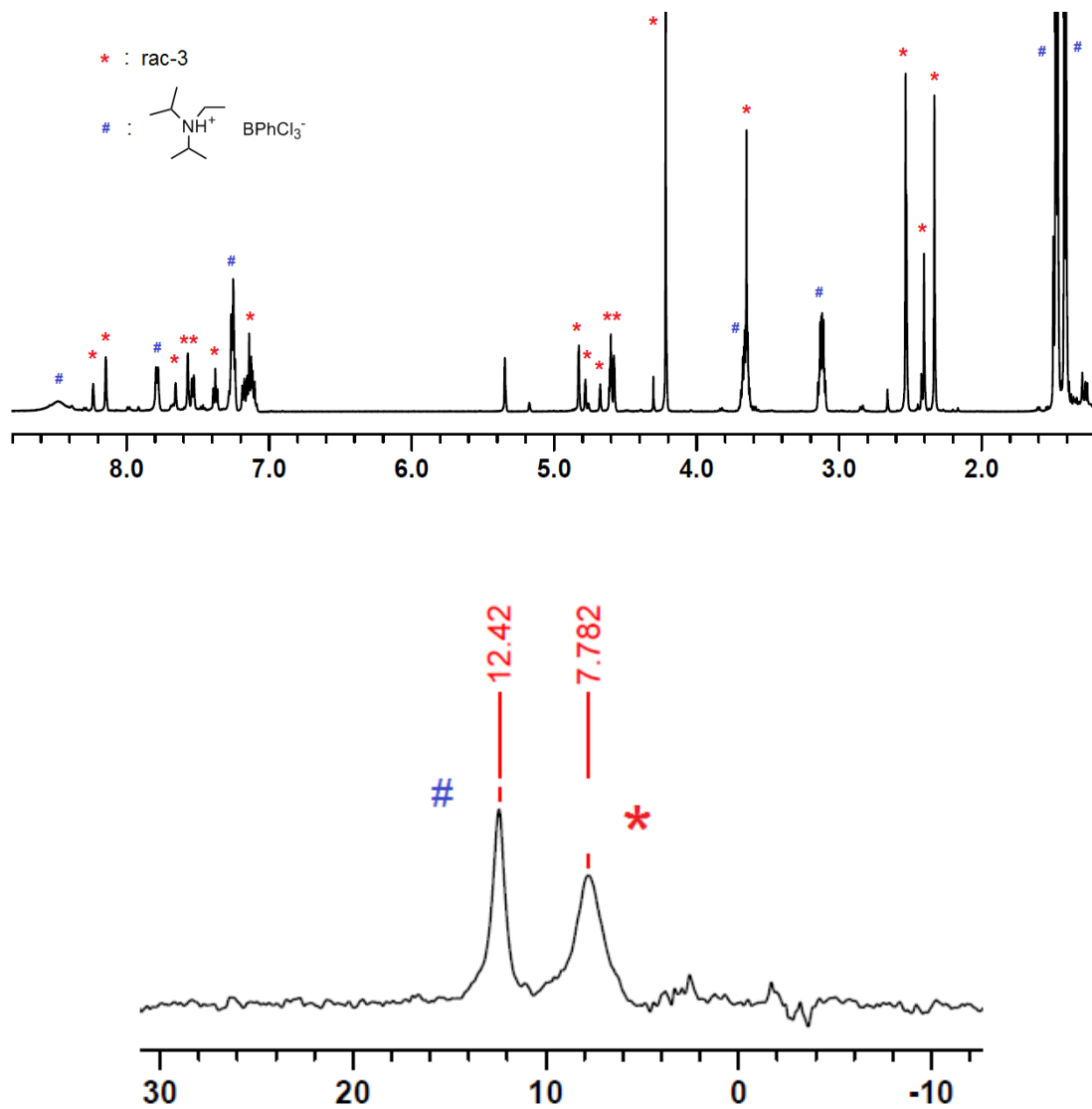
**Figure 3-9d.**  $^1\text{H}$  NMR spectrum of the product from treatment of (pS)-2Sn with an excess of  $\text{Me}_2\text{S}\cdot\text{BH}_3$  in  $\text{CDCl}_3$  for 48 h, followed by removal of all volatile components.



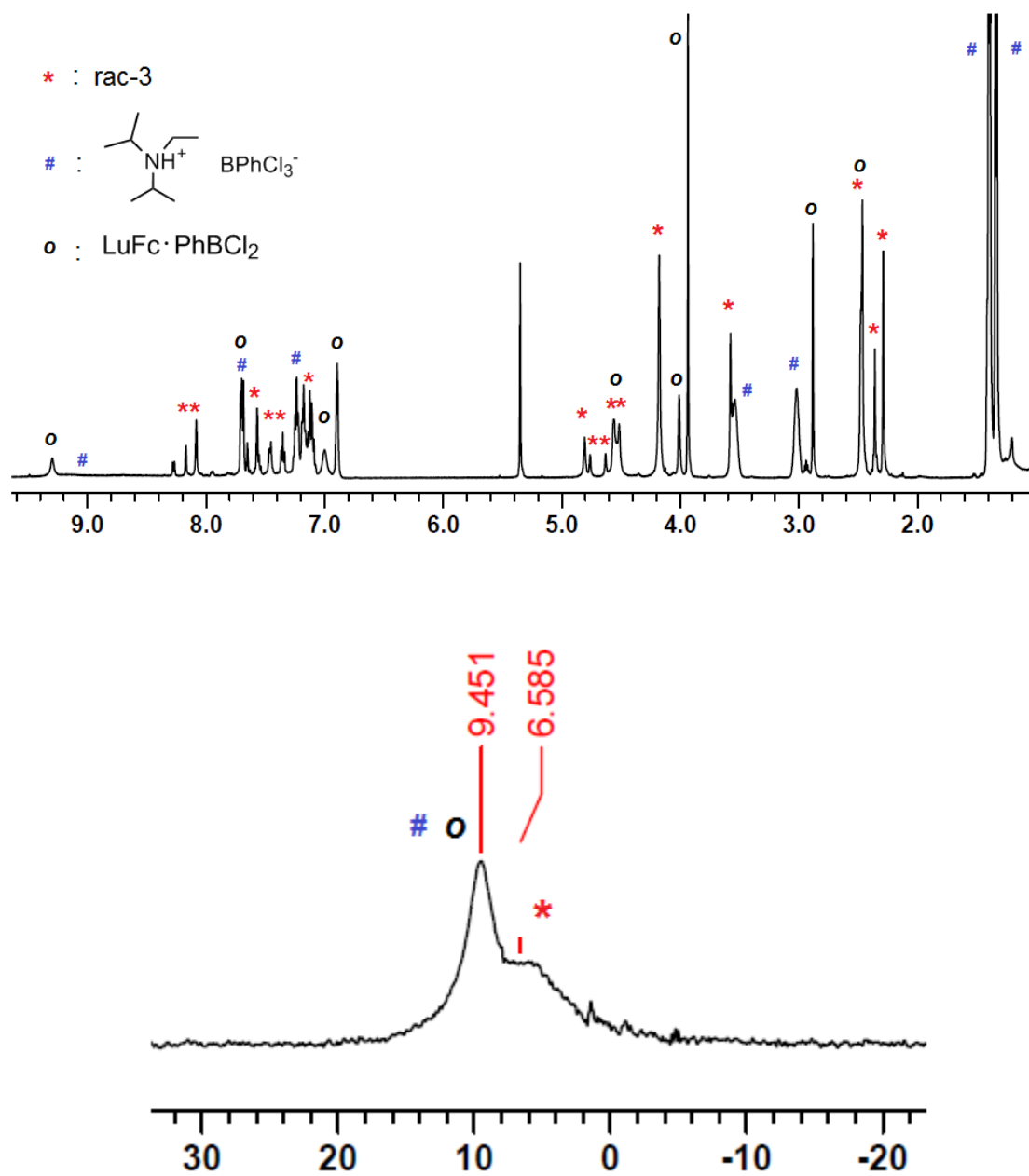
**Figure 3-9e.**  $^{11}\text{B}$  NMR spectrum of the reaction mixture from treatment of (pS)-2Sn with an excess of  $\text{Me}_2\text{S}\cdot\text{BH}_3$  in  $\text{CDCl}_3$  after 5 min. After removal of all volatile components no  $^{11}\text{B}$  NMR signal was observed.



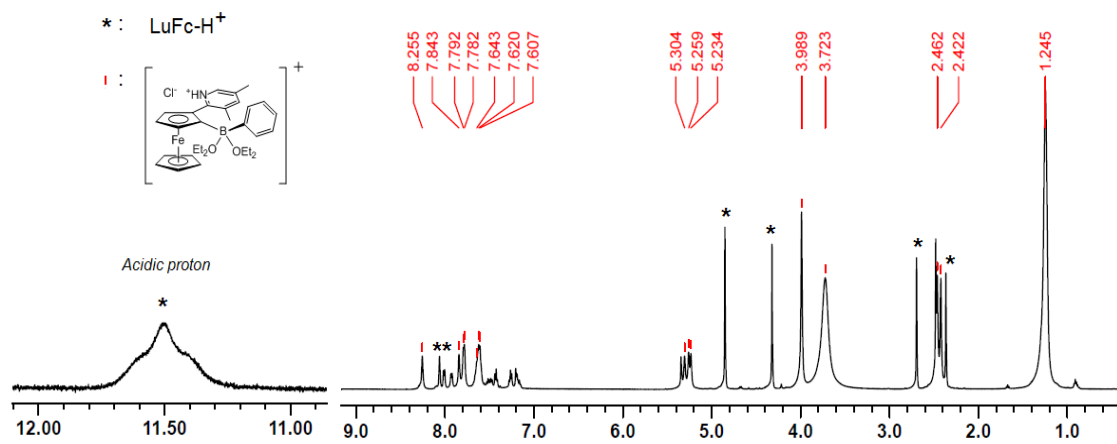
**Figure 3-9f.**  $^1\text{H}$  NMR spectra of the reaction mixtures from treatment of FcLu with (top)  $[\text{H}(\text{Et}_2\text{O})_2]^+[\text{B}(\text{C}_6\text{F}_5)_4]^-$  in  $\text{CD}_2\text{Cl}_2$  and (bottom)  $\text{B}(\text{C}_6\text{F}_5)_3$  in  $\text{CDCl}_3$ .



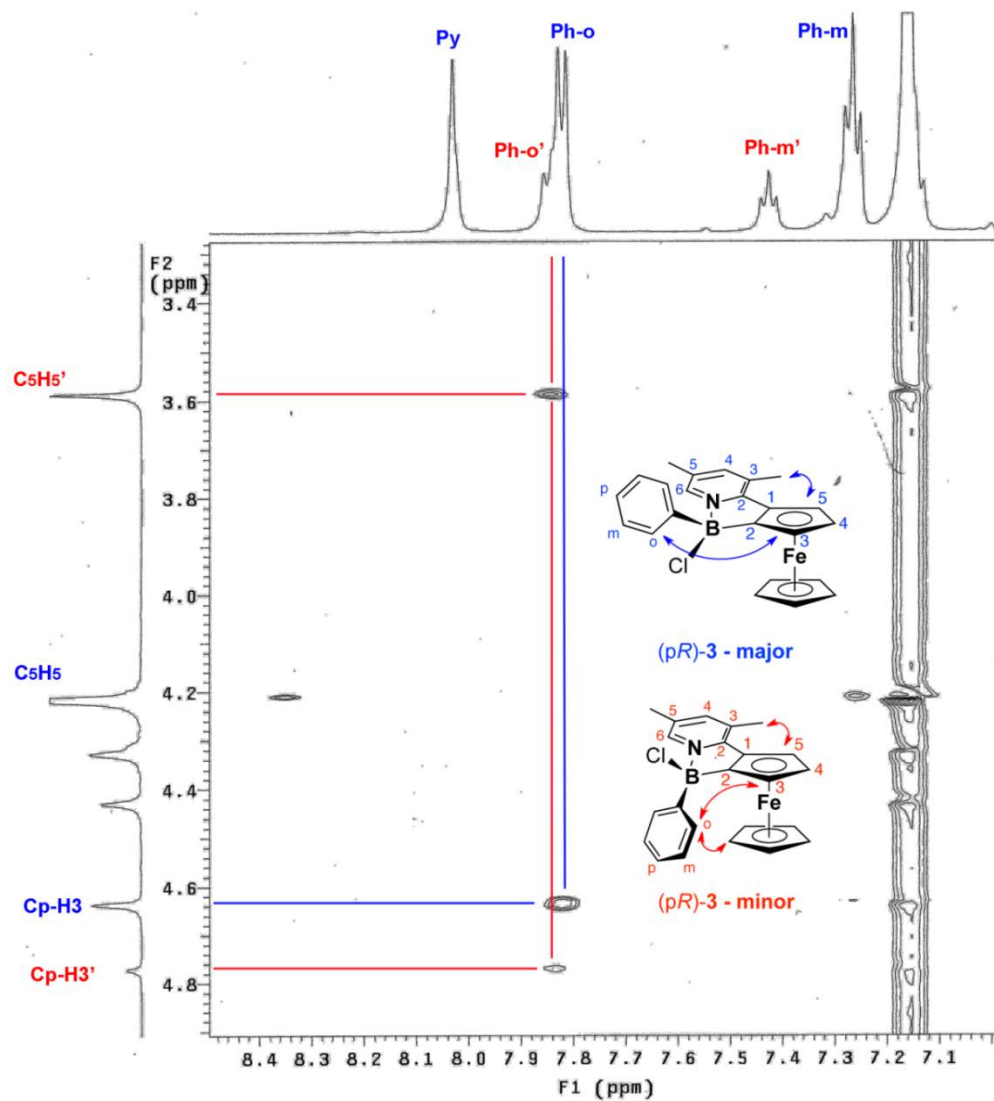
**Figure 3-9g.**  $^1\text{H}$  and  $^{11}\text{B}$  NMR spectra of the reaction mixture from treatment of FcLu with 2 equivs of  $\text{PhBCl}_2$  and 1 equiv of  $\text{EtN}(\text{iPr})_2$  in  $\text{CD}_2\text{Cl}_2$  at RT.



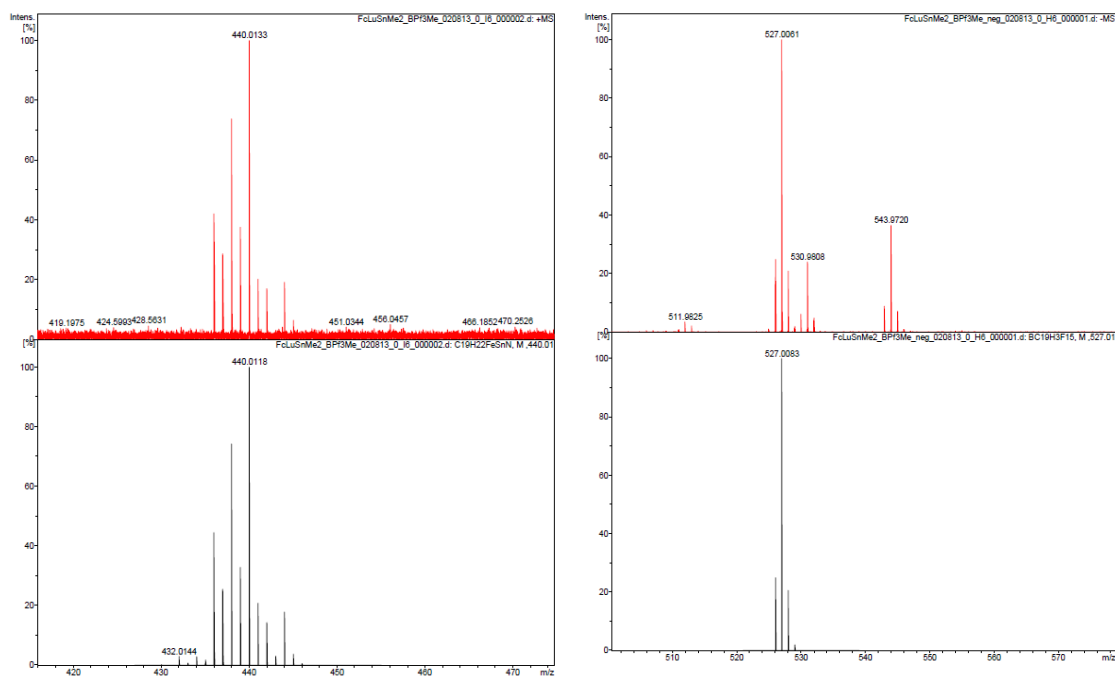
**Figure 3-9h.** <sup>1</sup>H and <sup>11</sup>B NMR spectra of the reaction mixture from treatment of FcLu with 2 equivs of PhBCl<sub>2</sub> and 1 equiv of EtN(*i*Pr)<sub>2</sub> in CD<sub>2</sub>Cl<sub>2</sub> at -70 °C.



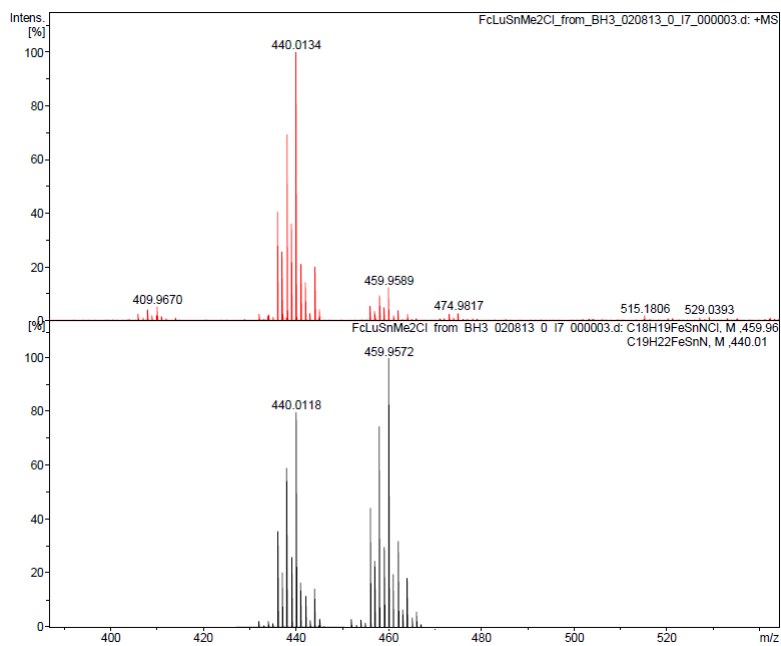
**Figure 3-9i.** <sup>1</sup>H NMR spectra of the reaction mixture from treatment of (pR)-**3** with [H(Et<sub>2</sub>O)<sub>2</sub>]<sup>+</sup>[B(C<sub>6</sub>F<sub>5</sub>)<sub>4</sub>]<sup>-</sup> in CD<sub>2</sub>Cl<sub>2</sub>.



**Figure 3-10.** Excerpt of the 2D-NOESY spectrum of compound (pR)-3 in  $C_6D_6$ .



**Figure 3- 11a.** High resolution MALDI-MS data of [(*pS*)-**4**]<sup>+</sup>[B(C<sub>6</sub>F<sub>5</sub>)<sub>3</sub>Me]<sup>-</sup> (left, pos. mode; right, neg. mode)



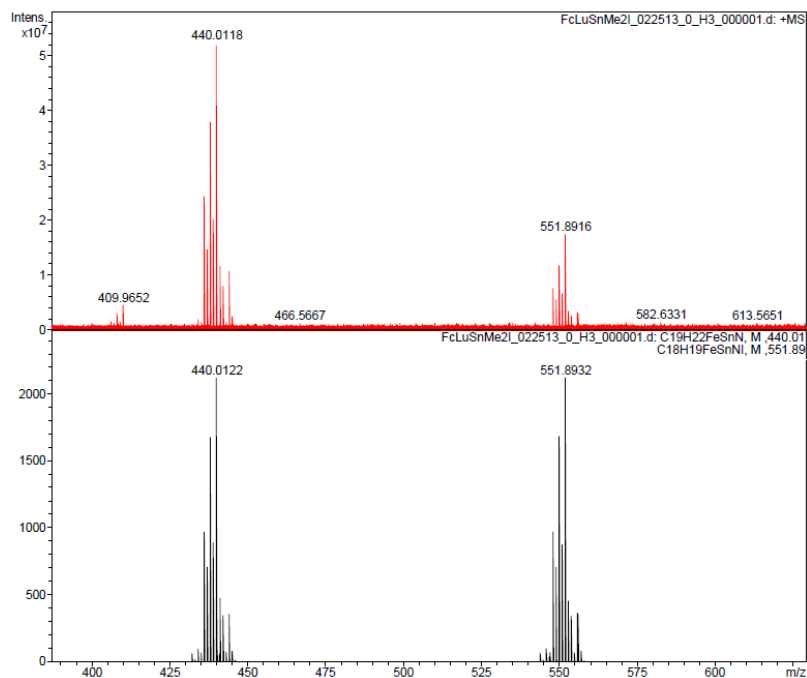


**Figure 3-11b.** High resolution (pos. mode) MALDI-MS data of (top) (pS)-4Cl and (bottom) (pS)-4I.

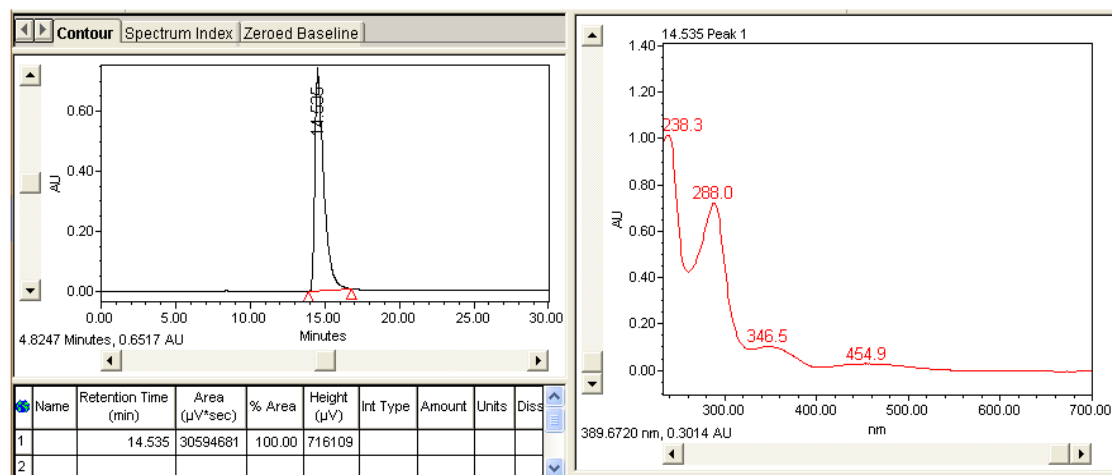


**Figure 3- 12.** HPLC trace (hexanes) and corresponding UV-visible spectrum of (pS)-2Sn.

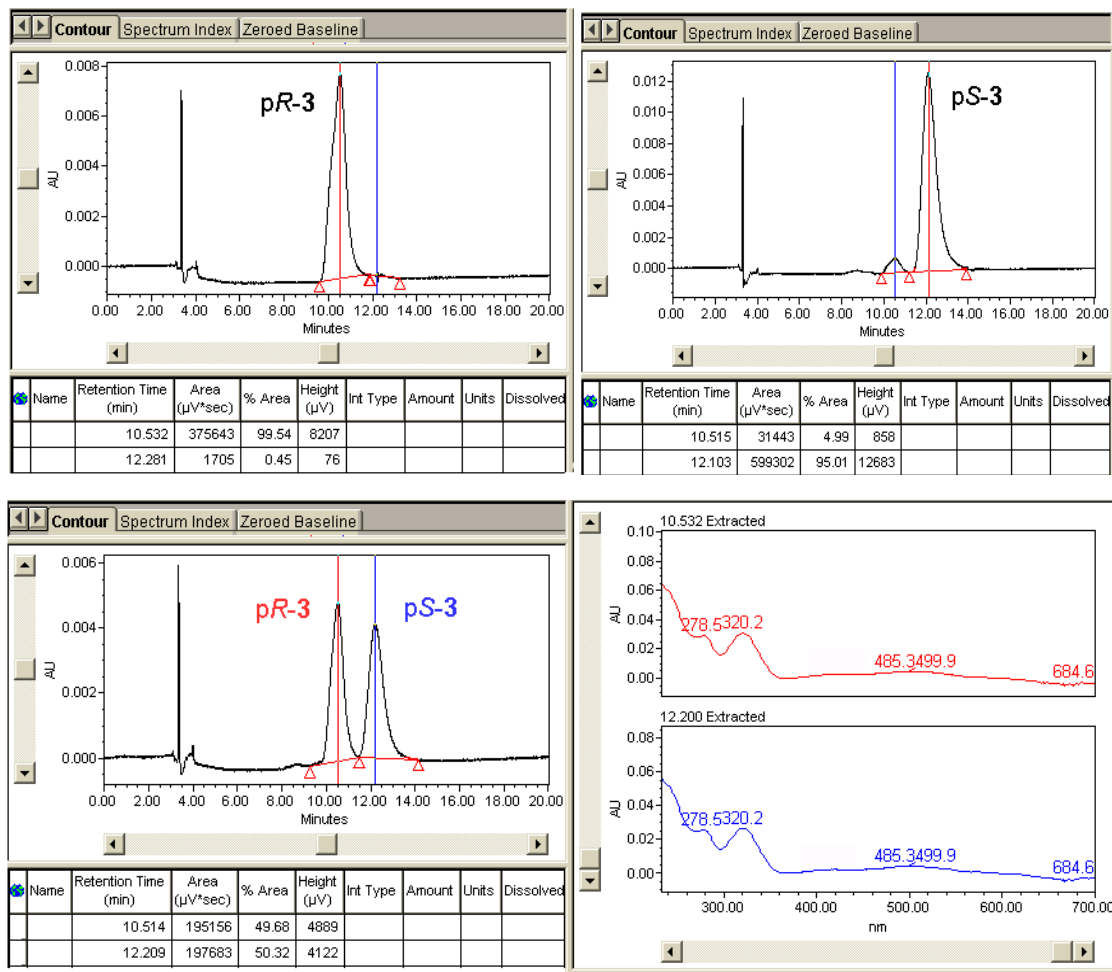


**Figure 3-13.** (top) HPLC traces of (pR)-3 and (pS)-3 (hexanes/THF: 93/7). (bottom) HPLC trace and the corresponding UV-visible spectra of racemic 3 (hexanes/THF: 93/7).

### 3.7 Notes and References

- Whisler, M. C.; MacNeil, S.; Snieckus, V.; Beak, P., *Angew. Chem. Int. Ed.* **2004**, *43*, 2206-2225.
- (a) Clososki, G. C.; Rohbogner, C. J.; Knochel, P., *Angew. Chem. Int. Ed.* **2007**, *46*, 7681-7684; (b) Mulvey, R. E., *Acc. Chem. Res.* **2009**, *42*, 743-755.
- (a) Hevia, E.; Honeyman, G. W.; Kennedy, A. R.; Mulvey, R. E.; Sherrington, D. C., *Angew. Chem. Int. Ed.* **2005**, *44*, 68-72; (b) Blair, V. L.; Carrella, L. M.; Clegg, W.; Klett, J.; Mulvey, R. E.; Rentschler, E.; Russo, L., *Chem. Eur. J.* **2009**, *15*, 856-863; (c) Balloch, L.; Garden, J. A.; Kennedy, A. R.; Mulvey, R. E.; Rantanen, T.; Robertson, S. D.; Snieckus, V., *Angew. Chem. Int. Ed.* **2012**, *51*, 6934-6937.
- Deng, W.-P.; Snieckus, V.; Metallinos, C., Chapter 2. Stereoselective Synthesis of Planar Chiral Ferrocenes. In *Chiral Ferrocenes in Asymmetric Catalysis: Synthesis and*

*Applications* Dai, L.-X.; Hou, X.-L., Eds. Wiley-VCH Verlag GmbH & Co. KGaA: Weinheim, Germany, 2010; pp 15-53.

5. (a) Colacot, T. J., *Chem. Rev.* **2003**, *103*, 3101; (b) Dai, L.-X.; Tu, T.; You, S.-L.; Deng, W.-P.; Hou, X.-L., *Acc. Chem. Res.* **2003**, *36*, 659; (c) Manoury, E.; Poli, R., Phosphine-Containing Planar Chiral Ferrocenes: Synthesis, Coordination Chemistry and Applications to Asymmetric Catalysis. In *Phosphorus Compounds: Advanced Tools in Catalysis and Material Sciences*, Peruzzini, M.; Gonsalvi, L., Eds. Springer Netherlands: 2011; Vol. 37, pp 121-149.

6. (a) deBiani, F. F.; Jäkle, F.; Spiegler, M.; Wagner, M.; Zanello, P., *Inorg. Chem.* **1997**, *36*, 2103-2111; (b) Zhang, F.; Morawitz, T.; Bieller, S.; Bolte, M.; Lerner, H.-W.; Wagner, M., *Dalton Trans.* **2007**, 4594-4598; (c) Mutseneck, E. V.; Bieller, S.; Bolte, M.; Lerner, H. W.; Wagner, M., *Inorg. Chem.* **2010**, *49*, 3540-3552.

7. (a) Grosche, M.; Herdtweck, E.; Peters, F.; Wagner, M., *Organometallics* **1999**, *18*, 4669-4672; (b) Heilmann, J. B.; Scheibitz, M.; Qin, Y.; Sundararaman, A.; Jäkle, F.; Kretz, T.; Bolte, M.; Lerner, H.-W.; Holthausen, M. C.; Wagner, M., *Angew. Chem. Int. Ed.* **2006**, *45*, 920-925; (c) Scheibitz, M.; Li, H.; Schnorr, J.; Sánchez Perucha, A.; Bolte, M.; Lerner, H.-W.; Jäkle, F.; Wagner, M., *J. Am. Chem. Soc.* **2009**, *131*, 16319-16329; (d) Braunschweig, H.; Breher, F.; Chiu, C. W.; Gamon, D.; Nied, D.; Radacki, K., *Angew. Chem. Int. Ed.* **2010**, *49*, 8975-8978.

8. Fournier, J. H.; Maris, T.; Wuest, J. D.; Guo, W. Z.; Galoppini, E., *J. Am. Chem. Soc.* **2003**, *125*, 1002-1006.

9. (a) Jensen, J. F.; Johannsen, M., *Org. Lett.* **2003**, *5*, 3025-3028; (b) Jensen, J. F.; Sotofte, I.; Sorensen, H. O.; Johannsen, M., *J. Org. Chem.* **2003**, *68*, 1258-1265; (c) Mamane, V., *Mini-Rev. Org. Chem.* **2008**, *5*, 303-312.

10. (a) Ruf, W.; Fueller, M.; Siebert, W., *J. Organomet. Chem.* **1974**, *64*, C45-C47; (b) Renk, T.; Ruf, W.; Siebert, W., *J. Organomet. Chem.* **1976**, *120*, 1-25; (c) Wrackmeyer, B.; Dörfler, U.; Herberhold, M., *Z. Naturforsch.* **1993**, *48 b*, 121-123; (d) Wrackmeyer, B.; Dörfler, U.; Rinck, J.; Herberhold, M., *Z. Naturforsch. B* **1994**, *49*, 1403-1406; (e) Appel, A.; Nöth, H.; Schmidt, M., *Chem. Ber.* **1995**, *128*, 621-626; (f) Reichert, A.; Bolte, M.; Lerner, H.-W.; Wagner, M., *J. Organomet. Chem.*, Ahead of Print.

11. (a) Jäkle, F.; Lough, A. J.; Manners, I., *Chem. Commun.* **1999**, 453-454; (b) Gamboa, J. A.; Sundararaman, A.; Kakalis, L.; Lough, A. J.; Jäkle, F., *Organometallics* **2002**, *21*, 4169-4181.

12. Eaborn, C., *J. Organomet. Chem.* **1975**, *100*, 43-57.

13. Zhao, Z.; Snieckus, V., *Org. Lett.* **2005**, *7*, 2523-2526.

14. Jäkle, F., Metallocene-Based Bidentate Lewis Acids. In *Group 13 Chemistry: From Fundamentals to Applications*, Shapiro, P. J.; Atwood, D., Eds. ACS: Washington, DC, 2002; Vol. Chapter 7.

15. Boshra, R.; Venkatasubbaiah, K.; Doshi, A.; Jäkle, F., *Organometallics* **2009**, *28*, 4141-4149.

16. (a) Sudhakar, P.; Thilagar, P., *J. Chem. Sci. (Bangalore, India)* **2013**, *125*, 41-49; (b) Chen, J.; Lalancette, R. A.; Jäkle, F., *Chem. Commun.* **2013**, *49*, 4893-4895; (c) Reichert, A.; Schmidt, J.; Bolte, M.; Wagner, M.; Lerner, H.-W., *Z. Anorg. Allg. Chem.*, Ahead of Print; (d) Siewert, I.; Vidovic, D.; Aldridge, S., *J. Organomet. Chem.* **2011**, *696*, 2528-2532.

17. The IUPAC-recommended Cahn–Ingold–Prelog (CIP) descriptors *pS* and *pR* are used throughout the manuscript to describe the planar chirality; see: Schlögl, K. *Top. Stereochem.* **1967**, *1*, 39
18. King, A. O.; Okukado, N.; Negishi, E.-i., *J. Chem. Soc., Chem. Commun.* **1977**, 683-684.
19. (a) Riant, O.; Argouarch, G.; Guillaneux, D.; Samuel, O.; Kagan, H. B., *J. Org. Chem.* **1998**, *63*, 3511-3514; (b) Pedersen, H. L.; Johannsen, M., *J. Org. Chem.* **2002**, *67*, 7982-7994; (c) Chen, J.; Venkatasubbaiah, K.; Pakkirisamy, T.; Doshi, A.; Yusupov, A.; Patel, Y.; Lalancette, R. A.; Jäkle, F., *Chem. Eur. J.* **2010**, *16*, 8861-8867.
20. Mantina, M.; Chamberlin, A. C.; Valero, R.; Cramer, C. J.; Truhlar, D. G., *J. Phys. Chem. A* **2009**, *113*, 5806-5812.
21. (a) For related organomercury compounds negative optical rotation values are consistently observed for the *pS*-isomer. For example,  $[\alpha]_D^{20}$  ( $c = 0.525$ ,  $\text{CHCl}_3$ ) =  $-395^\circ$  for the silylpyridine derivative (*pS*)-1-chloromercurio-2-(2-trimethylsilylpyrid-6-yl)ferrocene; see also: Djukic, J.-P.; Hijazi, A.; Flack, H. D.; Bernardinelli, G., *Chem. Soc. Rev.* **2008**, *37*, 406-425.
22. (a) Boshra, R.; Doshi, A.; Jäkle, F., *Angew. Chem. Int. Ed.* **2008**, *47*, 1134-1137; (b) Boshra, R.; Doshi, A.; Venkatasubbaiah, K.; Jäkle, F., *Inorg. Chim. Acta* **2010**, 162-166; (c) Thilagar, P.; Chen, J.; Lalancette, R. A.; Jäkle, F., *Organometallics* **2011**, *30*, 6734-6741; (d) Morgan, I. R.; Di Paolo, A.; Vidovic, D.; Fallis, I. A.; Aldridge, S., *Chem. Commun.* **2009**, 7288-7290.
23. We attribute this unusually large optical rotation to formation of an extended tricyclic ring system upon borane complexation.
24. The ee's for crude (*pR*)-**3** and (*pS*)-**3** were determined to be 90 and 58%, respectively.
25. Massey, A. G.; Park, A. J., *J. Organomet. Chem.* **1964**, *2*, 245-250.
26. Narula, C. K.; Nöth, H., *Inorg. Chem.* **1985**, *24*, 2532-9.
27. When (*pS*)-**2Sn** was treated with one equivalent of  $\text{PhBCl}_2$  in hexanes solution, a Me group on Sn was replaced with a chloro substituent and the resulting product, (*pS*)-**4Cl**, precipitated as an orange solid. Switching from hexanes to a 1:1 mixture of hexanes and toluene resulted in a mixture of (*pS*)-**4Cl** and (*pR*)-**3**. Clean conversion to the final product (*pR*)-**3** was observed with 2 equivs of  $\text{PhBCl}_2$ , which resulted in  $\text{Me}_2\text{SnCl}_2$  and  $\text{Me}_3\text{SnCl}$  as byproducts.
28. (a) Cunningham, A. F., *J. Am. Chem. Soc.* **1991**, *113*, 4864-4870; (b) Karlsson, A.; Broo, A.; Ahlberg, P., *Can. J. Chem.* **1999**, *77*, 628-633.
29. (a) De Vries, T. S.; Prokofjevs, A.; Vedejs, E., *Chem. Rev.* **2012**, *112*, 4246-4282; (b) Solomon, S. A.; Del Grosso, A.; Clark, E. R.; Bagutski, V.; McDouall, J. J. W.; Ingleson, M. J., *Organometallics* **2012**, *31*, 1908-1916; (c) Ishida, N.; Moriya, T.; Goya, T.; Murakami, M., *J. Org. Chem.* **2010**, *75*, 8709-8712; (d) Hatakeyama, T.; Hashimoto, S.; Seki, S.; Nakamura, M., *J. Am. Chem. Soc.* **2011**, *133*, 18614-18617.
30. We also explored the reactivity toward  $\text{BH}_3$ , which is a much smaller borane. Indeed, when (*pS*)-**2Sn** was mixed with an excess of  $\text{Me}_2\text{S}\cdot\text{BH}_3$  in  $\text{CDCl}_3$  at room temperature, ca. 20% of (*pS*)-**2Sn** was converted to the borane adduct (*pS*)-**2Sn** $\cdot\text{BH}_3$  according to  $^1\text{H}$  and  $^{11}\text{B}$  NMR analysis; in a follow-up reaction with the  $\text{CDCl}_3$  solvent, complete conversion to (*pS*)-**4Cl** occurred over a period of 48 h.

31. Jutzi, P.; Müller, C.; Stammler, A.; Stammler, H. G., *Organometallics* **2000**, *19*, 1442-1444.
32. Gros, P.; Viney, C.; Fort, Y., *Synlett* **2002**, *3*, 628-630.
33. Guillaneux, D.; Kagan, H. B., *J. Org. Chem.* **1995**, *60*, 2502-2505.
34. Krossing, I., *Chem. Eur. J.* **2001**, *7*, 490-502.

## Chapter 4 Synthesis and Characterization of Planar Chiral Lewis Pairs Derived from Pyridylferrocenes<sup>a</sup>

### 4.1 Introduction

As already mentioned in Chapter 1, the combination of sterically demanding electron-deficient Lewis acids (organoboranes, organoaluminum species, silylium cations, etc.) and bulky Lewis bases (phosphines, amines, pyridines and carbenes, etc.) results in so-called “frustrated Lewis pairs” (FLPs).<sup>1,2,3</sup> For example, Stephan *et al.* investigated a system consisting of tris(pentafluorophenyl)borane and 2,6-dimethylpyridine (**A**).<sup>4</sup> The Lewis adduct exists in thermal equilibrium with the free Lewis acid and base and is therefore capable of activating small molecules such as dihydrogen or THF.

In recent work in our group, we have pursued planar chiral ferrocene-based Lewis acids and their applications in small molecule activation and catalysis.<sup>5,6</sup> In chapter 3, we discussed the study of developing a stereoselective process for the synthesis of heterocycles.<sup>5e</sup> The goal of this chapter is to introduce a new class of planar chiral Lewis pairs based on the pyridylferrocenylborane framework. We postulated that if the B-N interaction in heterocycles (**B**) is sufficiently weakened, a thermally labile or “frustrated” planar chiral Lewis pair could be generated. We therefore prepared a series of new planar chiral Lewis pairs, in which we varied the steric demand of the pyridyl Lewis base and the steric and electron effect of the substituents attached to the borane Lewis acid moiety. We also investigated the effect of ferrocene oxidation on the Lewis pair properties.

---

<sup>a</sup> This chapter is adapted from a journal publication

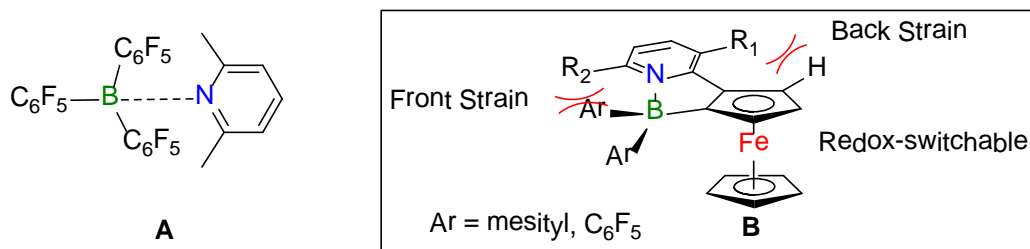
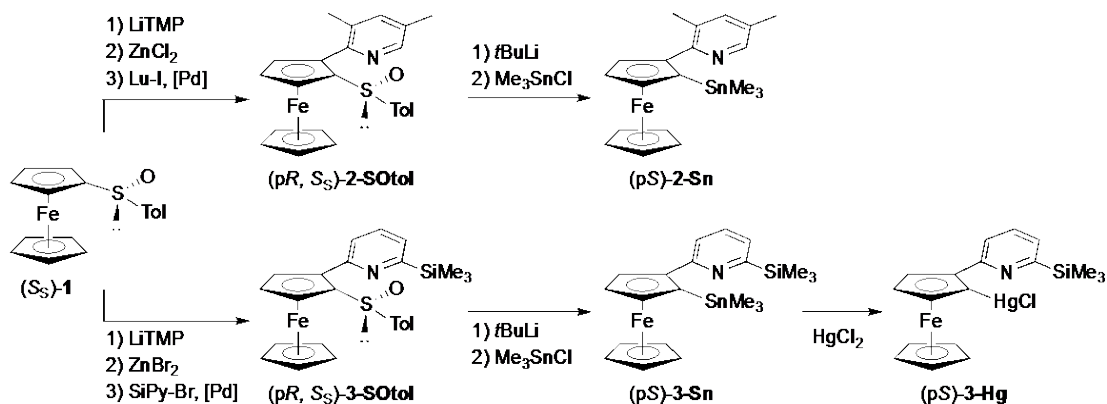


**Figure 4-1.** Examples of FLPs and planar chiral ferrocenes

## 4.2 Synthesis and Characterization

We explored two different methods for introducing steric bulk in the heterocyclic system **B**. A methyl group in the 5-position of the pyridyl ring was expected to result in steric repulsion with the hydrogen in 5-position of the substituted Cp ring, forcing the pyridyl moiety to rotate out of the Cp plane and thereby generating steric strain (back strain). In a second approach, we introduced a SiMe<sub>3</sub> substituent in the 6-position of the pyridyl group, which should directly interfere with the B-N bond formation (front strain). The corresponding stannylated or mercurated precursors, (*pS*)-2-(3,5-dimethylpyrid-2-yl)-1-(trimethylstannyl)ferrocene (**2-Sn**)<sup>5e</sup> and (*pS*)-2-(2-trimethylsilylpyrid-6-yl)-1-(chloromercurio)ferrocene (**3-Hg**), were prepared in enantiomerically pure form using the synthetic protocols outlined in Scheme 4-1.



Scheme 4-1. Synthesis of planar chiral pyridylferrocenes (pS)-2-Sn and (pS)-3-Hg (Lu = lutidyl or 3,5-dimethylpyrid-2-yl; SiPy-Br = 2-bromo-6-trimethylsilylpyridine; TMP = tetramethylpiperidyl)

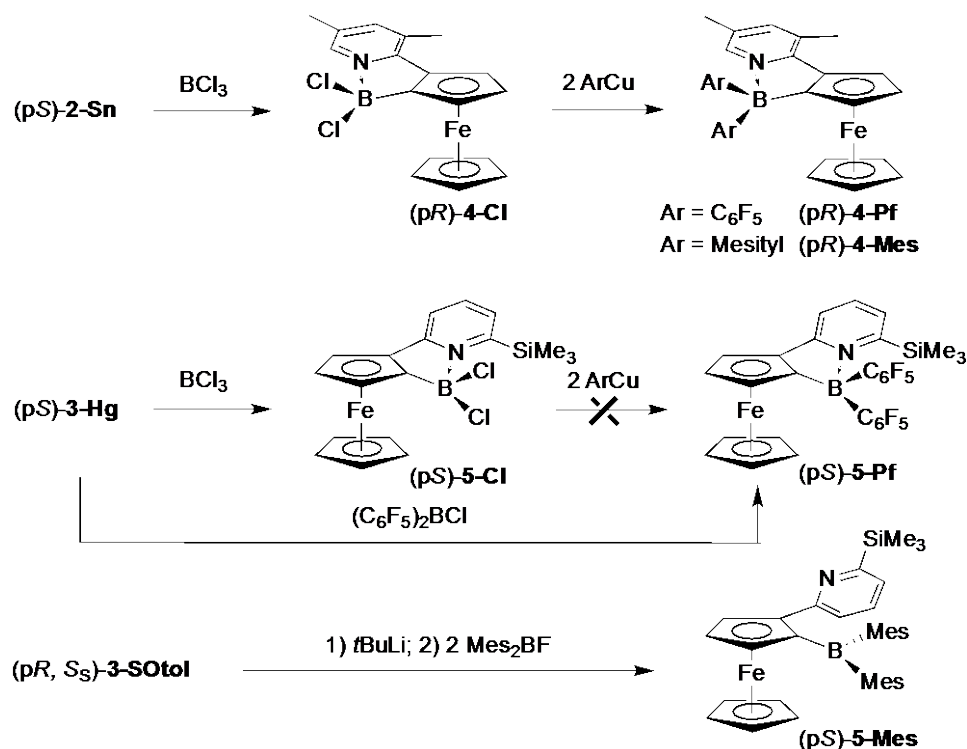
Following Kagan's protocol (S<sub>S</sub>)-1 was prepared from tri-*n*-butylstannylderrocene and then stereoselectively lithiated with LiTMP.<sup>7</sup> The chiral sulfinylferrocene species (pS, S<sub>S</sub>)-2-(3,5-dimethylpyrid-2-yl)-1-(*p*-tolylsulfinyl)ferrocene (**2-SOtol**)<sup>5c</sup> and (pS, S<sub>S</sub>)-2-(2-trimethylsilylpyrid-6-yl)-1-(*p*-tolylsulfinyl)ferrocene (**3-SOtol**) were obtained by Negishi coupling<sup>8</sup> of the corresponding zincated ferrocene species with 2-iodo-3,5-dimethylpyridine<sup>9</sup> and 2-bromo-6-trimethylsilylpyridine (SiPy-Br)<sup>10</sup>, respectively. Compounds **2-SOtol** and **3-SOtol** were then reacted with *tert*-BuLi at -78 °C, followed by treatment with a slight excess of trimethyltin chloride. After purification by column chromatography, <sup>1</sup>H NMR analysis revealed the desired stannylated product in the major fraction, but in each case it was accompanied by a small amount of protonated pyridylferrocene as a byproduct. While analytically pure **2-Sn** was readily obtained by recrystallization from MeOH, the more soluble **3-Sn** could not be isolated by crystallization. Hence, the crude product was treated with one equivalent of HgCl<sub>2</sub> in

acetone to give (*pS*)-1-(chloromercurio)-2-(2-trimethylsilylpyrid-6-yl)ferrocene (**3-Hg**), which was crystallized from hexanes and isolated in an overall yield of 71%.

Several strategies are available for the introduction of diarylborane moieties: The stannylated or mercurated ferrocene can either be reacted directly with a borane  $\text{Ar}_2\text{BX}$  ( $\text{X} = \text{Br}, \text{Cl}$ ) or it can be converted first to the ferrocenyldihaloborane, followed by reaction with a suitable organometallic reagent  $\text{ArM}$  (Scheme 4-2). The second approach tends to be more effective for the introduction of bulky aryl groups. Treatment of compound **2-Sn** with  $\text{BCl}_3$  in hexanes at  $-37\text{ }^\circ\text{C}$  led to almost quantitative conversion to the dichloroboryl species **4-Cl** according to  $^1\text{H}$  NMR analysis. After removing all volatile components under high vacuum the crude product was reacted with 2 equivs of  $\text{C}_6\text{F}_5\text{Cu}$  in toluene at  $80\text{ }^\circ\text{C}$  to afford (*pR*)-2-[bis(pentafluorophenyl)boryl]-1-(3,5-dimethylpyrid-2-yl)ferrocene (**4-Pf**), which was isolated as a purple solid in 66% yield after crystallization from hexanes. Using a similar procedure, **4-Mes** was obtained as a red solid from reaction of **4-Cl** with  $\text{MesCu}$  ( $\text{Mes} = 2,4,6\text{-trimethylphenyl}$ ). **4-Mes** was isolated in 51% yield by silica gel column chromatography using hexanes as the eluent.

Reaction of **3-Hg** with 1.1 equiv of  $\text{BCl}_3$  in hexanes resulted in formation of the corresponding (*pR*)-2-(dichloroboryl)-1-(2-trimethylsilylpyrid-6-yl)ferrocene (**5-Cl**) in a yield of 80% after recrystallization (see Supporting Information). However, subsequent treatment with two equivs of  $\text{C}_6\text{F}_5\text{Cu}$  did not yield the expected product, **5-Pf**; according to an NMR analysis of the crude product only one of the chloride substituents could be replaced with a  $\text{C}_6\text{F}_5$  group, even at elevated temperature, which might be due to steric hindrance. On the other hand, direct reaction of **3-Hg** with  $(\text{C}_6\text{F}_5)_2\text{BCl}$  proceeded readily at room temperature. The product, **5-Pf**, was obtained as a purple solid that proved to be

highly soluble in hexanes. Single crystals were grown from a minimum amount of hexanes over a period of a month at  $-37\text{ }^{\circ}\text{C}$  (34 % yield). Compound **5-Mes** was obtained using a different route, by lithiation of **3-SOtol** with *tert*-BuLi at  $-78\text{ }^{\circ}\text{C}$ , followed by treatment with a slight excess of  $\text{Mes}_2\text{BF}$ . Column chromatography on aluminum oxide with ether/hexanes (1/1) as the eluent, followed by recrystallization from hot methanol, provided the product as purple needle-shaped crystals in 39% yield.



**Scheme 4-2.** Synthesis of planar chiral 2-boryl-1-pyridylferrocenes (*pR*)-**4-Pf**, (*pR*)-**4-Mes**, (*pS*)-**5-Pf**, and (*pS*)-**5-Mes**.

The stereochemical assignments were confirmed by single crystal X-ray diffraction analysis (*vide infra*) and are consistent with our earlier studies on the borylation of pyridylferrocenes.<sup>5e</sup> With the stannylderrocene (*pS*)-**2-Sn** as the precursor the planar chirality of the borane product is inverted and optical rotations of  $[\alpha]_{\text{D}}^{20}$  ( $c = 0.115$ ,  $\text{CHCl}_3$ ) =  $+2078^{\circ}$  and  $[\alpha]_{\text{D}}^{20}$  ( $c = 0.10$ ,  $\text{CH}_2\text{Cl}_2$ ) =  $+1900^{\circ}$  were measured for (*pR*)-**4-Pf**

and (*pR*)-**4-Mes**, respectively. This result is attributed to attack of the borane at the Cp-H3 position of the substituted Cp ring, followed by a proton shift that results in the rearranged species (*pR*)-**4-Cl** as discussed previously.<sup>5e</sup> In contrast, reaction of the mercurioferrocene (*pS*)-**3-Hg** with (C<sub>6</sub>F<sub>5</sub>)<sub>2</sub>BCl occurs through direct Hg-C bond cleavage and results in retention of stereochemistry to give (*pS*)-**5-Pf**. Consequently, an optical rotation of  $[\alpha]_D^{20} (c = 0.10, \text{CH}_2\text{Cl}_2) = -1496^\circ$  of opposite sign was measured. Similarly, for (*pS*)-**5-Mes**, retention of stereochemistry results in an optical rotation of  $[\alpha]_D^{20} (c = 0.10, \text{CH}_2\text{Cl}_2) = -410^\circ$ . The lower absolute value of the optical rotation of (*pS*)-**5-Mes** is attributed to the open chain structure that is adopted (*vide infra*). To further confirm the enantiomeric purity of the pyridylferrocene derivatives, chiral HPLC measurements were carried out. **4-Pf** was selected for optimizing the conditions for separation since both enantiomers were available. For a sample of (*pR*)-**4-Pf** with about 40% ee the HPLC trace showed full separation into the individual enantiomers. All of the other compounds were measured under similar conditions and just one signal was observed, which could be correlated to the actual compound based on the corresponding UV-Vis absorption spectrum (PDA detector).

<sup>11</sup>B NMR resonances at 3.3 ppm (**4-Pf**), 2.5 (**4-Mes**), and -1.5 (**5-Pf**) suggest a tetracoordinate configuration for the boron center, even in the case of the bulky mesityl groups in **4-Mes** or the trimethylsilyl moiety in **5-Pf**. Only when we combined the bulky Mes group on boron with a 6-silyl substituent on the pyridyl group in **5-Mes** did we obtain a frustrated Lewis pair as evident from an <sup>11</sup>B NMR shift of 77.1 ppm. The <sup>19</sup>F NMR spectrum of **4-Pf** shows two sets of signals, which confirms that there is no exchange of the *endo*- and *exo*-C<sub>6</sub>F<sub>5</sub> rings, but the rotation of each ring about the C<sub>Pf</sub>-B

bond is not hindered. In contrast, **5-Pf** shows four sets of signals for the *ortho*- and *meta*-fluorines of the C<sub>6</sub>F<sub>5</sub> rings, indicating a higher degree of steric congestion, but still a closed B-N heterocyclic structure. The <sup>1</sup>H and <sup>13</sup>C NMR spectra are generally unremarkable; they are consistent with the proposed structures and show the typical pattern of 1,2-disubstituted ferrocenes. Of note is that the signal for the free Cp ring is upfield shifted to 3.60-3.67 ppm for all the compounds with a closed structure, which is attributed to the shielding effect of the aryl group in *endo*-position.

To further explore the strength of the B-N interaction we carried out X-ray diffraction experiments on single crystal of **4-Pf**, **4-Mes**, **5-Pf** and **5-Mes** (Figure 4-2). The X-ray structure of **4-Pf** shows the pyridine ring to be almost coplanar with the substituted Cp ring (Py//Cp 3.7(1)°). The B-N interaction is strong as evidenced by a relatively short distance of 1.631(3) Å, which falls into the classic B-N donor-acceptor bond range. Apparently the B-N interaction overcomes any back strain due to the methyl group on the 3-position of the pyridine ring. The B-N distance in compound **5-Pf** appears to be slightly longer at 1.647(4) Å, but this difference is not significant when applying 3σ error limits. Remarkably, however, the trimethylsilyl group is strongly bent away from the boryl moiety at an angle N1-C15-Si1 of 128.9(2)° that deviates significantly from the ideal angle of an sp<sup>2</sup> ring carbon.<sup>11</sup> Enhanced steric strain is also reflected in a larger tilt of the two Cp rings in **5-Pf** (7.3(1)°) relative to **4-Pf** (4.9(2)°). We conclude that despite the steric hindrance and strong distortion of the trimethylsilyl group, a B-N interaction to form the heterocycle remains favorable. The geometry for the mesityl derivative **4-Mes** is very similar to that of **4-Pf**, with a slightly greater B-N bond distance of 1.653(4) Å that is similar to that of **5-Pf**. These results are fully consistent with our solution NMR studies,

suggesting that the introduction of bulkier groups on boron has little impact on the B-N interaction. To our delight, for the most congested system **5-Mes**, single crystal X-ray diffraction analysis revealed a fully open conformation without any B-N interaction, which is consistent with the  $^{11}\text{B}$  NMR shift of 77.1 ppm in solution. A detailed investigation of the X-ray crystal structure indicated that the pyridyl group rotates away from the borane moiety to release some of the steric strain, resulting in a very long distance B-N distance of 4.468(4) Å. In this particular conformation further stabilization is achieved by a  $\pi$ -interaction between the pyridyl ring and one of the mesityl rings. The arene rings are oriented almost coplanar ( $11.1(1)^\circ$ ) and the shortest interatomic distance is  $\text{C11}\cdots\text{C21} = 3.054(3)$  Å. The  $\text{N1-C15-Si1}$  angle ( $114.17(18)^\circ$ ) is much smaller than that in **5-Pf** since steric strain due to B-N adduct formation is absent. **5-Mes** is characterized as a frustrated Lewis pair given that the Lewis base component is accessible and binds to boron in **5-Pf**, while the borane Lewis acid component binds to the less hindered dimethylpyridine in **4-Mes**. Thus, the Lewis acid and base sites are unquenched and cannot form a complex in **5-Mes** only due to steric constraints.

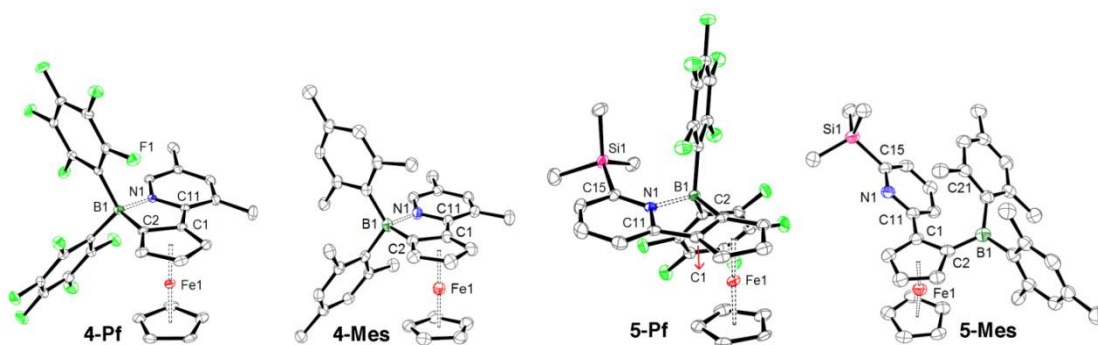


**Figure 4-2.** Ortep plots of (p*R*)-**4-Pf**, (p*R*)-**4-Mes**, (p*S*)-**5-Pf** and (p*S*)-**5-Mes** (50% thermal displacement ellipsoids).

Hydrogen atoms are omitted for clarity. Selected interatomic distances (Å) and angles ( $^\circ$ ): **4-Pf**: B1-N1 1.631(3), B1-C2 1.606(3), C1-C2-B1 109.31(17), C2-B1-N1 97.07(15), B1-N1-C11 112.61(16), N1-C11-C1 109.87(16), C11-C1-C2 111.04(17), Cp//Cp 4.9(2), Py//Cp 3.7(1). **4-Mes**: B1-N1 1.653(4), B1-C2 1.641(4), C1-C2-B1 110.4(2), C2-B1-N1

94.6(2), B1-N1-C11 114.4(2), N1-C11-C1 109.1(2), C11-C1-C2 111.5(2), Cp//Cp 6.8(2), Py//Cp 4.3(2). **5-Pf**: B1-N1 1.647(4), B1-C2 1.601(4), C1-C2-B1 108.9(3), C2-B1-N1 98.3(2), B1-N1-C11 110.4(2), N1-C11-C1 111.0(2), C11-C1-C2 111.4(3), N1-C15-Si1 128.9(2), Cp//Cp 7.3(1), Py//Cp 7.4(1). **5-Mes**: B1...N1 4.468(4), B1-C2 1.545(4), C1-C2-B1 131.0(2), N1-C11-C1 115.5(2), C11-C1-C2 128.0(2), N1-C15-Si1 114.17(18), Cp//Cp 6.2(2), Py//Cp 39.6(1), Py//Mes 11.1(1).

Compounds **4-Ar** (Ar = Mes, Pf) turned out to be quite robust and perfectly stable to air and moisture. Heating an NMR sample of **4-Pf** in  $d^8$ -toluene to 80 °C did not result in coalescence of the distinct sets of  $^{19}\text{F}$  NMR signals for each of the  $\text{C}_6\text{F}_5$  rings. Moreover, a  $^{19}\text{F}/^{19}\text{F}$  EXSY spectrum showed no exchange peaks even at elevated temperature (80 °C,  $d^8$ -toluene, mixing time: 1 s). This indicates that the B-N interaction is so strong that the B-N cycle does not open up even at high temperature. We also examined the reactivity of **4-Pf** with 4 bars of  $\text{H}_2$  at 100 °C in toluene, but no reaction was observed. Even the treatment with one equiv of Jutzi's acid,  $[\text{H}(\text{OEt}_2)_2]^+[\text{B}(\text{C}_6\text{F}_5)_4]^-$ , did not result in protonation of the pyridyl nitrogen with liberation of the tricoordinate boron center. All of the above experiments support the notion that the B-N interaction in **4-Pf** is exceptionally strong and prevents this system from behaving as an FLP.

We hypothesized that the additional steric strain that is present in compound **5-Pf** according to its X-ray structure should lead to enhanced reactivity. Upon heating of an NMR sample in  $d^8$ -toluene to 80 °C, the Pf ring that experiences less steric hindrance (tentatively assigned as *exo*-Pf) coalesces into one set of signals, while the other Pf ring (in the *endo*-position) retains two sets of signals. More importantly, a  $^{19}\text{F}/^{19}\text{F}$  EXSY spectrum (80 °C, mixing time: 1 s; Figure 4-3) showed clearly the presence of exchange peaks between the fluorine atoms of one Pf group and those of the other one. This observation strongly supports the notion that the B-N bond is cleaved at high

temperature, and the ensuing rapid rotation about the B-C<sub>Cp</sub> leads to exchange of the Pf groups in *exo*- and *endo*-position. The <sup>11</sup>B NMR resonance at 80 °C is almost identical to that at room temperature, indicating that the thermodynamic equilibrium still favors the tetracoordinate boron species, although, the exchange was facilitated at elevated temperature.

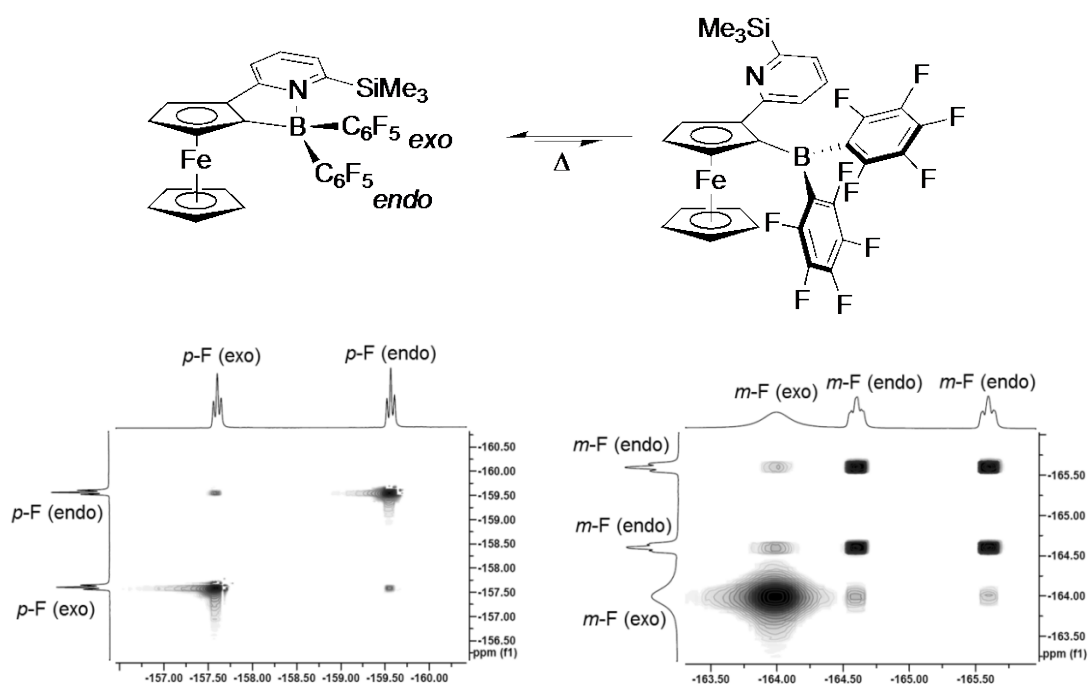
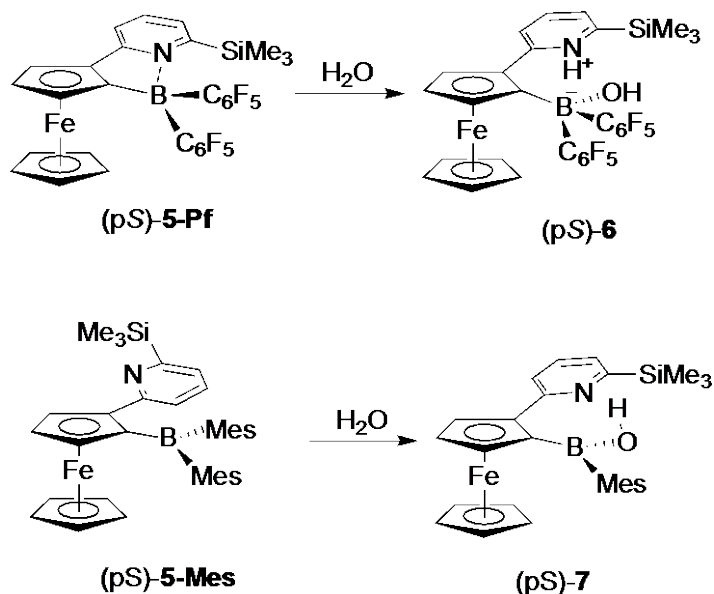


**Figure 4-3.** Sections of the <sup>19</sup>F-<sup>19</sup>F EXSY NMR spectrum of **5-Pf** and illustration of the equilibrium between ‘closed’ and ‘open’ forms of **5-Pf**.

In the case of the more strained species **5-Pf**, treatment with 4 bars of H<sub>2</sub> gas at 100 °C in toluene for 24 h did not result in any detectable hydrogenation products. Even in the presence of the ketamine *N*-(1-phenylethylidene)aniline as a hydrogen acceptor hydrogen activation and subsequent hydrogenation of the substrate could not be observed (4 bars of H<sub>2</sub> at 100 °C in toluene for 2 days). However, more potent reagents do lead to ring-opening. Unlike compounds **4-Pf** and **4-Mes**, when **5-Pf** was passed through a short plug

of silica gel, a new ring-opened species formed readily (Scheme 4-3). The  $^1\text{H}$  NMR spectrum of the product (**6**) showed the presence of 2 additional resonances at 18.24 and 3.23 ppm, which integrate as one proton each and correspond to the pyridinium proton and the OH group on boron. Single crystals of **6** were obtained from a 1:1 mixture of hexanes/ether and the X-ray structure unambiguously confirmed the addition of a water molecule (Figure 4-4). Hydrogen bonding occurs from the pyridinium donor Py-H1<sub>N</sub> to O1 as the acceptor as evident from the distance O1...H1<sub>N</sub> of 1.68(2) Å. A comparison of the X-ray data of **5-Pf** and **6** reveals significant release of ring strain upon addition of the water molecule. After ring-opening with H<sub>2</sub>O, the N1-C15-Si1 angle decreases from 128.9(2)° to 119.6(2)°, which is very close to the ideal value of 120° for a trigonal environment.<sup>12</sup> When the frustrated Lewis pair **5-Mes** was purified on a short plug of alumina gel, a later fraction was identified as compound **7**, generated by B-C<sub>Mes</sub> bond cleavage of **5-Mes** with one equivalent of H<sub>2</sub>O. The resulting borinic acid moiety in **7** forms an intramolecular hydrogen bond with the pyridine moiety. In contrast to compound **6**, the nitrogen in compound **7** serves as the hydrogen bond acceptor for the borinic acid proton (N1...H1 1.82(3) Å). The position of the acidic proton was unequivocally identified in the difference Fourier electron density contour map in Figure 4-5, which confirmed the connectivity between the highest electron residue (H1) and O1. The acidic proton in the crystal lattice could be refined without distance and displacement restraints and without significant geometry change compared to the riding mode. Interestingly, the  $^1\text{H}$  NMR resonance of the acidic proton in CDCl<sub>3</sub> was observed at 13.9 ppm, which is comparable to the protonation product of the pyridyl ferrocene derivative (p*S*)-2-(3,5-dimethylpyrid-2-yl)-1-(trimethylstannyl)ferrocene] ( $\delta$  = 12.2 ppm), but

strongly downfield shifted relative to typical H NMR resonances of borinic acids (6.0 – 7.0 ppm).<sup>13</sup>



**Scheme 4-3.** Reactions of (pS)-5-Pf and (pS)-5-Mes with H<sub>2</sub>O.

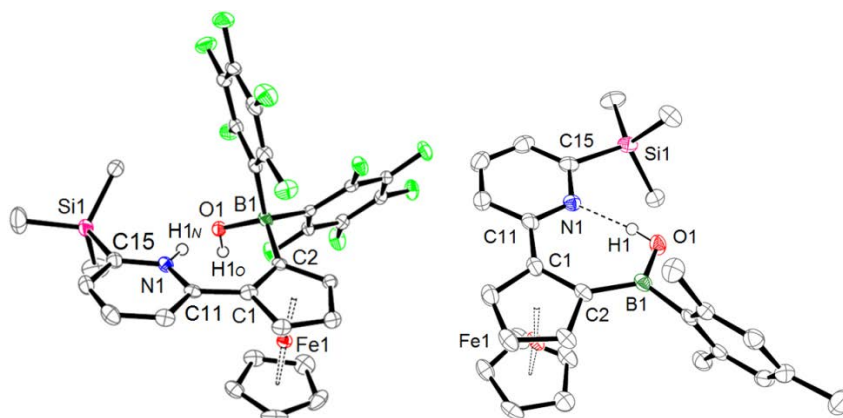


**Figure 4-4.** Ortep plot for the ring-opened products **6** and **7** (50% thermal displacement ellipsoids).

Hydrogen atoms are omitted for clarity except for those of the N-H and O-H groups. Selected interatomic distances (Å) and angles (°): For **6**: B1-C2 1.608(3), N1-H1<sub>N</sub> 0.92(2), O1...H1<sub>N</sub> 1.68(2), N1...O1 2.592(2), B1...N1 3.178(3), C1-C2-B1 131.11(17), C2-B1-O1 111.93(18), N1-C15-Si1 119.6(2), Cp//Cp 4.0(2), Py//Cp 8.7(1). For **7**: B1-C2 1.560(3), O1-H1 0.81(2), N1...H1 1.82(3), N1...O1 2.626(2), B1...N1 3.208(3), C1-C2-B1 134.19(18), C2-B1-O1 122.03(19), N1-C15-Si1 116.16(15), Cp//Cp 5.8(1), Py//Cp 5.3(1).

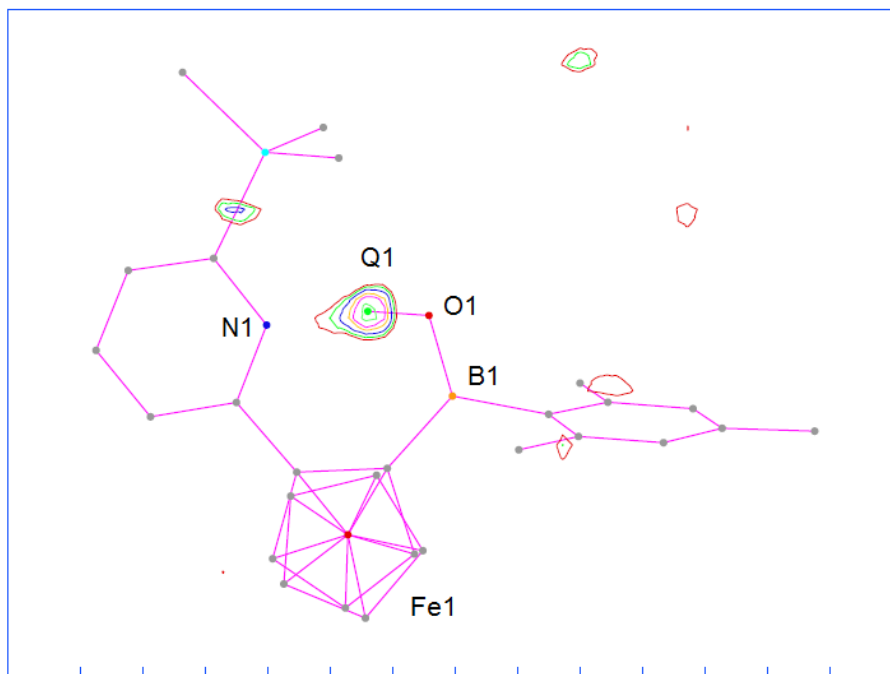


**Figure 4-5.** Difference Fourier electron density contour map of compound **7** before adding the acidic proton into the model. The highest electron residue (Q1) is located close to O1, clearly indicating that the acidic proton is bound to O1 rather than the pyridyl moiety in the solid state.

The presence of the redox-active ferrocenyl moieties provides another possible handle to tune the B-N interaction electronically. At the same time, the oxidation potential of the iron center provides an important indication of the Lewis acid strength of the boryl group. Compounds **4-Pf** and **5-Pf** show a similar reversible oxidation event at +120 and +134 mV, respectively, relative to the ferrocene/ferrocenium redox couple (Figure 4-6). These values are close to the potential measured for the Lewis acid-base complex of  $\text{NpFcB}(\text{C}_6\text{F}_5)_2$  with pyridine (+90 mV).<sup>5c</sup> They are significantly lower than for related uncomplexed ferrocenylboranes [cf.  $\text{NpFcB}(\text{C}_6\text{F}_5)_2$  <sup>5c</sup> +460 mV,  $\text{FcB}(\text{C}_6\text{F}_5)_2$  <sup>14</sup> +450 mV], in which an interaction between the electron-deficient borane and the iron center results in large anodic shifts of the Fe redox potential. As expected, compound **4-Mes** undergoes a reversible redox event at a more cathodic value (−174 mV) in comparison to

**4-Pf** (+120 mV), indicating that the more electron rich Mes groups decrease the electron density at the boron and iron centers. For the respective open-chain system **5-Mes** a significant interaction of the ferrocene unit and the tricoordinate boron is evident from the much larger redox potential of +145 mV (cf. +181 mV for FcBMes<sub>2</sub> in acetonitrile)<sup>15</sup> in comparison to that for **4-Mes**.

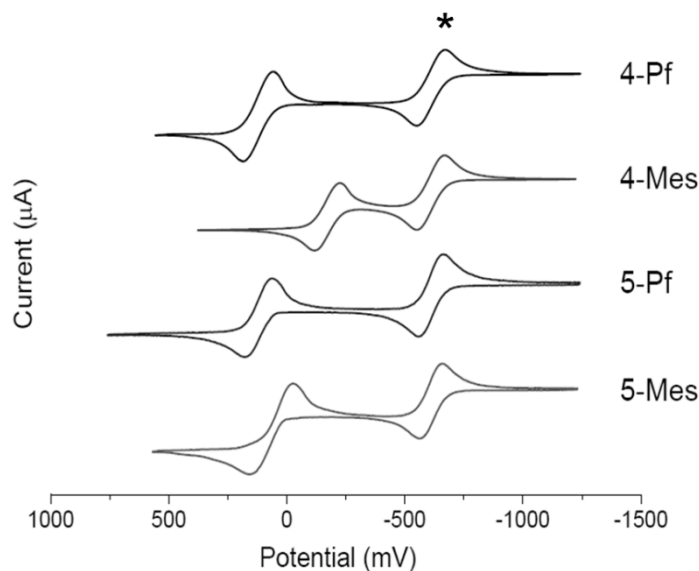
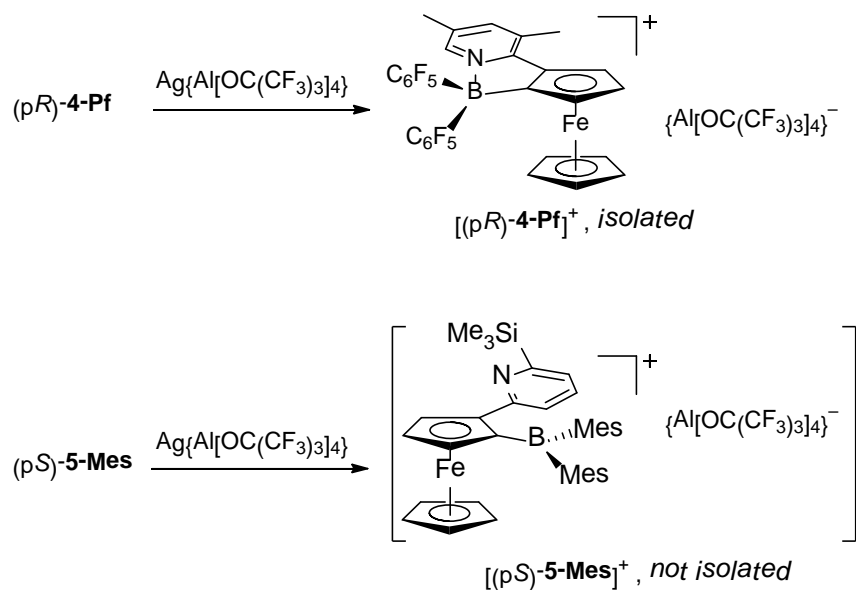


**Figure 4-6.** Cyclic voltammograms of compounds **4-Pf**, **4-Mes**, **5-Pf** and **5-Mes** (CH<sub>2</sub>Cl<sub>2</sub>, 0.05 M Bu<sub>4</sub>N[B[C<sub>6</sub>H<sub>3</sub>(CF<sub>3</sub>)<sub>2</sub>]<sub>4</sub>]); reported versus Fc/Fc<sup>+</sup>, which is taken as +610 mV versus Cp\*<sub>2</sub>Fe/Cp\*<sub>2</sub>Fe<sup>+</sup> (indicated with an asterisk, Cp\* = pentamethylcyclopentadienyl) as an internal reference.

Preparative oxidation of compound **4-Pf** to the corresponding ferrocenium species was accomplished by treatment with the silver derivative of Krossing's salt,<sup>16</sup> [Ag(CH<sub>2</sub>Cl<sub>2</sub>)]<sup>+</sup>[Al[OC(CF<sub>3</sub>)<sub>3</sub>]<sub>4</sub>]<sup>-</sup>. The product was isolated in the form of green crystals that were examined by X-ray diffraction analysis. The structure of one of two independent molecules of **4-Pf**<sup>+</sup> in the unit cell is shown in Figure 4-7. The major difference relative to neutral **4-Pf** is that the Cp<sub>CENT</sub>...Cp<sub>CENT</sub> distance increases from 3.3132(12) to 3.439(5) Å as expected for formation of a ferrocenium species. However,

the B-N distance of 1.644(9) Å proved to be very similar to that of the neutral precursor (**4-Pf** 1.631(3) Å). Upon oxidation, the pyridyl moiety would be expected to display a decreased Lewis basicity. However, prior studies show that the Lewis acidity of ferrocenylboranes is strongly enhanced upon oxidation of the iron center.<sup>17</sup> Based on the crystal structure data it appears that cancellation of these two effects results in a B-N interaction that is similar in strength to that of the neutral species. In this respect, the open system **5-Mes** was also oxidized with Krossing's Ag salt. The color of the mixture turned immediately from red to green and a precipitate formed, which was removed by filtration. <sup>1</sup>H NMR of the crude product showed the typical signals for an oxidized species in the region between 28 and 45 ppm, while the <sup>11</sup>B NMR resonance at around 65 ppm (**5-Mes**  $\delta = 77.1$  ppm) indicated that the boron remained tricoordinate. The combined evidence suggests that the oxidation of **5-Mes** does not likely promote the coordination from pyridyl to the boryl unit. Attempts to isolate the oxidized product failed due to the high reactivity. The color of a MALDI sample turned from green to red immediately after exposure to air. The high resolution mass spectrum indicated the species with oxygen insertion between boron and C<sub>Cp</sub> as the major decomposed product.



**Scheme 4-4.** Preparative oxidation of (pR)-4-Pf and (pS)-5-Mes.

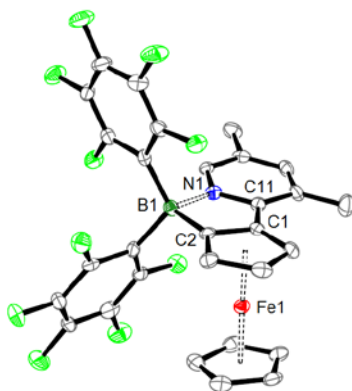


**Figure 4-7.** Ortep plot for compound **4-Pf**<sup>+</sup> (50% thermal displacement ellipsoids). Hydrogen atoms and the aluminate counterion are omitted for clarity. Selected interatomic distances (Å) and angles (°): B1-N1 1.644(9), B1-C2 1.626(11), Fe1-C<sub>Cp1</sub> 1.718(4), Fe1-C<sub>Cp2</sub> 1.721(4), C<sub>Cp1</sub>-C<sub>Cp2</sub> 3.439(5), C1-C2-B1 110.2(6), C2-B1-N1 95.6(5), B1-N1-C11 113.9(6), N1-C11-C1 108.5(6), C11-C1-C2 111.7(6), Cp//Cp 3.7(6), Py//Cp 1.0 (5). C<sub>Cp1</sub> = centroid of substituted Cp ring; C<sub>Cp2</sub> = centroid of unsubstituted Cp ring.

### 4.3 Conclusions

Two different methods were examined to influence the B-N interaction in ferrocene-based pyridine-borane Lewis pairs. While back strain induced by methylation of the pyridyl group in *meta*-position is overcome in the formation of the very stable B-N

adducts **4-Pf** and **4-Mes**, front strain due to a trimethylsilyl group in *ortho*-position of the pyridyl group in **5-Pf** and **5-Mes** decreases the B-N bond strength significantly. Although even for **5-Pf** the Lewis pair adopts a ‘closed form’ in solution and the solid state, EXSY NMR studies offer clear evidence for B-N cleavage at elevated temperature. A fully open conformation in **5-Mes** was achieved by incorporation of bulkier mesityl groups on boron. **5-Mes** is characterized as a frustrated Lewis pair given that the Lewis base component is accessible and binds to boron in **5-Pf**, while the borane Lewis acid component binds to the less hindered dimethylpyridine in **4-Mes**. Thus, the Lewis acid and base sites are unquenched and cannot form a complex in **5-Mes** only due to steric constraints. In the presence of H<sub>2</sub>O ring-opening of **5-Pf** occurred with formation of the corresponding pyridinium borate species **6**, which corresponds to the product of H<sub>2</sub>O addition across the B-N bond. In contrast, reaction of the open-chain species **5-Mes** with H<sub>2</sub>O yielded the B-C<sub>Mes</sub> cleavage product.

The influence of the electronic structure of the borane substituents on the redox potential of the iron center was also examined. The most significant difference was found when comparing the tetracoordinate ‘closed’ compounds with the tricoordinate species **5-Mes**; the latter experienced a strong anodic shift of the Fe oxidation potential, which is consistent with a pronounced interaction between the Lewis acidic borane moiety and the electron-rich Fe center.<sup>18</sup> On the other hand, the preparative oxidation of the ferrocene had little impact on the Lewis acid/base properties as **4-Pf** adopted a closed and **5-Mes** an open structure prior to and after oxidation. We attribute this unexpected result to a dual effect of ferrocene oxidation: while the Lewis acidity of the borane is enhanced, the Lewis basicity of the pyridine is diminished. In this respect, introduction of a non-

conjugated linker between the ferrocene and Lewis base units could prove beneficial for the future development of more redox-responsive Lewis pair systems. Another promising strategy for the development of more powerful Lewis pairs could be to incorporate borane substituents that promote higher electron-deficiency while offering sufficient steric bulk to stabilize the B-C bonds. Specifically, we expect the introduction of fluorinated mesityl groups to weaken the B-N bond due to steric constraints, while promoting FLP-type reactivity, hence allowing for activation of other small molecules such as the more challenging dihydrogen.

#### 4.4 Experimental Section

**Reagents and general methods.** Bis(dibenzylideneacetone)palladium(0), tri-*tert*-butylphosphine, Me<sub>3</sub>SnCl, ZnCl<sub>2</sub>, HgCl<sub>2</sub>, and *t*-butyl lithium (1.7 M in hexanes) were purchased from Aldrich and used without further purification. (*S*<sub>s</sub>)-*p*-Tolylsulfinylferrocene (**1**),<sup>7a</sup> 2,2,6,6-tetramethylpiperidyl lithium (TMPLi) was freshly prepared by addition of *n*-butyl lithium (1.6 M in hexanes) to a THF solution of 2,2,6,6-tetramethylpiperidine at 0 °C, 2-bromo-6-trimethylsilylpyridine,<sup>10</sup> (*pS*)-2-trimethylstannyl-1-(3,5-dimethylpyrid-2-yl)ferrocene (**2-Sn**),<sup>5e</sup> (C<sub>6</sub>F<sub>5</sub>)<sub>2</sub>BCl,<sup>19</sup> C<sub>6</sub>F<sub>5</sub>Cu,<sup>20</sup> MesCu,<sup>21</sup> and [Ag(CH<sub>2</sub>Cl<sub>2</sub>)] [Al(OC(CF<sub>3</sub>)<sub>3</sub>)<sub>4</sub>]<sup>16</sup> were prepared according to literature procedures. All reactions and manipulations were carried out under an atmosphere of prepurified nitrogen using either Schlenk techniques or an inert-atmosphere glove box (MBraun). 499.9 MHz <sup>1</sup>H NMR, 125.7 MHz <sup>13</sup>C NMR, 160.4 MHz <sup>11</sup>B NMR, 470.4 <sup>19</sup>F NMR, 99.3 MHz <sup>29</sup>Si, 186.4 MHz <sup>119</sup>Sn NMR and spectra were recorded on a Varian INOVA NMR spectrometer (Varian Inc., Palo Alto, CA) equipped with a boron-free 5

mm dual broadband gradient probe (Nalorac, Varian Inc., Martinez, CA). Solution  $^1\text{H}$  and  $^{13}\text{C}$  NMR spectra were referenced internally to solvent signals.  $^{11}\text{B}$  NMR spectra were acquired with boron-free quartz NMR tubes and referenced externally to  $\text{BF}_3 \cdot \text{Et}_2\text{O}$  ( $\delta = 0$ ),  $^{119}\text{Sn}$  NMR data to  $\text{SnMe}_4$  ( $\delta = 0$ ),  $^{29}\text{Si}$  NMR data to  $\text{SiMe}_4$  ( $\delta = 0$ ), and  $^{19}\text{F}$  NMR data to solvent signal. High resolution MALDI-MS data were obtained in positive mode on an Apex Ultra 7.0 Hybrid FTMS (Bruker Daltonics) using benzo[ $\alpha$ ]pyrene as the matrix. UV/Vis absorption data were acquired on a Varian Cary 500 UV/Vis/NIR spectrophotometer. Cyclic voltammetry measurements were carried out on a BAS CV-50W analyzer. The three-electrode system consisted of an Au disk as working electrode, a Pt wire as secondary electrode, and an Ag wire as the pseudo-reference electrode. The scans were referenced after the addition of a small amount of decamethylferrocene as internal standard. The potentials are reported relative to the ferrocene/ferrocenium couple ( $-610$  mV for  $\text{Cp}^*\text{Fe}/\text{Cp}^*\text{Fe}^+$  in  $\text{CH}_2\text{Cl}_2$  /  $0.05$  M  $\text{Bu}_4\text{N}[\text{B}(\text{C}_6\text{H}_3(\text{CF}_3)_2)_4]$ ). Optical rotation analyses were performed on an Autopol III polarimeter, Rudolph Research Analytical, using a tungsten-halogen light source operating at  $\lambda = 589$  nm. Chiral HPLC analyses were performed on a Waters Empower system equipped with a photodiode array detector and using a CHIRALPAK® IA-3 column. Elemental analyses were performed by Quantitative Technologies Inc., Whitehouse, NJ.

X-ray diffraction intensities were collected on a Bruker SMART APEX CCD Diffractometer using  $\text{CuK}\alpha$  ( $1.54178$  Å) radiation at  $100$  K. The structures were refined by full-matrix least squares based on  $F^2$  with all reflections.<sup>22</sup> Non-hydrogen atoms were refined with anisotropic displacement coefficients, and hydrogen atoms were treated as idealized contribution. SADABS (Sheldrick, 12 G.M. SADABS (2.01), Bruker/Siemens

Area Detector Absorption Correction Program; Bruker AXS: Madison, WI, 1998) absorption correction was applied. Crystallographic data for the structures of (p*R*)-**4-Pf**, (p*R*)-**4-Mes**, (p*S*)-**5-Pf**, (p*S*)-**5-Mes**, (p*S*)-**5-Cl**, (p*S*)-**6**, (p*S*)-**7** and [(p*S*)-**4-Pf**]<sup>+</sup>[Al(OC(CF<sub>3</sub>)<sub>3</sub>)<sub>4</sub>]<sup>-</sup> have been deposited with the Cambridge Crystallographic Data Center as supplementary publications CCDC 976017-976024. Copies of the data can be obtained free of charge on application to CCDC, 12 Union Road, Cambridge CB2 1EZ, UK (fax: (+44) 1223-336-033; email: [deposit@ccdc.cam.ac.uk](mailto:deposit@ccdc.cam.ac.uk)).

**Synthesis of (p*R*, *S*<sub>s</sub>)-2-(1-Trimethylsilylpyridyl)-1-(*p*-tolylsulfinyl)ferrocene (3-SOtol).** To a pre-cooled (-78 °C) solution of (*S*<sub>s</sub>)-*p*-tolylsulfinylferrocene (**1**) (2.00 g, 6.17 mmol) in THF (30 mL) was added dropwise a solution of LiTMP (0.5 M in THF, 14.8 mL, 7.40 mmol, 1.20 equiv) and the resulting mixture was kept stirring at the same temperature for 1 hour. A solution of ZnCl<sub>2</sub> (0.925 g, 6.79 mmol, 1.10 equiv) in THF (15 mL) was added. After 1 h at -78 °C the mixture was allowed to warm up and stirred for 1 h at 25 °C. For the cross-coupling reaction, bis(dibenzylideneacetone)palladium(0) (0.847 g, 0.926 mmol, 0.10 equiv), tri-*tert*-butylphosphine (0.374 g, 1.85 mmol, 0.20 equiv) and 2-bromo-6-trimethylsilylpyridine (3.55 g, 15.4 mmol, 2.50 equiv) were stirred in THF (20 mL) for 5 min and then added to the ferrocenylzinc reagent by syringe. The mixture was stirred for 2 days at 50 °C. After addition of saturated NH<sub>4</sub>Cl solution (50 mL), the mixture was extracted with CH<sub>2</sub>Cl<sub>2</sub> (3 × 30 mL). The combined organic layers were washed with brine and water, dried over sodium sulfate and then concentrated on a rotary evaporator. The residue was chromatographed on alumina with ethyl acetate/hexanes (1:2) as the eluent. Yield: 2.4 g (61%). <sup>1</sup>H NMR (499.9 MHz, CDCl<sub>3</sub>, 25

$^{\circ}\text{C}$ ):  $\delta = 7.84$  (d,  $J = 8.0$  Hz, 2H; tolyl), 7.54 (m, 2H; Py), 7.37 (m, 3H; py, tolyl), 5.04 (nr, 1H; Cp), 4.40 (nr,  $J = 2.0$  Hz, 1H; Cp), 4.07 (s, 5H; free Cp), 3.92 (nr, 1H; Cp), 2.47 (s, 3H; tolyl-Me), 0.43 (s, 9H; SiMe<sub>3</sub>).  $^{13}\text{C}$  NMR (125.69 MHz, CDCl<sub>3</sub>, 25  $^{\circ}\text{C}$ ):  $\delta = 168.0, 156.4, 141.2, 141.0, 133.9, 129.2, 126.2, 126.1, 120.5$  (py, tolyl), 93.1 (Cp), 86.9 (Cp), 71.2 (Cp), 71.2 (free Cp), 70.4 (Cp), 69.7 (Cp), 21.5 (Me), -1.7 (SiMe<sub>3</sub>).  $^{29}\text{Si}$  NMR (99.3 MHz, CHCl<sub>3</sub>, 25  $^{\circ}\text{C}$ )  $\delta = -5.4$ . Elemental analysis for C<sub>25</sub>H<sub>27</sub>FeNOSSi, calcd C 63.42, H 5.75, N 2.96, found C 63.34, H 5.80, N 2.76 %.

**Synthesis of (pS)-2-(2-Trimethylsilylpyrid-6-yl)-1-(chloromercurio)ferrocene (3-Hg).** A solution of *tert*-butyl lithium (1.04 mL, 1.78 mmol, 1.20 equiv) was added dropwise to a solution of **3-SOtol** (700 mg, 1.48 mmol) in THF (10 mL) at -78  $^{\circ}\text{C}$ . The reaction mixture was kept stirring for 10 min at the same temperature and then a solution of Me<sub>3</sub>SnCl (0.383 g, 1.92 mmol, 1.3 equiv) in THF (2 mL) was added via syringe. The resulting solution was stirred for 1 h and the temperature was then allowed to slowly raise to 25  $^{\circ}\text{C}$ . After addition of water the mixture was extracted with diethyl ether (3  $\times$  5 mL). The combined organic layers were washed with brine solution followed by water, dried over sodium sulfate and concentrated on a rotary evaporator. The residue was subjected to silica gel column chromatography with hexanes/triethylamine (100:1) as the eluent. A mixture of (2-trimethylsilylpyrid-6-yl)ferrocene and (pS)-2-(2-trimethylsilylpyrid-6-yl)-1-(trimethylstannyl)ferrocene (**3-Sn**) was obtained, which was further reacted without further purification. A solution of the crude product in acetone (20 mL) was added into a solution of HgCl<sub>2</sub> in acetone (20 mL). The mixture was stirred for 1 hour and then added to distilled water (100 mL) with stirring. Upon addition, a red precipitate formed, which was collected on a filter and dried under airflow. The solid was then taken up in hexanes.

Recrystallization at  $-37\text{ }^{\circ}\text{C}$  gave red crystals suitable for X-ray diffraction analysis. Yield: 600 mg (71%).  $^1\text{H}$  NMR (499.9 MHz,  $\text{CDCl}_3$ ,  $25\text{ }^{\circ}\text{C}$ ):  $\delta = 7.53$  (pst,  $J = 7.5$  Hz, 1H; Py), 7.38 (d,  $J = 7.5$  Hz, 1H; Py), 7.34 (d,  $J = 7.5$  Hz, 1H; Py), 4.98 (d,  $J = 1.5$  Hz, 1H; Cp), 4.61 (pst,  $J = 2.0$  Hz, 1H; Cp), 4.39 (nr, 1H; Cp), 4.06 (s, 5H; free Cp), 0.44 (s, 9H;  $\text{SiMe}_3$ ).  $^{13}\text{C}$  NMR (125.69 MHz,  $\text{CDCl}_3$ ,  $25\text{ }^{\circ}\text{C}$ ):  $\delta = 168.2$  (ipso-Py), 158.2 (ipso-Py), 134.5 (Py), 126.8 (Py), 119.5 (Py), 87.3 (ipso-Cp-C), 75.3 (Cp), 72.6 (Cp), 69.9 (free Cp), 68.0 (Cp),  $-1.1$  ( $\text{SiMe}_3$ ), ipso-Cp-Hg not observed.  $^{29}\text{Si}$  NMR (99.3 MHz,  $\text{CDCl}_3$ ,  $25\text{ }^{\circ}\text{C}$ )  $\delta = -5.1$ . Elemental analysis for  $\text{C}_{18}\text{H}_{20}\text{ClFeNSi}$ , calcd C 37.89, H 3.54, N 2.46, found C 37.83, H 3.49, N 2.36 %.

**Synthesis of (p*R*)-2-[Bis(pentafluorophenyl)boryl]-1-(3,5-dimethylpyrid-2-yl)ferrocene (4-Pf).** To a solution of **2-Sn** (100 mg, 0.22 mmol) in hexanes (20 mL) that was cooled to  $-37\text{ }^{\circ}\text{C}$  was added a solution of  $\text{BCl}_3$  (1 M in hexanes, 0.24 mL, 0.24 mmol, 1.10 equiv) dropwise under stirring. A red precipitate developed, which redissolved upon addition of 30 mL of toluene. After stirring for 2 hours solvents, excess  $\text{BCl}_3$  and the byproduct  $\text{Me}_3\text{SnCl}$  were removed under high vacuum. The crude product (p*R*)-2-dichloroboryl-1-(3,5-dimethylpyrid-2-yl)ferrocene (**4-Cl**) was further reacted without additional purification. To a pre-cooled solution of crude **4-Cl** in toluene (10 mL,  $-37\text{ }^{\circ}\text{C}$ ) was added a solution of  $\text{C}_6\text{F}_5\text{Cu}$  (101 mg, 0.44 mmol, 2.0 equiv) in toluene (5 mL). The reaction mixture was stirred at room temperature overnight and then at  $80\text{ }^{\circ}\text{C}$  for 2 hours. A white precipitate that had formed was removed by filtration and the filtrate was concentrated under vacuum. The residue was recrystallized from hot hexanes to give the product as dark red, X-ray quality crystals. Yield: 92 mg (66 %)  $[\alpha]_{\text{D}}^{20}$  ( $c = 0.115$ ,  $\text{CHCl}_3$ ) =  $2078^{\circ}$ ;  $^1\text{H}$  NMR (499.9 MHz,  $\text{CDCl}_3$ ,  $25\text{ }^{\circ}\text{C}$ ):  $\delta = 8.14$  (s, 1H; Lu), 7.53 (s, 1H;

Lu), 4.79 (d,  $J = 2.0$  Hz, 1H; Cp), 4.72 (br, 1H; Cp), 4.60 (pst,  $J = 2.0$  Hz, 1H; Cp), 3.67 (s, 5H; free Cp), 2.53 (s, 3H; Lu-Me), 2.32 (s, 3H; Lu-Me).  $^{13}\text{C}$  NMR (125.69 MHz,  $\text{CDCl}_3$ , 25 °C):  $\delta = 148.3$  (d,  $J(\text{C},\text{F}) = 237$  Hz, o- $\text{C}_6\text{F}_5$ ), 147.1 (d,  $J(\text{C},\text{F}) = 245$  Hz, o- $\text{C}_6\text{F}_5$ ), 139.9 (d,  $J(\text{C},\text{F}) = 256$  Hz, p- $\text{C}_6\text{F}_5$ ), 138.8(nr, p- $\text{C}_6\text{F}_5$ ), 137.1 (d,  $J(\text{C},\text{F}) = 253$  Hz, m- $\text{C}_6\text{F}_5$ ), 120.1 (br d, ipso- $\text{C}_6\text{F}_5$ ), 159.4, 143.7, 143.4, 129.6, 129.4 (Lu), 97.0 (br, ipso-Cp-B), 83.7 (ipso-Cp-C), 74.0 (Cp), 71.3 (Cp), 69.4 (free Cp), 64.2 (Cp), 18.5 (Me), 18.1 (Me).  $^{11}\text{B}$  NMR (160.4 MHz,  $\text{CDCl}_3$ , 25 °C)  $\delta = -3.3$  ( $w_{1/2} = 120$  Hz).  $^{19}\text{F}$  NMR (470.4 MHz,  $\text{CDCl}_3$ , 25 °C):  $\delta = -130.0$  (d,  $J(\text{F},\text{F}) = 17$  Hz, 2F; ortho-F),  $-134.0$  (d,  $J(\text{F},\text{F}) = 20$  Hz, 2F; ortho-F),  $-157.4$  (t,  $J(\text{F},\text{F}) = 20$  Hz, 1F; para-F),  $-159.7$  (t,  $J(\text{F},\text{F}) = 20$  Hz, 1F; para-F),  $-163.3$  (pst,  $J(\text{F},\text{F}) = 17$  Hz, 2F; meta-F),  $-163.6$  (pst,  $J(\text{F},\text{F}) = 18$  Hz, 2F; meta-F). High-resolution MALDI-MS (+ mode, benzo[ $\alpha$ ]pyrene):  $m/z$  635.0557 ( $[\text{M}]^+$ , 100%, calcd for  $^{12}\text{C}_{29}^{1}\text{H}_{16}^{11}\text{B}^{14}\text{N}^{19}\text{F}_{10}^{56}\text{Fe}$  635.0565). Elemental analysis for  $\text{C}_{29}\text{H}_{16}\text{BF}_{10}\text{FeN}$ , calcd C 54.81, H 2.54, N 2.21, found C 54.66, H 2.37, N 2.09 %

**Synthesis of (pR)-2-[bis(2,4,6-trimethylphenyl)boryl]-1-(3,5-dimethylpyrid-2-yl)ferrocene (4-Mes).** Compound **4-Cl** was synthesized as described above from a solution of **2-Sn** (50 mg, 0.22 mmol) in hexanes (10 mL) and  $\text{BCl}_3$  (1 M in hexanes, 0.12 mL, 0.12 mmol, 1.10 equiv). To a pre-cooled ( $-37$  °C) solution of crude **4-Cl** in toluene (5 mL) was added a solution of mesityl copper ( $\text{MesCu}$ ,  $\text{C}_9\text{H}_{11}\text{Cu}$ ) (40 mg, 0.48 mmol, 2.2 equiv) in toluene (5 mL). The reaction mixture was stirred at 90 °C overnight. A white precipitate that had formed was removed by filtration and the filtrate as concentrated under vacuum. The residue was subjected to chromatography using hexanes as the eluent. A dark red, fluffy solid formed after removal of the solvent. Yield: (30 mg) 51 %).  $[\alpha]_{\text{D}}^{20}$  ( $c = 0.10$ ,  $\text{CH}_2\text{Cl}_2$ ) = 1900°;  $^1\text{H}$  NMR (499.9 MHz,  $\text{CDCl}_3$ , 25 °C):  $\delta =$

8.10 (s, 1H; Lu), 7.41 (s, 1H; Lu), 6.80 (s, 1H; Mes), 6.72 (s, 1H; Mes), 6.57 (s, 1H; Mes), 6.53 (s, 1H; Mes), 4.71 (nr, 1H; Cp), 4.68 (nr, 1H; Cp), 4.47 (nr, 1H; Cp), 3.61 (s, 5H; free Cp), 2.54 (s, 3H; Lu-Me), 2.22 (s, 3H; Lu-Me), 2.20 (s, 3H; Mes-Me), 2.18 (s, 3H; Mes-Me), 2.10 (s, 3H; Mes-Me), 1.97 (s, 3H; Mes-Me), 1.73 (s, 3H; Mes-Me), 1.35 (s, 3H; Mes-Me).  $^{13}\text{C}$  NMR (125.69 MHz,  $\text{CDCl}_3$ , 25 °C):  $\delta$  = 159.2, 145.5, 142.7, 142.3, 142.0, 141.1, 136.1, 134.4, 132.5, 129.9, 129.2, 129.2, 129.1, 129.1, 128.6, (Lu + Mes), 151.3 (ipso-Mes-B), 111.5 (ipso-Cp-B), 85.7 (ipso-Cp-C), 72.0 (Cp), 71.7 (Cp), 68.9 (free Cp), 62.1 (Cp), 26.2, 25.2, 24.8, 24.2, 20.7, 20.7, 18.8, 18.3 (Me).  $^{11}\text{B}$  NMR (160.4 MHz,  $\text{CDCl}_3$ , 25 °C)  $\delta$  = 2.5 ( $w_{1/2}$  = 800 Hz). High-resolution MALDI-MS (+ mode, benzo[ $\alpha$ ]pyrene):  $m/z$  539.2474 ( $[\text{M}]^+$ , 50%, calcd for  $^{12}\text{C}_{35}\text{H}_{38}\text{B}^{11}\text{N}^{14}\text{N}^{56}\text{Fe}$  539.2447), 420.1609 ( $[\text{M-Mes}]^+$ , 100%, calcd for  $^{12}\text{C}_{26}\text{H}_{27}\text{B}^{11}\text{N}^{14}\text{N}^{56}\text{Fe}$  420.1585). Elemental analysis for  $\text{C}_{35}\text{H}_{38}\text{BFeN}$ , calcd C 77.90, H 7.10, N 2.60, found C 77.30, H 7.06, N 2.43 %.

**Synthesis of (pS)-2-(bis(pentafluorophenyl)boryl)-1-(2-trimethylsilylpyrid-6-yl)ferrocene (5-Pf).** To a solution of **3-Hg** (100 mg, 0.175 mmol) in toluene (10 mL) that was cooled down to  $-37$  °C was added a solution of  $(\text{C}_6\text{F}_5)_2\text{BCl}$  (70 mg, 0.184 mmol, 1.1 equiv) in toluene (5 mL). Upon addition the color of the solution turned purple. After stirring over night at room temperature the solvent was removed under vacuum. The residue was re-dissolved in 5 mL of hexanes and a small amount of a black solid was filtered off. The filtrate was kept at  $-37$  °C for one month to give X-ray quality crystals of the product. Yield: 40 mg (34%).  $[\alpha]_D^{20}$  ( $c = 0.10$ ,  $\text{CH}_2\text{Cl}_2$ ) =  $-1496^\circ$ .  $^1\text{H}$  NMR (499.9 MHz,  $\text{CDCl}_3$ , 25 °C):  $\delta$  = 7.81 (pst,  $J = 7.5$  Hz, 1H; Py), 7.56 (d,  $J = 7.5$  Hz, 1H; Py), 7.54 (d,  $J = 8.0$  Hz, 1H; Py), 4.71 (d,  $J = 1.5$  Hz, 1H; Cp), 4.56 (nr, 1H; Cp), 4.54 (nr, 1H; Cp), 3.60 (s, 5H; free Cp), 0.05 (s, 9H;  $\text{SiMe}_3$ ).  $^{13}\text{C}$  NMR (125.69 MHz,  $\text{CDCl}_3$ , 25 °C):  $\delta$

= 150-135 (br unresolved; *ortho*-, *meta*-, *para*-C<sub>6</sub>F<sub>5</sub>), 168.3, 166.2, 138.9, 128.2, 119.0 (Py), 85.2 (ipso-Cp-B), 73.2 (Cp), 70.9 (Cp), 70.8 (Cp), 69.4 (free Cp), 60.1 (Cp), 0.5 (SiMe<sub>3</sub>). <sup>11</sup>B NMR (160.4 MHz, CDCl<sub>3</sub>, 25 °C)  $\delta = -1.5$  ( $w_{1/2} = 150$  Hz). <sup>19</sup>F NMR (470.4 MHz, CDCl<sub>3</sub>, 25 °C):  $\delta = -127.1$  (br, 1F; *ortho*-F),  $-130.1$  (br, 1F; *ortho*-F),  $-133.2$  (dd,  $J(\text{F},\text{F}) = 24$  Hz, 7 Hz, 1F; *ortho*-F),  $-134.2$  (br, 1F; *ortho*-F),  $-157.1$  (t,  $J(\text{F},\text{F}) = 20$  Hz, 1F; *para*-F),  $-159.2$  (t,  $J(\text{F},\text{F}) = 20$  Hz, 1F; *para*-F),  $-163.1$  (br, 1F; *meta*-F),  $-163.9$  (br, 1F; *meta*-F),  $-164.5$  (m, 1F; *meta*-F),  $-165.0$  (m, 1F; *meta*-F). High-resolution MALDI-MS (+ mode, benzo[ $\alpha$ ]pyrene):  $m/z$  679.0670 ([M]<sup>+</sup>, 100%, calcd for <sup>12</sup>C<sub>30</sub><sup>1</sup>H<sub>20</sub><sup>11</sup>B<sup>14</sup>N<sup>19</sup>F<sub>10</sub><sup>29</sup>Si<sup>56</sup>Fe 679.0648). Elemental analysis for C<sub>30</sub>H<sub>20</sub>BF<sub>10</sub>FeNSi, calcd C 53.02, H 2.97, N 2.06, found C 52.90, H 2.87, N 1.95 %.

**Synthesis of Ring-opened Species 6.** Compound **3-Hg** (100 mg, 0.175 mmol) was first converted to **5-Pf** as described above. Instead of recrystallization, the crude product was passed through a short silica gel column using ether/hexanes (1:1) as the eluent. A purple colored solid was obtained, which can be recrystallized in hot ether/hexanes (1:1). Yield: 50 mg (41%).  $[\alpha]_{\text{D}}^{20}$  ( $c = 0.10$ , CH<sub>2</sub>Cl<sub>2</sub>) =  $-462^\circ$ . <sup>1</sup>H NMR (499.9 MHz, CDCl<sub>3</sub>, 25 °C):  $\delta = 18.24$  (br, 1H; Py-H<sup>+</sup>), 7.86 (pst,  $J = 8.0$  Hz, 1H; Py), 7.66 (d,  $J = 8.5$  Hz, 1H; Py), 7.41 (d,  $J = 7.0$  Hz, 1H; Py), 4.76 (nr, 1H; Cp), 4.61 (nr, 1H; Cp), 4.31 (nr, 1H; Cp), 4.08 (s, 5H; free Cp), 3.22 (s, 1H; B-OH), 0.39 (s, 9H; SiMe<sub>3</sub>). <sup>13</sup>C NMR (125.69 MHz, CDCl<sub>3</sub>, 25 °C):  $\delta = 150-135$  (br unresolved; *ortho*-, *meta*-, *para*-C<sub>6</sub>F<sub>5</sub>), 158.4, 154.2, 136.0, 121.6, 118.8 (Py), 90.9 (ipso-Cp-B), 76.1 (Cp), 71.4 (Cp), 67.6 (Cp), 65.2 (free Cp), 63.0 (Cp),  $-7.1$  (SiMe<sub>3</sub>). <sup>11</sup>B NMR (160.4 MHz, CDCl<sub>3</sub>, 25 °C)  $\delta = -2.7$  ( $w_{1/2} = 90$  Hz). <sup>19</sup>F NMR (470.4 MHz, CDCl<sub>3</sub>, 25 °C):  $\delta = -133.0$  (d,  $J(\text{F},\text{F}) = 16$  Hz, 2F; *ortho*-F),  $-135.4$  (br, 2F; *ortho*-F),  $-160.0$  (t,  $J(\text{F},\text{F}) = 20$  Hz, 1F; *para*-F),  $-160.6$  (t,  $J(\text{F},\text{F}) = 20$  Hz, 1F;

para-F),  $-164.4$  (m, 2F; meta-F),  $-165.1$  (m, 2F; meta-F). High-resolution MALDI-MS (+ mode, benzo[ $\alpha$ ]pyrene):  $m/z$  679.0669 ( $[M-H_2O]^+$ , 100%, calcd for  $^{12}C_{30}^{1}H_{20}^{11}B^{14}N^{19}F_{10}^{29}Si^{56}Fe$  679.0648). Elemental analysis for  $C_{30}H_{22}BF_{10}FeNOSi$ , calcd C 51.65, H 3.18, N 2.01, found C 51.46, H 3.15, N 2.13 %.

**Synthesis of (pS)-2-bis(2,4,6-trimethylphenyl)jboryl-1-(2-trimethylsilylpyrid-6-yl)ferrocene (5-Mes) and Compound 7.** A solution of *tert*-butyllithium (0.42 mL, 0.72 mmol, 1.1 equiv) was added dropwise to a solution of **3-SOtol** (310 mg, 0.66 mmol) in THF (10 mL) at  $-78$  °C. The reaction mixture was kept stirring for 10 min at the same temperature and then a solution of  $Mes_2BF$  (211 mg, 0.79 mmol, 1.2 equiv) in THF (5 mL) was added via syringe. The resulting solution was stirred for 1 h and the temperature was then allowed to slowly raise to 25 °C. After concentration under high vacuum the residue was redissolved in minimum amount of hexanes. The mixture was subjected to aluminum oxide column chromatography with hexanes/ether (1:1) as the eluent. The first band that was collected was purple colored. Recrystallization in methanol at  $-37$  °C gave purple crystals suitable for X-ray diffraction analysis. Yield: 150 mg (39%).  $[\alpha]_D^{20}$  ( $c = 0.10$ ,  $CH_2Cl_2$ ) =  $-410^\circ$ .  $^1H$  NMR (499.9 MHz,  $CDCl_3$ , 25 °C):  $\delta = 7.00$  (d,  $J = 6.5$  Hz, 1H; Py), 6.87 (d + pst, 2H; Py), 6.55 (s, 4H, Mes), 5.30 (nr, 1H; Cp), 4.73 (nr, 1H; Cp), 4.56 (nr, 1H; Cp), 4.11 (s, 5H; free Cp), 2.19(s, 12H, Mes-Me), 2.16 (s, 6H, Mes-Me), 0.32 (s, 9H;  $SiMe_3$ ).  $^{13}C$  NMR (125.69 MHz,  $CDCl_3$ , 25 °C):  $\delta = 165.3$ , 158.3, 139.2, 137.0, 130.8, 127.7, 124.6, 124.5 (Py + Mes), 142.8 (ipso-Mes-B), 92.7 (ipso-Cp-B), 83.9 (Cp), 82.3 (ipso-Cp-C), 74.6 (Cp), 72.0 (Cp), 71.2 (free Cp), 23.8, 20.9 (Mes-Me)-1.7 (Si-Me).  $^{11}B$  NMR (160.4 MHz,  $CDCl_3$ , 25 °C)  $\delta = 77.1$  ( $w_{1/2} = 1600$  Hz).  $^{29}Si$  NMR (99.3 MHz,  $CDCl_3$ , 25 °C)  $\delta = -6.4$ . High-resolution MALDI-MS (+ mode,

benzo[ $\alpha$ ]pyrene):  $m/z$  583.2527 ( $[M]^+$ , 100%, calcd for  $^{12}C_{36}^{1}H_{42}^{11}B^{14}N^{29}Si^{56}Fe$  583.2531). Elemental analysis for  $C_{36}H_{42}BFeNSi$ , calcd C 74.08, H 7.26, N 2.40, found C 73.60, H 7.28, N 2.12 %. When the crude product of **5-Mes** (see above) was subjected to aluminum oxide column chromatography with hexanes/ether (1:1) as the eluent, a second orange band was isolated at a longer retention time. Recrystallization in hexanes at  $-37$  °C gave red crystals suitable for X-ray diffraction analysis. Yield: 100 mg (32%). Compound **7** also formed upon treatment of pure **5-Mes** with silica gel similar to the procedure used to prepare compound **6** from **5-Pf**.  $[\alpha]_D^{20}$  ( $c = 0.10$ ,  $CH_2Cl_2$ ) =  $-316^\circ$ .  $^1H$  NMR (499.9 MHz,  $CDCl_3$ , 25 °C):  $\delta = 13.89$  (s, 1H, OH) 7.62 (pst,  $J = 7.5$  Hz, 1H; Py), 7.51 (d,  $J = 8.0$  Hz, 1H; Py), 7.41 (d,  $J = 7.0$  Hz, 1H; Py), 6.26 (br, 2H, Mes), 5.04 (nr, 1H; Cp), 4.54 (nr, 1H; Cp), 4.26 (nr, 1H; Cp), 4.03 (s, 5H; free Cp), 2.67 (br, 3H, Mes-Me), 2.30 (s, 3H, Mes-Me), 2.15 (br, 3H, Mes-Me), 0.45 (s, 9H;  $SiMe_3$ ).  $^{13}C$  NMR (125.69 MHz,  $CDCl_3$ , 25 °C):  $\delta = 166.3$ , 161.0, 136.7, 135.4, 127.2, 126.1, 120.6 (Py + Mes), 139.3 (ipso-Mes-B), ipso-Cp-B not observed, 87.5 (ipso-Cp-C), 81.0 (Cp), 72.7 (Cp), 71.7 (Cp), 70.2 (free Cp), 22.6, 21.2 (Mes-Me), -1.8 (Si-Me).  $^{11}B$  NMR (160.4 MHz,  $CDCl_3$ , 25 °C)  $\delta = 48.4$  ( $w_{1/2} = 1400$  Hz).  $^{29}Si$  NMR (99.3 MHz,  $CDCl_3$ , 25 °C)  $\delta = -4.3$ . High-resolution MALDI-MS (+ mode, benzo[ $\alpha$ ]pyrene):  $m/z$  481.1696 ( $[M]^+$ , 100%, calcd for  $^{12}C_{27}^{1}H_{32}^{11}B^{14}N^{29}Si^{56}Fe$  481.1696). Elemental analysis for  $C_{27}H_{32}BFeNOSi$ , calcd C 67.35, H 6.70, N 2.91, found C 67.46, H 6.88, N 2.75 %.

**Synthesis of  $[4-Pf]^+[Al[OC(CF_3)_3]_4]^-$ .** To a solution of **4-Pf** (10.9 mg, 0.017 mmol) in  $CHCl_3$  (1 mL) that was cooled down to  $-37$  °C was added a solution of  $[Ag(CH_2Cl_2)]Al[OC(CF_3)_3]_4$  (20 mg, 0.017 mmol, 1.0 equiv) in  $CHCl_3$  (0.5 mL) under stirring. The color of the mixture turned from purple to green. After removal of a white

precipitate by filtration, the solvent was removed under vacuum. The residue was redissolved in 1 mL of  $\text{CH}_2\text{Cl}_2$  and the product crystallized at  $-37\text{ }^\circ\text{C}$ . Yield: 20 mg (73 %).  $^1\text{H}$  NMR (499.9 MHz,  $\text{CD}_2\text{Cl}_2$ ,  $25\text{ }^\circ\text{C}$ ):  $\delta = 39.5$  (br, 1H; Cp), 35.9 (br, 1H; Cp), 31.1 (br, 5H; free Cp), 29.9 (br, 1H; Cp), 0.63 (s, 1H; Lu), 0.24 (s, 1H; Lu),  $-5.75$  (s, 3H; Lu-Me),  $-16.5$  (br, 3H; Lu-Me).  $^{11}\text{B}$  NMR (160.4 MHz,  $\text{CDCl}_3$ ,  $25\text{ }^\circ\text{C}$ )  $\delta = 1.1$  ( $w_{1/2} = 180$  Hz).  $^{19}\text{F}$  NMR (470.4 MHz,  $\text{CD}_2\text{Cl}_2$ ,  $25\text{ }^\circ\text{C}$ ):  $\delta = -76.2$  (s, 36F;  $\text{CF}_3$ ),  $-148.7$  (br, 2F; ortho-F),  $-150.1$  (br, 2F; ortho-F),  $-151.4$  (t,  $J(\text{F},\text{F}) = 20$  Hz, 1F; para-F),  $-153.7$  (t,  $J(\text{F},\text{F}) = 19$  Hz, 1F; para-F),  $-156.7$  (pst, 2F; meta-F),  $-170.0$  (br, 2F, meta-F). Elemental analysis for  $\text{C}_{45}\text{H}_{16}\text{AlBF}_4\text{FeNO}_4$ , calcd C 33.73, H 1.01, N 0.87, found C 33.62, H 0.76, N 1.65%.

**NMR scale reaction for  $[\mathbf{5}\text{-Mes}]^+[\text{Al}[\text{OC}(\text{CF}_3)_3]_4]^-$ .** To a solution of **5-Mes** (9.9 mg, 0.017 mmol) in  $\text{CDCl}_3$  (0.5 mL) that was cooled down to  $-37\text{ }^\circ\text{C}$  was added a solution of  $[\text{Ag}(\text{CH}_2\text{Cl}_2)]\text{Al}[\text{OC}(\text{CF}_3)_3]_4$  (20 mg, 0.017 mmol, 1.0 equiv) in  $\text{CDCl}_3$  (0.5 mL) under stirring. The color of the mixture turned from red to green. After removal of a white precipitate by filtration, the filtrate was transfer to a J Young's NMR tube for acquisition of the  $^1\text{H}$  and  $^{11}\text{B}$  NMR. Attempts to isolate the oxidized species failed due to high reactivity of the product.  $^1\text{H}$  NMR (499.9 MHz,  $\text{CDCl}_3$ ,  $25\text{ }^\circ\text{C}$ ):  $\delta = 43.8$  (br, 1H; Cp), 32.0 (br, 2H; Cp), 29.4 (br, 5H; free Cp), 19.0 (br, 1H), 15.1 (br, 1H), 5.40 (br), 2.52 (br), 0.15 (br),  $-1.34$  (br),  $-2.52$  (br),  $-3.71$  (br),  $-21.0$  (br).  $^{11}\text{B}$  NMR (160.4 MHz,  $\text{CDCl}_3$ ,  $25\text{ }^\circ\text{C}$ )  $\delta = 64.5$  ( $w_{1/2} = 600$  Hz).

## 4.5 Supporting Information

**Table 4-1.** Crystal data and structure refinement details for **4-Pf**, **5-Pf**, **4-Mes**, **5-Mes**, **4-Pf<sup>+</sup>**, **5-Cl**, **6** and **7**.

Compound	<b>4-Pf</b>	<b>5-Pf</b>	<b>4-Mes</b>	<b>5-Mes</b>
empirical formula	C <sub>29</sub> H <sub>16</sub> BF <sub>10</sub> FeN	C <sub>30</sub> H <sub>20</sub> BF <sub>10</sub> FeNSi	C <sub>35</sub> H <sub>38</sub> BFeN	C <sub>36</sub> H <sub>42</sub> BFeNSi
MW	634.09	679.22	539.32	583.46
<i>T</i> , K	100(2)	100(2)	100(2)	100(2)
wavelength, Å	1.54178	1.54178	1.54178	1.54178
crystal system	Orthorhobic	monoclinic	orthorhobic	orthorhobic
space group	<i>P</i> 2 <sub>1</sub> 2 <sub>1</sub> 2 <sub>1</sub>	<i>P</i> 2 <sub>1</sub>	<i>P</i> 2 <sub>1</sub> 2 <sub>1</sub> 2 <sub>1</sub>	<i>P</i> 2 <sub>1</sub> 2 <sub>1</sub> 2 <sub>1</sub>
<i>a</i> , Å	11.1678(2)	9.4484(5)	8.9154(2)	8.1450(2)
<i>b</i> , Å	13.4185(2)	11.9287(6)	17.5500(4)	18.4095(3)
<i>c</i> , Å	17.0146(2)	12.8027(6)	17.8546(4)	20.7312(4)
<i>α</i> , deg	90	90	90	90
<i>β</i> , deg	90	103.529(2)	90	90
<i>γ</i> , deg	90	90	90	90
<i>V</i> , Å <sup>3</sup>	2549.73(7)	1402.92(12)	2793.62(11)	3108.55(11)
<i>Z</i>	4	2	4	4
$\rho_{\text{calc}}$ , g cm <sup>-3</sup>	1.654	1.608	1.282	1.247
$\mu$ (Mo/Cu K $\alpha$ ), mm <sup>-1</sup>	5.62	5.54	4.49	4.43
crystal size, mm	0.26×0.23×0.21	0.47×0.40×0.24	0.22×0.13×0.13	0.37×0.17×0.13
$\theta$ range, deg	4.2-70.9	3.6-71.2	3.5-69.7	3.2-69.4
limiting indices	-13≤ <i>h</i> ≤12	-10≤ <i>h</i> ≤10	-10≤ <i>h</i> ≤10	-9≤ <i>h</i> ≤8
	-16≤ <i>k</i> ≤15	-13≤ <i>k</i> ≤14	-20≤ <i>k</i> ≤21	-21≤ <i>k</i> ≤21
	-20≤ <i>l</i> ≤19	-15≤ <i>l</i> ≤12	-21≤ <i>l</i> ≤21	-24≤ <i>l</i> ≤23
reflns collected	21887	11293	27036	27578
independent reflns	4026 [ <i>R</i> (int) = 0.024]	3986 [ <i>R</i> (int) = 0.051]	4970 [ <i>R</i> (int) = 0.153]	5551 [ <i>R</i> (int) = 0.057]
absorption correction	Numerical	Numerical	Numerical	Numerical
data/restraints/ parameters	4026 / 0 / 382	3986 / 1 / 401	4970 / 180 / 351	5551 / 0 / 370
goodness-of-fit on <i>F</i> <sup>2</sup>	1.05	1.06	0.99	1.01
final <i>R</i> indices	<i>R</i> 1 = 0.022	<i>R</i> 1 = 0.037	<i>R</i> 1 = 0.053	<i>R</i> 1 = 0.034
[ <i>I</i> > 2σ( <i>I</i> )] <sup>[a]</sup>	w <i>R</i> 2 = 0.059	w <i>R</i> 2 = 0.095	w <i>R</i> 2 = 0.103	w <i>R</i> 2 = 0.080
<i>R</i> indices (all data) <sup>[a]</sup>	<i>R</i> 1 = 0.023	<i>R</i> 1 = 0.038	<i>R</i> 1 = 0.059	<i>R</i> 1 = 0.042
	w <i>R</i> 2 = 0.060	w <i>R</i> 2 = 0.095	w <i>R</i> 2 = 0.106	w <i>R</i> 2 = 0.084
peak <sub>max</sub> /hole <sub>min</sub> (e Å <sup>-3</sup> )	0.20 / -0.18	0.47 / -0.39	0.53 / -0.45	0.34 / -0.23
absolute structure parameter	0.013(3)	0.036(4)	-0.010(4)	0.019(4)

$$[\text{a}] R1 = \sum ||F_o| - |F_c|| / \sum |F_o|; wR2 = [\sum [w(F_o^2 - F_c^2)^2] / \sum w(F_o^2)^2]^{1/2}$$

Compound	<b>6</b>	<b>5-Cl</b>	<b>4-Pf<sup>+</sup></b>	<b>7</b>
empirical formula	C <sub>30</sub> H <sub>22</sub> BF <sub>10</sub> FeN OSi	C <sub>18</sub> H <sub>20</sub> BCl <sub>2</sub> FeNSi	C <sub>29</sub> H <sub>16</sub> BF <sub>10</sub> FeN· C <sub>16</sub> AlF <sub>36</sub> O <sub>4</sub>	C <sub>27</sub> H <sub>32</sub> BFeNOS i
MW	697.24	416.00	1602.23	481.29
<i>T</i> , K	100(2)	100(2)	100(2)	100(2)
wavelength, Å	1.54178	1.54178	1.54178	1.54178
crystal system	orthorhobic	orthorhobic	monoclinic	orthorhobic
space group	<i>P</i> 2 <sub>1</sub> 2 <sub>1</sub> 2 <sub>1</sub>	<i>P</i> 2 <sub>1</sub> 2 <sub>1</sub> 2 <sub>1</sub>	<i>P</i> 2 <sub>1</sub>	<i>P</i> 2 <sub>1</sub> 2 <sub>1</sub> 2 <sub>1</sub>
<i>a</i> , Å	10.4751(1)	8.1701(1)	10.3925(3)	9.9836(2)
<i>b</i> , Å	15.4500(2)	14.7737(3)	15.6591(4)	15.1922(2)
<i>c</i> , Å	17.8813(2)	15.5140(3)	17.4152(4)	16.9599(3)
<i>α</i> , deg	90	90	90	90
<i>β</i> , deg	90	90	106.114(2)	90
<i>γ</i> , deg	90	90	90	90
<i>V</i> , Å <sup>3</sup>	2893.91(6)	1872.58(6)	2722.75(12)	2572.36(8)
<i>Z</i>	4	4	2	4
$\rho_{\text{calc}}$ , g cm <sup>-3</sup>	1.600	1.476	1.954	1.243
$\mu$ (Mo/Cu K $\alpha$ ), mm <sup>-1</sup>	5.42	9.68	4.31	5.28
crystal size, mm	0.41×0.31×0.14	0.34×0.21×0.21	0.35×0.14×0.03	0.31×0.30×0.23
$\theta$ range, deg	3.8–71.1	4.1–71.1	2.6–66.9	3.9–69.2
limiting indices	–12 ≤ <i>h</i> ≤ 12 –18 ≤ <i>k</i> ≤ 18 –21 ≤ <i>l</i> ≤ 20	–10 ≤ <i>h</i> ≤ 9 –17 ≤ <i>k</i> ≤ 17 –18 ≤ <i>l</i> ≤ 18	–12 ≤ <i>h</i> ≤ 12 –18 ≤ <i>k</i> ≤ 18 –20 ≤ <i>l</i> ≤ 19	–11 ≤ <i>h</i> ≤ 10 –17 ≤ <i>k</i> ≤ 18 –19 ≤ <i>l</i> ≤ 20
reflns collected	26229	17487	19080	21668
independent reflns	4881 [R(int) = 0.031]	3126 [R(int) = 0.028]	7790 [R(int) = 0.056]	4288 [R(int) = 0.037]
absorption correction	Numerical	Numerical	Numerical	Numerical
data/restraints/ parameters	4881 / 0 / 410	3126 / 0 / 220	7790 / 1 / 895	4288 / 0 / 297
goodness-of-fit on <i>F</i> <sup>2</sup>	1.14	1.01	1.24	1.07
final <i>R</i> indices	<i>R</i> 1 = 0.024	<i>R</i> 1 = 0.023	<i>R</i> 1 = 0.063	<i>R</i> 1 = 0.025
[ <i>I</i> > 2σ( <i>I</i> ) ] <sup>[a]</sup>	w <i>R</i> 2 = 0.052	w <i>R</i> 2 = 0.058	w <i>R</i> 2 = 0.086	w <i>R</i> 2 = 0.068
<i>R</i> indices (all data) <sup>[a]</sup>	<i>R</i> 1 = 0.027 w <i>R</i> 2 = 0.052	<i>R</i> 1 = 0.025 w <i>R</i> 2 = 0.058	<i>R</i> 1 = 0.106 w <i>R</i> 2 = 0.101	<i>R</i> 1 = 0.027 w <i>R</i> 2 = 0.070
peak <sub>max</sub> /hole <sub>min</sub> (e Å <sup>-3</sup> )	0.26 / –0.21	0.38 / –0.17	0.61 / –0.56	0.21 / –0.16
absolute structure parameter	0.006(3)	0.004(4)	0.023(6)	0.019(4)

**Synthesis of (p*S*)-5-Cl.** To a solution of **3-Hg** (68 mg, 0.12 mmol) in hexanes (10 mL) that was cooled down to  $-37\text{ }^{\circ}\text{C}$  was added a solution of  $\text{BCl}_3$  (1.0 M in hexanes, 0.13 mL, 0.13 mmol, 1.10 equiv) dropwise under stirring. A red precipitate developed, which redissolved upon addition of 10 mL of toluene. The reaction mixture was stirred overnight at room temperature and then for 2 hours at  $80\text{ }^{\circ}\text{C}$ . The solvents were removed under vacuum and the residue was re-dissolved in hot toluene/hexanes (1:1). An insoluble black solid was filtered off and the filtrate was kept at  $-37\text{ }^{\circ}\text{C}$  for recrystallization. Yield: 40 mg (80%).  $^1\text{H}$  NMR (499.9 MHz,  $\text{CDCl}_3$ ,  $25\text{ }^{\circ}\text{C}$ ):  $\delta$  = 7.76 (t,  $J$  = 8.0 Hz, 1H; Py), 7.62 (d,  $J$  = 8.0 Hz, 1H; Py), 7.38 (d,  $J$  = 8.0 Hz, 1H; Py), 4.79 (d,  $J$  = 2.0 Hz, 1H; Cp), 4.74 (d,  $J$  = 2.0 Hz, 1H; Cp), 4.63 (pst,  $J$  = 2.0 Hz, 1H; Cp), 4.06 (s, 5H; free Cp), 0.66 (s, 9H;  $\text{SiMe}_3$ ).  $^{11}\text{B}$  NMR (160.4 MHz,  $\text{CDCl}_3$ ,  $25\text{ }^{\circ}\text{C}$ )  $\delta$  = 7.53 ( $w_{1/2}$  = 110 Hz).

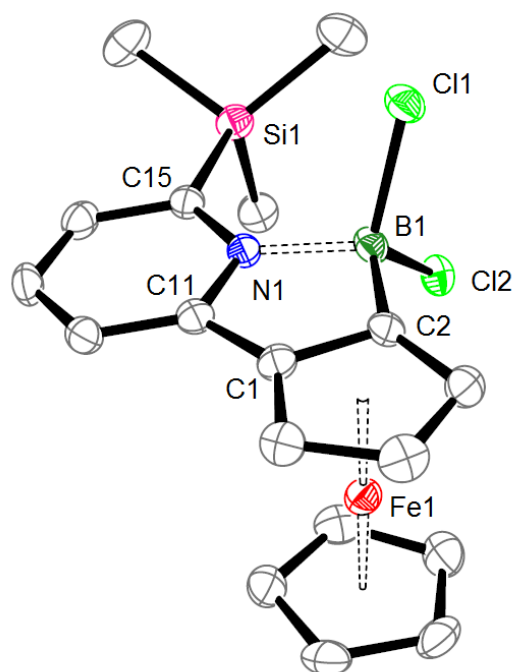


**Figure 4-8.** Ortep plot for compound **5-Cl** (50% thermal displacement ellipsoids). Hydrogen atoms are omitted for clarity. Selected interatomic distances ( $\text{\AA}$ ) and angles ( $^{\circ}$ ): B1-N1 1.614(3), B1-C2 1.571(4), B1-Cl1 1.878(3), B1-Cl2 1.857(3), C1-C2-B1 107.6(2), C2-B1-N1 100.66(19), B1-N1-C11 109.63(19), N1-C11-C1 110.3(2), C11-C1-C2 111.4(3), N1-C15-Si1 128.98(16), Cp//Cp 1.97, Py//Cp 4.88.

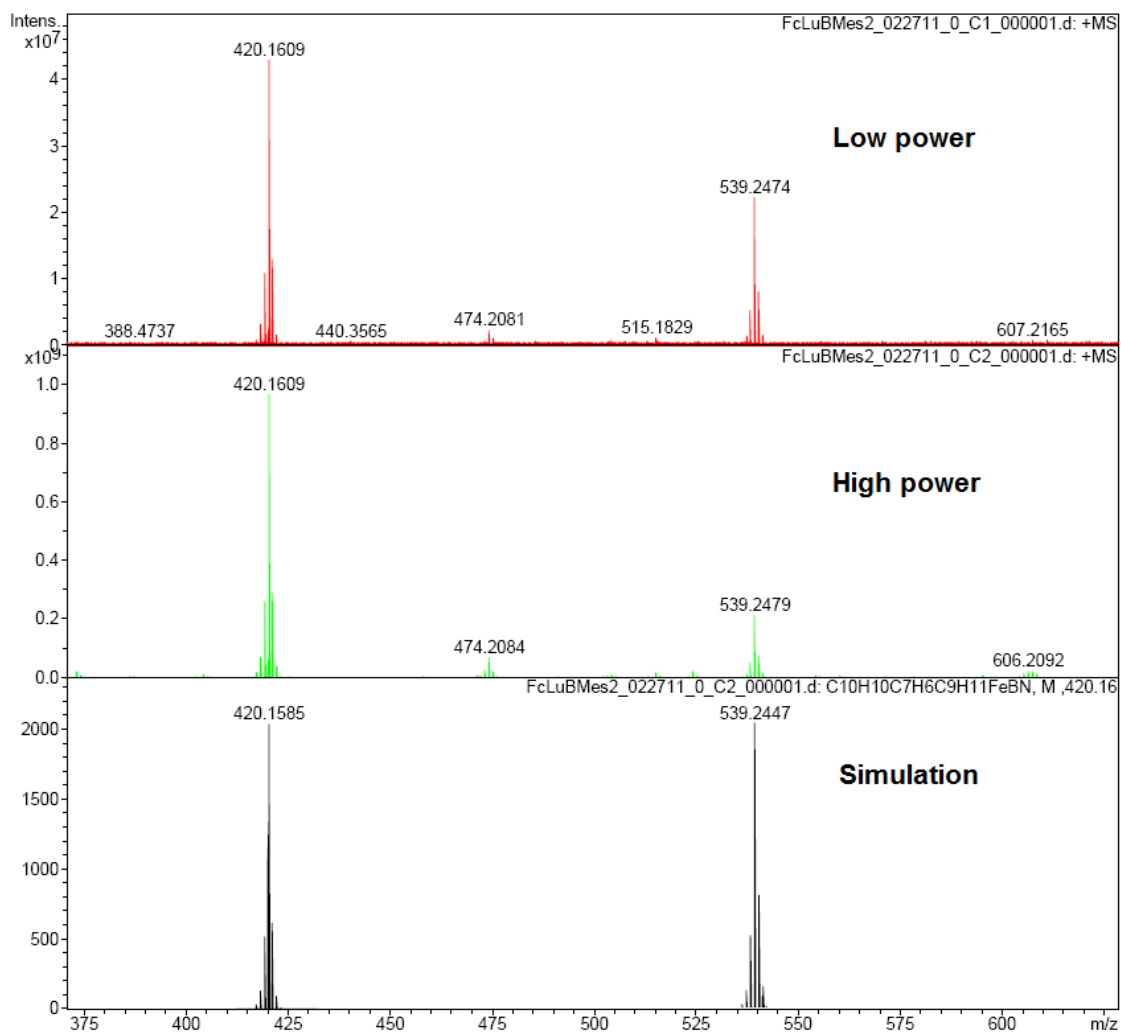


**Figure 4-9.** MALDI-MS data of compound 4-Mes.

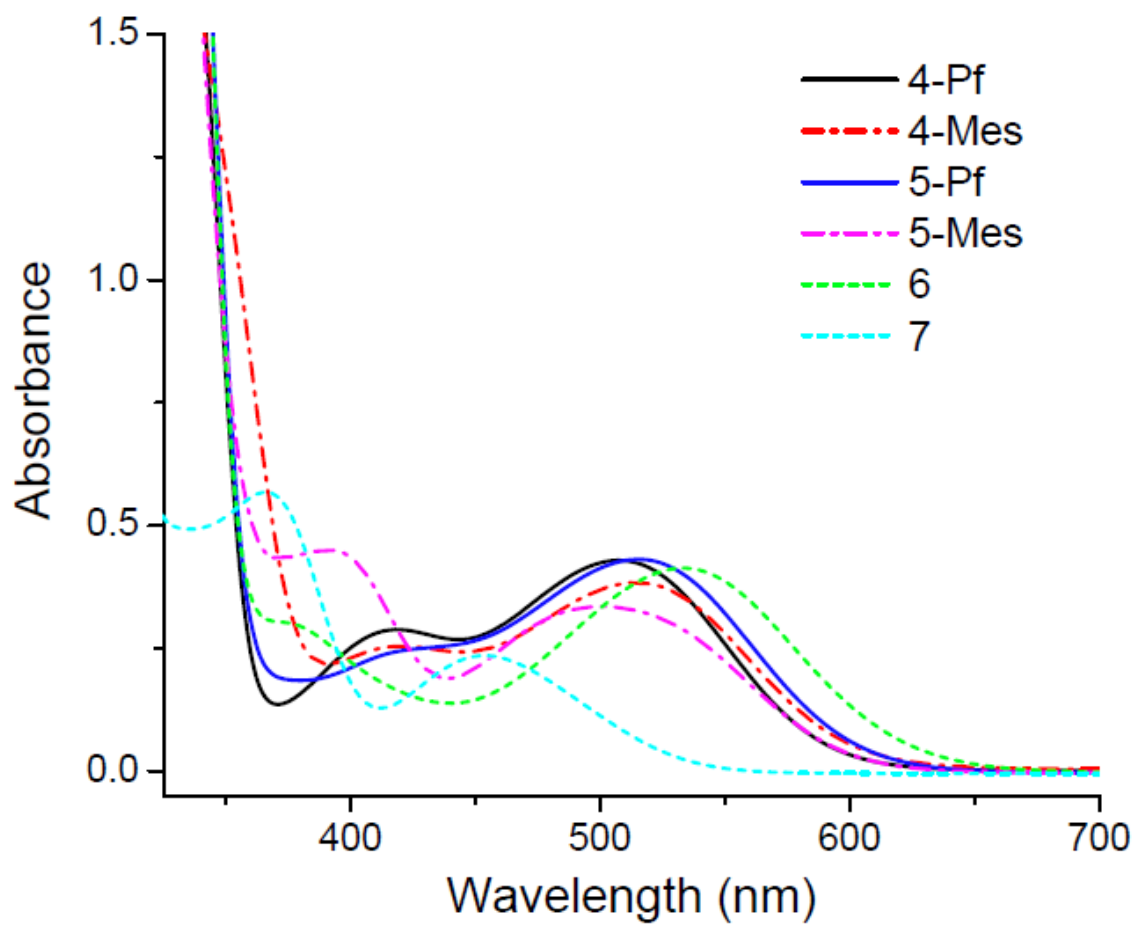


**Figure 4-10.** Comparison of UV-Vis absorption spectra in  $\text{CHCl}_3$ .

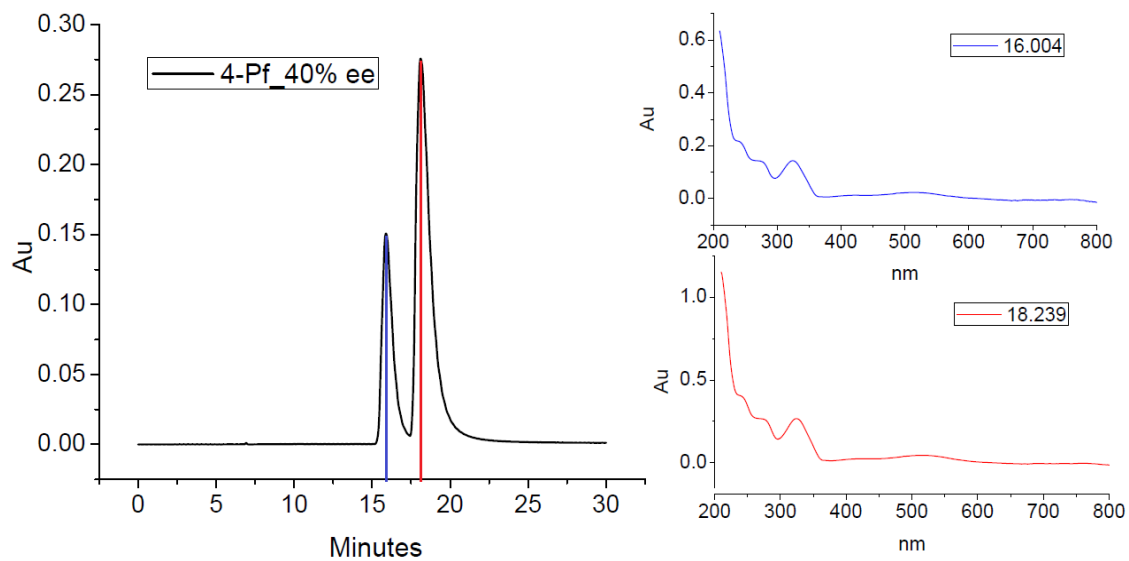


**Figure 4-11.** Chiral HPLC trace and the corresponding UV-Vis spectrum of **4-Pf** (40% ee).

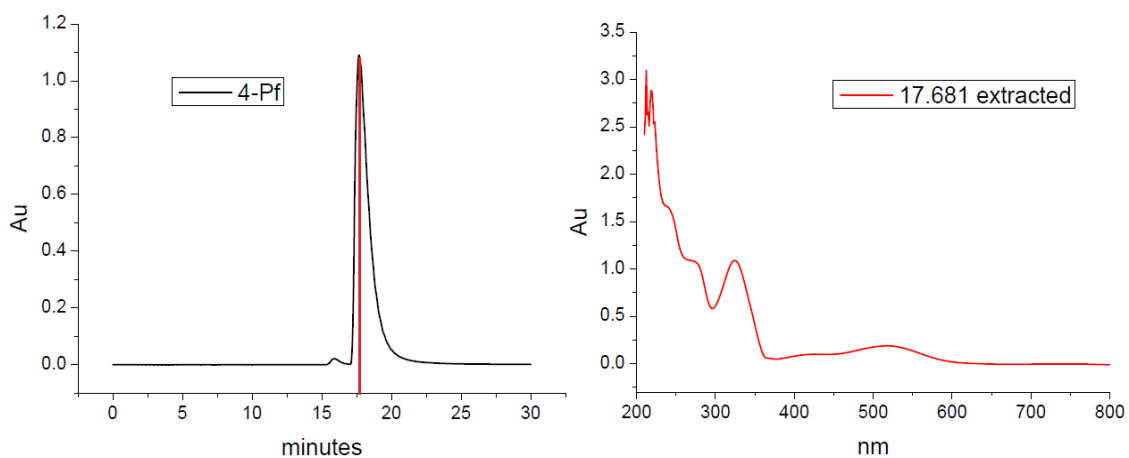


**Figure 4-12.** Chiral HPLC trace and the corresponding UV-Vis spectrum of (pR)-**4-Pf**.

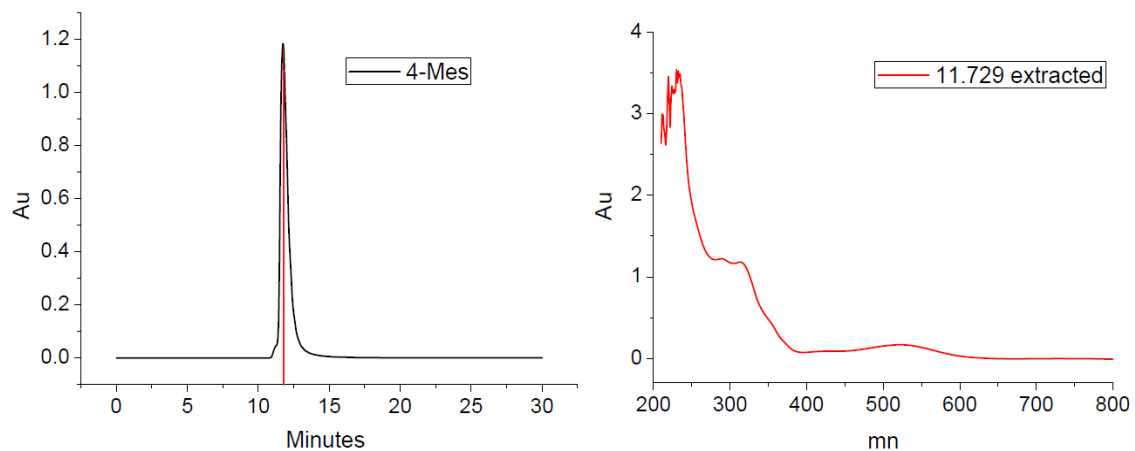


**Figure 4-13.** Chiral HPLC trace and the corresponding UV-Vis spectrum of (pR)-4-Mes.

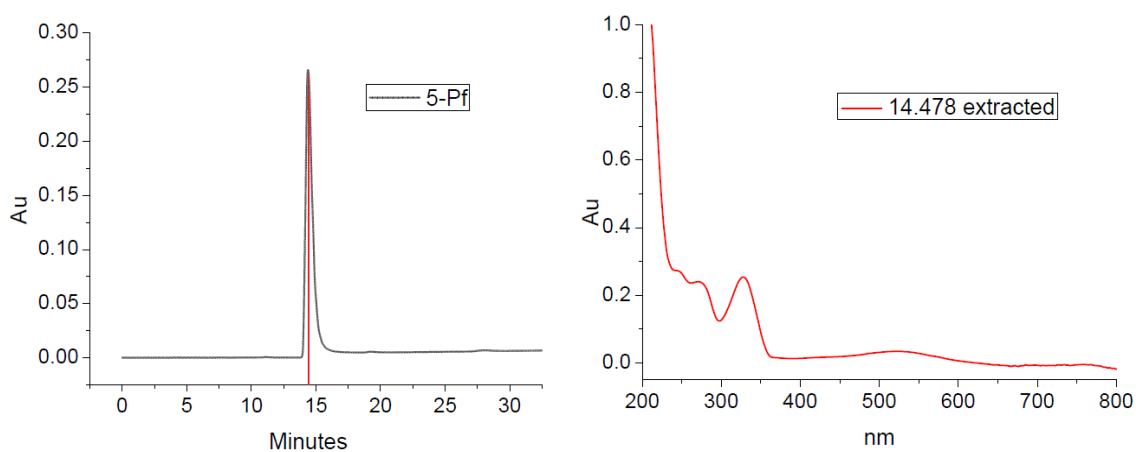


**Figure 4-14.** Chiral HPLC trace and the corresponding UV-Vis spectrum of (pS)-5-Pf.

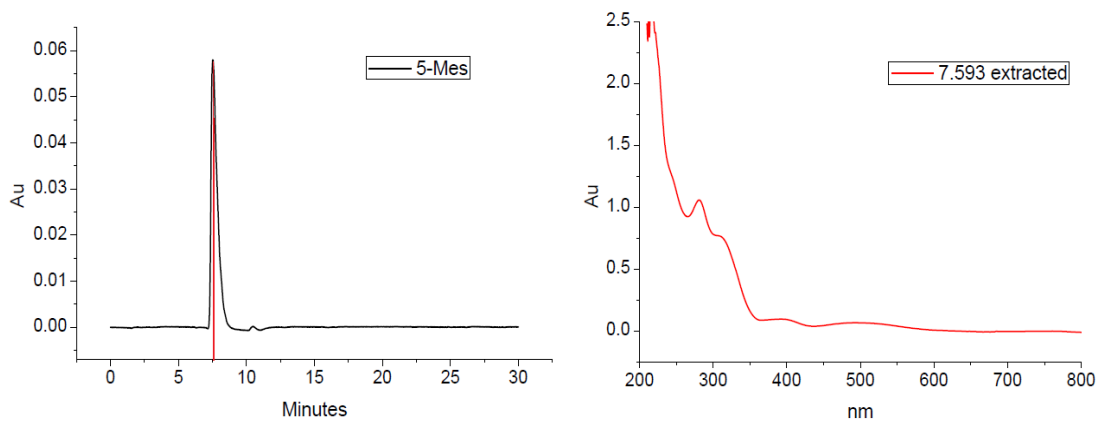


**Figure 4-15.** Chiral HPLC trace and the corresponding UV-Vis spectrum of (pS)-5-Mes.

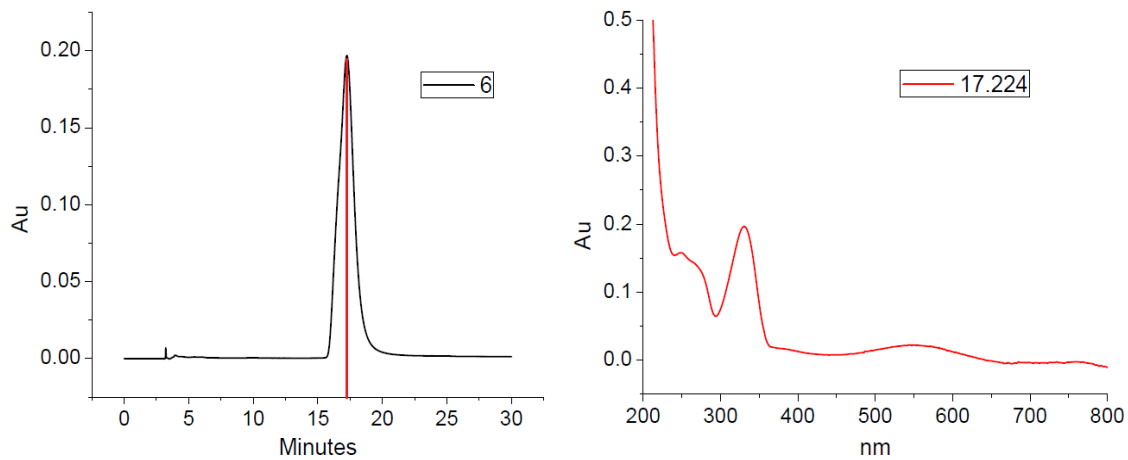


**Figure 4-16.** Chiral HPLC trace and the corresponding UV-Vis spectrum of (pS)-6.

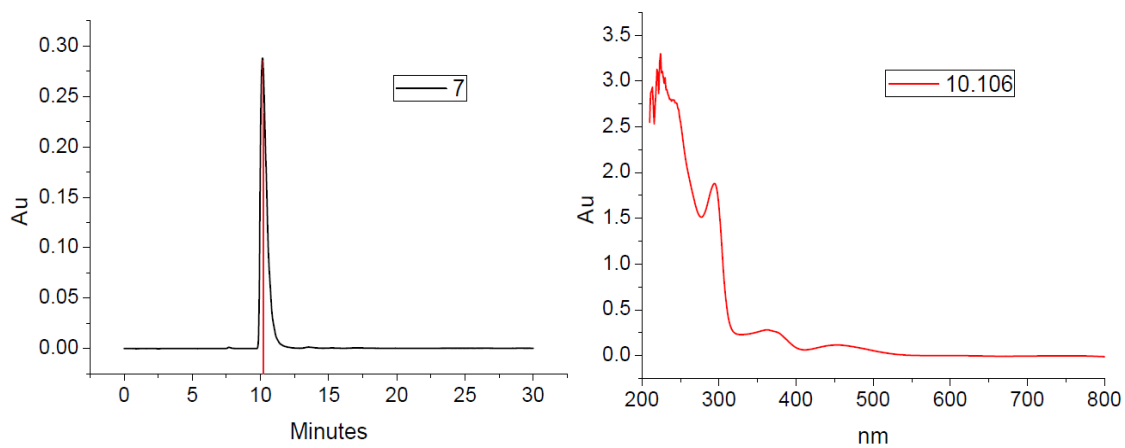


**Figure 4-17.** Chiral HPLC trace and the corresponding UV-Vis spectrum of (pS)-7.

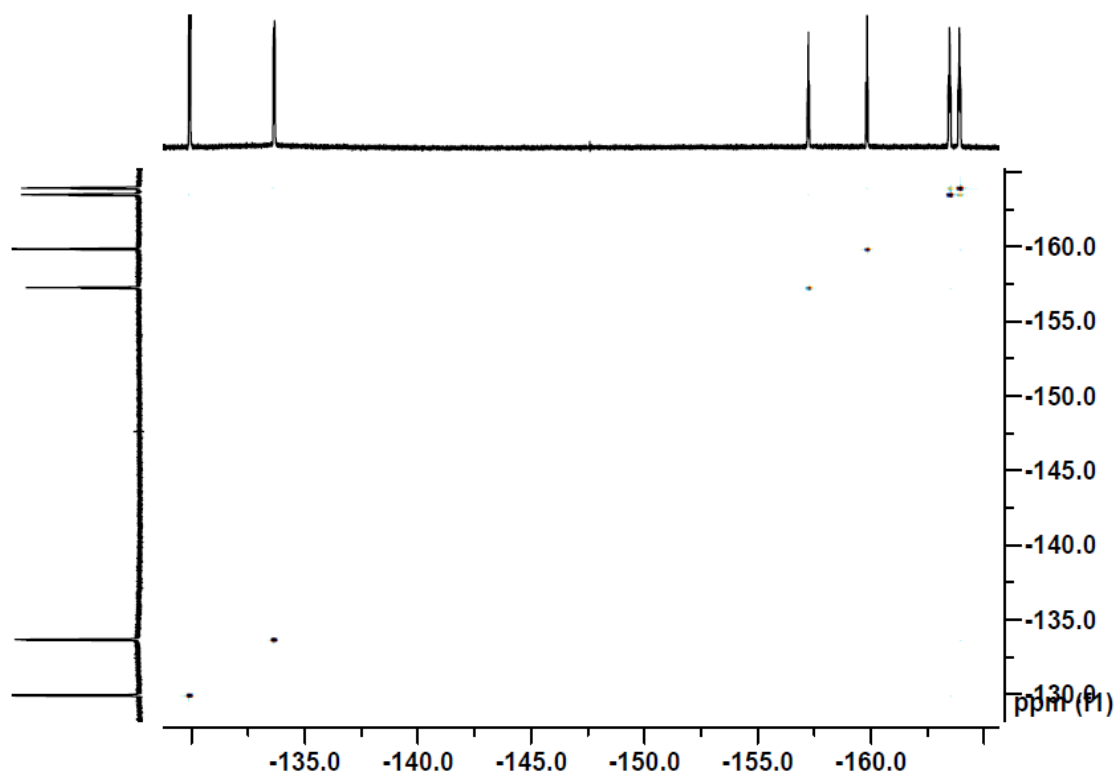


**Figure 4-18.**  $^{19}\text{F}$ - $^{19}\text{F}$  EXSY spectrum of **4-Pf** at 80 °C in  $d_8$ -toluene.

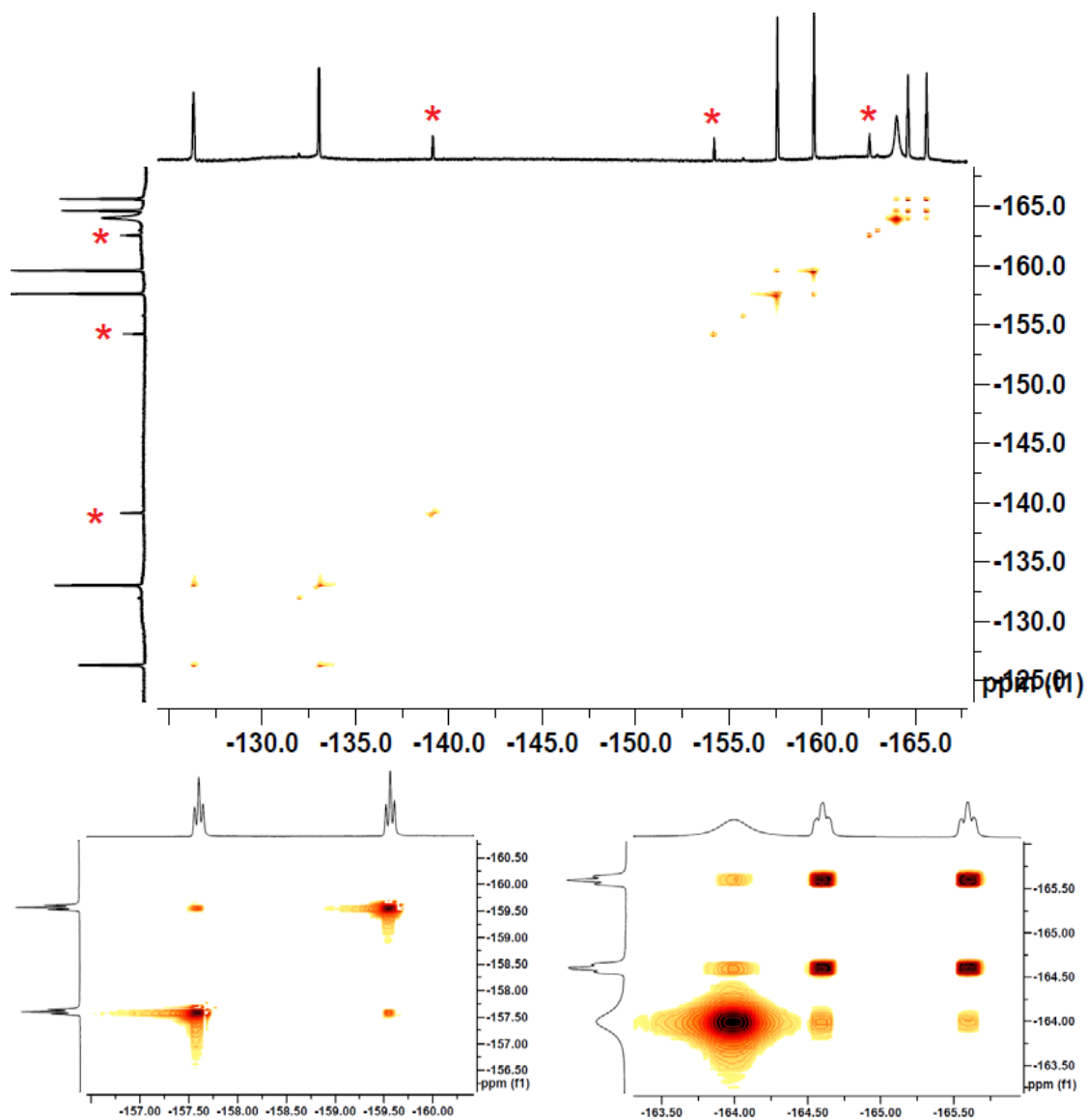


**Figure 4-19.**  $^{19}\text{F}$ - $^{19}\text{F}$  EXSY spectrum of **5-Pf** at 80 °C in  $\text{d}_3$ -toluene. Trace impurity is due to hydrolysis and subsequent boroxine formation with  $\text{C}_6\text{F}_5\text{H}^*$  as impurity signals.

#### 4.6 Notes and References

- (a) Stephan, D. W.; Erker, G., *Angew. Chem. Int. Ed.* **2010**, *49*, 46-76; (b) Stephan, D. W., *Dalton Trans.* **2012**, *41*, 9015; (c) Welch, G. C.; San Juan, R. R.; Masuda, J. D.; Stephan, D. W., *Science* **2006**, *314*, 1124-1126.
- (a) Kenward, A. L.; Piers, W. E., *Angew. Chem. Int. Ed.* **2008**, *47*, 38-41; (b) Neu, R. C.; Otten, E.; Lough, A.; Stephan, D. W., *Chem. Sci.* **2010**, *2*, 170-176; (c) Zhao, X.; Stephan, D. W., *Chem. Commun.* **2011**, *47*, 1833-1835; (d) Holschumacher, D.; Daniliuc, C. G.; Jones, P. G.; Tamm, M., *Z. Naturforsch. B* **2011**, *66*, 371-377; (e) Marwitz, A. J. V.; Dutton, J. L.; Mercier, L. G.; Piers, W. E., *J. Am. Chem. Soc.* **2011**, *133*, 10026-10029; (f) Theuergarten, E.; Schloesser, J.; Schluens, D.; Freytag, M.; Daniliuc, C. G.; Jones, P. G.; Tamm, M., *Dalton Trans.* **2012**, *41*, 9101-9110; (g) Sajid, M.; Stute, A.; Cardenas, A. J. P.; Culotta, B. J.; Hepperle, J. A. M.; Warren, T. H.; Schirmer, B.; Grimme, S.; Studer, A.; Daniliuc, C. G.; Froehlich, R.; Petersen, J. L.; Kehr, G.; Erker, G., *J. Am. Chem. Soc.* **2012**, *134*, 10156-10168; (h) Zhang, Y.; Miyake, G. M.; Chen, E. Y. X., *Angew. Chem. Int. Ed.* **2010**, *49*, 10158-10162; (i) Heiden, Z. M.; Stephan, D. W., *Chem. Commun.* **2011**, *47*, 5729-5731; (j) Piers, W. E.; Marwitz, A. J. V.; Mercier, L. G., *Inorg. Chem.* **2011**, *50*, 12252-12262; (k) Rosorius, C.; Kehr, G.; Froehlich, R.; Grimme, S.; Erker, G., *Organometallics* **2011**, *30*, 4211-4219; (l) Greb, L.; Ona-Burgos, P.; Schirmer, B.; Grimme, S.; Stephan, D. W.; Paradies, J., *Angew. Chem. Int. Ed.* **2012**, *51*, 10164-10168; (m) Stephan, D. W., *Org. Biomol. Chem.* **2012**, *10*, 5740-5746; (n) Zhang, Y.; Miyake, G. M.; John, M. G.; Falivene, L.; Caporaso, L.; Cavallo, L.; Chen, E. Y. X., *Dalton Trans.* **2012**, *41*, 9119-9134.
- (a) Chen, D. J.; Wang, Y. T.; Klankermayer, J., *Angew. Chem. Int. Ed.* **2010**, *49*, 9475-9478; (b) Mewald, M.; Fröhlich, R.; Oestreich, M., *Chem. Eur. J.* **2011**, *17*, 9406-9414; (c) Ghattas, G.; Chen, D. J.; Pan, F. F.; Klankermayer, J., *Dalton Trans.* **2012**, *41*, 9026-9028; (d) Chen, D. J.; Leich, V.; Pan, F. F.; Klankermayer, J., *Chem. Eur. J.* **2012**, *18*, 5184-5187; (e) Mewald, M.; Oestreich, M., *Chem. Eur. J.* **2012**, *18*, 14079-14084.
- Geier, S. J.; Gille, A. L.; Gilbert, T. M.; Stephan, D. W., *Inorg. Chem.* **2009**, *48*, 10466-10474.
- (a) Boshra, R.; Doshi, A.; Jäkle, F., *Angew. Chem. Int. Ed.* **2008**, *47*, 1134-1137; (b) Boshra, R.; Venkatasubbaiah, K.; Doshi, A.; Jäkle, F., *Organometallics* **2009**, *28*, 4141-4149; (c) Chen, J.; Venkatasubbaiah, K.; Pakkirisamy, T.; Doshi, A.; Yusupov, A.; Patel, Y.; Lalancette, R. A.; Jäkle, F., *Chem. Eur. J.* **2010**, *16*, 8861-8867; (d) Thilagar, P.; Chen, J.; Lalancette, R. A.; Jäkle, F., *Organometallics* **2011**, *30*, 6734-6741; (e) Chen, J.; Lalancette, R. A.; Jäkle, F., *Organometallics* **2013**, *32*, 5843-5851; (f) Chen, J.; Lalancette, R. A.; Jäkle, F., *Chem. Commun.* **2013**, *49*, 4893-4895.
- (a) Huber, D. P.; Kehr, G.; Bergander, K.; Froehlich, R.; Erker, G.; Tanino, S.; Ohki, Y.; Tatsumi, K., *Organometallics* **2008**, *27*, 5279-5284; (b) Morgan, I. R.; Di Paolo, A.; Vidovic, D.; Fallis, I. A.; Aldridge, S., *Chem. Commun.* **2009**, 7288-7290; (c) Schwendemann, S.; Tumay, T. A.; Axenov, K. V.; Peuser, I.; Kehr, G.; Fröhlich, R.; Erker, G., *Organometallics* **2010**, *29*, 1067-1069; (d) Siewert, I.; Vidovic, D.; Aldridge, S., *J. Organomet. Chem.* **2011**, *696*, 2528-2532; (e) Voss, T.; Sortais, J. B.; Fröhlich, R.; Kehr, G.; Erker, G., *Organometallics* **2011**, *30*, 584-594; (f) Sudhakar, P.; Thilagar, P., *J. Chem. Sci.* **2013**, *125*, 41-49.

7. (a) Guillaneux, D.; Kagan, H. B., *J. Org. Chem.* **1995**, *60*, 2502-2505; (b) Riant, O.; Argouarch, G.; Guillaneux, D.; Samuel, O.; Kagan, H. B., *J. Org. Chem.* **1998**, *63*, 3511-3514.
8. King, A. O.; Okukado, N.; Negishi, E.-i., *J. Chem. Soc., Chem. Commun.* **1977**, 683-684.
9. Gros, P.; Viney, C.; Fort, Y., *Synlett* **2002**, *4*, 628-630.
10. Rodriguez, A.; Romero, J.; Garcia-Vasquez, J. A.; Duran, M. L.; Sousa-Pedrares, A.; Sousa, A.; Zubieta, J., *Inorg. Chim. Acta.* **1999**, *284*, 133-138.
11. A very similar observation is made for the chloro-substituted species 5-Cl. The B-N distance of 1.615(3) Å suggests a strong Lewis acid-base interaction, which forces the trimethylsilyl group to bend away from the boryl moiety (N1-C15-Si1 = 129.0(2)°). See Supporting Information for details of the X-ray structure of 5-Cl.
12. A direct comparison of the N1-C15-Si1 angles in compounds 5-Pf [128.9(2)°], 6 [119.6(2)°] and 5-Mes [114.2(2)°] reveals that the steric congestion at the Lewis base decreases from pyridine-borane pair to pyridinium, then to free pyridine. The angle for 5-Mes is less than 120° due to the lower steric demand at N versus the C-H in ortho-position.
13. Thilagar, P.; Murillo, D.; Chen, J.; Jäkle, F., *Dalton Trans.* **2013**, *42*, 665-670.
14. Carpenter, B. E.; Piers, W. E.; Parvez, M.; Yap, G. P. A.; Rettig, S. J., *Can. J. Chem.* **2001**, *79*, 857-867.
15. Broomsgrove, A. E. J.; Addy, D. A.; Bresner, C.; Fallis, I. A.; Thompson, A. L.; Aldridge, S., *Chem. Eur. J.* **2008**, *14*, 7525-7529.
16. Reisinger, A.; Himmel, D.; Krossing, I., *Angew. Chem. Int. Ed.* **2006**, *45*, 6997-7000.
17. (a) Scheibitz, M.; Bolte, M.; Bats, J. W.; Lerner, H.-W.; Nowik, I.; Herber, R. H.; Krapp, A.; Lein, M.; Holthausen, M.; Wagner, M., *Chem. Eur. J.* **2005**, *11*, 584-603; (b) Venkatasubbaiah, K.; Nowik, I.; Herber, R. H.; Jäkle, F., *Chem. Commun.* **2007**, 2154-2156.
18. Scheibitz, M.; Bolte, M.; Bats, J. W.; Lerner, H.-W.; Nowik, I.; Herber, R. H.; Krapp, A.; Lein, M.; Holthausen, M.; Wagner, M., *Chem. Eur. J.* **2005**, *11*, 584-603.
19. Sundararaman, A.; Jäkle, F., *J. Organomet. Chem.* **2003**, *681*, 134-142.
20. (a) Cairncross, A.; Omura, H.; Sheppard, W. A., *J. Am. Chem. Soc.* **1971**, *93*, 248-249; (b) Cairncross, A.; Sheppard, W. A.; Wonchoba, E.; Guildford, W. J.; House, C. B.; Coates, R. M., *Org. Synth.* **1980**, *59*, 122-131; (c) Sundararaman, A.; Lalancette, R. A.; Zakharov, L. N.; Rheingold, A. L.; Jäkle, F., *Organometallics* **2003**, *22*, 3526-3532.
21. (a) Meyer, E. M.; Gambarotta, S.; Floriani, C.; Chiesi-Villa, A.; Guastini, C., *Organometallics* **1989**, *8*, 1067-1079; (b) Eriksson, H.; Håkansson, M., *Organometallics* **1997**, *16*, 4243-4244.
22. Sheldrick, G. M. *SHELXTL, Version 6.14*, Bruker AXS Inc.: Madison, WI, 2004.

## Chapter 5 Catalytic Application of Planar Chiral Ferrocenyl Lewis Acids: Studies of Lewis Acidity, Substrate Binding and Asymmetric Process<sup>a</sup>

### 5.1 Introduction

In this chapter we describe the first planar chiral ferrocenylborenium species (*pR*)-**3**<sup>+</sup>, which is obtained in enantiopure form by halide abstraction from the corresponding chloroborane adduct (*pR*)-**2** using Krossing's salt. Competition experiments suggest that the Lewis acidity of (*pR*)-**3**<sup>+</sup> is higher than that of B(C<sub>6</sub>F<sub>5</sub>)<sub>3</sub> towards anions and slightly lower towards neutral Lewis bases. The ferrocenylborenium species (*pR*)-**3**<sup>+</sup> is examined as a catalyst for the stereoselective hydrosilylation of ketones.

Highly Lewis acidic organoboranes continue to attract tremendous interest and current applications range from Lewis acid catalysis of organic transformations<sup>1</sup> and polymerization reactions<sup>2</sup> to small molecule activation,<sup>3</sup> sensors for anions,<sup>4</sup> and the development of new and unusual electronic materials.<sup>5</sup> Many of the earlier studies have focused on installing electron withdrawing fluorine substituents onto organoboranes as a means of increasing the electron-deficient character of boron, and B(C<sub>6</sub>F<sub>5</sub>)<sub>3</sub> is nowadays broadly applied not only in academia but has also found its way into a wide range of industrial processes.<sup>6</sup> An alternative approach involves the incorporation of tricoordinate boron into antiaromatic cyclics as in borole and diborabenzene derivatives. In this case, Lewis acid-base adduct formation is energetically favored by conversion to non-aromatic species.<sup>7</sup> Most recently, highly reactive borenium species<sup>8</sup> have been introduced, in

---

<sup>a</sup> This chapter is adapted from a journal publication

which the cationic charge further enhances the potency of tricoordinate borane Lewis acids.<sup>9</sup>

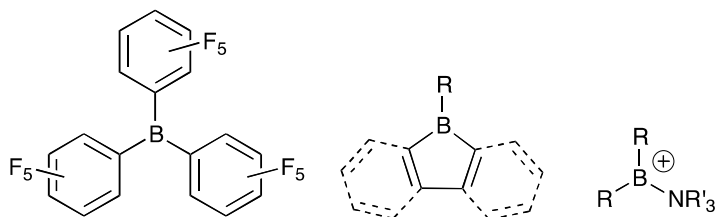
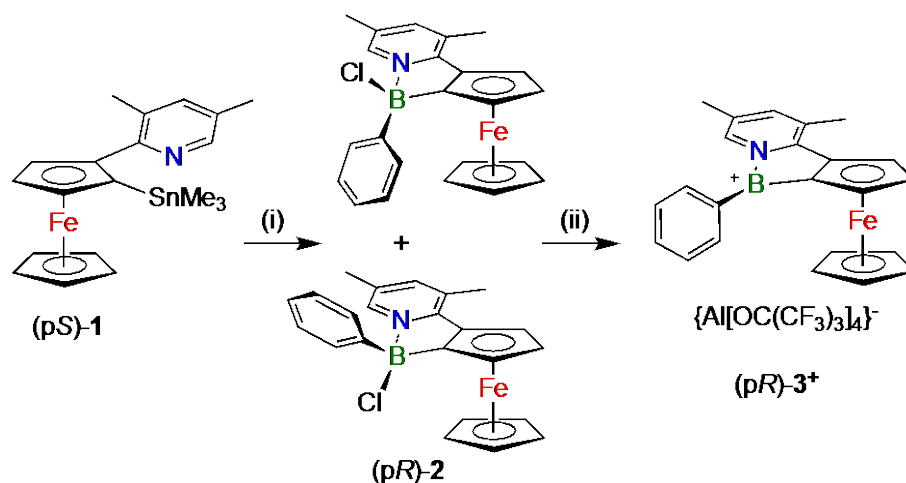


**Figure 5-1.** Examples of highly Lewis acidic organoboranes

Borenium species have proven highly advantageous especially in the promotion of electrophilic aromatic substitution chemistries.<sup>8b, 10</sup> Very recently the first studies of their use in hydrogenation and hydroboration catalysis have also been reported.<sup>11</sup> For broad application in organic synthesis it is desirable to develop and utilize chiral borenium Lewis acids. Chiral alkyl- and arylboranes, including fluorinated derivatives, are widely applied as reagents and catalysts in stereoselective synthesis.<sup>14-16</sup> We have over the past several years pursued planar chiral ferrocene-based Lewis acids.<sup>15, 17-19</sup> We have demonstrated, for example, the utility of a bifunctional ferrocene-based Lewis acid as a stereoselective reagent for the allylation of ketones with ee's of up to 80%.<sup>12</sup> We have also introduced fluorinated arylboranes attached to a chiral naphthylferrocenyl framework.<sup>13</sup> Related planar-chiral  $\eta^5$ -1,2-azaborolyll iron complexes have been utilized by Fu and coworkers in Mukayama aldol reactions and in stereoselective additions to imines.<sup>14</sup> Interestingly, planar chiral borenium cations were proposed as intermediates in these processes. We describe in here the first synthesis of an isolable planar-chiral ferrocenylborenium cation, discuss the Lewis acid properties and present a proof-of-principle investigation of its utility in the hydrosilylation of ketones.

## 5.2 Synthesis and Characterization



### Scheme 5-1. Synthesis of (pR)-3<sup>+</sup>

(i) 2 PhBCl<sub>2</sub>, toluene/hexanes, -37 °C to rt. (ii) Method A: [Ag(CH<sub>2</sub>Cl<sub>2</sub>)]{Al[OC(CF<sub>3</sub>)<sub>3</sub>]<sub>4</sub>}, CHCl<sub>3</sub>, -37 °C to rt; Method B: Li{Al[OC(CF<sub>3</sub>)<sub>3</sub>]<sub>4</sub>}, CDCl<sub>3</sub>, rt.

The chloroborane adduct (pR)-3 was prepared by treatment of the organotin compound (pS)-1<sup>15</sup> with an excess of PhBCl<sub>2</sub> in hexanes/toluene mixture (Scheme 5-1).<sup>16,17</sup> Based on <sup>1</sup>H NMR studies (Figure 5-2a) two different species (ratio 2.5:1) are present in solution, which are attributed to the *exo*-Ph and *endo*-Ph isomers of (pR)-2. According to a 2D NOESY experiment,<sup>†</sup> the major isomer features the Ph group in *exo*-position and the minor isomer in *endo*-position. Coalescence was not observed in the 1D <sup>1</sup>H NMR spectra even at temperatures up to 70 °C. This indicates that isomerization is slow on the NMR time scale.

We initially attempted to prepare the corresponding borenium cation by Cl<sup>-</sup> abstraction with B(C<sub>6</sub>F<sub>5</sub>)<sub>3</sub>. Indeed, when compound (pR)-3 was mixed with one equivalent of B(C<sub>6</sub>F<sub>5</sub>)<sub>3</sub>, coalescence into a single set of broad <sup>1</sup>H NMR resonances was observed (Figure 5-2b). However, the Lewis acid strength of B(C<sub>6</sub>F<sub>5</sub>)<sub>3</sub> proved to be far too low to

bring about complete abstraction of  $\text{Cl}^-$ . In contrast, treatment of (p*R*)-**2** with 1 equiv of Crossing's salt<sup>18</sup>

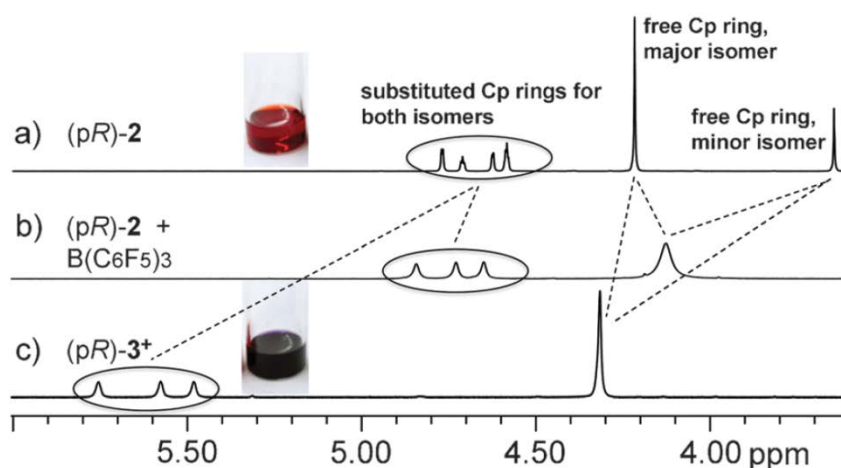


**Figure 5-2.** Expansion of the Cp region of the  $^1\text{H}$  NMR spectra for a) (p*R*)-**2** (*exo*- and *endo*-isomers), b) (p*R*)-**2** +  $\text{B}(\text{C}_6\text{F}_5)_3$  and c) (p*R*)-**3**<sup>+</sup> ( $\text{CDCl}_3$ ) and photographs illustrating the associated color change.

$[\text{Ag}(\text{CH}_2\text{Cl}_2)]\{\text{Al}[\text{OC}(\text{CF}_3)_3]_4\}$  or  $\text{Li}\{\text{Al}[\text{OC}(\text{CF}_3)_3]_4\}$  in  $\text{CHCl}_3$  led to quantitative chloride abstraction with formation of the tricoordinate borenium cation (p*R*)-**3**<sup>+</sup> (Scheme 5-1). The  $^1\text{H}$  NMR spectrum showed strongly downfield shifted signals at 5.75, 5.58 and 5.48 ppm for the substituted Cp ring, consistent with attachment of a highly electron-deficient borenium cation (Figure 5-2c). In the  $^{11}\text{B}$  NMR spectrum a broad signal was observed at 45.4 ppm for the cation and in the  $^{19}\text{F}$  NMR spectrum a sharp signal at  $-75.4$  ppm for the anion. Another characteristic feature of the borenium cation (p*R*)-**3**<sup>+</sup> is its deep purple color (Figure 5-2,  $\lambda_{\text{max}} = 566$  nm,  $\varepsilon = 2200$   $\text{M}^{-1}\text{cm}^{-1}$ ). This unusual color is likely due to enhanced charge transfer from iron to the more extended and highly electron-deficient  $\pi$ -system of the pyridylborenium heterocycle in (p*R*)-**3**<sup>+</sup>.<sup>19</sup>

A single crystal X-ray diffraction analysis confirmed retention of the planar chirality upon halide abstraction from (p*R*)-**2** to give (p*R*)-**3**<sup>+</sup> (Figure 5-3a). As expected, the

highly electron-deficient nature of the borenium moiety results in a strong interaction between B and the electron-rich Fe, which is reflected in pronounced bending of the boryl group out of the Cp plane, towards the iron center. The tilt angles for the boryl groups in two independent cations are  $14.1^\circ$  ( $\text{Fe}\cdots\text{B}$  2.925 Å) and  $14.5^\circ$  ( $\text{Fe}\cdots\text{B}$  2.907 Å), respectively, which is similar to Piers' perfluorophenyl-substituted  $\text{FcB}(\text{C}_6\text{F}_5)_2$ <sup>20</sup> ( $16^\circ$ ,  $\text{Fe}\cdots\text{B}$  2.924 Å) and  $\text{FcBBr}_2$ <sup>21</sup> ( $17.7, 18.9^\circ$ ;  $\text{Fe}\cdots\text{B}$  2.856/2.840 Å).<sup>22</sup> Noteworthy is that the  $\text{Cp}_{\text{CENT}}\cdots\text{Cp}_{\text{CENT}}$  distance of 3.316 Å is consistent with a neutral ferrocene,<sup>23</sup> supporting the assignment of  $(pR)\text{-3}^+$  as a borenium-substituted ferrocene rather than a borane-substituted ferrocenium species.<sup>24</sup> Another interesting aspect is that the planar  $\pi$ -conjugated structure of  $(pR)\text{-3}^+$  favors formation of inter-molecular  $\pi$ - $\pi$  dimers that consist of two independent cations.†

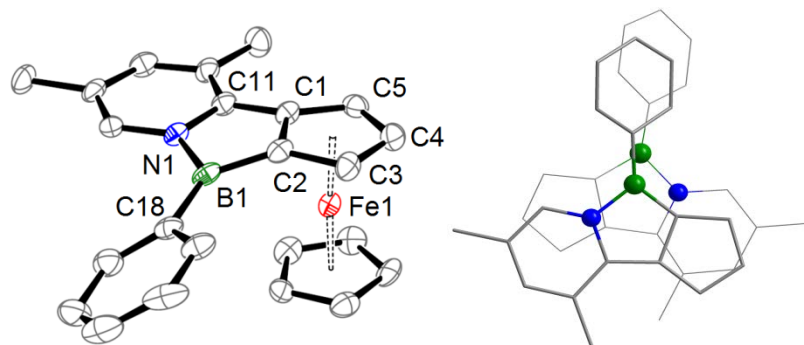


**Figure 5-3.** a) Ortep plot of  $(pR)\text{-3}^+$  (50% thermal ellipsoids); counteranions and H atoms are omitted. Selected distances (Å) and angles ( $^\circ$ ) [ $2^{\text{nd}}$  independent molecule]: B1-N1 1.544(7) [1.550(9)], B1-C2 1.519(9) [1.539(9)], B1-C18 1.524(9) [1.504(10)], C2-B1-N1 102.2(5) [100.6(5)], C2-B1-C18 131.4(5) [132.2(6)], C18-B1-N1 126.3(5) [127.1(6)]. (b) A  $\pi$  dimer consisting of two independent molecules of  $(pR)\text{-3}^+$  (only substituted Cp rings shown).

### 5.3 Lewis Acidity Determination and Substrate Binding

A first indication of the high Lewis acidity of  $(pR)\text{-3}^+$  came from the fact that the reaction of  $(pR)\text{-2}$  with an equimolar amount of  $\text{B}(\text{C}_6\text{F}_5)_3$  led to only a very modest

downfield shift of the Cp resonances (see Figure 5-2b). This implies that only partial abstraction ( $\ll 50\%$ ) of chloride from (pR)-**2** occurs and suggests that (pR)-**3**<sup>+</sup> as a cation has a higher affinity than B(C<sub>6</sub>F<sub>5</sub>)<sub>3</sub> towards anionic Lewis bases such as Cl<sup>-</sup>.

According to Gutman-Beckett's method,<sup>25</sup> the <sup>31</sup>P NMR shift difference of Et<sub>3</sub>PO before and after complexation to a Lewis acid could serve as a measurement of Lewis acidity. The larger downfield chemical shift is an indication of higher Lewis acid strength. This method was utilized to examine the relative Lewis acidity of (pR)-**3**<sup>+</sup>. The chemical shift difference  $\Delta\delta$  is larger for (pR)-**3**<sup>+</sup> (32.6 ppm) than for B(C<sub>6</sub>F<sub>5</sub>)<sub>3</sub> (26.5 ppm), which would indicate higher Lewis acidity of (pR)-**3**<sup>+</sup> toward Et<sub>3</sub>PO (Figure 5-4).

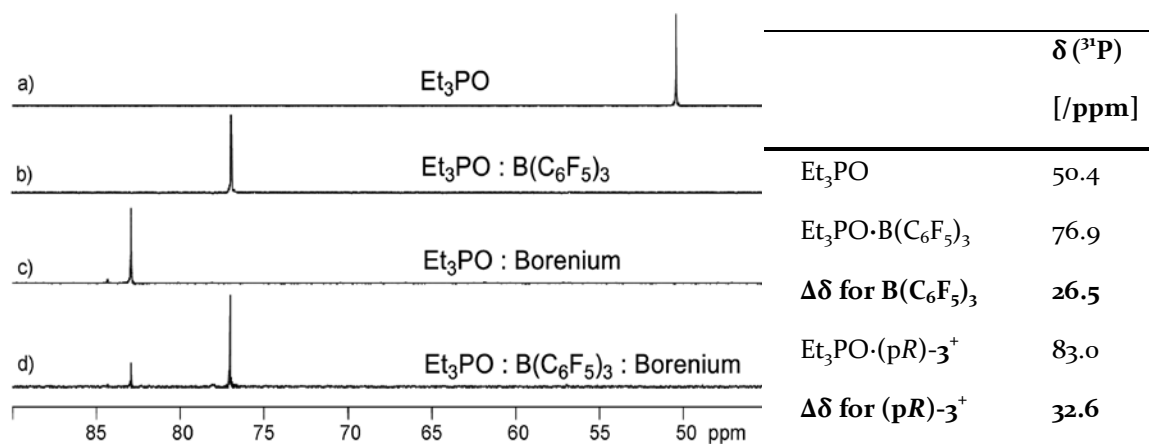


**Figure 5-4.** Competitive binding of (pR)-**3**<sup>+</sup> and B(C<sub>6</sub>F<sub>5</sub>)<sub>3</sub> to Et<sub>3</sub>PO examined by <sup>31</sup>P NMR spectroscopy in CD<sub>2</sub>Cl<sub>2</sub> at room temperature (0.02 M solutions). a) Et<sub>3</sub>PO; b) Et<sub>3</sub>PO + B(C<sub>6</sub>F<sub>5</sub>)<sub>3</sub>. c) Et<sub>3</sub>PO + (pR)-**3**<sup>+</sup>. d) Et<sub>3</sub>PO + 1.0 (pR)-**3**<sup>+</sup> + 1.0 B(C<sub>6</sub>F<sub>5</sub>)<sub>3</sub>.

However, to gain more insight into the Lewis acid properties of (pR)-**3**<sup>+</sup> we performed a competitive binding study, in which a mixture of the borenium species (pR)-**3**<sup>+</sup> and B(C<sub>6</sub>F<sub>5</sub>)<sub>3</sub> was treated with an equimolar amount of the neutral Lewis base Et<sub>3</sub>PO (Figure 5-5). The complexes Et<sub>3</sub>PO·(pR)-**3**<sup>+</sup> and Et<sub>3</sub>PO·B(C<sub>6</sub>F<sub>5</sub>)<sub>3</sub> are present in a ratio of 1:3.6 at

room temperature, which shows that slightly more  $\text{Et}_3\text{PO}$  binds to  $\text{B}(\text{C}_6\text{F}_5)_3$  than to  $(pR)\text{-}\mathbf{3}^+$ , indicating that  $\text{B}(\text{C}_6\text{F}_5)_3$  is a stronger Lewis acid toward  $\text{Et}_3\text{PO}$ . The fact that the  $^{31}\text{P}$  chemical shift difference is larger for the binding of  $\text{Et}_3\text{PO}$  to  $(pR)\text{-}\mathbf{3}^+$  could be related to delocalization of the positive charge on the phosphorous. Clearly, the Gutmann-Beckett method cannot be used to directly compare the Lewis acidity of ionic and neutral borane species, instead a competition experiment has to be performed. We conclude that  $(pR)\text{-}\mathbf{3}^+$  has a higher affinity than  $\text{B}(\text{C}_6\text{F}_5)_3$  towards anionic Lewis bases such as  $\text{Cl}^-$  and is only slightly less Lewis acidic than  $\text{B}(\text{C}_6\text{F}_5)_3$  towards neutral Lewis bases such as  $\text{Et}_3\text{PO}$ . In short,  $(pR)\text{-}\mathbf{3}^+$  proved to be a remarkably strong Lewis acid.

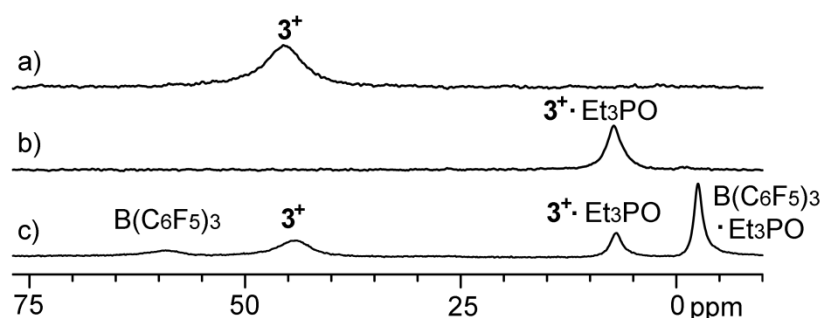


**Figure 5-5.** Competitive binding of  $(pR)\text{-}\mathbf{3}^+$  and  $\text{B}(\text{C}_6\text{F}_5)_3$  to  $\text{Et}_3\text{PO}$  examined by  $^{11}\text{B}$  NMR spectroscopy in  $\text{CD}_2\text{Cl}_2$  at room temperature (0.02 M solutions). a)  $(pR)\text{-}\mathbf{3}^+$ ; b)  $(pR)\text{-}\mathbf{3}^+$  +  $\text{Et}_3\text{PO}$ ; c) 1.0  $(pR)\text{-}\mathbf{3}^+$  + 1.0  $\text{B}(\text{C}_6\text{F}_5)_3$  + 1.0  $\text{Et}_3\text{PO}$ . The ratios in plot c) are consistent with those obtained by  $^{31}\text{P}$  NMR (see Figure 5-4).

An application of Lewis acids in organic synthesis that has attracted considerable interest is the metal-free hydrosilylation of ketones. This process was first studied for  $\text{B}(\text{C}_6\text{F}_5)_3$  by Piers and coworkers.<sup>26</sup> Piers demonstrated that activation of the Si-H functionality in silanes with  $\text{B}(\text{C}_6\text{F}_5)_3$  plays a key role<sup>3c</sup> and more recent studies by Oestreich further support this notion.<sup>27</sup> However, the development of enantioselective versions of this process continues to be a challenge.<sup>28</sup>

We first examined the reactivity of (p*R*)-**3**<sup>+</sup> toward ketones and silanes, respectively. When (p*R*)-**3**<sup>+</sup> was mixed with 1 equiv of HSiEt<sub>3</sub> in CDCl<sub>3</sub> at RT, the <sup>1</sup>H NMR spectra of both components were unchanged. However, at elevated temperature a loss of *H*-Si-CH<sub>2</sub> coupling was clearly observed (Figure 5-6), which is consistent with an R'<sub>3</sub>Si-H⋯BR<sub>3</sub> interaction according to studies by Bergman and coworkers<sup>29</sup> on related Al-based systems. Treatment of compound (p*R*)-**3**<sup>+</sup> with acetophenone resulted in a distinct color change from deep purple to orange-red due to adduct formation. The Lewis acid strength of (p*R*)-**3**<sup>+</sup> toward acetophenone proved to be about one order of magnitude lower than that of B(C<sub>6</sub>F<sub>5</sub>)<sub>3</sub> according to the competition study (see Figure 5-14). The complex (p*R*)-**3**<sup>+</sup>(acetophenone) can be readily isolated as a crystalline solid and its single crystal X-ray structure shows binding of the acetophenone from the *endo*-side of the ferrocene (B-O = 1.560(8) [1.577(8)] Å, Figure 5-7).

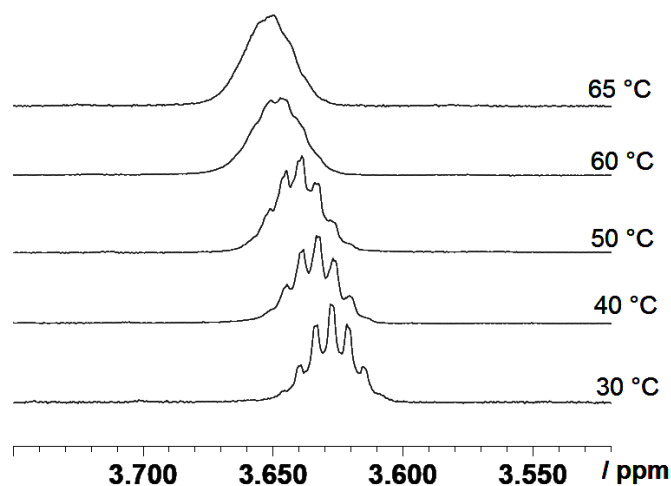
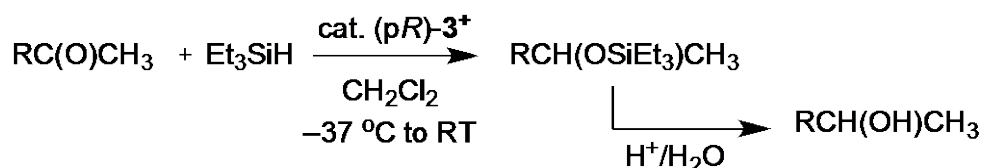


**Figure 5-6.** VT <sup>1</sup>H NMR spectra for a mixture of (p*R*)-**3**<sup>+</sup> and Et<sub>3</sub>SiH in CDCl<sub>3</sub>.



silane Ph<sub>3</sub>SiH (entry 3), only trace amount of product was detected. This observation is consistent with the silane activation mechanism, in which the ketones with higher degree of steric hindrance and silanes with lower degree of steric hindrance are favored since the Si-H activation becomes more accessible.



**Scheme 5-2.** Hydrosilylation of ketones catalyzed by (pR)-3<sup>+</sup>.

**Table 5-1.** Hydrosilylation of different ketones with silanes in the presence of (pR)-3<sup>+</sup> as catalyst.

Entry	Ketone	Silane	Cat. (%)	Conv. (%) <sup>a</sup>	ee (%)
1	R <sup>1</sup> =Ph, R <sup>2</sup> =Me	Et <sub>3</sub> SiH	5	65	20 <sup>b</sup> R-(+)
2	R <sup>1</sup> =Ph, R <sup>2</sup> =Me	PhMe <sub>2</sub> SiH	5	92	6 <sup>b</sup> R-(+)
3	R <sup>1</sup> =Ph, R <sup>2</sup> =Me	Ph <sub>3</sub> SiH	5	trace	ND
4	R <sup>1</sup> = <i>t</i> Bu, R <sup>2</sup> =Me	Et <sub>3</sub> SiH	2	>95	5 <sup>c</sup> S-(+)
5	R <sup>1</sup> = <i>t</i> Bu, R <sup>2</sup> =Me	PhMe <sub>2</sub> SiH	2	>95	5 <sup>c</sup> S-(+)
6	R <sup>1</sup> =1-Np, R <sup>2</sup> =Me	Et <sub>3</sub> SiH	3	29	ND
7	R <sup>1</sup> =1-Np, R <sup>2</sup> =Me	PhMe <sub>2</sub> SiH	3	44	ND

<sup>a</sup> Conversion determined by <sup>1</sup>H NMR (reaction time: ca. 12 h except for entries 4,5 which went to completion within 10 min).

<sup>b</sup> The silylated product was first converted to the corresponded alcohol, then the ee was determined by chiral GC-FID (Entry 1) or HPLC (Entry 2).

<sup>c</sup> The silylated product was converted to the corresponded alcohol, isolated by distillation, and then reacted with the chemical shift reagent (S)-(+)- $\alpha$ -methoxy- $\alpha$ -trifluoromethylphenylacetyl chloride as described by Mosher.<sup>30</sup>

In conclusion, halide abstraction from the Lewis acid-base pair (pR)-2 was accomplished using the Ag or Li derivative of Krossing's salt, resulting in a novel planar-

chiral borenium-type Lewis acid. The Lewis acid strength of chiral (*pR*)-**3**<sup>+</sup> proved to be comparable to that of B(C<sub>6</sub>F<sub>5</sub>)<sub>3</sub>. While modest enantiomeric excess was achieved in the hydrosilylation of ketones with (*pR*)-**3**<sup>+</sup> as a catalyst, this study represents the first application of a planar-chiral borenium Lewis acid in the stereoselective reduction of ketones. Further modification of the steric demand of the pyridyl ligand and the exocyclic boron substituent is expected to allow for significantly enhanced selectivities, while the activity can likely be optimized through tuning of the electronic effect of the exocyclic B-aryl group.

## 5.5 Experimental Section

**Reagents and General Methods.** PhBCl<sub>2</sub> and Et<sub>3</sub>PO were purchased from Aldrich and used without further purification. (*pS*)-**1**,<sup>31</sup> Mosher's acid,<sup>30</sup> and the Krossing salts<sup>18, 32</sup> were prepared according to literature procedures. All reactions and manipulations were carried out under an atmosphere of prepurified nitrogen using either Schlenk techniques or an inert-atmosphere glove box (MBraun). 499.9 MHz <sup>1</sup>H NMR, 125.7 MHz <sup>13</sup>C NMR, 160.4 MHz <sup>11</sup>B NMR, and 470.4 MHz <sup>19</sup>F spectra were recorded on a Varian INOVA NMR spectrometer (Varian Inc., Palo Alto, CA) equipped with a boron-free 5 mm dual broadband gradient probe (Nalorac, Varian Inc., Martinez, CA). Solution <sup>1</sup>H and <sup>13</sup>C NMR spectra were referenced internally to solvent signals. <sup>11</sup>B NMR spectra were acquired with boron-free quartz NMR tubes and referenced to BF<sub>3</sub> · Et<sub>2</sub>O (δ = 0). The following abbreviations are used for signal assignments: Lu = 3,5-dimethylpyrid-2-yl, Fc = ferrocenyl, Cp = cyclopentadienyl. High resolution MALDI-MS data (benzo[α]pyrene as matrix) were obtained in positive mode on an Apex Ultra 7.0 Hybrid FTMS (Bruker

Daltonics). UV/Vis absorption data were acquired on a Varian Cary 500 UV/Vis/NIR spectrophotometer. Optical rotation analyses were performed on an Autopol III polarimeter, Rudolph Research Analytical, using a tungsten-halogen light source operating at  $\lambda = 589$  nm. GC-FID analyses were performed on a Varian CP3800 GC instrument using an Rt-BetaDex-sm chiral column. Chiral HPLC analyses were performed on a Waters Empower system equipped with a 717plus autosampler, a 1525 binary HPLC pump, and a 2998 photodiode array detector; a CHIRALPAK® IA-3 column was used for separation. Elemental analyses were performed by Quantitative Technologies Inc., Whitehouse, NJ.

X-ray diffraction intensities were collected on a Bruker SMART APEX CCD Diffractometer using  $\text{CuK}\alpha$  (1.54178 Å) radiation at 100 K. The structures were refined by full-matrix least squares based on  $F^2$  with all reflections (SHELXTL V5.10; G. Sheldrick, Siemens XRD, Madison, WI). Non-hydrogen atoms were refined with anisotropic displacement coefficients, and hydrogen atoms were treated as idealized contribution. SADABS (Sheldrick, 12 G.M. SADABS (2.01), Bruker/Siemens Area Detector Absorption Correction Program; Bruker AXS: Madison, WI, 1998) absorption correction was applied. Crystallographic data for the structures of (pR)-**3**<sup>+</sup> and (pR)-**3**<sup>+</sup>(**acetophenone**) have been deposited with the Cambridge Crystallographic Data Center as supplementary publications CCDC 907178-907179. Copies of the data can be obtained free of charge on application to CCDC, 12 Union Road, Cambridge CB2 1EZ, UK (fax: (+44) 1223-336-033; email: [deposit@ccdc.cam.ac.uk](mailto:deposit@ccdc.cam.ac.uk)).

**Synthesis of [(pR)-LuFcB(C<sub>6</sub>H<sub>5</sub>)Cl · 0.5 C<sub>7</sub>H<sub>8</sub>] ((pR)-2).** A solution of (pS)-1 (100 mg, 0.22 mmol) in a mixture of hexanes/toluene (10/10 mL) was cooled down to -37 °C and then a solution of PhBCl<sub>2</sub> (70 mg, 0.44 mmol, 2.0 equiv) in toluene (2 mL) was added dropwise under stirring. The mixture was stirred over night at room temperature before applying high vacuum to remove the solvents. The residue was taken back up in a mixture of hot hexanes/toluene (1/1). When stored at -37 °C crystals were obtained that contain half an equivalent of toluene. Yield: 55 mg (55%).  $[\alpha]_D^{20}$  (c = 0.10, CH<sub>2</sub>Cl<sub>2</sub>) = 2110°. <sup>1</sup>H NMR (499.9 MHz, CDCl<sub>3</sub>, 25 °C): Major : Minor = 2.5 : 1;  $\delta$  = 8.23 (s, 1H, Lu; Minor), 8.13 (s, 1H; Lu, Major), 7.58 (s, 1H; Lu, Minor), 7.53 (d, *J* = 7 Hz, 2H; *o*-Ph, Minor), 7.48 (s, 1H; Lu, Major), 7.37 (pst, *J* = 7 Hz, 2H; *m*-Ph, Minor), 7.32 (d, *J* = 7 Hz, 2H; *o*-Ph, Major), 7.26 (nr, 1H, *p*-Ph, Minor), 7.16 (pst, *J* = 7 Hz, 2H; *m*-Ph, Major), 7.13 (m, 1H, *p*-Ph, Major), 4.77 (dd, *J* = 2.5 Hz, 1.0 Hz, 1H; Cp, Major), 4.71 (overlapped, 2H; Cp, Minor), 4.62 (dd, *J* = 2.5 Hz, 1.0 Hz, 1 H; Cp, Major), 4.58 (m, 2H; Cp, Major + Minor), 4.22 (s, 5H; free Cp, Major), 3.65 (s, 5H; free Cp, Minor), 2.52 (s, 3H; Lu-Me, Major), 2.51 (s, 3H; Lu-Me, Minor), 2.38 (s, 3H; Lu-Me, Minor), 2.30 (s, 3H; Lu-Me, Major). <sup>11</sup>B NMR (160.4 MHz, CDCl<sub>3</sub>, 25° C)  $\delta$  = 6.0 (*w*<sub>1/2</sub> = 210 Hz). <sup>13</sup>C NMR (125.69 MHz, CDCl<sub>3</sub>, 25 °C)  $\delta$  = 158.3, 157.3, 143.3, 142.8, 142.4, 141.5, 131.5, 131.5, 130.4, 130.3, 129.5, 128.9, 127.3, 127.3, 126.4, 126.2 (Lu + Ph), ipso-Ph-B not observed, 84.0 (ipso-Cp-C, Major), 82.5 (ipso-Cp-C, Minor), 74.7 (Cp, Minor), 74.4 (Cp, Major), 70.3 (ipso-Cp-B, Major), 70.2 (ipso-Cp-B, Minor), 70.1 (free Cp, Major), 69.8 (free Cp, Minor), 64.6 (Cp, Minor), 64.5 (Cp, Major), 18.3 (Lu-Me, Major), 18.3 (Lu-Me, Minor), 18.2 (Lu-Me, Minor), 18.1 (Lu-Me, Major). UV-Vis (CH<sub>2</sub>Cl<sub>2</sub>):  $\lambda_{\max}$  = 413 ( $\epsilon$  = 1900 M<sup>-1</sup> cm<sup>-1</sup>), 503 ( $\epsilon$  = 2700 M<sup>-1</sup> cm<sup>-1</sup>). High-resolution MALDI-MS (+ mode, benzo[ $\alpha$ ]pyrene):

$m/z$  413.0828 ( $[M]^+$ , 40%, calcd for  $^{12}\text{C}_{23}^{1}\text{H}_{21}^{11}\text{B}^{14}\text{N}^{35}\text{Cl}^{56}\text{Fe}$  413.0804);  $m/z$  378.1137 ( $[M-\text{Cl}]^+$ , 100%, calcd for  $^{12}\text{C}_{23}^{1}\text{H}_{21}^{11}\text{B}^{14}\text{N}^{56}\text{Fe}$  378.1115).

**Synthesis of  $[(pR)\text{-LuFcB}(\text{C}_6\text{H}_5)]^+\{\text{Al}[\text{OC}(\text{CF}_3)_3]_4\}^- ((pR)\text{-3}^+)$ . Method A:** To a solution of  $\text{LuFcB}(\text{C}_6\text{H}_5)\text{Cl} \cdot 0.5 \text{C}_7\text{H}_8$  ( $(pR)\text{-2}$ ; 4.9 mg, 0.0106 mmol) in  $\text{CHCl}_3$  (0.5 mL) that was cooled down to  $-37^\circ\text{C}$  was added a solution of  $[\text{Ag}(\text{CH}_2\text{Cl}_2)]\{\text{Al}[\text{OC}(\text{CF}_3)_3]_4\}$  (14.0 mg, 0.012 mmol, 1.1 equiv) in  $\text{CHCl}_3$  (0.5 mL) under stirring. The color of the solution turned from red to purple. After filtering off a small amount of a white precipitate, the filtrate was carefully layered with 1 mL of hexanes and kept at  $-37^\circ\text{C}$  for recrystallization. Yield: 6.0 mg (42 %). **Method B:** To a sample of  $\text{Li}\{\text{Al}[\text{OC}(\text{CF}_3)_3]_4\}$  (13.4 mg, 0.0138 mmol) in a 10 mL Schlenk flask was added a solution of  $\text{LuFcB}(\text{C}_6\text{H}_5)\text{Cl} \cdot 0.5 \text{C}_7\text{H}_8$  ( $(pR)\text{-2}$ ; 6.3 mg, 0.0138 mmol) in  $\text{CDCl}_3$  (1 mL) under vigorous stirring. Upon addition the color of the solution turned from red to purple. The mixture was stirred for 2 hours and then filtered.  $^1\text{H}$  NMR analysis showed complete conversion to the product.  $^1\text{H}$  NMR (499.9 MHz,  $\text{CDCl}_3$ ,  $25^\circ\text{C}$ ):  $\delta = 8.31$  (s, 1H; Lu), 7.95 (d,  $J = 7$  Hz, 2H; *o*-Ph), 7.83 (s, 1H; Lu), 7.81 (nr, 1H; *p*-Ph), 7.67 (pst,  $J = 7$  Hz, 2H; *m*-Ph), 5.75 (nr, 1H; Cp), 5.58 (nr, 1H; Cp), 5.48 (nr, 1H; Cp), 4.32 (s, 5H; free Cp), 2.40 (s, 3H; Lu-Me), 2.39 (s, 3H; Lu-Me).  $^{13}\text{C}$  NMR (125.69 MHz,  $\text{CDCl}_3$ ,  $25^\circ\text{C}$ ):  $\delta = 156.4, 148.0, 140.1, 134.6, 134.5, 134.1, 131.6, 129.9$ , (Lu + Ph), 121.2 (q,  $J(\text{C},\text{F}) = 293$  Hz,  $\text{CF}_3$ ), 85.7 (Cp), 82.9 (ipso-Cp-C), ipso-Cp-B not observed, 79.2 (Cp), 76.6 (Cp), 76.5 (free Cp), 17.7 (Lu-Me), 17.2 (Lu-Me).  $^{11}\text{B}$  NMR (160.4 MHz,  $\text{CDCl}_3$ ,  $25^\circ\text{C}$ )  $\delta = 45.4$  ( $w_{1/2} = 750$  Hz).  $^{19}\text{F}$  NMR (470.4 MHz,  $\text{CDCl}_3$ ,  $25^\circ\text{C}$ ):  $\delta = -75.4$ . UV-Vis ( $\text{CH}_2\text{Cl}_2$ ):  $\lambda_{\text{max}} = 407$  ( $\epsilon = 2000 \text{ M}^{-1} \text{ cm}^{-1}$ ), 566 ( $\epsilon = 2200 \text{ M}^{-1} \text{ cm}^{-1}$ ). Elemental analysis

for  $C_{39}H_{21}AlBF_3FeNO_4$ , calcd C 34.82, H 1.57, N 1.04, found C 34.32, H 1.27, N 0.96%.

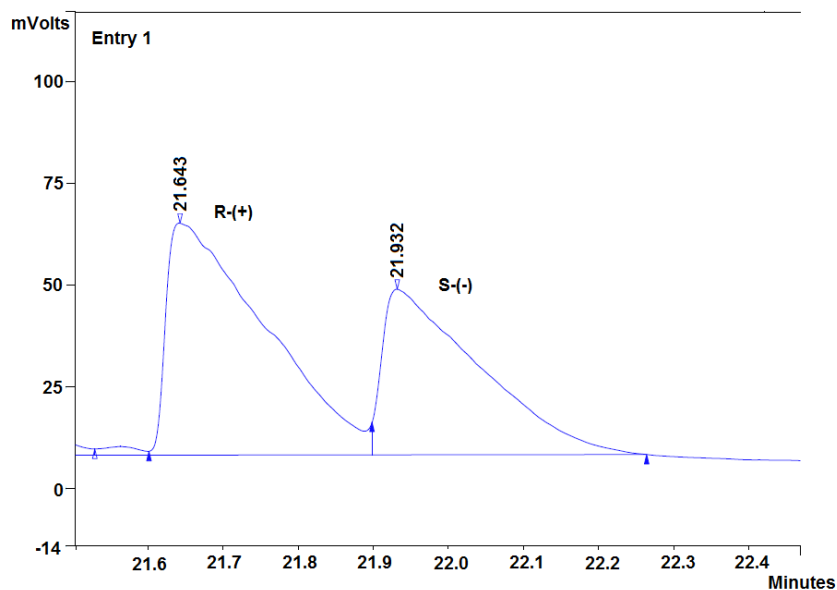
**Synthesis of [(*pR*)-LuFcB(C<sub>6</sub>H<sub>5</sub>)·PhC(O)CH<sub>3</sub>]<sup>+</sup>{Al[OC(CF<sub>3</sub>)<sub>3</sub>]<sub>4</sub>}<sup>-</sup> ((*pR*)-**3<sup>+</sup>**(acetophenone)).** In a glove box, a solution of LuFcB(C<sub>6</sub>H<sub>5</sub>)Cl · 0.5 C<sub>7</sub>H<sub>8</sub> ((*pR*)-**2**; 11.0 mg, 0.0242 mmol) in CH<sub>2</sub>Cl<sub>2</sub> (5 mL) was added to a sample of Li{Al[OC(CF<sub>3</sub>)<sub>3</sub>]<sub>4</sub>} (23.5 mg, 0.0242 mmol) in a vial under vigorous stirring. Upon addition the color of the solution turned from red to purple. The mixture was stirred for 2 hours and then a solution of PhC(O)CH<sub>3</sub> in CH<sub>2</sub>Cl<sub>2</sub> (1.0 M, 0.0242 mmol, 0.0242 mL) was added. The color of the solution turned from purple to red. The solution was filtered and concentrated under high vacuum. The residue was re-dissolved in CH<sub>2</sub>Cl<sub>2</sub> (5 mL), carefully layered with hexanes (5 mL) and then placed in a freezer at -37 °C to obtain purple red crystals. Yield: 20 mg (57 %). <sup>1</sup>H NMR (499.9 MHz, CD<sub>2</sub>Cl<sub>2</sub>, 25 °C): δ = 8.31, 8.03, 7.76, 7.37 (br, 10H; Ph), 8.22 (s, 1H; Lu), 7.76 (s, 1H; Lu), 5.16 (br, 1H; Cp), 5.02 (br, 1H; Cp), 4.72 (br, 1H; Cp), 4.02 (s, 5H; free Cp), 3.15 (br, 3H; Me), 2.54 (s, 3H; Lu-Me), 2.42 (s, 3H; Lu-Me). <sup>1</sup>H NMR (499.9 MHz, CD<sub>2</sub>Cl<sub>2</sub>, -20 °C): δ = 8.43 (d, *J* = 8 Hz, 2H; *o*-Ph), 8.17 (s, 1H; Lu), 8.11 (t, *J* = 8 Hz, 1H; *p*-Ph), 7.82 (t, *J* = 8 Hz, 2H; *m*-Ph), 7.72 (s, 1H; Lu), 7.32-7.26 (m, 3H; *m*-Ph + *p*-Ph), 7.22 (d, *J* = 7 Hz, 2H; *o*-Ph), 5.09 (nr, 1H; Cp), 4.90 (nr, 1H; Cp), 4.60 (nr, 1H; Cp), 3.94 (s, 5H; free Cp), 3.26 (s, 3H; Me), 2.53 (s, 3H; Lu-Me), 2.39 (s, 3H; Lu-Me). <sup>11</sup>B NMR (160.4 MHz, CDCl<sub>3</sub>, 25 °C) δ = 10.7 (*w*<sub>1/2</sub> = 960 Hz). Elemental analysis for C<sub>47</sub>H<sub>29</sub>AlBF<sub>3</sub>FeNO<sub>5</sub>, calcd C 38.52, H 1.99, N 0.96, found C 38.36, H 2.04, N 0.95%.

**Hydrosilylation Catalysis.** Stock solutions (1.0 M) of the ketones and silanes were prepared in CH<sub>2</sub>Cl<sub>2</sub>. A predetermined quantity of (*pR*)-**3<sup>+</sup>** was dissolved in a minimum

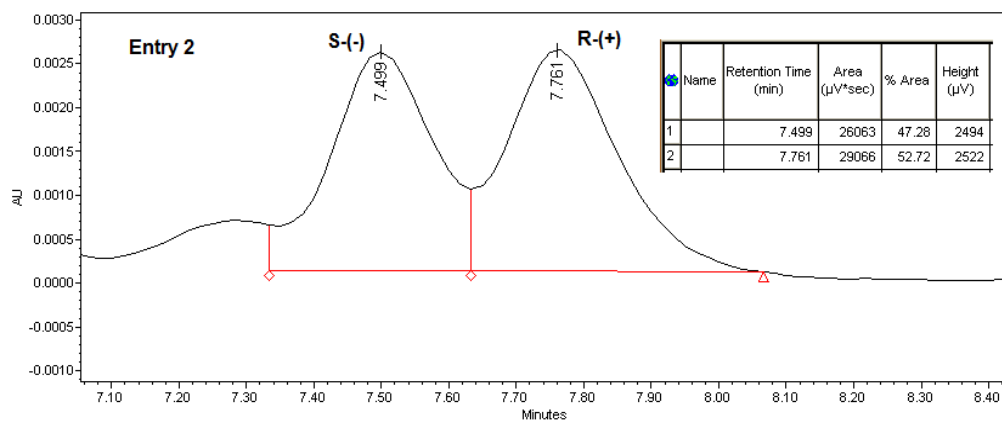
amount of  $\text{CH}_2\text{Cl}_2$  and the corresponding amount of the silane solution was added. The mixture was cooled down to  $-37\text{ }^\circ\text{C}$ , an equimolar amount of the ketone solution was added and the progress of the reaction was monitored by taking an aliquot and measuring the  $^1\text{H}$  NMR in  $\text{CD}_2\text{Cl}_2$ . After completion of the reaction, the mixture was treated with dilute  $\text{HCl}$  (aq.) solution and stirred vigorously overnight. To determine the enantioselectivity, the resulting (desilylated) alcohol was either directly examined by chiral GC-FID or HPLC, or isolated by distillation and then reacted with the chemical shift reagent (S)-(+)- $\alpha$ -methoxy- $\alpha$ -trifluoromethylphenylacetyl chloride as described by Mosher<sup>30</sup>. In a typical procedure, to a solution of the alcohol (5 mg) in 0.7 mL of  $\text{CDCl}_3$  in a NMR tube is added 1 equivalent of Mosher's chemical shift reagent and an excess amount of pyridine- $d_5$ . The mixture is heated to  $50\text{ }^\circ\text{C}$  for 2 days and then filtered. The filtrate is transferred to another NMR tube and measured directly.

## 5.6 Supporting Information

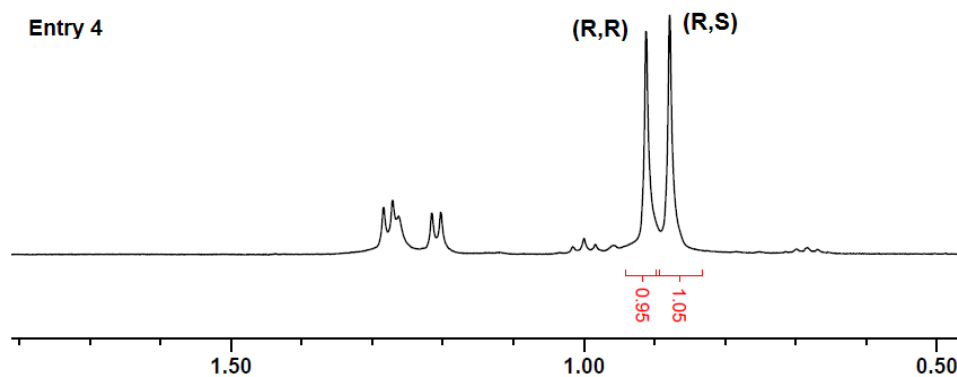
(a) Data corresponding to Entry 1 in Table 5-1 – Chiral GC-FID analysis of 1-phenylethanol:



**(b) Data corresponding to Entry 2 in Table 5-1 – Chiral HPLC analysis of 1-phenylethanol:**



**(c) Data corresponding to Entry 4 in Table 5-1 –  $^1\text{H}$  NMR spectrum of the product from reaction of 3,3-dimethyl-2-butanol with Mosher's chemical shift reagent:**



**(d) Data corresponding to Entry 5 in Table 5-1 –  $^1\text{H}$  NMR spectrum of the product from reaction of 3,3-dimethyl-2-butanol with Mosher's chemical shift reagent:**

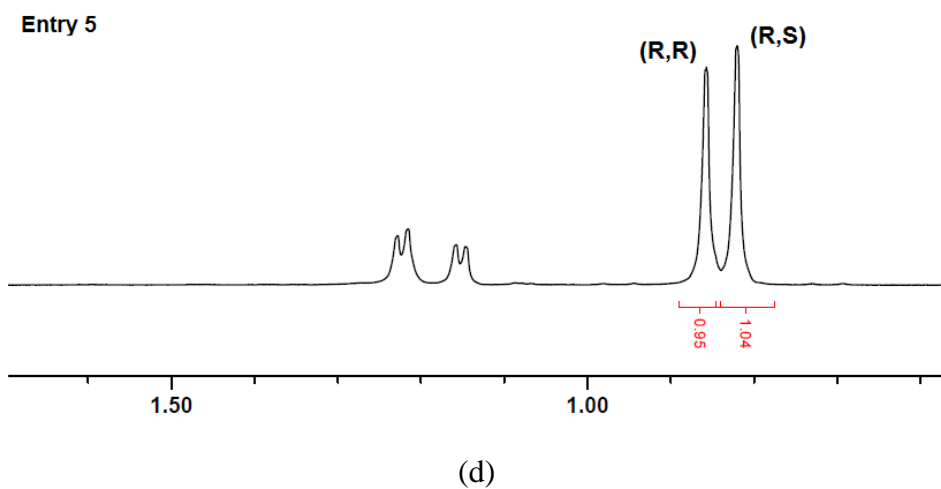


**Figure 5-8.** Data corresponding to determination of enantiomeric excess of catalysis products.

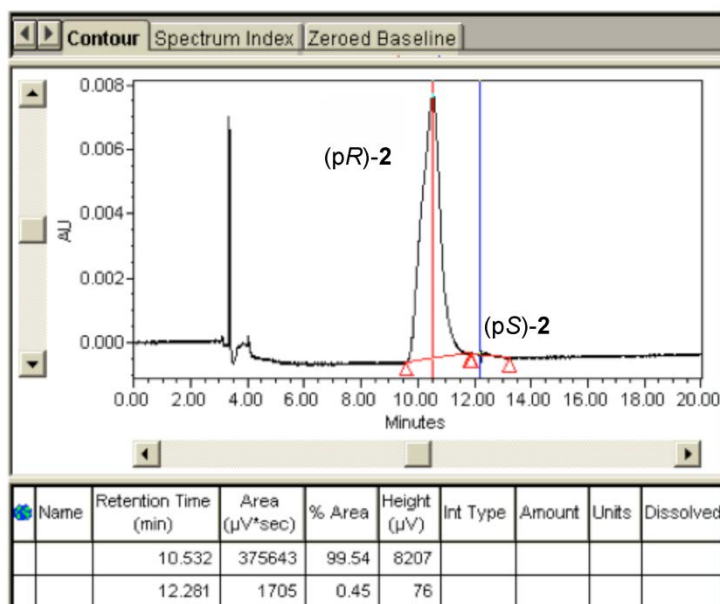


**Figure 5-9.** Chiral HPLC analysis for compound (pR)-2 (99% ee) in 93:7 hexanes:THF.

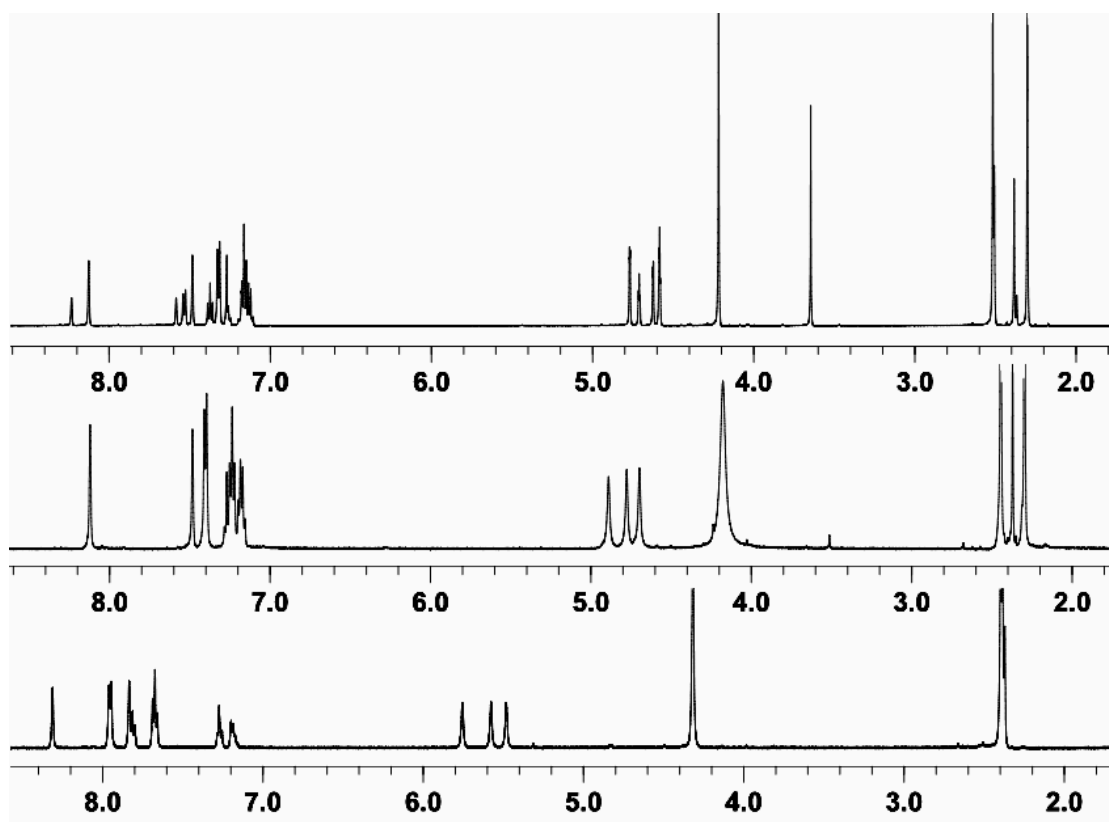


**Figure 5-10.** Complete  $^1\text{H}$  NMR spectra of (pR)-2 (top), (pR)-2 +  $\text{B}(\text{C}_6\text{F}_5)_3$  (middle), and (pR)-3 $^+$  (bottom) in  $\text{CDCl}_3$ .

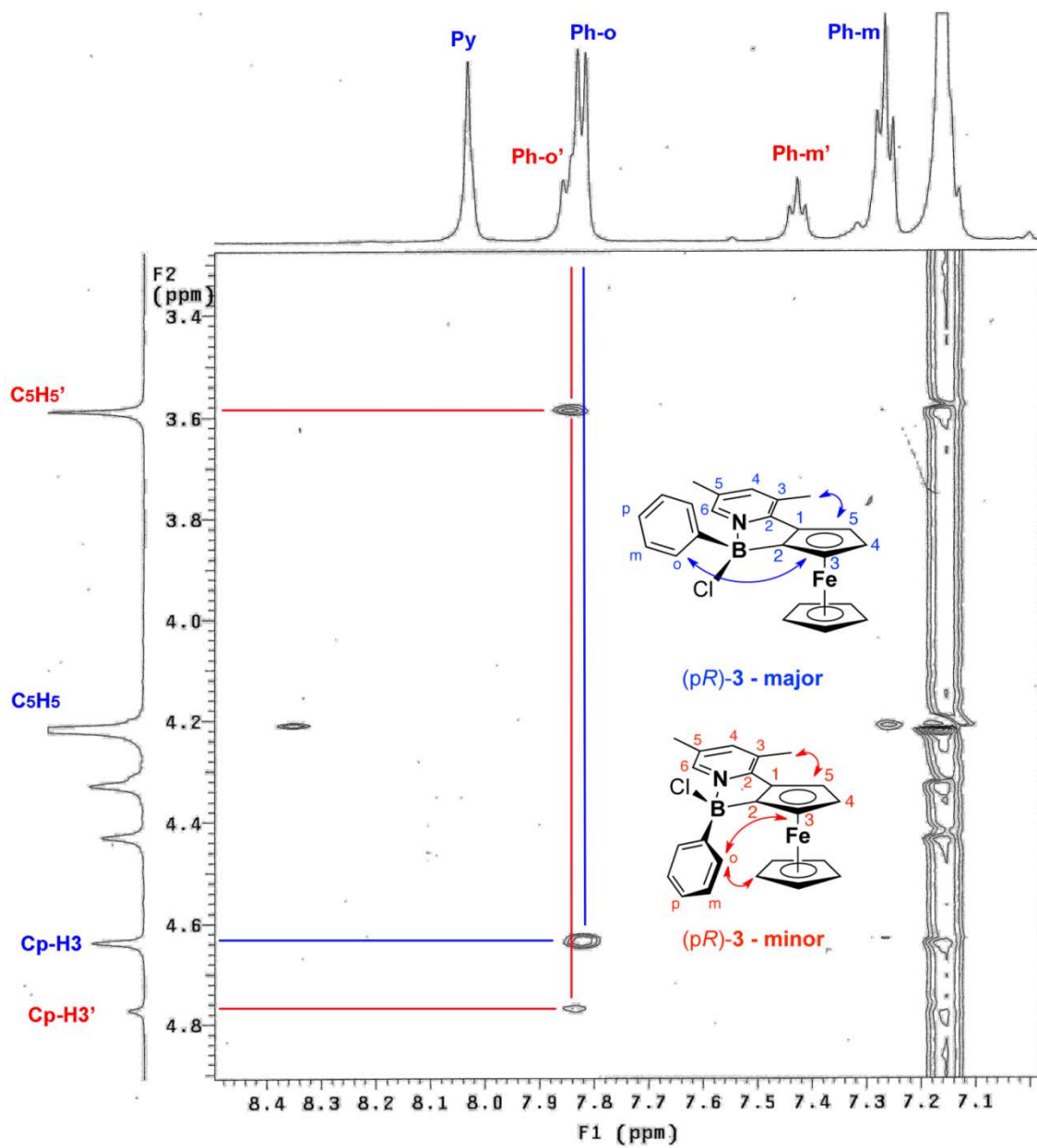
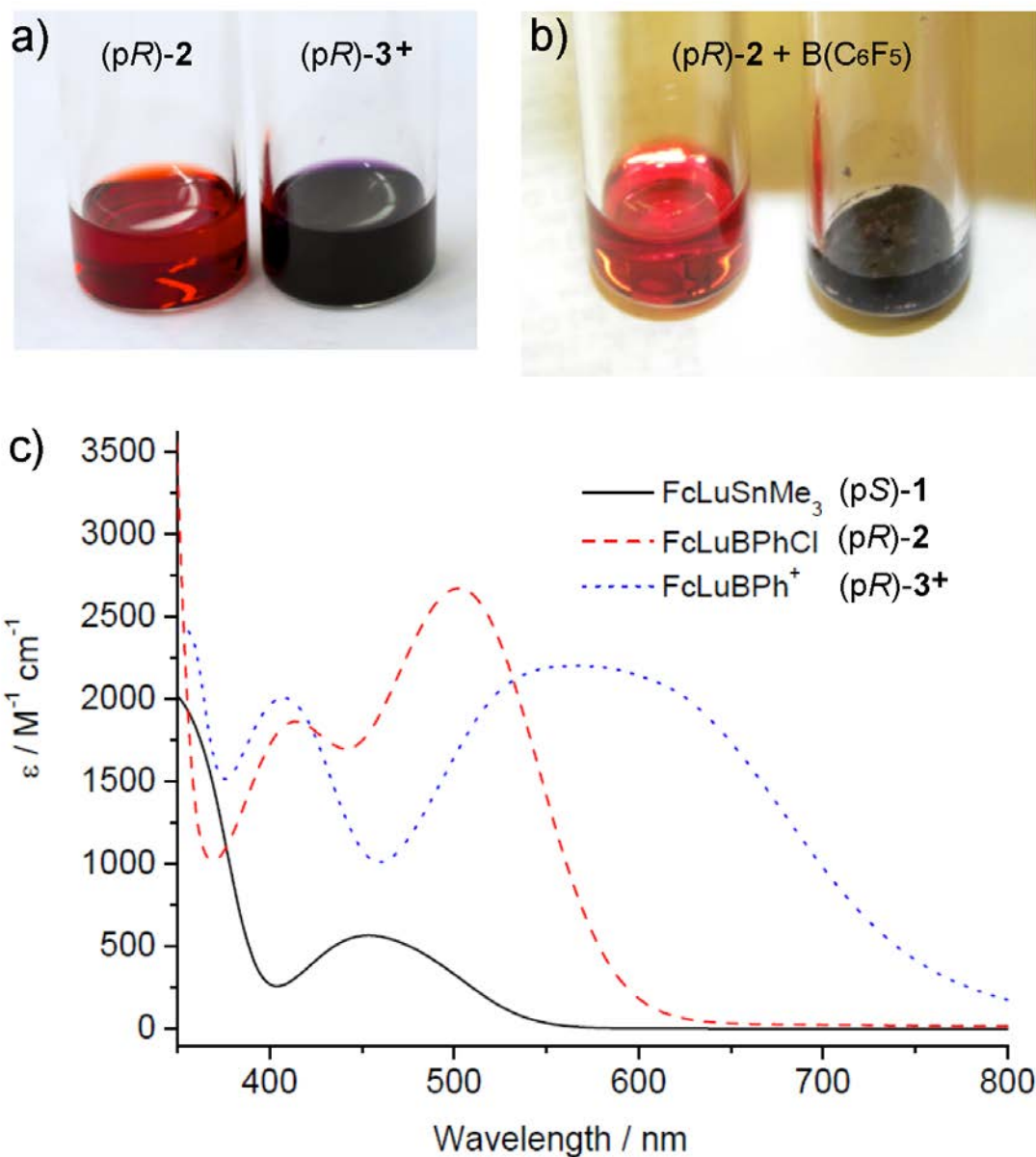
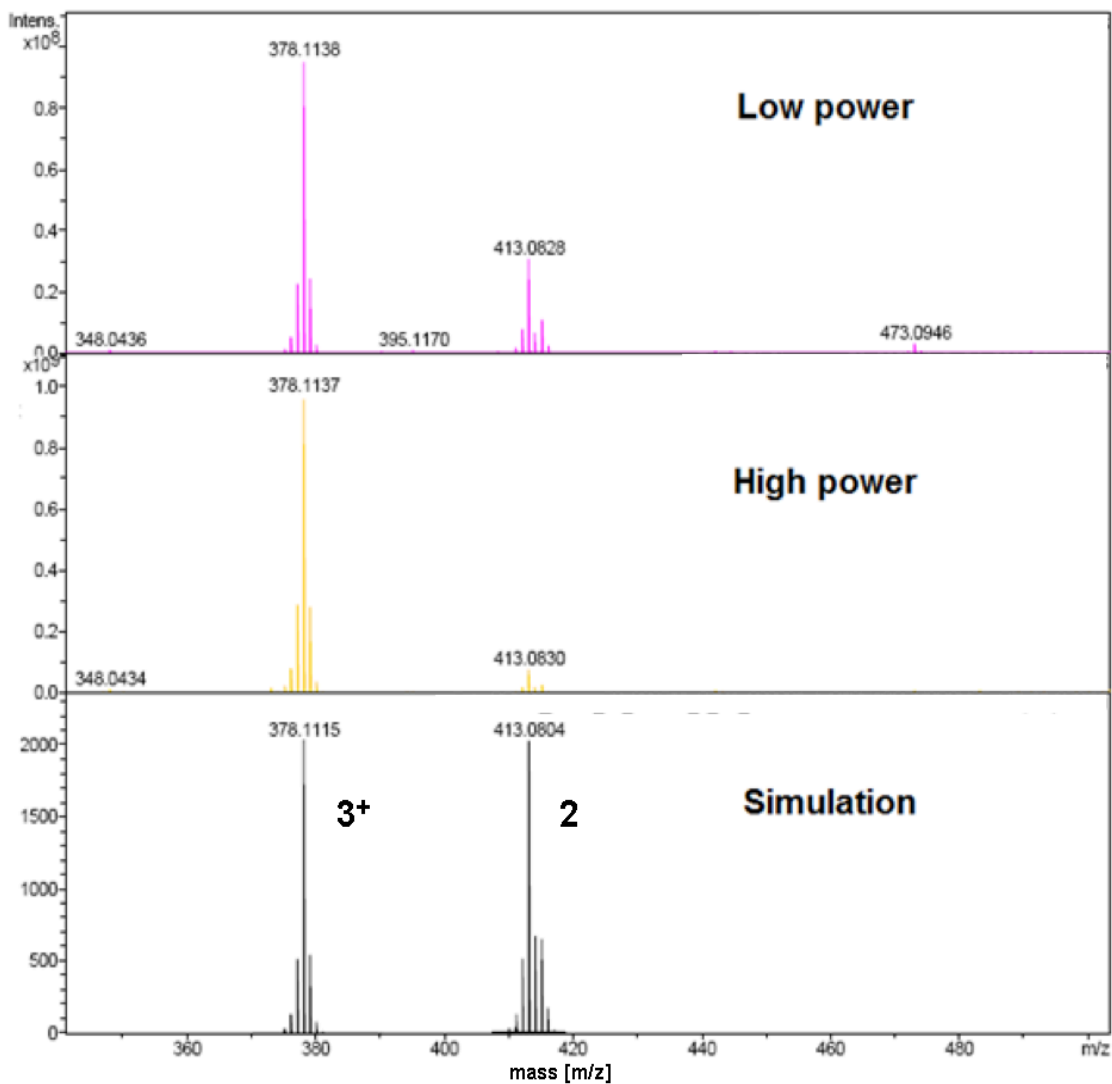


Figure 5-11. 2D-NOESY spectra of compound (pR)-2 in  $C_6D_6$ .



**Figure 5-12.** a) Photographs of  $\text{CH}_2\text{Cl}_2$  solutions of compounds (pR)-2 and (pR)-3<sup>+</sup>. b) Photographs of a mixture of (pR)-2 +  $\text{B}(\text{C}_6\text{F}_5)_3$  in  $\text{CH}_2\text{Cl}_2$  solution and in the solid state after solvent removal. c) Comparison of UV-Vis spectra of compounds (pS)-1 ( $\text{CHCl}_3$ ), (pR)-2 and (pR)-3<sup>+</sup> ( $\text{CH}_2\text{Cl}_2$ ).

Note that the color change upon removal of solvent from the mixture of (pR)-2 +  $\text{B}(\text{C}_6\text{F}_5)_3$  in  $\text{CH}_2\text{Cl}_2$  suggests that halide abstraction by  $\text{B}(\text{C}_6\text{F}_5)_3$  with formation of (pR)-3<sup>+</sup> becomes more favorable in the absence of the solvent  $\text{CH}_2\text{Cl}_2$ .



**Figure 5-13.** High-resolution MALDI-MS spectra of compound (pR)-2 acquired at different laser power levels and comparison to simulated spectra of (pR)-2 and (pR)-3<sup>+</sup>. With increasing laser power, the ion (pR)-3<sup>+</sup> becomes more dominant, suggesting facile Cl<sup>-</sup> abstraction under these conditions.

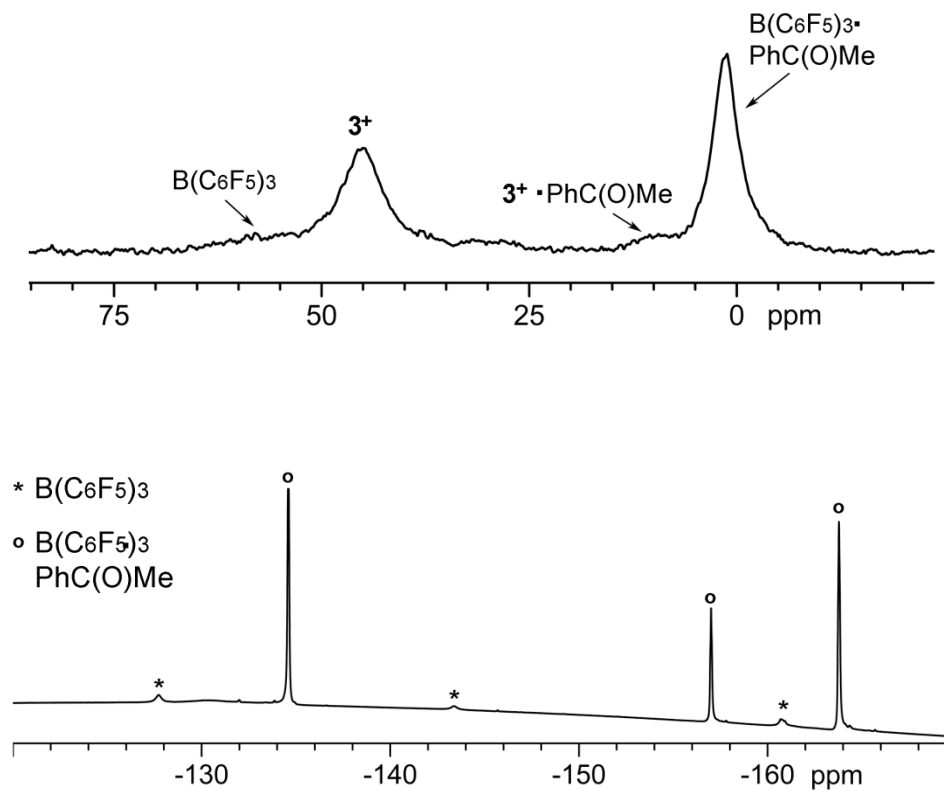


**Figure 5-14.** (top) Competitive binding of (*pR*)- $3^+$  and  $\text{B}(\text{C}_6\text{F}_5)_3$  to acetophenone (ratio of 1.0 (*pR*)- $3^+$  : 1.0  $\text{B}(\text{C}_6\text{F}_5)_3$  : 1.0  $\text{PhC}(\text{O})\text{Me}$ ) examined by  $^{11}\text{B}$  NMR spectroscopy in  $\text{CD}_2\text{Cl}_2$  at  $-20^\circ\text{C}$ . (bottom) Corresponding  $^{19}\text{F}$  NMR data. The ratio of complexation products was estimated to be ca. 10:1 in favor of complex formation with  $\text{B}(\text{C}_6\text{F}_5)_3$ , which is significantly larger than in the case of  $\text{Et}_3\text{PO}$ .

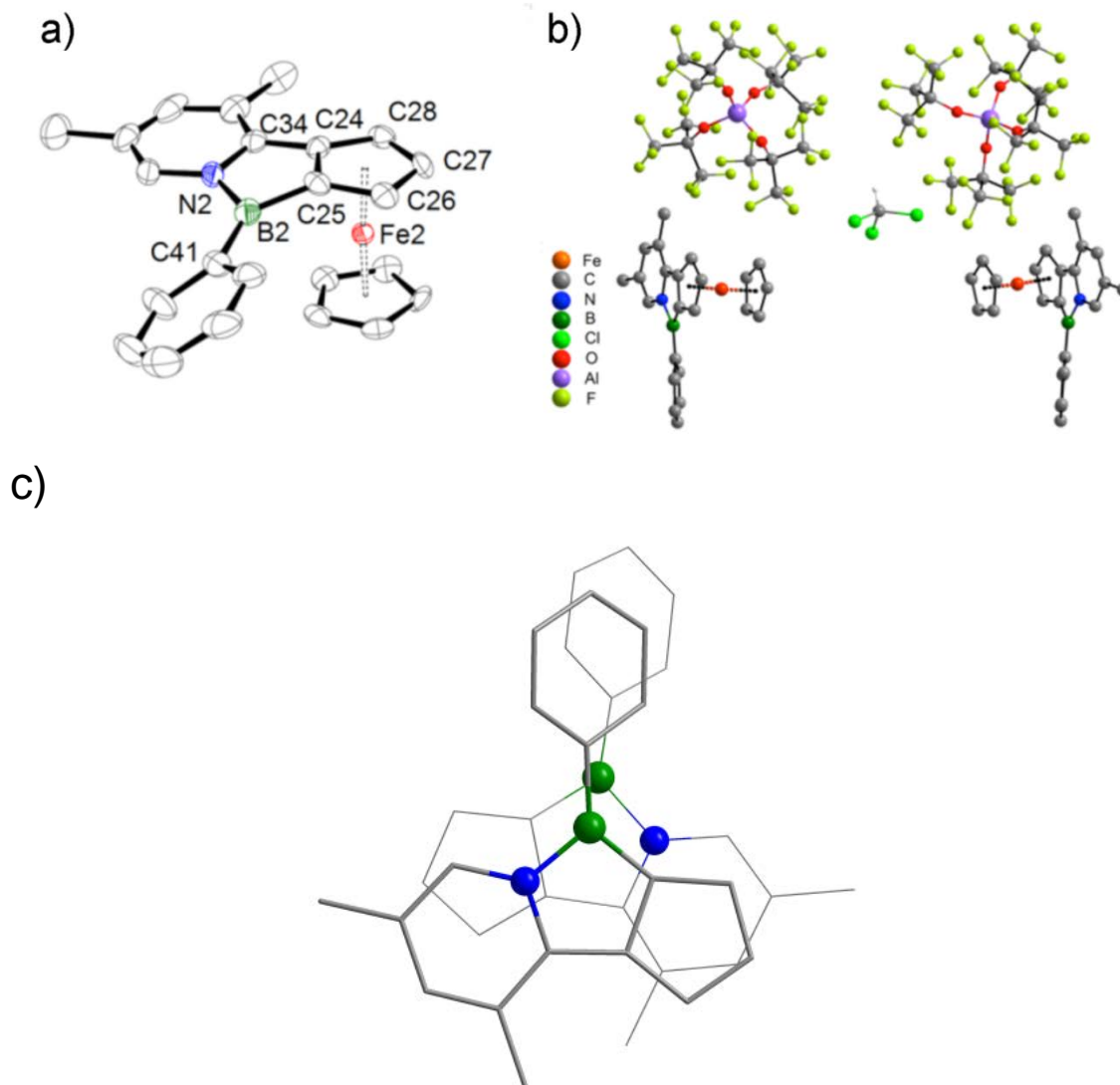


**Figure 5-15.** a) Ortep plot of the second independent molecule of (p*R*)-**3**<sup>+</sup> (50% thermal displacement ellipsoids). Hydrogen atoms and the counterion are omitted for clarity. Selected interatomic distances (Å) and angles (°): B2-N2 1.550(9), B2-C25 1.539(9), B2-C41 1.504(10), C25-B2-N2 100.6(5), C25-B2-C41 132.2(6), C41-B2-N2 127.1(6). b) Asymmetric unit of compound (p*R*)-**3**<sup>+</sup> (hydrogen atoms are omitted for clarity except in CHCl<sub>3</sub>). Although the data set was acquired at 100 K, the anions were slightly disordered due to free rotation of the perfluorinated *t*-butyl groups. c) A  $\pi$  dimer consisting of two independent molecules of (p*R*)-**3**<sup>+</sup> (only substituted Cp rings shown).

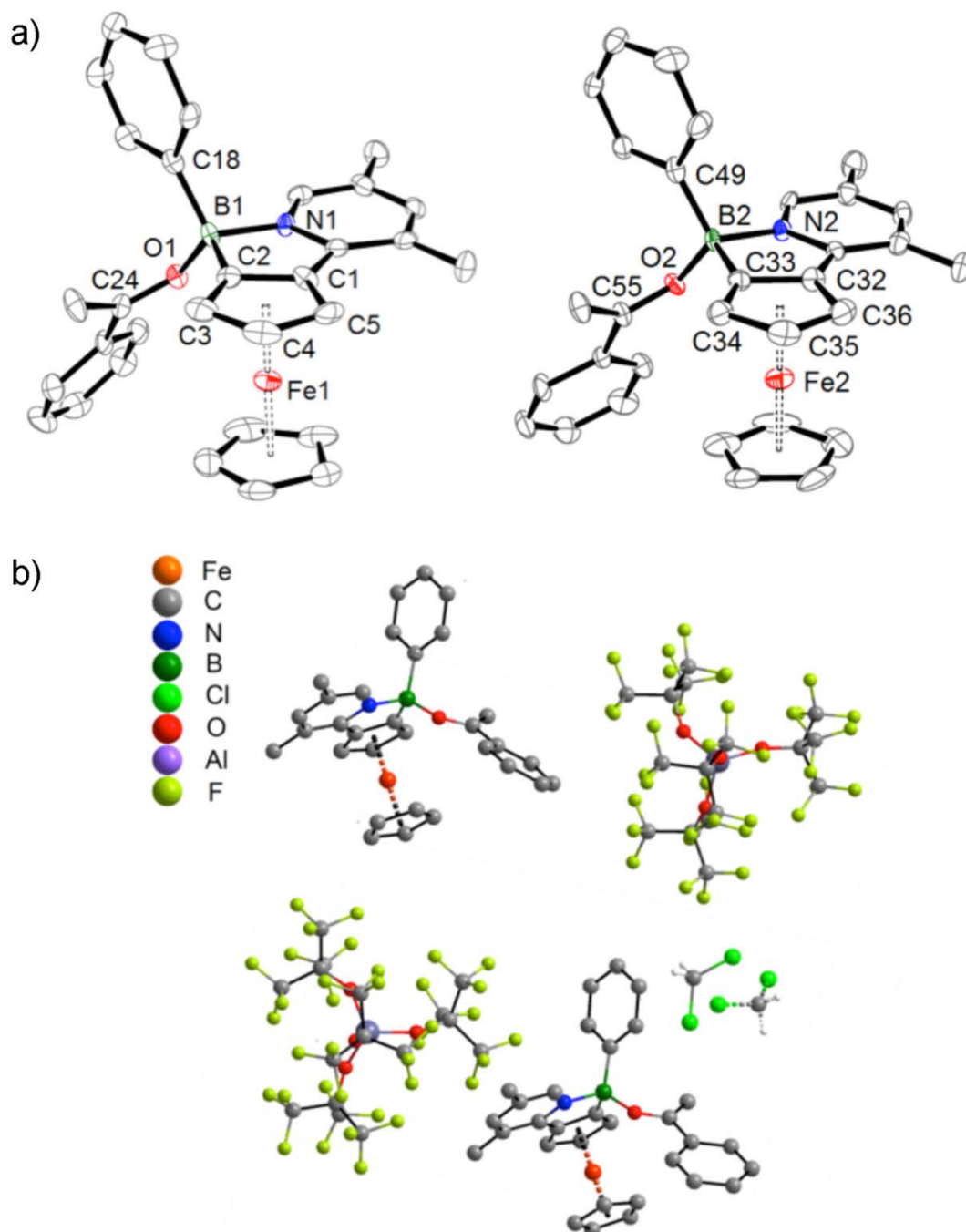


**Figure 5-16.** a) Orteplote of two independent molecules of (*pR*)-**3<sup>+</sup>(acetophenone)** (50% thermal displacement ellipsoids). Hydrogen atoms and the counterions are omitted for clarity. Selected distances (Å) [second independent molecule]: B1-N1 1.603(9) [1.592(9)], B1-O1 1.560(8) [1.577(8)], B1-C2 1.580(11) [1.593(10)], B1-C18 1.603(11) [1.594(10)], O1-C24 1.257(8) [1.255(8)]. b) Asymmetric unit of compound (*pR*)-**3<sup>+</sup>(acetophenone)** (hydrogen atoms are omitted for clarity except in CH<sub>2</sub>Cl<sub>2</sub>). The positional disorder of the solvent CH<sub>2</sub>Cl<sub>2</sub> could be modeled and refined as two parts

without any problems. Both sites of the disordered  $\text{CH}_2\text{Cl}_2$  are shown in the asymmetric cell; the site occupancy factors are 0.54 (solid) and 0.46 (dash).

**Table 5-2.** Details of X-ray analyses of (p*R*)-**3** and (p*R*)-**3**<sup>+</sup>(acetophenone).

Compound	(p <i>R</i> )- <b>3</b> <sup>+</sup>	(p <i>R</i> )- <b>3</b> <sup>+</sup> • PhC(O)Me
CCDC	907178	907179
empirical formula	2 [C <sub>23</sub> H <sub>21</sub> BF <sub>3</sub> N] <sup>+</sup> [C <sub>16</sub> AlF <sub>36</sub> O <sub>4</sub> ] <sup>-</sup> · CHCl <sub>3</sub>	2 [C <sub>31</sub> H <sub>29</sub> BF <sub>3</sub> NO] <sup>+</sup> [C <sub>16</sub> AlF <sub>36</sub> O <sub>4</sub> ] <sup>-</sup> · CH <sub>2</sub> Cl <sub>2</sub>
MW	2809.78	3015.62
<i>T</i> , K	100(2)	100(2)
wavelength, Å	1.54178	1.54178
crystal system	Orthorhombic	Monoclinic
space group	P2 <sub>1</sub> 2 <sub>1</sub> 2 <sub>1</sub>	P2 <sub>1</sub>
<i>a</i> , Å	15.9616 (6)	19.2119(3)
<i>b</i> , Å	20.3519 (6)	14.9703(3)
<i>c</i> , Å	30.5167 (8)	19.5719(3)
$\alpha$ , deg	90	90
$\beta$ , deg	90	92.512(1)
$\gamma$ , deg	90	90
<i>V</i> , Å <sup>3</sup>	9913.3 (5)	5623.62(17)
<i>Z</i>	4	2
$\rho_{\text{calc}}$ , g cm <sup>-3</sup>	1.883	1.781
$\mu$ (Cu K $\alpha$ ), mm <sup>-1</sup>	5.04	4.30
Crystal size, mm	0.43 × 0.28 × 0.27	0.45 × 0.32 × 0.26
$\theta$ range, deg	2.6-71.6	2.3-72.0
limiting indices	-18 ≤ <i>h</i> ≤ 18 -23 ≤ <i>k</i> ≤ 20 -36 ≤ <i>l</i> ≤ 35	-22 ≤ <i>h</i> ≤ 23 -15 ≤ <i>k</i> ≤ 17 -23 ≤ <i>l</i> ≤ 23
reflns collected	17455	51856

independent reflns	15330[R(int) = 0.034]	16806 [R(int) = 0.038]
Absorption correction	Numerical	Numerical
data/restraints/para's	15330 / 15 / 1535	16808 / 50 / 1718
goodness-of-fit on $F^2$	1.02	1.03
final R indices	R1 = 0.068	R1 = 0.075
[ $I > 2\sigma(I)$ ] <sup>[a]</sup>	wR2 = 0.180	wR2 = 0.189
R indices (all data) <sup>[a]</sup>	R1 = 0.076	R1 = 0.088
	wR2 = 0.187	wR2 = 0.201
Peak <sub>max</sub> /hole <sub>min</sub> (e Å <sup>-3</sup> )	1.37 / -0.69	1.56 / -0.66
Absolute structure parameter	0.019(5)	0.022(6)

---

[a]  $R1 = \sum |F_o| - |F_c| / \sum |F_o|$ ;  $wR2 = \{ \sum [w(F_o^2 - F_c^2)^2] / \sum [w(F_o^2)^2] \}^{1/2}$ .

## 5.7 Notes and References

1. Yamamoto, H., *Lewis Acids in Organic Synthesis*. Wiley VCH: Weinheim, New York, Chichester, Brisbane, Singapore, Toronto, 2000.
2. Chen, E. Y.-X.; Marks, T. J., *Chem. Rev.* **2000**, *100*, 1391-1434.
3. (a) Stephan, D. W.; Erker, G., *Angew. Chem. Int. Ed.* **2009**, *49*, 46-76; (b) Sumerin, V.; Schulz, F.; Atsumi, M.; Wang, C.; Nieger, M.; Leskelae, M.; Repo, T.; Pyykko, P.; Rieger, B., *J. Am. Chem. Soc.* **2008**, *130*, 14117-14119; (c) Piers, W. E.; Marwitz, A. J. V.; Mercier, L. G., *Inorg. Chem.* **2011**, *50*, 12252-12262.
4. (a) Wade, C. R.; Broomsgrove, A. E. J.; Aldridge, S.; Gabbai, F. P., *Chem. Rev.* **2010**, *110*, 3958-3984; (b) Hudson, Z. M.; Wang, S., *Acc. Chem. Res.* **2009**, *42*, 1584-1596.
5. (a) Lorbach, A.; Hubner, A.; Wagner, M., *Dalton Trans.* **2012**, *41*, 6048-6063; (b) Jäkle, F., *Chem. Rev.* **2010**, *110*, 3985-4022; (c) Entwistle, C. D.; Marder, T. B., *Angew. Chem. Int. Ed.* **2002**, *41*, 2927-2931.
6. (a) Piers, W. E., *Adv. Organomet. Chem.* **2005**, *52*, 1-76; (b) Piers, W. E.; Chivers, T., *Chem. Soc. Rev.* **1997**, *26*, 345-354.
7. (a) Braunschweig, H.; Kupfer, T., *Chem. Commun.* **2011**, *47*, 10903-10914; (b) Iida, A.; Sekioka, A.; Yamaguchi, S., *Chem. Sci.* **2012**, *3*, 1461-1466; (c) Fukazawa, A.; Dutton, J. L.; Fan, C.; Mercier, L. G.; Houghton, A. Y.; Wu, Q.; Piers, W. E.; Parvez, M., *Chem. Sci.* **2012**, *3*, 1814-1818; (d) Pakkirisamy, T.; Venkatasubbaiah, K.; Kassel, W. S.; Rheingold, A. L.; Jäkle, F., *Organometallics* **2008**, *27*, 3056-3064; (e) Venkatasubbaiah, K.; Zakharov, L. N.; Kassel, W. S.; Rheingold, A. L.; Jäkle, F., *Angew. Chem. Int. Ed.* **2005**, *44*, 5428-5433; (f) Metz, M. V.; Schwartz, D. J.; Stern, C. L.; Nickias, P. N.; Marks, T. J., *Angew. Chem. Int. Ed.* **2000**, *39*, 1312-1316.

8. (a) Kolle, P.; Nöth, H., *Chem. Rev.* **1985**, *85*, 399-418; (b) De Vries, T. S.; Prokofjevs, A.; Vedejs, E., *Chem. Rev.* **2012**, *112*, 4246-4282.
9. (a) Solomon, S. A.; Del Grosso, A.; Clark, E. R.; Bagutski, V.; McDouall, J. J. W.; Ingleson, M. J., *Organometallics* **2012**, *31*, 1908-1916; (b) Mansaray, H. B.; Rowe, A. D. L.; Phillips, N.; Niemeyer, J.; Kelly, M.; Addy, D. A.; Bates, J. I.; Aldridge, S., *Chem. Commun.* **2011**, *47*, 12295-12297; (c) Prokofjevs, A.; Vedejs, E., *J. Am. Chem. Soc.* **2011**, *133*, 20056-20059; (d) Matsumoto, T.; Gabbai, F. P., *Organometallics* **2009**, *28*, 4252-4253.
10. Prokofjevs, A.; Kampf, J. W.; Vedejs, E., *Angew. Chem. Int. Ed.* **2011**, *50*, 2098-2101.
11. (a) Farrell, J. M.; Hatnean, J. A.; Stephan, D. W., *J. Am. Chem. Soc.* **2012**, *134*, 15728-15731; (b) Eisenberger, P.; Bailey, A. M.; Crudden, C. M., *J. Am. Chem. Soc.* **2012**, *134*, 17384-17387.
12. Boshra, R.; Doshi, A.; Jäkle, F., *Angew. Chem. Int. Ed.* **2008**, *47*, 1134-1137.
13. Chen, J.; Venkatasubbaiah, K.; Pakkirisamy, T.; Doshi, A.; Yusupov, A.; Patel, Y.; Lalancette, R. A.; Jäkle, F., *Chem. Eur. J.* **2010**, *16*, 8861-8867.
14. (a) Liu, S.-Y.; Hills, I. D.; Fu, G. C., *J. Am. Chem. Soc.* **2005**, *127*, 15352-15353; (b) Liu, S. Y.; Lo, M. M. C.; Fu, G. C., *Tetrahedron* **2006**, *62*, 11343-11349.
15. The IUPAC-recommended Cahn–Ingold–Prelog (CIP) descriptors *pS* and *pR* are used throughout the manuscript to describe the planar chirality; see: Schlögl, K. *Top. Stereochem.* **1967**, *1*, 39
16. The selective formation of (*pR*)-**2** is surprising, because the isomer (*pS*)-**2** of opposite planar chirality would be expected in an *ipso*-borodestannylation reaction. Mechanistic details of this unusual rearrangement is discussed in Chapter 3.
17. A single crystal X-ray structure of (*pR*)-**2** confirmed the stereochemical assignment and revealed the *exo*-Ph isomer as the only stereoisomer in the solid state.
18. Krossing, I., *Chem. Eur. J.* **2001**, *7*, 490-502.
19. For studies of the charge transfer properties of dipyritylboronium-functionalized ferrocenes see: Thomson, M. D.; Novosel, M.; Roskos, H. G.; Müller, T.; Scheibitz, M.; Wagner, M.; de Biani, F. F.; Zanello, P., *J. Phys. Chem. A* **2004**, *108*, 3281-3291.
20. Carpenter, B. E.; Piers, W. E.; Parvez, M.; Yap, G. P. A.; Rettig, S. J., *Can. J. Chem.* **2001**, *79*, 857-867.
21. Appel, A.; Jäkle, F.; Priermeier, T.; Schmid, R.; Wagner, M., *Organometallics* **1996**, *15*, 1188-1194.
22. To date, the largest dip angle of any borylferrocene derivative was found in the antiaromatic ferrocenylborole FcBC<sub>4</sub>Ph<sub>4</sub> (29.4°; Fe...B 2.664 Å). Braunschweig, H.; Breher, F.; Chiu, C.-W.; Gamon, D.; Nied, D.; Radacki, K., *Angew. Chem. Int. Ed.* **2010**, *49*, 8975-8978.
23. Venkatasubbaiah, K.; Doshi, A.; Nowik, I.; Herber, R. H.; Rheingold, A. L.; Jäkle, F., *Chem. Eur. J.* **2008**, *14*, 444-458.
24. For a related discussion on boryl-phosphonium vs. borenium species, see Dureen, M. A.; Lough, A.; Gilbert, T. M.; Stephan, D. W., *Chem. Commun.* **2008**, 4303-4305.
25. (a) Gutmann, V., *Coor. Chem. Rev.* **1976**, *18*, 225-255; (b) Mayer, U.; Gutmann, V.; Gerger, W., *Monatsh. Chem.* **1975**, *106*, 1235-1257; (c) Beckett, M. A.; Brassington, D. S.; Light, M. E.; Hursthouse, M. B., *J. Chem. Soc. Dalton Trans.* **2001**, 1768-1772; (d)

- Beckett, M. A.; Strickland, G. C.; Holland, J. R.; Sukumar Varma, K., *Polymer* **1996**, *37*, 4629-4631.
26. Parks, D. J.; Piers, W. E., *J. Am. Chem. Soc.* **1996**, *118*, 9440-9441.
27. Mewald, M.; Oestreich, M., *Chem. Eur. J.* **2012**, *18*, 14079-14084.
28. (a) Chen, D. J.; Leich, V.; Pan, F. F.; Klankermayer, J., *Chem. Eur. J.* **2012**, *18*, 5184-5187; (b) Mewald, M.; Fröhlich, R.; Oestreich, M., *Chem. Eur. J.* **2011**, *17*, 9406-9414.
29. Koller, J.; Bergman, R. G., *Organometallics* **2012**, *31*, 2530-2533.
30. Dale, J. A.; Mosher, H. S., *J. Am. Chem. Soc.* **1973**, *95*, 512-519.
31. Chen, J.; Lalancette, R. A.; Jäkle, F., *Organometallics* **2013**, *32*, 5843-5851.
32. Reisinger, A.; Trapp, N.; Krossing, I., *Organometallics* **2007**, *26*, 2096-2105.

## Chapter 6 Planar Chiral Diferrocene Systems

### 6.1 Introduction

In this chapter we describe our efforts towards a novel class of chiral Lewis acids and Lewis pairs based on two ferrocenes that are doubly linked by heteroatoms. A survey of the recent literature reveals that only the 1,2-di-silylated (**A**) and 1,2-di-borylated species (**B**) have been reported. For the doubly silyl-bridged ferrocene derivatives, the synthesis involved addition of  $\text{FeCl}_2$  to a mixture of disila-s-indacene dianion and  $\text{CpNa}$  (excess amount). The desired product was isolated from the crude mixture, which consisted of anti-isomer (**A**), syn-isomer, and other multi-nuclear species that contain more than two ferrocene units.<sup>1</sup> In a different way, system **B** was obtained by the boron-tin exchange of a 1,2-distannylated ferrocene and  $\text{BCl}_3$ . After the first boron-tin exchange, the intermediate, a 1-stannyl-2-boryl-ferrocene, could further undergo a second transmetalation to give the doubly boryl-bridged ferrocenes. Replacement of the chlorine atoms on the boron with aromatic substituents allows for tuning of the electronic properties of these systems. Due to the presence of a weak interaction between the iron and boron centers, the boryl units are bent away from the plane of the substituted Cp rings. Remarkably, this type of interaction could be interrupted by the oxidation of the ferrocene unit, reduction of the boryl moiety, or Lewis base complexation to the boron center, resulting in a geometry change to a more co-planar conformation.<sup>2</sup> Related 1,1'-disubstituted ferrocene derivatives have attracted considerable efforts during the past two decades. This family of compounds can be readily obtained from the 1,1'-dilithiated ferrocene precursor. Elements ranging from group 13 and 14 such as B,<sup>3</sup> Si,<sup>4</sup> Sn,<sup>5</sup> Pb,<sup>6</sup> Al<sup>7</sup>

and Ga<sup>8</sup> were incorporated as bridges. One of the examples showing very intriguing properties in supramolecular chemistry is the complex **C** reported by Wagner and coworkers. This diferrocene system served as a lithium ion scavenger to form complex **C**, where a Li<sup>+</sup> is positioned in the middle of a diferrocenyl diborate framework and stabilized by the electron rich borate and Fe(II) moieties. Interestingly, the system was able to expel the Li<sup>+</sup> ion after oxidation of the diferrocene unit.<sup>3</sup>

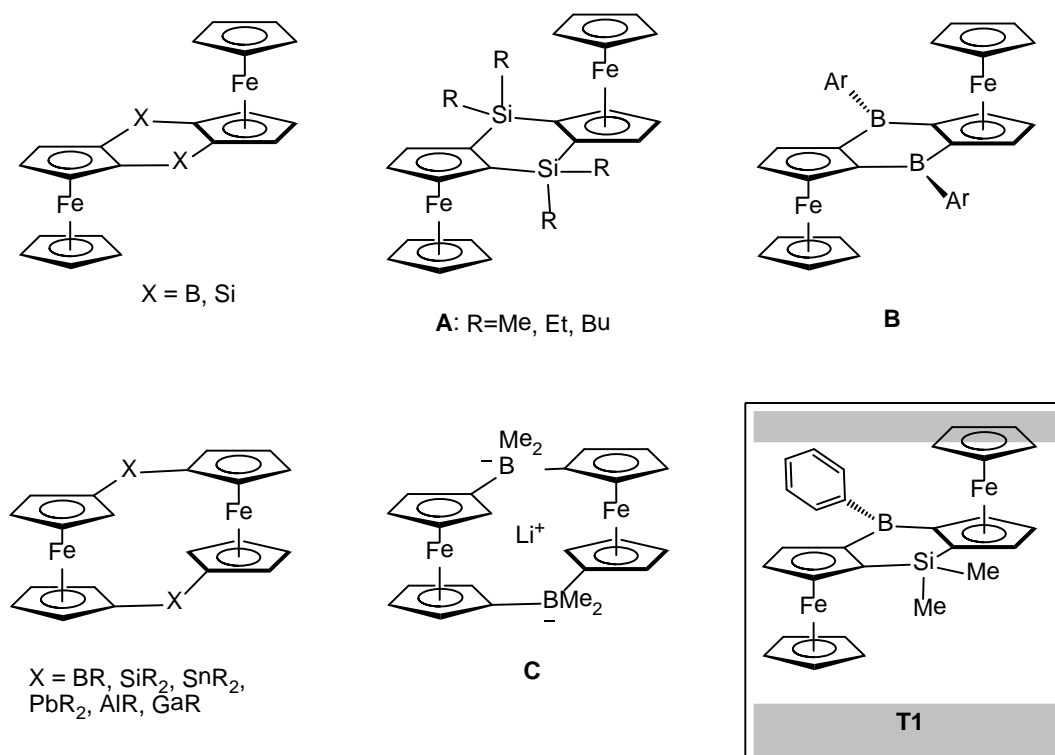


**Figure 6-1.** Representative examples of element-bridged diferrocenes.

We envisioned that replacement of one of the boron atoms with silicon or phosphorus will break the symmetry in compound **B** resulting in chiral Lewis acids. With phosphorus an ambiphilic system would be generated that features both a Lewis acidic boron and a Lewis basic phosphorus center. Related benzene-based ambiphilic phosphaborin systems (**D**) have been reported by Kawashima and coworkers.<sup>9</sup> Studies on

electronic and optical properties indicated an intramolecular charge transfer from phosphorus to boron upon photo excitation. Moreover, the alkylation of phosphorus resulted in the formation of a cationic phosphonium species, which became more soluble in polar solvents and had a high affinity towards anions such as fluoride and bromide.<sup>10</sup> A lot of effort has also been directed to applications where boron and phosphorus could work in a cooperative manner. For instance, borane-phosphine systems can serve as FLPs and be utilized to activate small molecules as discussed in Chapter 1. In addition, these types of amphoteric molecules could coordinate to transition metals in different and unique ways. Ligands for transition metal coordination can be classified as the following three types: 2e-donor ligands (L), 1e-donor ligands (X) and 0e-donors/2e-acceptors (Z).<sup>11</sup> Ambiphilic ligands can be described as molecules bearing donor moieties (L and/or X) and at least one Lewis acid unit (Z). Last but not least, in order to retain the ambiphilic features, it is imperative to prevent the strong interaction between the Lewis basic and Lewis acidic units by tuning both electronic and steric properties of the appendant substituents. There are also several coordination modes that could be involved: (1) the metal binds solely to the Lewis base moiety (L) and the Lewis acid (Z) interacts with an incoming substrate (S) (Figure 6-2a); (2) the Lewis acid (Z) can interact with the ligand (X) within the coordination sphere of the metal (Figure 6-2b); (3) the Lewis acid could bind cooperatively to a nucleophilic metal center, forming a dative interaction from the metal to the Lewis acid (Figure 6-2c). The first type of coordination mode mimics the working behavior of enzymes in nature. The second and third types have also been studied extensively in the past decade. For example, by tuning the Lewis acidity of the boron center, the ambiphilic ligands **E** bind to the metal via  $P \rightarrow M \rightarrow B$  or  $P \rightarrow M \rightarrow Cl \rightarrow B$

interactions (M: rhodium or gold).<sup>12</sup> This rare interacting mode (M→Z  $\sigma$ -donation) provides an opportunity to investigate the coordination of various Lewis acids (B, Al, Ga, In, Si, Sn) to different transition metals (Rh, Ni, Pd, Pt, Cu, Ag, Au etc.).<sup>13</sup> The increasing interest and successful examples in this emerging area raised a fundamental question on the nature of such interactions. For example, Bourissou and coworkers carried out comparative studies on the structural geometry and the electronic configuration of an ambiphilic complex [ $\{\kappa^3\text{-}(o\text{-}(\text{iPr}_2\text{P})_2\text{C}_6\text{H}_4)\text{BPh}\}\text{AuCl}$ ]. The solid state structure indicated a square planar geometry, which is usually adopted by Au<sup>III</sup> d<sup>8</sup> complexes. However, the computational data suggested that the dative Au→B interaction did not lead to the formal two-electron oxidation of Au<sup>I</sup> to Au<sup>III</sup>, which was also supported by the Mössbauer spectroscopic analysis. As a result, the Au metal retained a d<sup>10</sup> configuration with an unexpected square planar geometry.

Herein we describe the synthesis of the first examples of planar chiral diferrocenylsilaborin Lewis acid (**T1**) and an ambiphilic diferrocenylphosphaborin derivative (**T2**). We also discuss the redox properties, binding behavior in the presence of external Lewis acids or transition metals to (**T2**), as well as an investigation of the electron donating property in the corresponding Vaska-type complex.

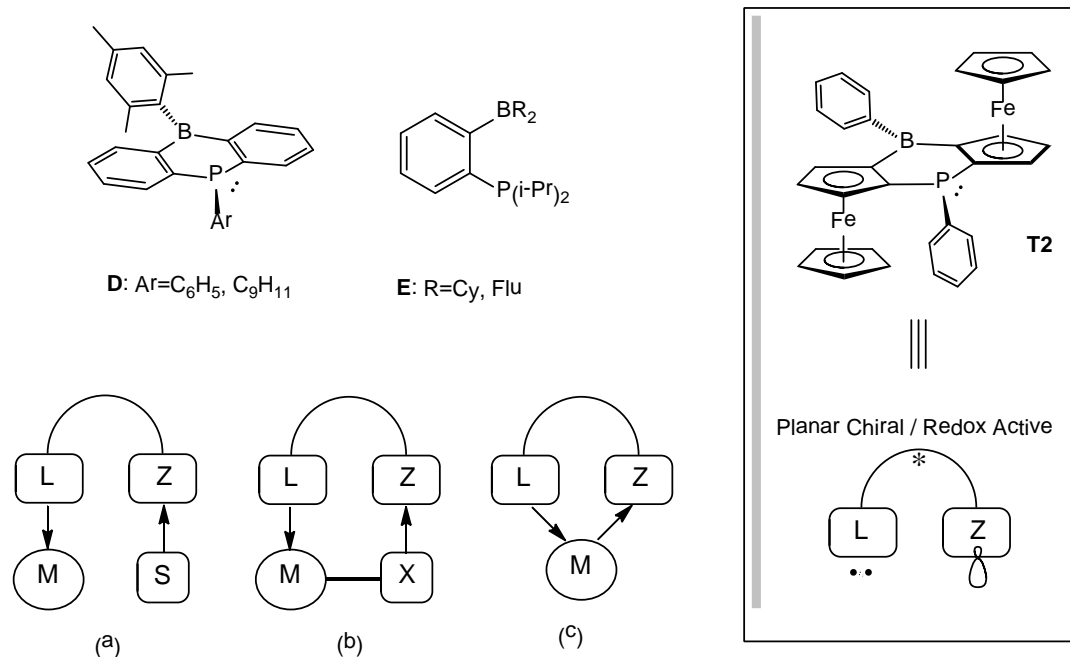
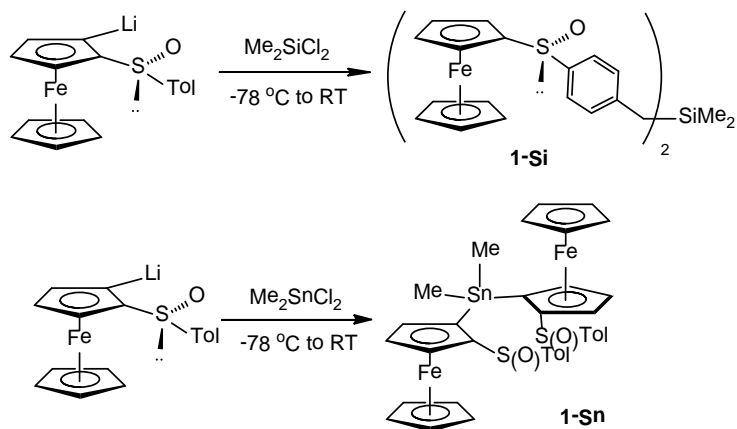


**Figure 6-2.** Examples of ambiphilic ligands, the different coordination modes and the targeted diferrocenylphosphaborin compound **T2**.

## 6.2 Results and Discussions

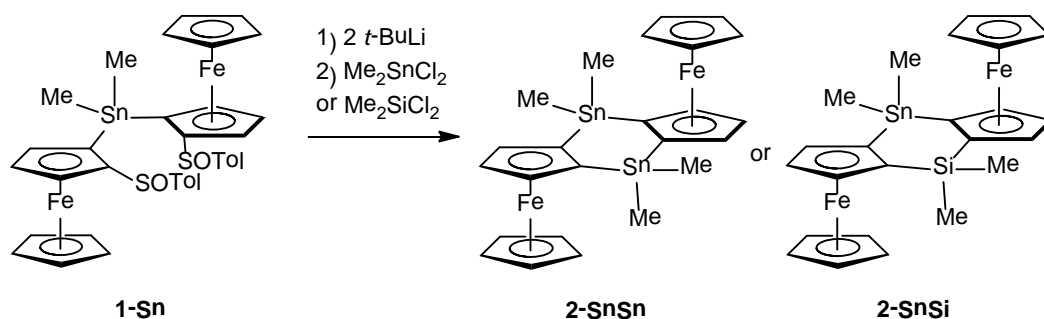
Initially, we explored methods to link two ferrocene units with different hetero atoms. Li-Fc-SOTol, prepared by diastereoselective lithiation of FcSOTol with LDA according to Kagan's method,<sup>14</sup> was chosen as the precursor because of its facile preparation and excellent stereoselectivity in the synthesis of planar chiral 1,2-disubstituted ferrocenes. The lithiated species was then treated with  $\text{Me}_2\text{SiCl}_2$ ,  $\text{PhPCl}_2$  or  $\text{Me}_2\text{SnCl}_2$ . In the case of  $\text{Me}_2\text{SiCl}_2$ , a yellow solid was isolated after chromatography. However, NMR studies indicated a mono-substituted ferrocene derivative (**1-Si**). We propose that the Li-Fc-Tol was not able to attack  $\text{Me}_2\text{SiCl}_2$  due to steric effects. As the temperature increased, isomerization occurred to give a benzyl anion with less steric hindrance, which could undergo the nucleophilic substitution at the silicon atom and give the corresponding unexpected ferrocene dimer. In the reaction with  $\text{PhPCl}_2$ , several fractions of unidentified

species formed, which could not be separated well by chromatography. Fortunately, switching to a better electrophile  $\text{Me}_2\text{SnCl}_2$  provided the expected bridged product. Column chromatography followed by crystallization gave the desired product (**1-Sn**) in a yield of 80% (Scheme 6-1).



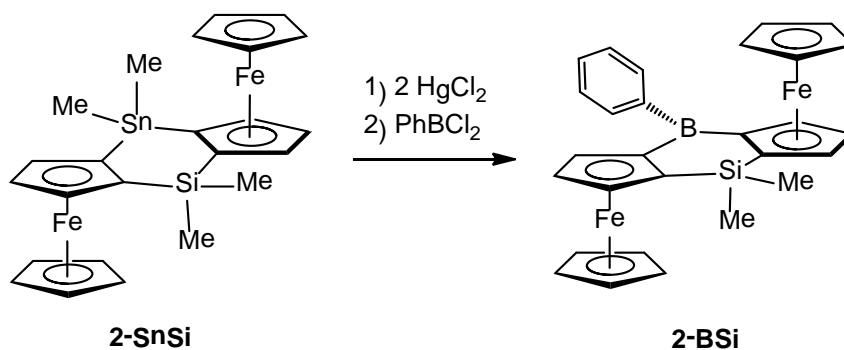
**Scheme 6-1.** Synthesis of planar chiral tin-bridged diferrocene **1-Sn**.

The dilithiation of compound **1-Sn** proceeded readily upon treatment with 2 equivalents of *t*-BuLi at  $-78\text{ }^\circ\text{C}$ . Cyclic systems **2-SnSn** and **2-SnSi** were obtained after the metathesis of the dilithiated species with the corresponding element dichloride ( $\text{Me}_2\text{SnCl}_2$  and  $\text{Me}_2\text{SiCl}_2$ , respectively). Compounds **2-SnSn** and **2-SnSi** (Scheme 6-2) were purified by silica gel column chromatography using hexanes as eluent, followed by crystallization in methanol (yield of 65% for **2-SnSn** and 62% for **2-SnSi**). Only one set of 1,2-disubstituted Cp signals is observed in the  $^1\text{H}$  NMR, which is consistent with the  $\text{C}_2$  symmetry of the molecules.



**Scheme 6-2.** Synthesis of planar chiral cycles **2-SnSn** and **2-SnSi**.

We next investigated the replacement of the dimethylstannyl unit in **2-SnSi** by a boryl unit. Reaction of **2-SnSi** with 2 equivalents of  $\text{HgCl}_2$  in acetone (1 h) resulted in the complete conversion into the corresponding dimercurated species.  $^1\text{H}$  NMR showed the typical patterns for the 1,2-disubstituted ferrocene derivative and the absence of the Sn-Me signal suggested the replacement of tin with mercury. The product reacted readily with  $\text{PhBCl}_2$  in toluene at  $90^\circ\text{C}$  overnight to give a new cycle **2-BSi** in a yield of 47% (Scheme 6-3). The incorporation of boron is evident from multinuclear NMR data.  $^1\text{H}$  NMR indicates a set of aromatic B-*Ph* signals as well as a downfield shift for the substituted Cp ring due to the electron deficiency of the boron. An  $^{11}\text{B}$  NMR resonance at  $\delta = 53.9$  denotes a typical tricoordinate boron (Figure 6-3).



**Scheme 6-3.** Synthesis of planar chiral cycle **2-BSi**.

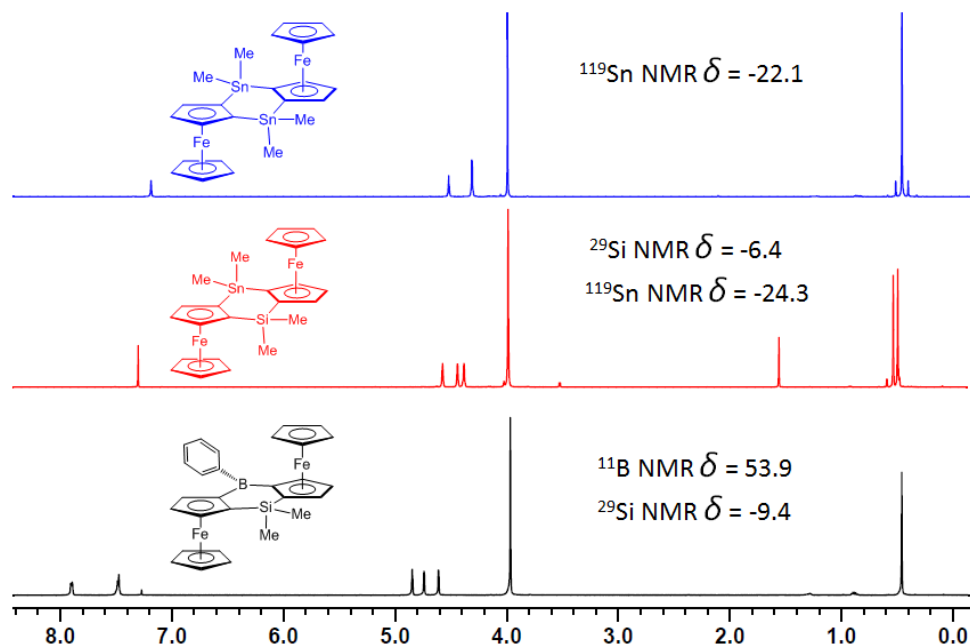


**Figure 6-3.** Comparison of NMR data for cycles **2-SnSn**, **2-SnSi**, **2-BSi**.

The solid state characterization of the achiral system, **2-SnSn**, is hampered by the unsolved disorder of the ferrocenyl units. The chiral derivative **2-SnSi** suffered minor disorder as well. Nonetheless, its structure could be solved in the chiral  $C_2$  space group. In both of the independent molecules of **2-SnSi**, the tin and silicon atoms are almost coplanar with the substituted Cp rings. The ferrocene units are positioned in an anti-fashion and adopt a  $pR$  configuration according to the CIP protocol. The introduction of boron resulted in a dramatic change of the solid state structure. The B-Si compound crystallized in the  $P2_1$  space group with an unchanged  $pR$  configuration for the diferrocene unit (Figure 6-4). Selective distances and angles are summarized in Table 6-1. The bridge angles ( $\gamma$ , see Chapter 1) in **2-SnSi** are  $101.7(5)^\circ$  [ $102.4(6)^\circ$ ] at the Sn center and  $108.7(8)^\circ$  [ $111.2(7)^\circ$ ] at the Si center. The bridge angles in compound **2-BSi** are  $102.60(11)^\circ$  at the Si and  $118.4(2)^\circ$  at the B. The large difference between  $\gamma$  for **2-**

**SnSi** and **2-BSi** can be attributed to the planarization upon changing the tetrahedral geometry of Sn to a trigonal geometry of B. A considerable interaction between the tricoordinate electron deficient boryl unit and the iron center is deduced from the dip angles of the boron out of the Cp planes ( $13.9^\circ$  and  $13.7^\circ$ ) ( $\alpha$ , see Chapter 1), towards the metal centers (Figure 6-4). As a result, the substituted Cp rings in **2-BSi** are positioned in a distorted orientation with the dihedral angle (Cp//Cp) of  $14.12^\circ$ , which is very different from cycle **2-SnSi**. The substituted Cp rings in **2-SnSi** are coplanar due to the  $C_2$  symmetry.

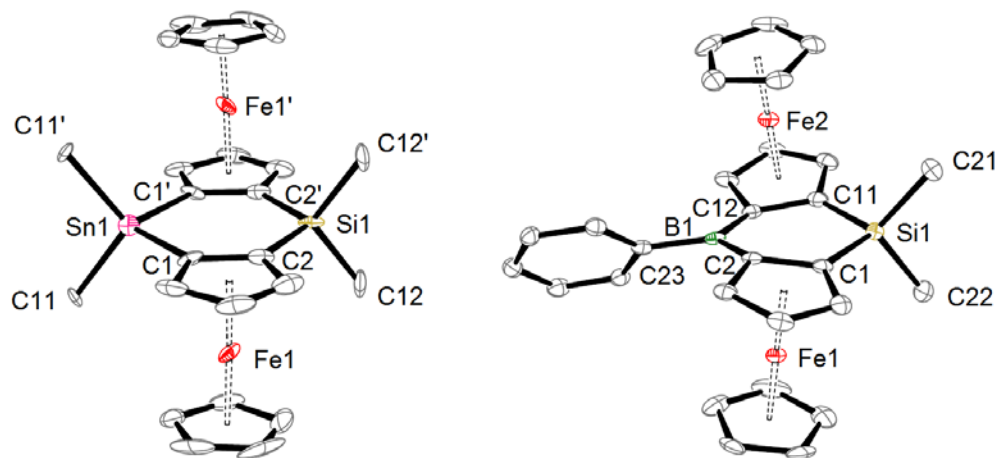


**Figure 6-4.** a) Ortep plot of **2-SnSi** and **2-BSi** (50% thermal ellipsoids); H atoms are omitted.

**Table 6-1.** Selected distances (Å), angles ( $^\circ$ ) and parameters of **2-SnSi** and **2-BSi**.

	<b>2-SnSi</b> [2 <sup>nd</sup> molecule]	<b>2-BSi</b>
Bond length (Å)	Sn1-C1: 2.115(9) [2.137(9)];	Si1-C1: 1.861(3);
	Sn1-C11: 2.149(9) [2.147(9)];	Si1-C11: 1.851(3);
	Si1-C2: 1.882(12) [1.878(11)];	Si1-C21: 1.878(3);
	Si1-C12: 1.856(12) [1.881(12)];	Si1-C22: 1.879(3);
		B1-C2: 1.543(4);
	B1-C12: 1.555(4);	
	B1-C23: 1.570(4);	
Dip angle <sup>a</sup> ( $^\circ$ )	--	13.9 & 13.7
Bridge angle ( $^\circ$ )	C1-Sn1-C1' 101.7(5) [102.4(6)];	C2-B1-C12 118.4(2);
	C2-Si1-C2' 108.7(8) [111.2(7)];	C1-Si1-C11 102.60(11);

Tilt angle <sup>b</sup> (°)	3.99 [1.96]	0.72 & 0.97
Cp//Cp <sup>c</sup> (°)	0 [0]	14.12
$\Sigma_{\angle C-E-C}$ <sup>d</sup> (°)	--	B1: 360
Flack parameter	0.114(17)	0.007(3)

[a] Applied to cycles with boron bridges;

[b] Data correspond to lower Fc and upper Fc;

[c] Dihedral angles of two substituted Cp planes;

[d] Sum of bond angles around the bridging element B or P.

The electrochemistry of **2-SnSn**, **2-SnSi** and **2-BSi** was examined by cyclic voltammetry and square wave voltammetry (Figure 6-5). CV data show that all compounds undergo quasi-reversible mono- and di- oxidation for the diferrocene moieties. The peak separations for **2-SnSn**, **2-SnSi** and **2-BSi** are 374, 394 and 574 mV, respectively. The redox behavior of compounds **2-SnSn** and **2-SnSi** is almost identical, suggesting that the switching between tin and silicon bridges has just a minor influence on the geometry and electronic coupling between the ferrocene units. In contrast, incorporation of boron resulted in dramatic anodic shifts of both the 1<sup>st</sup> and 2<sup>nd</sup> oxidation potentials, as well as an enlargement of the peak separation (Table 6-2). Interestingly, **2-SnSn** and **2-SnSi** exhibited two redox waves with equal intensities, while compound **2-BSi** showed a considerably smaller current for the 2<sup>nd</sup> oxidation. Notably, Compton and coworkers studied the double reduction behavior of anthraquinone in low electrolyte support and observed the same phenomenon.<sup>15</sup> They attribute this phenomenon to a fast comproportionation rate that leads to accumulation of the mono- anion, hence the transport of it becomes rate-limiting. The fast comproportionation is thermodynamically more favorable if the peak separation for two redox processes is larger. In the case of low electrolyte support, the diffusion of the mono- anion is reduced by repulsion from the negatively charged reaction layer. As a result, the magnitude for the 2<sup>nd</sup> reduction is

decreased. Although we already used a relatively well-supported system (ca. 50 fold amount of the electrolyte compared to the substrates), we still observe this similar phenomenon due to ineffective screening of the electric field in compound **2-BSi** as well as other compounds with large peak separation (*vide infra*). The cycle **2-BSi** was also chemically oxidized by treatment with 2 equivalents of the Ag derivative of Krossing's salt. The  $^1\text{H}$  NMR resonances shifted to 44.4 ppm for the free Cp and 29.0, 22.4, 18.1 ppm for the substituted Cp ring. Unfortunately, attempts to characterize the product by crystallography failed. Under ambient conditions a hydrolyzed species precipitated from a  $\text{CH}_2\text{Cl}_2$  solution of the oxidized compound and was analyzed by single-crystal X-ray diffraction (**Figure 6-6**). The oxidation of both ferrocene units was evident from the distances of the centroids of two Cp rings (3.420 Å), which falls into the typical range for oxidized ferrocene.

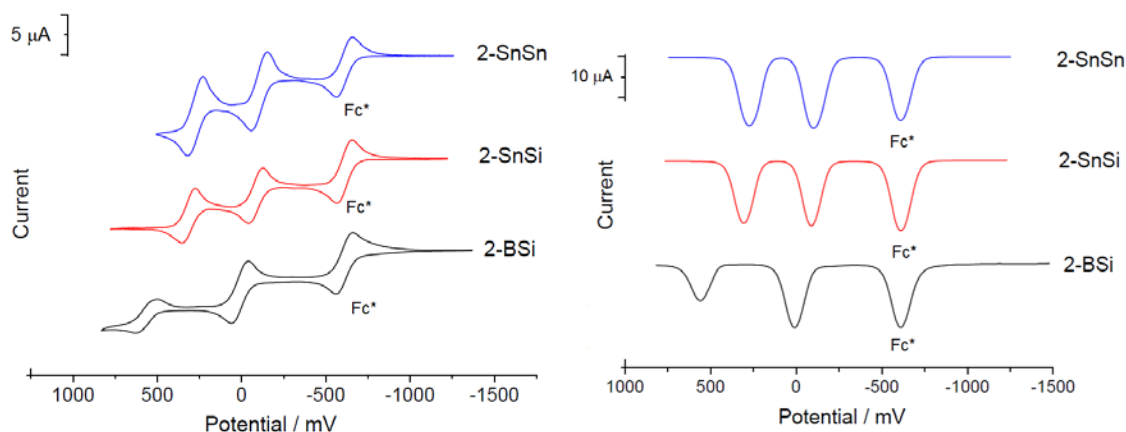


**Figure 6-5.** Left: cycle voltammetry data for **2-SnSn**, **2-SnSi**, **2-BSi** ( $\text{CH}_2\text{Cl}_2$ , 25 mV/s, 0.05 M  $\text{Bu}_4\text{N}[\text{B}(\text{C}_6\text{H}_3(\text{CF}_3)_2)_4]$  as electrolyte, reported versus  $\text{Fc}/\text{Fc}^+$ , which is taken as +610 mV versus  $\text{Fc}^*/\text{Fc}^{*+}$  as an internal reference); Right: square wave voltammetry data for **2-SnSn**, **2-SnSi**, **2-BSi**.

**Table 6-2.** Redox potentials derived from cyclic voltammetry or square-wave voltammetry data; CH<sub>2</sub>Cl<sub>2</sub>, 0.05 M Bu<sub>4</sub>N[B(C<sub>6</sub>H<sub>3</sub>(CF<sub>3</sub>)<sub>2</sub>)<sub>4</sub>] as electrolyte, reported vs Fc/Fc<sup>+</sup>

	$E_{1/2}$ (1) (mV)	$E_{1/2}$ (2) (mV)	$\Delta E_{1/2}$ (mV)
<b>2-SnSn</b> <sup>a</sup>	-101	273	374
<b>2-SnSi</b> <sup>a</sup>	-88	306	394
<b>2-BSi</b> <sup>a</sup>	10	557	547
BPh-BPh <sup>b</sup>	60	570	510

[a] Calculated from square-wave voltammetry data

[b] Cyclic voltammetry Data from ref. [2a]

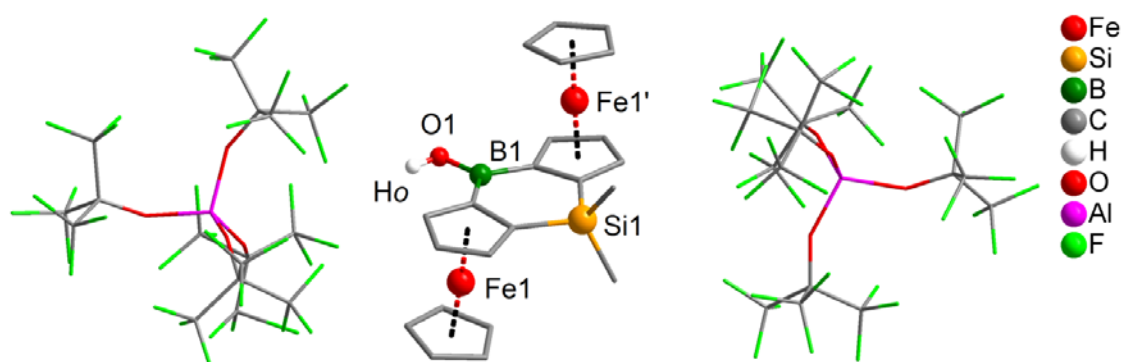
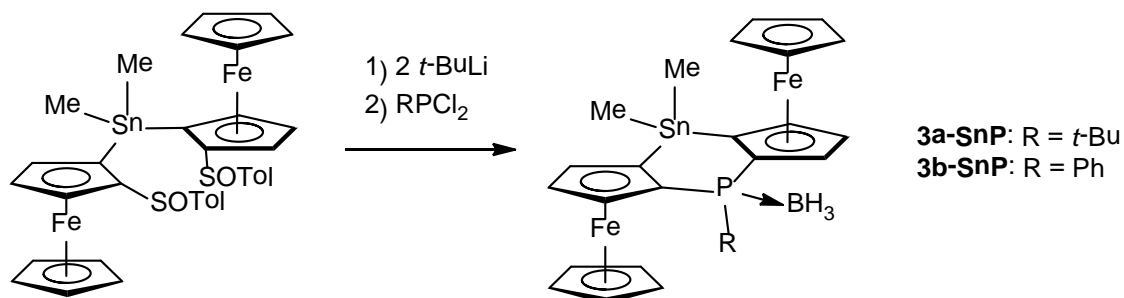


**Figure 6-6.** Solid state structure of a doubly oxidized species derived from **2-BSi** (Hydrogen atoms omitted except for B-OH).

Following a similar strategy as described for the chiral Lewis acid **2-BSi**, **1-Sn** was dilithiated and treated with dichlorophosphines for the synthesis of ambiphilic phosphorus-containing cycles (Scheme 6-4). An initial attempt with the alkyl phosphine *t*-BuPCl<sub>2</sub> followed by reaction with BH<sub>3</sub> in THF led to a trace amount of the product **3a-SnP**, which is complexed with BH<sub>3</sub> to avoid oxidation of the phosphorus. The steric bulk as well as the electron rich character of the *t*-butyl group possibly hampered the efficient nucleophilic replacement of the chlorine atoms with the ferrocene units. Switching to the

aryl phosphine  $\text{PhPCl}_2$ , a better electrophile with less steric hindrance, led to an increase in the yield to 40% for the product **3b-SnP**. Both compounds formed red crystals suitable for structure determination. They crystallize in the  $P2_12_12_1$  space group with one independent molecule for the *t*-butyl derivative and two for the phenyl derivative in the unit cell. The structural parameters are generally very similar as they adopt very similar geometries (Figure 6-7 and Table 6-3). But the individual ferrocene moieties experience different spatial environments. While one is closer to the  $\text{BH}_3$  group, the other is adjacent to the *t*-butyl or phenyl group on phosphorus. Due to the bulky pendent groups on the phosphorus, the substituted Cp rings adopt a butterfly orientation, rather than a coplanar conformation. The dihedral angles (Cp//Cp) of the substituted Cp rings are measured to be  $43.76^\circ$  and  $53.78^\circ$  [ $45.49^\circ$ ] for **3a-SnP** and **3b-SnP**, respectively. The bridge angles in **3a-SnP** are  $96.16(10)^\circ$  at the Sn center and  $107.18(11)^\circ$  at the P center. The bridge angles in **3b-SnP** are  $95.87(10)^\circ$  [ $95.99(10)^\circ$ ] at the Sn center and  $105.00(12)^\circ$  [ $106.07(12)^\circ$ ] at the P center. The steric hindrance is also reflected in the tilt angles ( $\gamma$ ) of the ferrocene moiety that is closest to the P substituent, which are  $11.86^\circ$  for the *t*-butyl derivative and  $4.96^\circ$  [ $6.17^\circ$ ] for the phenyl derivative. The difference in the tilt angle is consistent with the lower yield for the ring formation in the case of *t*-BuPCl<sub>2</sub>.



**Scheme 6-4.** Synthesis of planar chiral cycles **3a-SnP** and **3b-SnP**.

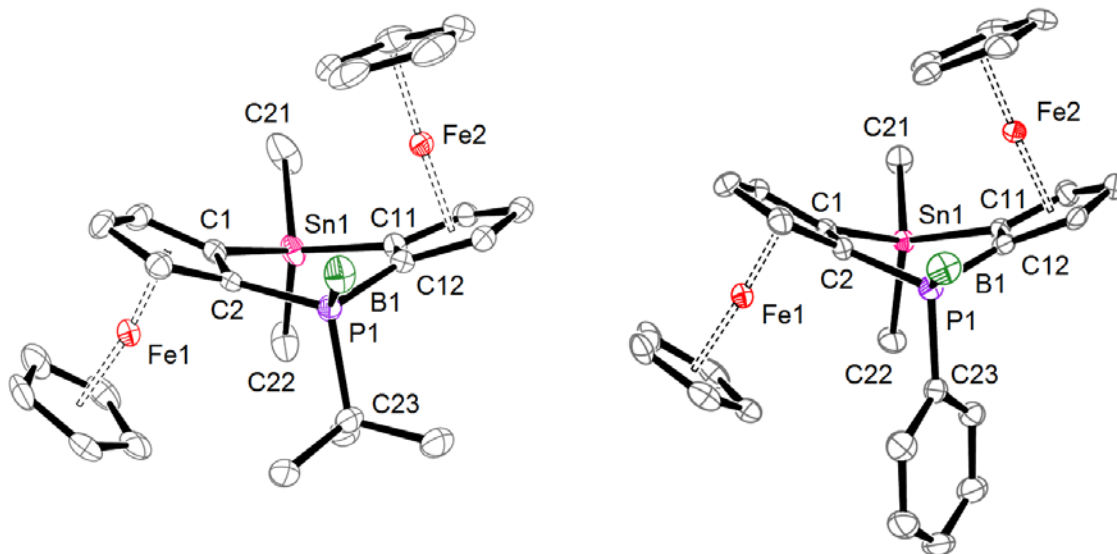


**Figure 6-7.** a) Ortep plots of **3a-SnP** and **3b-SnP** (50% thermal ellipsoids); H atoms are omitted.

**Table 6-3.** Selected distances (Å), angles (°) and parameters of **3a-SnP** and **3b-SnP**.

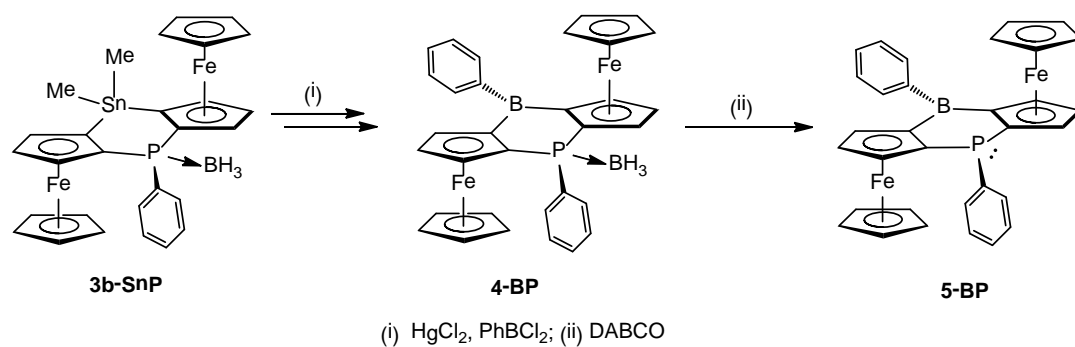
	<b>3a-SnP</b>	<b>3b-SnP</b> [2 <sup>nd</sup> molecule]
Bond length (Å)	Sn1-C1: 2.128(2); Sn1-C11: 2.135(3); Sn1-C21: 2.139(3); Sn1-C22: 2.146(3); P1-C2: 1.815(2); P1-C12: 1.805(3); P1-C23: 1.866(3); P1-B1: 1.932(3);	Sn1-C1: 2.126(3) [2.133(3)]; Sn1-C11: 2.142(3) [2.138(3)]; Sn1-C21: 2.134(3) [2.132(3)]; Sn1-C22: 2.132(3) [2.143(3)]; P1-C2: 1.799(3) [1.810(3)]; P1-C12: 1.797(3) [1.799(3)]; P1-C23: 1.825(3) [1.817(3)]; P1-B1: 1.924(3) [1.925(3)];
Bridge angle (°)	C1-Sn1-C11: 96.16(10); C2-P1-C12: 107.18(11);	C1-Sn1-C11: 95.87(10) [95.99 (10)]; C2-P1-C12: 105.00(12) [106.07(12)];
Tilt angle <sup>a</sup> (°)	11.86 & 3.79	4.93 [6.17] & 1.68 [1.78]
Cp//Cp <sup>a</sup> (°)	43.76	53.78 [45.49]
$\Sigma_{\angle C-E-C}$ (°)	P1: 320.47	P1: 320.14 [318.40]
Flack parameter	0.008(4)	0.013(3)

[a] Data correspond to upper Fc and lower Fc;

[b] Dihedral angles of two substituted Cp planes;

[c] Sum of bond angles around the bridging element B or P.

The phenyl derivative **3b-SnP** was used as precursor for the synthesis of a **4-BP** because of its higher yield. Similar to the previous synthetic protocol, **3b-SnP** was initially treated with 2 equiv of  $\text{HgCl}_2$  for the synthesis of the dimercurated species. However,  $^1\text{H}$  NMR indicated that only 1 equivalent of  $\text{HgCl}_2$  had reacted. Cleavage of only one of the  $\text{Sn-C}_{\text{Cp}}$  bonds results in the formation of a species bearing a chlorodimethylstannyl and a chloromercurio group. The retention of the chlorodimethylstannyl group was evident from the  $^1\text{H}$  NMR resonances at 1.05 and 1.32 ppm that each integrated as 3 protons. Attempts to use longer reaction times led to no further conversion and higher reaction temperature resulted in the loss of the chloromercurio group. Fortunately, the intermediate reacted smoothly with  $\text{PhBCl}_2$  to give the desired product. After heating in toluene to 90 °C for 12 h and subsequent column chromatography, the analytically pure cycle **4-BP** was obtained in a yield of 49 %. The broad signals at 1.16 ppm in the  $^1\text{H}$  NMR and a signal at -35.2 ppm in the  $^{11}\text{B}$  NMR indicate the attachment of the  $\text{BH}_3$  group. On the other hand, MALDI-MS data show a major signal corresponding to the loss of  $\text{BH}_3$ . In the solid state, **4-BP** crystallizes in the  $\text{P2}_1$  space group. The  $\Sigma_{\angle\text{C-B-C}}$  around boron is 360.0°, indicating that B adopts an almost perfect trigonal planar geometry.  $\Sigma_{\angle\text{C-P-C}}$  around phosphorus is 314.33°, which is consistent with pyramidalization at phosphorus. The bridge angles were measured to be 117.0(3)° at the B and 101.97(13)° at the P. The dip angles of the boron towards the iron centers are 13.5° and 14.5°, respectively (Figure 6-8 and Table 6-4).



**Scheme 6-5.** Synthesis of the ambiphilic ligand **5-BP**.

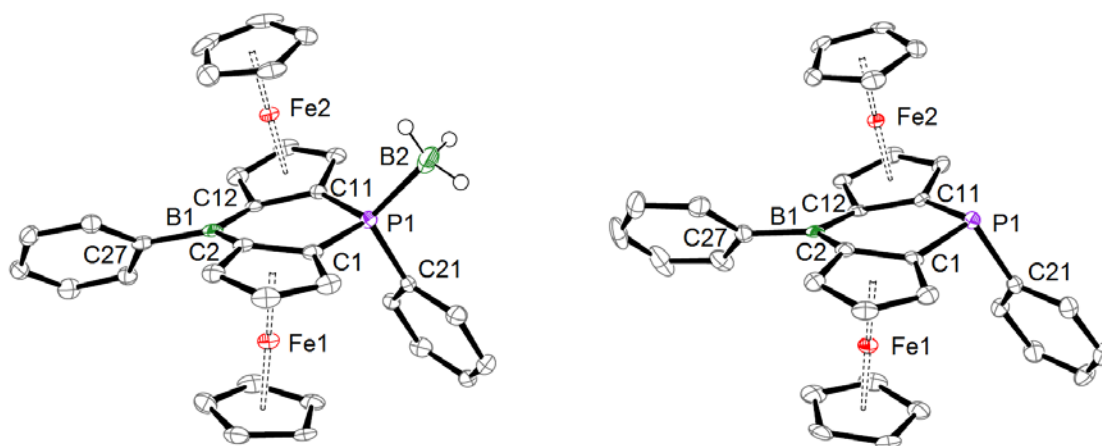


**Figure 6-8.** a) Ortep plots of **4-BP** and **5-BP** (50% thermal ellipsoids); H atoms (except  $\text{BH}_3$ ) are omitted

**Table 6-4.** Selected distances ( $\text{\AA}$ ) and angles ( $^\circ$ ) of **4-BP** and **5-BP**.

	<b>4-BP</b>	<b>5-BP</b>
Bond length ( $\text{\AA}$ )	B1-C2: 1.547(5);	B1-C2: 1.533(4);
	B1-C12: 1.531(5);	B1-C12: 1.544(4);
	B1-C27: 1.570(5);	B1-C27: 1.568(4);
	P1-C1: 1.800(3);	P1-C1: 1.823(2);
	P1-C11: 1.789(3);	P1-C11: 1.809(2);
	P1-C21: 1.818(3);	P1-C21: 1.846(2);
	P1-B2: 1.897(4);	
Dip angle <sup>a</sup> ( $^\circ$ )	13.5 & 14.5	14.6 & 15.6
Bridge angle ( $^\circ$ )	C2-B1-C12: 117.0(3);	C2-B1-C12: 117.2(2);
	C1-P1-C11: 101.97(13);	C1-P1-C11: 99.48(11);
Tilt angle <sup>b</sup> ( $^\circ$ )	3.69 & 0.97	2.53 & 2.23

Cp//Cp <sup>c</sup> (°)	18.03	15.05
$\Sigma_{\angle C-E-C}^d$ (°)	B1: 360.0 P1: 314.33	B1: 360.0 P1: 305.7
Flack parameter	0.012(4)	0.004(3)

[a] Applied to cycles with boron bridges;

[b] Data correspond to lower Fc and upper Fc;

[c] Dihedral angles of two substituted Cp planes;

[d] Sum of bond angles (C-E-C) around the bridging element B or P.

The cleavage of BH<sub>3</sub> under MALDI-MS spectrometry conditions encouraged us to explore synthetic methods to prepare the free cycle **5-BP**. Reaction of **4-BP** with a slight excess of DABCO at 50 °C for 2 days led to formation of the deprotected species, which was purified by aluminum oxide column chromatography with THF/hexanes (1:1) as the eluent in a glovebox. <sup>1</sup>H, <sup>11</sup>B and <sup>31</sup>P NMR spectroscopy confirmed the successful removal of the BH<sub>3</sub> group in the product. The compound **5-BP** crystallized in the P3<sub>2</sub> space group after slow evaporation of a hexanes solution (Figure 6-8). The bending of the boron (dip angle,  $\alpha$ ) towards the iron centers is 14.6° and 15.6°, respectively. The  $\Sigma_{\angle C-P-C}$  around the phosphorus is 305.7° (314.33° for **4-BP**). The lone pair of electrons of the tricoordinate phosphorus typically makes only a very small contribution to the conjugation of  $\pi$  systems, hence the phosphorus usually adopts a pyramidal structure.<sup>9a</sup> Removal of the BH<sub>3</sub> group has very little impact on the P-C bonds distances. The geometry around boron ( $\Sigma_{\angle C-B-C}$  of 360.0°) remained similar when compared to **4-BP** (Table 6-4). After exposure to the air, **5-BP** was converted to a new species (see Supporting Information). The <sup>31</sup>P NMR signal shifted from -24.9 to 29.0 ppm and the MALDI-MS spectrum indicated the addition of an oxygen atom to the molecule, suggesting that the phosphine unit had been oxidized to the phosphine oxide, likely due to the electron-rich environment provided by the biferrocene framework.

For the chiral cyclic compounds, it is crucial to investigate the stereo-selectivity for each step. One method is the absolute configuration as determined by the Flack parameter. We determined the Flack parameters for compounds **2-SnSi** [0.114(17)], **2-BSi** [0.007(3)], **3a-SnP** [0.008(4)], **3b-SnP** [0.013(3)] and **4-BP** [0.012 (4)] and **5-BP** [0.004(3)]. All of the values fell into the satisfactory range except that for cycle **2-SnSi**. We attribute it to the minor disorder (see Supporting Information) in the crystal lattice of **2-SnSi**. The Flack parameter could also be affected by any unsolved disorder problem. To further confirm the enantiopurity of these compounds, the same batches of crystals were used for chiral HPLC and optical rotation measurements for **2-SnSi**, **2-BSi**, **3b-SnP** and **4-BP**. All of them showed one major signal from the chiral HPLC trace, which was identified as the individual cycle with the PDA detector by comparison with UV-Vis spectra of pure cycles. The chiral HPLC and optical rotation measurements for the free ligand **5-BP** were not carried out due to its susceptibility to oxidation under ambient condition. However, it is reasonable to believe that the deprotection of  $\text{BH}_3$  to form **5-BP** occurs with chiral retention.

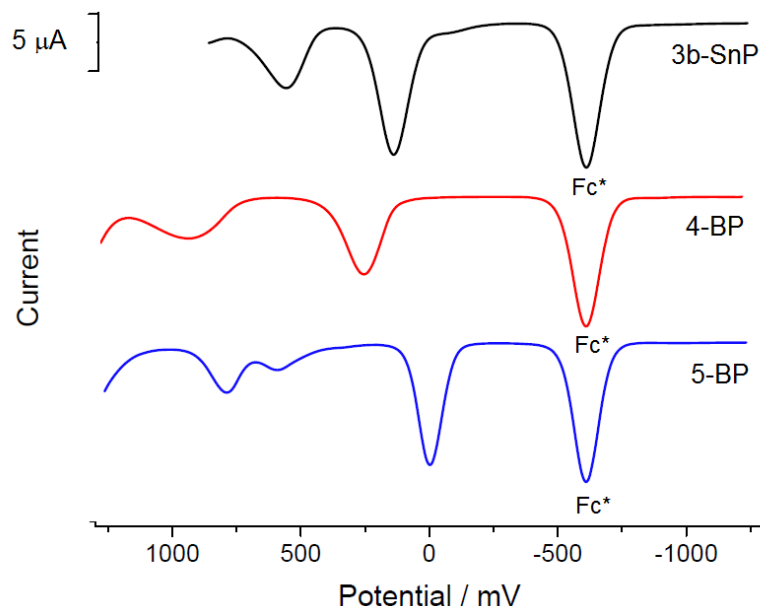


**Figure 6-9.** Square-wave voltammetry data for **3b-SnP**, **4-BP**, **5-BP** ( $\text{CH}_2\text{Cl}_2$ , 0.05 M  $\text{Bu}_4\text{N}[\text{B}(\text{C}_6\text{H}_3(\text{CF}_3)_2)_4]$  as electrolyte, reported versus  $\text{Fc}/\text{Fc}^+$ , which is taken as +610 mV versus  $\text{Fc}^*/\text{Fc}^{*+}$  as an internal reference)

**Table 6-5.** Redox potentials derived from square wave voltammetry data;  $\text{CH}_2\text{Cl}_2$ , 0.05 M  $\text{Bu}_4\text{N}[\text{B}(\text{C}_6\text{H}_3(\text{CF}_3)_2)_4]$  as electrolyte, reported vs  $\text{Fc}/\text{Fc}^+$ .

	$E_{1/2}(1)$ (mV)	$E_{1/2}(2)$ (mV)	$\Delta E_{1/2}$ (mV)
<b>3b-SnP</b>	138	557	419
<b>4-BP</b>	255	940	685
<b>5-BP</b>	-2	591 / 787	-

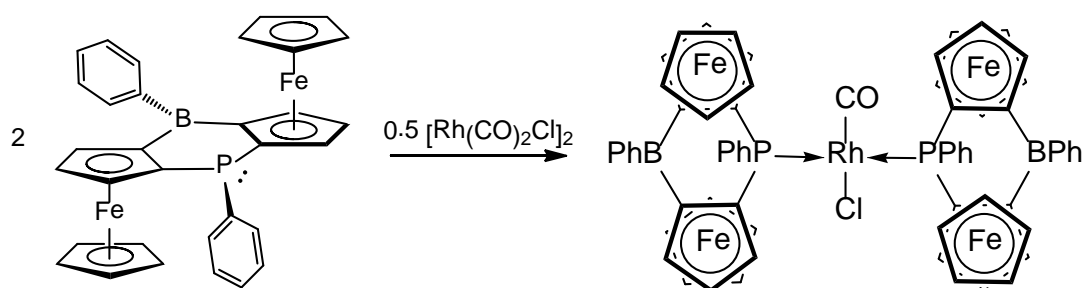
The redox properties of **3b-SnP**, **4-BP** and **5-BP** were studied by cyclic and square wave voltammetry (Figure 6-9 and Table 6-5). For the  $\text{BH}_3$ -protected species, a reversible 1<sup>st</sup> oxidation and quasi-reversible 2<sup>nd</sup> oxidation were observed. Incorporation of B resulted in an anodic shift for both potentials as well as an enlarged peak separation. For the free cycle **5-BP**, the removal of the  $\text{BH}_3$  renders an increase of electron density of

the system, leading to a cathodic shift for the 1<sup>st</sup> redox process ( $E_{1/2}(1) = -2$  mV). Another two signals at higher potential were recorded (591 and 787 mV). Although we were not able to assign them unequivocally, we postulate that one of them corresponds to the 2<sup>nd</sup> oxidation of the diferrocene backbone, while the other might be derived from the electron transfer between the ferrocene and the phosphine moieties, followed by reaction with trace amount of water.<sup>16</sup>

The **5-BP** system could be potentially used as a tunable tertiary phosphine ligand. The compound reacted readily with 0.25 equiv of  $[\text{Rh}(\text{CO})_2\text{Cl}]_2$  to give the corresponding Vaska-type rhodium complex (Scheme 6-6). For such a complex, the monodentate phosphine ligands usually occupy the trans positions, which is consistent with the observation that only one set of  $^1\text{H}$  NMR signals is present for the ligand. The  $^{31}\text{P}$  NMR resonance at 7.6 ppm (doublet) is downfield shifted when compared to that of the free ligand (-24.9 ppm), due to reduced electron density after binding to the rhodium. Moreover, the direct bonding between the Rh and P is evident from the  $^2J(^{103}\text{Rh},\text{P})$  coupling constant of 124 Hz (Figure 6-10). The MADLI-MS data further confirmed the incorporation of two ligands into the complex. The signal with highest intensity at  $m/z$  1110.0461 was assigned to be  $[\text{M}-\text{CO}-\text{Cl}-\text{FeCp}]^+$ , corresponding to loss of the CO and Cl ligands as well as a CpFe fragment.

The coordination of the phosphine to the rhodium stabilizes the lone pair of electrons and removes the electron density from the ferrocene. As a consequence, the diferrocenyl moieties exhibited more reversible and anodic oxidation processes compared to the free ligand (Figure 6-11). In fact, the redox behavior of the Rh complex is quite similar to that of the  $\text{BH}_3$  complex. More interestingly, due to the presence of two redox-active ligands

(namely  $L_1$  and  $L_2$ ), the oxidations are split into two-step single-electron processes. The potentials and peak separations measured by square-wave voltammetry are summarized in Table 6-6. The signals at 130 and 862 mV were assigned as the 1<sup>st</sup> and 2<sup>nd</sup> oxidations of the diferrocenyphosphino ligand  $L_1$ . Similarly, the signals at 254 and 1000 mV were attributed to the second ligand  $L_2$ . The peak separations (732 and 746 mV) are the largest in this series of diferrocene derivatives.



**Scheme 6-6.** Synthesis of a Vaska-type rhodium compound.

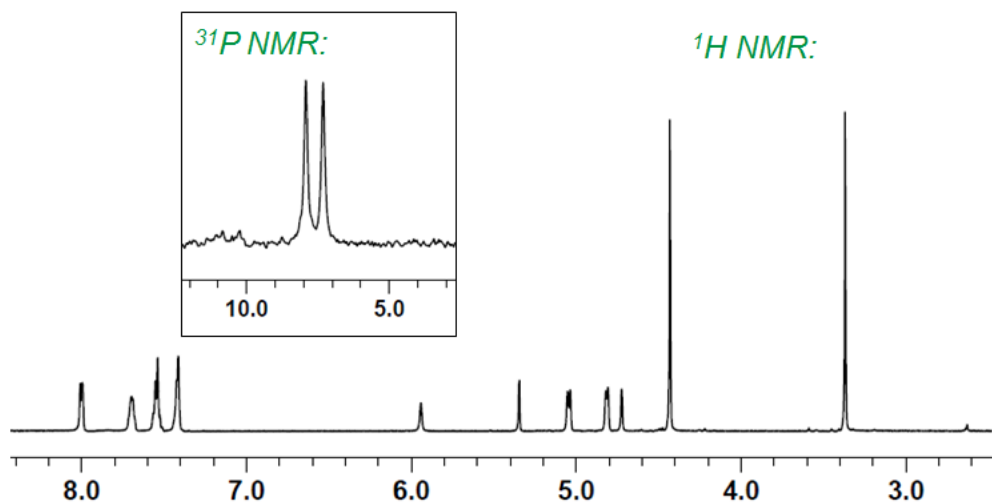


**Figure 6-10.**  $^1\text{H}$  and  $^{31}\text{P}$  NMR spectra for complex  $(5\text{-BP})_2\text{Rh}(\text{CO})\text{Cl}$  in  $\text{CD}_2\text{Cl}_2$ .

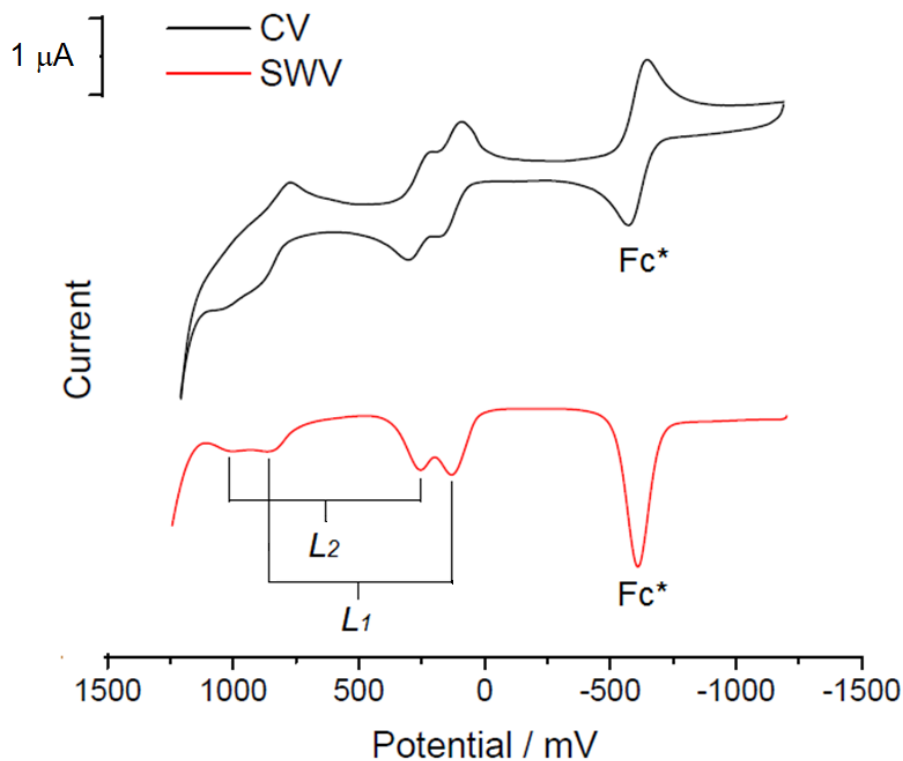


**Figure 6-11.** Cyclic voltammetry ( $\text{CH}_2\text{Cl}_2$ , 50 mV/s, 0.05 M  $\text{Bu}_4\text{N}[\text{B}(\text{C}_6\text{H}_3(\text{CF}_3)_2)_4]$  as electrolyte, reported versus  $\text{Fc}/\text{Fc}^+$ , which is taken as +610 mV versus  $\text{Fc}^*/\text{Fc}^{*+}$  as an internal reference) and square-wave voltammetry data for  $(\mathbf{5-BP})_2\text{Rh}(\text{CO})\text{Cl}$  complex.

**Table 6-6.** Redox potentials derived from square-wave voltammetry data of  $(\mathbf{5-BP})_2\text{Rh}(\text{CO})\text{Cl}$ ;  $\text{CH}_2\text{Cl}_2$ , 0.05 M  $\text{Bu}_4\text{N}[\text{B}(\text{C}_6\text{H}_3(\text{CF}_3)_2)_4]$  as electrolyte, reported vs  $\text{Fc}/\text{Fc}^+$ .

	$E_{1/2}(1)$ (mV)	$E_{1/2}(2)$ (mV)	$\Delta E_{1/2}$ (mV)
$\mathbf{L}_1$	130	862	732
$\mathbf{L}_2$	254	1000	746

The synthesis of a Vaska-type Rh(I) complex allows us to monitor the CO stretching frequency in the presence of different cis- phosphine ligands.<sup>17</sup> This IR band can serve as a probe for the steric and electronic properties of the phosphine ligand. The  $\nu(\text{CO})$  of

1965  $\text{cm}^{-1}$  for **(5-BP)<sub>2</sub>Rh(CO)Cl** (Figure 6-12, blackline) lies in between that of the acyclic mono-ferrocenyl ligand ( $\text{PPh}_2\text{Fc}$ , 1970  $\text{cm}^{-1}$ ) and diferrocenyl ( $\text{PPhFc}_2$ , 1957  $\text{cm}^{-1}$ ) complexes. Apparently, the incorporation of boron results in some degree of electron density reduction when compared to the unfunctionalized derivative. More interestingly, after addition of an excess amount of tetrabutylammonium fluoride to the rhodium complex, the  $\nu(\text{CO})$  shifted dramatically to 1937  $\text{cm}^{-1}$ , suggesting a pronounced enhancement of the “electron releasing” characteristic of the ligand after the fluoride binding (Figure 6-12). A possible explanation is that an increase of the electron density at the metal center and the resulting enhanced  $d-\pi^*$  back bonding leads to a weakening of the  $\text{C}\equiv\text{O}$  bond. In a control experiment, the addition of tetra-*n*-butylammonium fluoride to  $(\text{PPh}_3)_2\text{Rh}(\text{CO})\text{Cl}$  did not affect the  $\nu(\text{CO})$ , which excludes other possibilities such as ligand exchange. In comparison, substitution of the para-position of triphenylphosphine as the ligand with electron-donating groups such as  $-\text{OMe}$  or electron-withdrawing groups such as  $-\text{F}$  and  $-\text{Cl}$  results in only a slight change in the CO stretching frequency (within  $\Delta 5 \text{ cm}^{-1}$  even all of the substituents in the phosphorus are replaced).<sup>17</sup> On the other hand, Peters *et al.* pointed out that the formal charge of the entire metal complex should be considered, since cationic late transition metal ions can have a strong polarization effect on the CO, which leads to a higher CO stretching frequency. They synthesized two families of metal complexes: one consists of zwitterionic complexes with bis(phosphino)borate ligands and the other of cationic complexes with the corresponding bis(phosphino)silane ligands. For the cationic platinum species, the  $\pi$ -back-bonding is weak due to the net positive charge, which results in a high energy CO stretching frequency (2094  $\text{cm}^{-1}$ ). For the borate platinum complex they mentioned, this

polarization effect is reduced because of the negative charge on the boron (regardless of whether the complex is in zwitterion form or not, as long as the overall charge is 0). As a consequence, the  $\nu(\text{CO})$  shifts to lower energy ( $2070 \text{ cm}^{-1}$ ). Therefore, the absolute shift of  $\nu(\text{CO})$  is a result of a polarization effect and the electronic contributions. In our case, it is reasonable to believe the fluoborate ligand is more electron-donating,<sup>18</sup> but the polarization effect of the overall negative charge of the complex likely also contributes to the increased backbonding and lower  $\nu(\text{CO})$ .

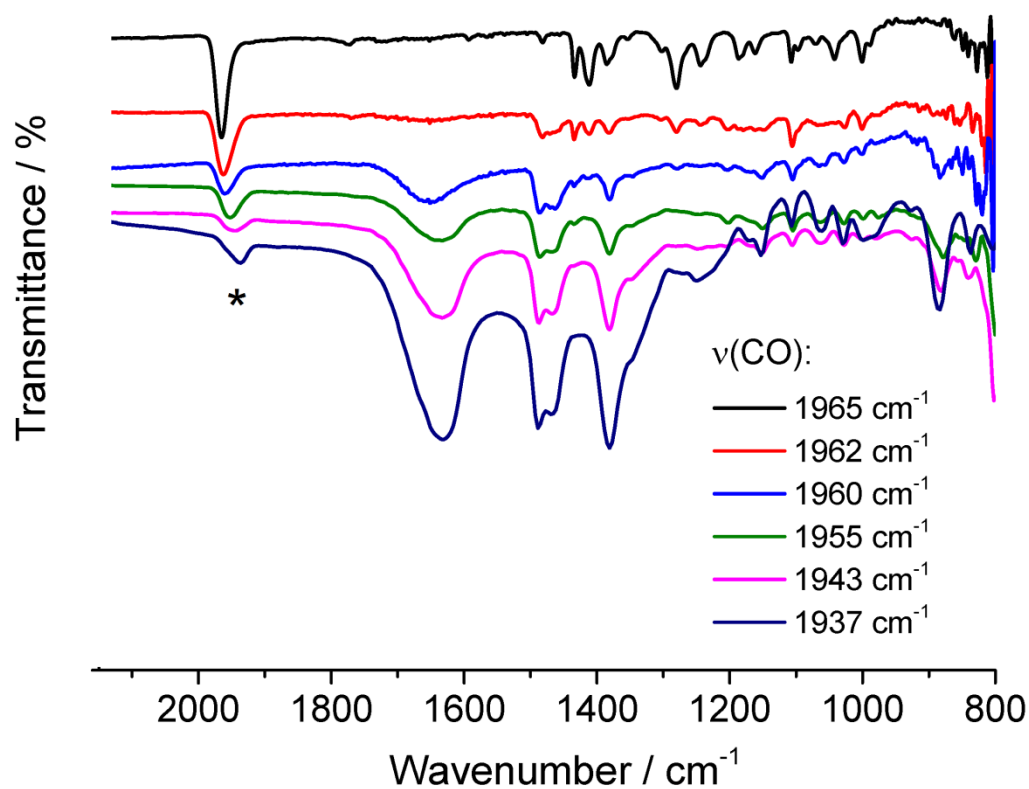


**Figure 6-12.** IR spectra for complex  $(5\text{-BP})_2\text{Rh}(\text{CO})\text{Cl}$  (black line, transmission mode) before and after addition of increasing amounts of F. (The CO stretching band is indicated by an asterisk)

### 6.3 Conclusions

We have established a practical protocol for the synthesis of a number of hetero-atom linked differrocenes, ranging from group 13 to group 15 elements such as boron, silicon, tin and phosphorus. While the compounds with tricoordinate boron feature a trigonal fragment, the others adopt tetrahedral configurations. The successful introduction of planar chirality was supported by single-crystal X-ray crystallography, chiral HPLC and optical rotation measurements. Electrochemical studies reveal that the cycles **2-SnSn**, **2-SnSi** and **2-BSi** undergo 2-step reversible oxidations for the Fc units. The introduction of boron results in anodic shifts for both of the potentials. For the most interesting system, **5-BP**, the 1<sup>st</sup> quasi-reversible process suggests the possibility to serve as a redox responsive ligand. In the solid state structure of **5-BP**, the tricoordinate phosphorus adopts a pyramidal conformation, indicating very little contribution of its lone pair of electrons to the extended  $\pi$  system. The **5-BP** cycle is a relatively strongly basic ligand as is evident from the  $\nu(\text{CO})$  stretching frequency ( $1965\text{ cm}^{-1}$ ) of the corresponding Vaska-type rhodium complex. More interestingly, the binding of  $\text{F}^-$  to the boron shifts the  $\nu(\text{CO})$  to  $1937\text{ cm}^{-1}$ , which is similar to the respective complex with the highly electron-rich alkyl phosphine  $\text{PCy}_3$  complex at  $\nu(\text{CO})$  of  $1943\text{ cm}^{-1}$ .

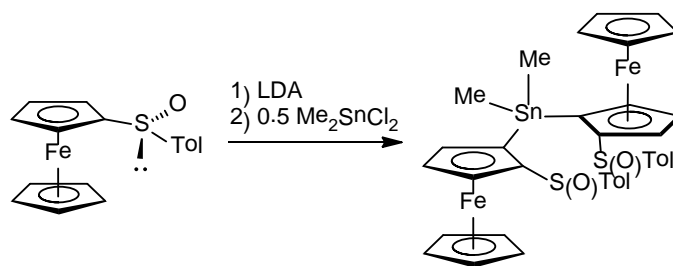
### 6.4 Experimental Section

**Reagents and General Methods.**  $\text{Me}_2\text{SnCl}_2$ ,  $\text{PhBCl}_2$ ,  $t\text{-BuPCl}_2$ ,  $\text{BH}_3$  (1.0 M in THF),  $t$ -butyl lithium (1.7 M in hexanes), 1,4-diazabicyclo[2.2.2]octane (DABCO), di- $\mu$ -chlorotetracarbonyldirrhodium ( $[\text{Rh}(\text{CO})_2\text{Cl}]_2$ ) and tetra- $n$ -butylammonium fluoride were purchased from Aldrich and used without further purification.  $\text{PhPCl}_2$  was purchased

from Aldrich and distilled prior to use.  $\text{Me}_2\text{SiCl}_2$  was purchased from Aldrich and distilled over  $\text{CaH}_2$  prior to use. Lithium diisopropylamide (LDA) was freshly prepared by addition of *n*-butyl lithium (1.6 M in hexanes) to a THF solution of diisopropylamine at 0 °C. (pS)-**1**,<sup>19</sup> and the Crossing salts<sup>20</sup> were prepared according to literature procedures. All reactions and manipulations were carried out under an atmosphere of prepurified nitrogen using either Schlenk techniques or an inert-atmosphere glove box (MBraun). 499.9 MHz  $^1\text{H}$  NMR, 125.7 MHz  $^{13}\text{C}$  NMR, 160.4 MHz  $^{11}\text{B}$  NMR, 470.4 MHz  $^{19}\text{F}$  NMR, 99.3 MHz  $^{29}\text{Si}$  NMR, 202.4 MHz  $^{31}\text{P}$  NMR and 186.4 MHz  $^{119}\text{Sn}$  NMR spectra were recorded on a Varian INOVA NMR spectrometer (Varian Inc., Palo Alto, CA) equipped with a boron-free 5 mm dual broadband gradient probe (Nalorac, Varian Inc., Martinez, CA).  $^1\text{H}$ ,  $^{13}\text{C}$ ,  $^{19}\text{F}$ ,  $^{29}\text{Si}$ ,  $^{31}\text{P}$  and  $^{119}\text{Sn}$  NMR spectra were referenced internally to solvent signals.  $^{11}\text{B}$  NMR spectra were acquired with boron-free quartz NMR tubes and referenced to  $\text{BF}_3 \cdot \text{Et}_2\text{O}$  ( $\delta = 0$ ). The following abbreviations are used for signal assignments: Ph = phenyl, Fc = ferrocenyl, Cp = cyclopentadienyl. High resolution MALDI-MS data (benzo[ $\alpha$ ]pyrene as matrix) were obtained in positive mode on an Apex Ultra 7.0 Hybrid FTMS (Bruker Daltonics). UV/Vis absorption data were acquired on a Varian Cary 500 UV/Vis/NIR spectrophotometer. Optical rotation analyses were performed on an Autopol III polarimeter, Rudolph Research Analytical, using a tungsten-halogen light source operating at  $\lambda = 589$  nm. Chiral HPLC analyses were performed on a Waters Empower system equipped with a 717plus autosampler, a 1525 binary HPLC pump, and a 2998 photodiode array detector; a CHIRALPAK® IA-3 column was used for separation. Elemental analyses were performed by Quantitative Technologies Inc., Whitehouse, NJ. IR Measurements were carried out on a Thermo

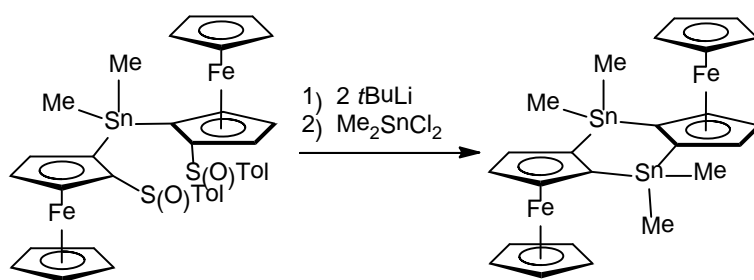
Nicolet 6700 spectrometer (Thermo Electron Corporation, Madison, WI, USA) of a  $\text{CH}_2\text{Cl}_2$  solution by either transmission or ATR mode.

X-ray diffraction intensities were collected on a Bruker SMART APEX CCD Diffractometer using  $\text{CuK}\alpha$  (1.54178 Å) radiation at 100 K. The structures were refined by full-matrix least squares based on  $F^2$  with all reflections (SHELXTL V5.10; G. Sheldrick, Siemens XRD, Madison, WI). Non-hydrogen atoms were refined with anisotropic displacement coefficients, and hydrogen atoms were treated as idealized contribution. SADABS (Sheldrick, 12 G.M. SADABS (2.01), Bruker/Siemens Area Detector Absorption Correction Program; Bruker AXS: Madison, WI, 1998) absorption correction was applied. Crystallographic data for the structures of **1-Sn**, **2-SnSn**, **2-SnSi**, **2-BSi**, **3a-SnP**, **3b-SnP**, **4-BP** and **5-BP** will be deposited with the Cambridge Crystallographic Data Center as supplementary publications. Copies of the data can be obtained free of charge on application to CCDC, 12 Union Road, Cambridge CB2 1EZ, UK (fax: (+44) 1223-336-033; email: [deposit@ccdc.cam.ac.uk](mailto:deposit@ccdc.cam.ac.uk)).



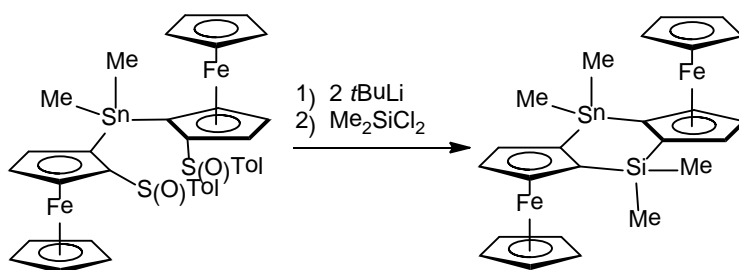
**Synthesis of  $\text{Fc}(\text{SOTol})(\mu\text{-SnMe}_2)\text{Fc}(\text{SOTol})$ .** To a pre-cooled ( $-78\text{ }^\circ\text{C}$ ) solution of  $\text{FcSOTol}$  (4.00 g, 12.3 mmol) in THF (60 mL) was added a pre-made LDA solution (0.50 M, 27.2 mL, 13.6 mmol, 1.10 equiv) dropwise and the mixture was kept stirring for 1 hour.  $\text{Me}_2\text{SnCl}_2$  (1.63 g, 7.38 mmol, 0.60 equiv) in THF (10 mL) was added slowly. The reaction mixture was kept stirring at the same temperature for 1 hour and then allowed to

warm up overnight before quenching with water. The mixture was extracted with  $\text{CH}_2\text{Cl}_2$  ( $3 \times 50$  mL). The combined organic layers were washed with brine and water, dried over sodium sulfate and concentrated. The residue was chromatographed on a silica column with THF/hexanes/triethyl amine (25: 75: 1) as the eluent. X-ray quality crystals were obtained by recrystallization in hot THF. Yield: 3.9 g (80 %).  $[\alpha]_D^{20}$  ( $c = 0.10$ ,  $\text{CH}_2\text{Cl}_2$ ) =  $-34^\circ$ ;  $^1\text{H}$  NMR (499.9 MHz,  $\text{CDCl}_3$ ,  $25^\circ\text{C}$ ):  $\delta = 7.44$  (d,  $J = 8.0$  Hz, 4H; tolyl), 7.10 (d,  $J = 8.0$  Hz, 4H; tolyl), 4.48 (nr, 2H; Cp), 4.39 (nr, 2H; Cp), 4.37 (nr, 2H; Cp), 4.29 (s, 10H; free Cp), 2.33 (s, 6H; Me), 0.80 (s/d,  $J(^{117/119}\text{Sn},\text{H}) = 60$  Hz, 6H;  $\text{SnMe}_2$ ).  $^{13}\text{C}$  NMR (125.69 MHz,  $\text{CDCl}_3$ ,  $25^\circ\text{C}$ ):  $\delta = 142.5$ , 140.8, 129.3, 125.2 (tolyl), 97.6 (s/d,  $^2J(^{117/119}\text{Sn},\text{C}) = 39$  Hz; ipso-Cp-S), 77.6 (s/d,  $^2J(^{117/119}\text{Sn},\text{C}) = 41$  Hz, Cp), 73.2 (s/d,  $^3/4J(^{117/119}\text{Sn},\text{C}) = 38$  Hz, Cp), 70.6 (ipso-Cp-Sn), 69.9 (free Cp), 69.0 (s/d,  $^3/4J(^{117/119}\text{Sn},\text{C}) = 27$  Hz; Cp), 21.4 (Me),  $-3.8$  (s/d,  $^1J(^{117/119}\text{Sn},\text{C}) = 422/442$  Hz;  $\text{SnMe}_2$ ).  $^{119}\text{Sn}$  NMR (186.4 MHz,  $\text{C}_6\text{D}_6$ ,  $25^\circ\text{C}$ )  $\delta = -25.5$ . Elemental analysis for  $\text{C}_{36}\text{H}_{36}\text{Fe}_2\text{O}_2\text{S}_2\text{Sn}$ , calcd C 54.38, H4.56, found C 54.56, H 4.21



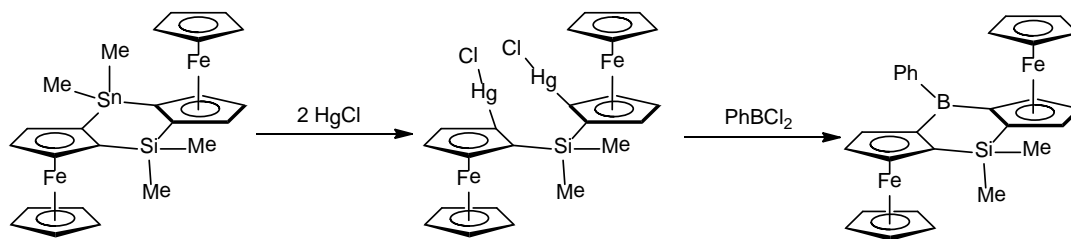
**Synthesis of  $\text{Fc}_2\text{Sn}_2\text{Me}_4$ .** A solution of  $\text{Fc}(\text{SOTol})(\mu\text{-SnMe}_2)\text{Fc}(\text{SOTol})$  (100 mg, 0.126 mmol) in THF (10 mL) was cooled to  $-78^\circ\text{C}$  and a solution of *t*-butyl lithium in hexanes (0.155 mL, 0.264 mmol, 2.10 equiv) was added dropwise under stirring. The reaction mixture was kept stirring for 10 min at the same temperature and a solution of

Me<sub>2</sub>SnCl<sub>2</sub> (0.029 g, 0.132 mmol, 1.05 equiv) in THF (1.5 mL) was added via syringe. The resulting solution was stirred for 1 h and the temperature was slowly raised to 25 °C. After addition of water the mixture was extracted with diethyl ether (3 × 5 mL). The combined organic layers were washed with brine solution followed by water, dried over sodium sulfate and concentrated. The residue was subjected to silica gel column chromatography with hexanes/triethylamine (100:1) as the eluent to give the product as a red solid. Yield: 54 mg (65%). <sup>1</sup>H NMR (499.9 MHz, C<sub>6</sub>D<sub>6</sub>, 25 °C): δ = 4.51 (t, 2H, *J* = 2.5 Hz; Cp), 4.30 (d, 4H, *J* = 2.5 Hz; Cp), 3.99 (s, 10H; free Cp), 0.48 (s/d, *J*(<sup>117/119</sup>Sn,H) = 54/56 Hz, 12H; SnMe<sub>2</sub>). <sup>13</sup>C NMR (125.69 MHz, C<sub>6</sub>D<sub>6</sub>, 25 °C): δ = 77.1 (s/d, <sup>1</sup>*J*(<sup>117/119</sup>Sn,C) = 513/535 Hz; ipso-Cp-Sn), 77.1 (s/d, <sup>2/3</sup>*J*(<sup>117/119</sup>Sn,C) = 46/63 Hz; Cp), 73.2 (s/d, <sup>3</sup>*J*(<sup>117/119</sup>Sn,C) = 40 Hz; Cp), 69.1 (free Cp), -6.5 (s/d, <sup>1</sup>*J*(<sup>117/119</sup>Sn,C) = 350/366 Hz; SnMe<sub>2</sub>). <sup>119</sup>Sn NMR (186.4 MHz, C<sub>6</sub>D<sub>6</sub>, 25 °C) δ = -22.1 (s/d, <sup>3</sup>*J*(<sup>117</sup>Sn, <sup>119</sup>Sn) = 122 Hz). UV-Vis (CH<sub>2</sub>Cl<sub>2</sub>): λ<sub>max</sub> = 460 (ε = 310 M<sup>-1</sup> cm<sup>-1</sup>). High-resolution MALDI-MS (+ mode, benzo[α]pyrene): *m/z* 650.8678 ([M-Me]<sup>+</sup>, 40%, calcd for <sup>12</sup>C<sub>23</sub><sup>1</sup>H<sub>25</sub><sup>56</sup>Fe<sub>2</sub><sup>119</sup>Sn<sub>2</sub> 650.8702), 665.8913 ([M]<sup>+</sup>, 100%, calcd for <sup>12</sup>C<sub>24</sub><sup>1</sup>H<sub>28</sub><sup>56</sup>Fe<sub>2</sub><sup>119</sup>Sn<sub>2</sub> 665.8937).



**Synthesis of Fc<sub>2</sub>SnMe<sub>2</sub>SiMe<sub>2</sub>.** A solution of Fc(SOTol)(μ-SnMe<sub>2</sub>)Fc(SOTol) (400 mg, 0.504 mmol) in THF (40 mL) was cooled to -78 °C and a solution of *t*-butyl lithium in hexanes (0.62 mL, 1.06 mmol, 2.10 equiv) was added dropwise under stirring. The

reaction mixture was kept stirring for 10 min at the same temperature and a solution of  $\text{Me}_2\text{SiCl}_2$  (0.091 g, 0.706 mmol, 1.4 equiv) in THF (1.5 mL) was added via syringe. The resulting solution was stirred for 1 h and the temperature was slowly raised to 25 °C. After addition of water the mixture was extracted with diethyl ether (3 × 20 mL). The combined organic layers were washed with brine solution followed by water, dried over sodium sulfate and concentrated. The residue was subjected to silica gel column chromatography with hexanes/triethylamine (100:1) as the eluent to give the product as a red solid. Recrystallization in hot methanol at -37 °C gave X-ray quality crystals. Yield: 179 mg (62%).  $[\alpha]_D^{20}$  (c = 0.10,  $\text{CH}_2\text{Cl}_2$ ) = -88° ;  $^1\text{H}$  NMR (499.9 MHz,  $\text{CDCl}_3$ , 25 °C):  $\delta$  = 4.55 (nr, 2H; Cp), 4.42 (nr, 2H; Cp), 4.36 (nr, 2H; Cp), 3.96 (s, 10H; free Cp), 0.52 (s/d,  $^2J(^{117/119}\text{Sn},\text{C})$  = 56 Hz, 6H;  $\text{SnMe}_2$ ), 0.48 (s, 6H;  $\text{SiMe}_2$ ).  $^{13}\text{C}$  NMR (125.69 MHz,  $\text{C}_6\text{D}_6$ , 25 °C):  $\delta$  = 78.5 (ipso-Cp), 77.4 (s/d,  $J(^{117/119}\text{Sn},\text{C})$  = 59 Hz; Cp), 76.5 (ipso-Cp), 76.1 (s/d,  $J(^{117/119}\text{Sn},\text{C})$  = 43 Hz; Cp), 73.2 (s/d,  $J(^{117/119}\text{Sn},\text{C})$  = 41 Hz; Cp), 69.2 (free Cp), 2.3 ( $\text{SiMe}_2$ ), -6.7 (s/d,  $^1J(^{117/119}\text{Sn},\text{C})$  = 349, 370 Hz;  $\text{SnMe}_2$ ).  $^{29}\text{Si}$  NMR (99.3 MHz,  $\text{C}_6\text{D}_6$ , 25 °C)  $\delta$  = -6.4.  $^{119}\text{Sn}$  NMR (186.4 MHz,  $\text{C}_6\text{D}_6$ , 25 °C)  $\delta$  = -24.3. UV-Vis ( $\text{CH}_2\text{Cl}_2$ ) :  $\lambda_{\text{max}}$  = 461 ( $\epsilon$  = 280  $\text{M}^{-1} \text{cm}^{-1}$ ). High-resolution MALDI-MS (+ mode, benzo[ $\alpha$ ]pyrene): m/z 575.9671 ( $[\text{M}]^+$ , 100%, calcd for  $^{12}\text{C}_{24}^1\text{H}_{28}^{29}\text{Si}^{56}\text{Fe}_2^{119}\text{Sn}$  575.9680).



**Synthesis of  $\text{Fc}_2\text{SiMe}_2\text{Hg}_2\text{Cl}_2$ .** A solution of  $\text{Fc}_2\text{SiMe}_2\text{SnMe}_2$  (0.129 g, 0.224 mmol) in acetone (10 mL) was added into a solution of  $\text{HgCl}_2$  (0.112 g, 0.448 mmol, 2.0 equiv) in acetone (10 mL). The mixture was stirred for 1 hour before adding it to water (50 mL). Upon addition, a yellow precipitate was formed, which was collected on a filter paper, washed with hexanes (10 mL) and dried under air flow. Yield: 185 mg (71%).  $^1\text{H}$  NMR (499.9 MHz,  $\text{CDCl}_3$ , 25 °C):  $\delta$  = 4.75 (nr, 2H; Cp), 4.54 (nr, 2H; Cp), 4.37 (nr, 2H; Cp), 4.23 (s, 10H; free Cp), 0.64 (s, 6H;  $\text{SiMe}_2$ ).  $^{13}\text{C}$  NMR (125.69 MHz,  $\text{C}_6\text{D}_6$ , 25 °C):  $\delta$  = 90.1 (ipso-Cp-Hg), 77.3 (Cp), 75.6 (ipso-Cp-Si), 75.5 (Cp), 73.6 (Cp), 68.8 (free Cp), 0.1 ( $\text{SiMe}_2$ ).  $^{29}\text{Si}$  HNMR (99.3 MHz,  $\text{C}_6\text{D}_6$ , 25 °C)  $\delta$  = -6.8.

**Synthesis of  $\text{Fc}_2\text{SiMe}_2\text{BPh}$ .** To a solution of  $\text{Fc}_2\text{SiMe}_2\text{Hg}_2\text{Cl}_2$  (0.225g, 0.250 mmol) in toluene (20 mL) was added a solution of  $\text{PhBCl}_2$  (0.047g, 0.300 mmol, 1.2 equiv) in toluene (2 mL) at -37 °C inside a glove box. The mixture was then heated to 90 °C overnight in a sealed flask. A grey solid formed, which was removed by filtration. The filtrate was concentrated, taken back up in hot hexanes and kept at -37 °C for recrystallization. Yield: 60 mg (47%).  $[\alpha]_D^{20}$  (c = 0.10,  $\text{CH}_2\text{Cl}_2$ ) = -2122° ;  $^1\text{H}$  NMR (499.9 MHz,  $\text{CDCl}_3$ , 25 °C):  $\delta$  = 7.90 (m, 2H; o-Ph), 7.48 (m, 3H; m-Ph, p-Ph), 4.85 (pst, J = 2.0 Hz, 2H; Cp), 4.74 (nr, 2H; Cp), 4.61 (nr, 2H; Cp), 3.97 (s, 10H; free Cp), 0.46 (s, 6H;  $\text{SiMe}_2$ ).  $^{13}\text{C}$  NMR (125.69 MHz,  $\text{CDCl}_3$ , 25 °C):  $\delta$  = 132.6 (Ph), 128.2 (Ph), 127.3 (Ph), ipso-Ph-B not observed, 80.3 (ipso-Cp-B), 78.8 (Cp), 78.7 (Cp), 77.5 (ipso-Cp-Si), 77.1 (Cp), 69.5 (free Cp), 2.2 ( $\text{SiMe}_2$ ).  $^{11}\text{B}$  NMR (160.4 MHz,  $\text{CDCl}_3$ , 25 °C)  $\delta$  = 53.9 ( $w_{1/2}$  = 750 Hz).  $^{29}\text{Si}$  NMR (99.3 MHz,  $\text{CDCl}_3$ , 25 °C)  $\delta$  = -9.4. UV-Vis ( $\text{CH}_2\text{Cl}_2$ ):  $\lambda_{\text{max}}$  = 367 ( $\epsilon$  = 5460  $\text{M}^{-1} \text{cm}^{-1}$ ), 471 ( $\epsilon$  = 7060  $\text{M}^{-1} \text{cm}^{-1}$ ). High-resolution MALDI-MS (+

mode, benzo[ $\alpha$ ]pyrene):  $m/z$  514.0683 ( $[M]^+$ , 100%, calcd for  $^{12}\text{C}_{28}^{1}\text{H}_{27}^{11}\text{BSi}^{56}\text{Fe}_2$  514.0669).

**Synthesis of  $\text{Fc}_2\text{SnMe}_2\text{P}(\text{BH}_3)t\text{Bu}$ .** A solution of  $\text{Fc}(\text{SOTol})(\mu\text{-SnMe}_2)\text{Fc}(\text{SOTol})$  (0.500 g, 0.628 mmol) in THF (40 mL) was cooled to  $-78\text{ }^\circ\text{C}$  and a solution of *t*-butyl lithium in hexanes (0.760 mL, 1.29 mmol, 2.05 equiv) was added dropwise under stirring. The reaction mixture was kept stirring for 10 min at the same temperature and a solution of *t*BuPCl<sub>2</sub> (0.105 g, 0.66 mmol, 1.05 equiv) in THF (5 mL) was added via syringe. After subsequent addition of a  $\text{BH}_3\cdot\text{THF}$  solution (1.0 M, 0.75 mL, 1.2 equiv), the resulting solution was stirred for 1 h and the temperature was slowly raised to  $25\text{ }^\circ\text{C}$ . An aqueous  $\text{NaHCO}_3$  solution was added and the mixture was extracted with diethyl ether (3  $\times$  20 mL). The combined organic layers were washed with brine solution followed by water, dried over sodium sulfate and concentrated. The residue was subjected to silica gel column chromatography with hexanes/triethylamine (100:1) as the eluent to give the product as a red solid. Recrystallization in hexanes at  $-37\text{ }^\circ\text{C}$  gave X-ray quality crystals. Yield: 40 mg (10%).  $^1\text{H}$  NMR (499.9 MHz,  $\text{CDCl}_3$ ,  $25\text{ }^\circ\text{C}$ ):  $\delta$  = 5.11 (nr, 1H; Cp), 4.83 (nr, 1H; Cp), 4.79 (d,  $J$  = 2.0 Hz, 1H; Cp), 4.58 (d,  $J$  = 2.0 Hz, 1H; Cp), 4.54 (nr, 1H; Cp), 4.34 (nr, 1H; Cp), 4.26 (s, 5H; free Cp), 3.83 (s, 5H; free Cp), 1.35 (d,  $J$  = 2.5 Hz, 9H, *t*-Bu), 1.0 (very br, 3H;  $\text{BH}_3$ ), 0.60 (s/d,  $^2J(^{117}/^{119}\text{Sn},\text{H})$  = 58 Hz, 3H; SnMe), 0.60 (s/d,  $^2J(^{117}/^{119}\text{Sn},\text{H})$  = 56 Hz, 3H; SnMe).  $^{13}\text{C}$  NMR (125.69 MHz,  $\text{CDCl}_3$ ,  $25\text{ }^\circ\text{C}$ ):  $\delta$  = 79.2 (d,  $J$  = 20 Hz; Cp), 77.8 (d,  $J$  = 18 Hz; Cp), 76.6 (d,  $J$  = 5 Hz; ipso-Cp-Sn), 76.4 (overlapped d; ipso-Cp-P), 76.3 (d,  $J$  = 7 Hz; Cp), 73.9 (d, 63 Hz; ipso-Cp-P), 73.5 (d,  $J$  = 9 Hz; Cp), 72.3 (d,  $J$  = 9 Hz; Cp) 71.8 (d,  $J$  = 4 Hz; ipso-Cp-Sn), 70.2 (free Cp), 70.0

(free Cp), 30.8 (d,  $^1J = 34$  Hz; *t*Bu), 26.4 (d,  $^2J = 3$  Hz; Cp), -3.5 (s/d,  $^1J(^{117/119}\text{Sn},\text{C}) = 377,390$  Hz; SnMe), -6.8 (SnMe s/d,  $^1J(^{117/119}\text{Sn},\text{C}) = 377,395$  Hz); one Cp resonance not observed due to solvent signal overlap.  $^{11}\text{B}$  NMR (160.4 MHz,  $\text{CDCl}_3$ , 25 °C)  $\delta = -39.0$  (m,  $w_{1/2} = 400$  Hz).  $^{31}\text{P}\{^1\text{H}\}$  NMR (202.4 MHz,  $\text{CDCl}_3$ , 25 °C)  $\delta = 28.9$ .  $^{119}\text{Sn}\{^1\text{H}\}$  NMR (186.4 MHz,  $\text{CDCl}_3$ , 25 °C)  $\delta = -28.0$  (d,  $^3J(^{31}\text{P},^{119}\text{Sn}) = 5$  Hz). High-resolution MALDI-MS (+ mode, benzo[ $\alpha$ ]pyrene):  $m/z$  548.9182 ( $[\text{M}-\text{BH}_3-t\text{Bu}]^+$ , 100%, calcd for  $^{12}\text{C}_{22}^1\text{H}_{22}^{31}\text{P}^{56}\text{Fe}_2^{120}\text{Sn}$  548.9179);  $m/z$  605.9888 ( $[\text{M}-\text{BH}_3]^+$ , 1%, calcd for  $^{12}\text{C}_{26}^1\text{H}_{31}^{31}\text{P}^{56}\text{Fe}_2^{120}\text{Sn}$  605.9884).

**Synthesis of  $\text{Fc}_2\text{SnMe}_2\text{P}(\text{BH}_3)\text{Ph}$ .** A solution of  $\text{Fc}(\text{SOTol})(\mu\text{-SnMe}_2)\text{Fc}(\text{SOTol})$  (1.60 g, 2.01 mmol) in THF (150 mL) was cooled to -78 °C and a solution of *t*-butyl lithium in hexanes (2.49 mL, 4.23 mmol, 2.10 equiv) was added dropwise under stirring. The reaction mixture was kept stirring for 10 min at the same temperature and a solution of  $\text{PhPCl}_2$  (0.396 g, 2.21 mmol, 1.1 equiv) in THF (5 mL) was added via syringe. After subsequent addition of a  $\text{BH}_3\cdot\text{THF}$  solution (1.0 M, 3.02 mL, 1.50 equiv), the resulting solution was stirred for 1 h and the temperature was slowly raised to 25 °C. All volatile components were removed under high vacuum. The residue was redissolved in  $\text{CH}_2\text{Cl}_2$ , an aqueous  $\text{NaHCO}_3$  solution added and the aqueous phase was extracted with diethyl ether ( $3 \times 50$  mL). The combined organic layers were washed with brine solution followed by water, dried over sodium sulfate and concentrated. The residue was subjected to aluminum oxide column chromatography with THF/hexanes/triethylamine (20:80:1) as the eluent to give the product as a red solid. Recrystallization in hexanes at -37 °C gave X-ray quality crystals. Yield: 510 mg (40%).  $[\alpha]_D^{20}$  ( $c = 0.10$ ,  $\text{CH}_2\text{Cl}_2$ ) =

+206° ; <sup>1</sup>H NMR (499.9 MHz, CDCl<sub>3</sub>, 25 °C): δ = 7.82 (m, 2H; *m*-Ph), 7.41 (br, 3H; *o*-Ph, *p*-Ph), 5.20 (nr, 1H; Cp), 4.88 (nr, 1H; Cp), 4.66 (nr, 1H; Cp), 4.63 (d, *J* = 2.0 Hz, 1H; Cp), 4.52 (nr, 1H; Cp), 4.40 (nr, 1H; Cp), 3.92 (s, 5H; free Cp), 3.67 (s, 5H; free Cp), 1.2 (br, 3H, BH<sub>3</sub>), 0.64 (s/d, <sup>2</sup>*J*(<sup>117/119</sup>Sn,H) = 58 Hz, 3H; SnMe), 0.60 (s/d, <sup>2</sup>*J*(<sup>117/119</sup>Sn,H) = 58 Hz, 3H; SnMe). <sup>13</sup>C NMR (125.69 MHz, CDCl<sub>3</sub>, 25 °C): δ = 136.4 (d, <sup>1</sup>*J* = 56 Hz; ipso-Ph-P), 132.0 (d, *J* = 11 Hz; *o*-Ph), 130.4 (br; *p*-Ph), 127.9 (d, *J* = 9 Hz; *m*-Ph), 79.9 (d, <sup>1</sup>*J* = 67 Hz; ipso-Cp-P), 77.8 (d, *J* = 7 Hz; Cp), 76.4 (d, *J* = 8 Hz; Cp), 76.0 (d, *J* = 8 Hz; Cp), 73.8 (d, *J* = 10 Hz; Cp), 73.7 (d, <sup>1</sup>*J* = 75 Hz; ipso-Cp-P), 73.7 (d, *J* = 5 Hz; ipso-Cp-Sn), 72.4 (d, *J* = 5 Hz; ipso-Cp-Sn), 71.7 (d, *J* = 11 Hz; Cp), 70.3 (free Cp), 69.2 (free Cp), -4.6 (s/d, <sup>1</sup>*J*(<sup>117/119</sup>Sn,C) = 370, 386 Hz; SnMe), -8.2 (s/d, <sup>1</sup>*J*(<sup>117/119</sup>Sn,C) = 377, 393 Hz; SnMe). <sup>11</sup>B NMR (160.4 MHz, CDCl<sub>3</sub>, 25 °C) δ = -38.6 (*w*<sub>1/2</sub> = 350 Hz). <sup>31</sup>P{<sup>1</sup>H} NMR (202.4 MHz, CDCl<sub>3</sub>, 25 °C) δ = 10.3 (m). <sup>119</sup>Sn{<sup>1</sup>H} NMR (186.4 MHz, CDCl<sub>3</sub>, 25 °C) δ = -26.9 (d, <sup>3</sup>*J*(<sup>31</sup>P, <sup>119</sup>Sn) = 10 Hz). High-resolution MALDI-MS (+ mode, benzo[*a*]pyrene): *m/z* 625.9557 ([M-BH<sub>3</sub>]<sup>+</sup>, 1%, calcd for <sup>12</sup>C<sub>28</sub><sup>1</sup>H<sub>27</sub><sup>31</sup>P<sup>56</sup>Fe<sub>2</sub><sup>120</sup>Sn 625.9572).

**Synthesis of Fc<sub>2</sub>SnMe<sub>2</sub>ClHgClP(BH<sub>3</sub>)Ph.** A solution of **Fc<sub>2</sub>SnMe<sub>2</sub>P(BH<sub>3</sub>)Ph** (0.120 g, 0.188 mmol) in acetone (3 mL) was added into a solution of HgCl<sub>2</sub> (0.051 g, 0.188 mmol, 1.0 equiv) in acetone (2 mL). The mixture was stirred for 1 hour before adding it to water (50 mL). Upon addition, a yellow precipitate formed, which was collected on a filter paper, washed with hexanes (10 mL), dried under high vacuum at 60 °C overnight and used in the next step without further purification. **Fc<sub>2</sub>SnMe<sub>2</sub>ClHgClP(BH<sub>3</sub>)Ph:** Yield: 145 mg (85%). Purity: ca. 90% by <sup>1</sup>H NMR. <sup>1</sup>H NMR (499.9 MHz, CDCl<sub>3</sub>, 25

°C):  $\delta = 7.84$  (pst,  $J = 9$  Hz, 2H; *m*-Ph), 7.51 (m, 3H; *o*-Ph + *p*-Ph), 5.13 (nr, 1H; Cp), 4.85 (nr, 1H; Cp), 4.80 (nr, 1H; Cp), 4.79 (nr, 1H; Cp), 4.70 (nr, 1H; Cp), 4.32 (nr, 1H; Cp), 4.10 (s, 5H; free Cp), 3.84 (s, 5H; free Cp), 1.6 (br, 3H; BH<sub>3</sub>), 1.31 (s/d,  $^2J(^{117/119}\text{Sn,H}) = 67$  Hz, 3H; SnMe), 1.05 (s/d,  $^2J(^{117/119}\text{Sn,H}) = 62$  Hz, 3H; SnMe).  $^{11}\text{B}$  NMR (160.4 MHz, CDCl<sub>3</sub>, 25 °C)  $\delta = -37.4$  (m,  $w_{1/2} = 320$  Hz).  $^{31}\text{P}\{^1\text{H}\}$  NMR (202.4 MHz, CDCl<sub>3</sub>, 25 °C)  $\delta = 8.7$  (m).  $^{119}\text{Sn}\{^1\text{H}\}$  NMR (186.4 MHz, CDCl<sub>3</sub>, 25 °C)  $\delta = 65.6$  (d,  $J = 30$  Hz).

**Synthesis of Fc<sub>2</sub>BPhP(BH<sub>3</sub>)Ph.** To a solution of **Fc<sub>2</sub>SnMe<sub>2</sub>ClHgClP(BH<sub>3</sub>)Ph** (0.145 g, 0.159 mmol) in toluene (10 mL) was added a solution of PhBCl<sub>2</sub> (0.028 mg, 0.175 mmol, 1.2 equiv) in toluene (2 mL) at -37 °C inside a glove box. The mixture was stirred at room temperature for 2 days before heated to 90 °C overnight in a sealed flask. A grey solid formed, which was removed by filtration. The filtrate was concentrated and then subjected to silica gel column chromatography using THF/hexanes/triethylamine (20:80:1) as eluent. The product was obtained as an analytically pure red solid by recrystallization in hot hexanes. **Fc<sub>2</sub>BPhP(BH<sub>3</sub>)Ph**: Yield: 45 mg (49%).  $[\alpha]_{\text{D}}^{20}$  (c = 0.10, CH<sub>2</sub>Cl<sub>2</sub>) = -1484°.  $^1\text{H}$  NMR (499.9 MHz, CDCl<sub>3</sub>, 25 °C):  $\delta = 8.00$  (br, 2H; Ph), 7.62 (br, 2H; Ph), 7.52 (br, 3H; Ph), 7.44 (br, 3H; Ph), 5.21 (nr, 1H; Cp), 5.09 (nr, 1H; Cp), 5.0 (nr, 1H; Cp), 4.90 (nr, 1H; Cp), 4.80 (nr, 2H; Cp), 4.22 (s, 5H; free Cp), 3.38 (s, 5H; free Cp), 1.2 (br, 3H; BH<sub>3</sub>).  $^{13}\text{C}$  NMR (125.69 MHz, CDCl<sub>3</sub>, 25 °C):  $\delta = 142.2$  (ipso-Ph-B), 137.1 (d,  $^1J = 54$  Hz; ipso-Ph-P), 132.7 (BPh), 131.2 (d,  $J = 10$  Hz; PPh), 130.4 (br; PPh), 129.1 (BPh), 128.1 (d,  $J = 10$  Hz; PPh), 127.9 (BPh), 79.7 (d,  $^2J = 16$  Hz; Cp), 79.1 (d,  $^3J = 5$  Hz; Cp) 78.3 (d,  $^1J = 62$  Hz; ipso-Cp-P), 78.2 (d,  $^3J = 10$  Hz; Cp), 76.5 (d,  $^3J = 8$  Hz; Cp), 76.2 (d,  $^2J = 18$  Hz; Cp), 73.3 (d,  $J = 74$  Hz; ipso-Cp-P), 71.8 (free Cp), 70.2 (free

Cp), ipso-Cp-B and one of the Cp resonance not observed due to solvent signal overlap.  $^{11}\text{B}$  NMR (160.4 MHz,  $\text{CDCl}_3$ , 25 °C)  $\delta = 52.1$  ( $w_{1/2} = 800$  Hz),  $-35.2$  ( $w_{1/2} = 400$  Hz).  $^{31}\text{P}\{^1\text{H}\}$  NMR (202.4 MHz,  $\text{CDCl}_3$ , 25 °C)  $\delta = 11.2$ . High-resolution MALDI-MS (+ mode, benzo[ $\alpha$ ]pyrene):  $m/z$  564.0575 ( $[\text{M-BH}_3]^+$ , 100%, calcd for  $^{12}\text{C}_{32}^{1}\text{H}_{26}^{11}\text{B}^{31}\text{P}^{56}\text{Fe}_2$  564.0565).

**Synthesis of  $\text{Fc}_2\text{BPhPPH}$**  To a  $\text{CDCl}_3$  (0.7 mL) solution of  $\text{Fc}_2\text{BPhP}(\text{BH}_3)\text{Ph}$  (35.0 mg, 0.061 mmol) was added an equimolar amount of DABCO (7.47 mg, 0.067 mmol) at room temperature. The solution was transferred into a J. Young's NMR tube and heated to 50 °C.  $^1\text{H}$  NMR data confirmed the full conversion to product after 2 days. The reaction mixture was subjected to a short aluminium oxide column with THF/hexanes (1:4) as eluent. Yield: 30 mg (88%).  $^1\text{H}$  NMR (499.9 MHz,  $\text{CDCl}_3$ , 25 °C):  $\delta = 7.95$  (m, 2H; Ph), 7.51 (m, 3H; Ph), 7.44 (t,  $J = 7$  Hz, 2H; Ph), 7.38 (t,  $J = 7$  Hz, 2H; Ph), 7.34 (t,  $J = 7$  Hz, 1H; Ph), 5.07 (nr, 1H; Cp), 4.92 (nr, 1H; Cp), 4.74 (nr, 1H; Cp), 4.71 (nr, 1H; Cp), 4.70 (nr, 2H; Cp), 4.62 (nr, 1H; Cp), 4.02 (s, 5H; free Cp), 3.42 (s, 5H; free Cp).  $^{13}\text{C}$  NMR (125.69 MHz,  $\text{CDCl}_3$ , 25 °C):  $\delta = 144.2$  (d,  $J = 23$  Hz; ipso-Ph-P), 143.1 (ipso-Ph-B), 132.8 (Ph), 131.1 (d,  $J = 18$  Hz; Ph), 128.7 (Ph), 127.9 (br, 2 signals overlapping; Ph), 127.6 (Ph), 88.0 (ipso-Cp-B), 80.1 (d,  $J = 26$  Hz; Cp), 79.0 (Cp), 75.5 (Cp), 75.4 (d,  $J = 23$  Hz; Cp), 70.9 (free Cp), 70.0 (free Cp).  $^{11}\text{B}$  NMR (160.4 MHz,  $\text{CDCl}_3$ , 25 °C)  $\delta = 53.0$  ( $w_{1/2} = 1000$  Hz).  $^{31}\text{P}\{^1\text{H}\}$  NMR (202.4 MHz,  $\text{CDCl}_3$ , 25 °C)  $\delta = -24.9$ . High-resolution MALDI-MS (+ mode, benzo[ $\alpha$ ]pyrene):  $m/z$  564.0575 ( $[\text{M}]^+$ , 100%, calcd for  $^{12}\text{C}_{32}^{1}\text{H}_{26}^{11}\text{B}^{31}\text{P}^{56}\text{Fe}_2$  564.0565).

**Synthesis of  $(\text{Fc}_2\text{BPhPPH})_2\text{Rh}(\text{CO})\text{Cl}$ .** To a solution of  $\text{Fc}_2\text{BPhPPH}$  (10 mg, 0.018 mmol) in  $\text{CD}_2\text{Cl}_2$  (0.7 mL) was added di- $\mu$ -chloro-tetracarbonyldirrhodium (1.72 mg,

0.0044 mmol, 0.25 equiv).  $^1\text{H}$  NMR measurement indicated full conversion. All volatile components were removed under high vacuum. Analytically pure compound was obtained by slow diffusion of hexanes vapor into an acetone solution of the crude product. Yield: 11 mg (92%).  $^1\text{H}$  NMR (499.9 MHz,  $\text{CDCl}_3$ , 25 °C):  $\delta$  = 8.00 (d,  $J$  = 7 Hz, 4H; Ph), 7.69 (nr, 4H; Ph), 7.54 (m, 6H; Ph), 7.41 (m, 6H; Ph), 5.94 (nr, 4H; Cp), 5.05 (nr, 4H; Cp), 5.04 (nr, 4H; Cp), 4.82 (nr, 4H; Cp), 4.81 (nr, 4H; Cp), 4.72 (s, 4H; free Cp), 4.43 (s, 10H; free Cp), 3.37 (s, 10H; free Cp).  $^{13}\text{C}$  NMR (125.69 MHz,  $\text{CD}_2\text{Cl}_2$ , 25 °C):  $\delta$  = 144.5 (br, ipso-Ph-B), 142.3 (t,  $J$  = 21 Hz; ipso-Ph-P), 134.7 (BPh), 133.7 (t,  $J$  = 6 Hz; PPh), 131.0 (BPh), 130.7 (PPh), 129.6 (BPh), 129.5 (t,  $J$  = 5 Hz; PPh), 86.8 (t,  $J$  = 26 Hz; ipso-Cp-P), 84.7 (t,  $J$  = 8 Hz; Cp), 80.4 (Cp), 80.2 (t,  $J$  = 5 Hz; Cp), 80.0 (t,  $J$  = 10 Hz; Cp), 78.5 (br; ipso-Cp-B), 78.1 (t,  $J$  = 5 Hz; Cp), 78.0 (t,  $J$  = 3 Hz; Cp), 77.5 (t,  $J$  = 28 Hz; ipso-Cp-P), 73.9 (free Cp), 72.3 (free Cp), one of the ipso-Cp-B is not observed.  $^{11}\text{B}$  NMR (160.4 MHz,  $\text{CD}_2\text{Cl}_2$ , 25 °C)  $\delta$  = 52.2 ( $w_{1/2}$  = 2800 Hz).  $^{31}\text{P}\{\text{H}\}$  NMR (202.4 MHz,  $\text{CD}_2\text{Cl}_2$ , 25 °C)  $\delta$  = 7.61 (d,  $^2J(^{103}\text{Rh},\text{P})$  = 121 Hz). High-resolution MALDI-MS (+ mode, benzo[ $\alpha$ ]pyrene):  $m/z$  1231.0218 ( $[\text{M-CO-Cl}]^+$ , 20%, calcd for  $^{12}\text{C}_{64}^1\text{H}_{52}^{11}\text{B}_2^{31}\text{P}_2^{56}\text{Fe}_4^{103}\text{Rh}$  1231.0203) 1110.0461 ( $[\text{M-CO-Cl-FeCp}]^+$ , 100%, calcd for  $^{12}\text{C}_{59}^1\text{H}_{47}^{11}\text{B}_2^{31}\text{P}_2^{56}\text{Fe}_3^{103}\text{Rh}$  1110.0459).

### NMR Scale Reactions:

**Synthesis of  $\text{Fc}_2\text{BPhP}(\text{O})\text{Ph}$ .** A solution of  $\text{Fc}_2\text{BPhPPH}$  in  $\text{CDCl}_3$  was exposed to air and stirred for one hour.  $^1\text{H}$  NMR showed full conversion to the oxidized product.  $^1\text{H}$  NMR (499.9 MHz,  $\text{CDCl}_3$ , 25 °C):  $\delta$  = 7.94 (br, 2H; BPh), 7.83 (br m, 2H; PPh), 7.53 (br, 3H; Ph), 7.49 (br, 3H; Ph), 5.24 (nr, 1H; Cp), 5.16 (nr, 1H; Cp), 5.07 (nr, 1H; Cp),

4.93 (nr, 1H; Cp), 4.81 (nr, 1H; Cp), 4.72 (nr, 1H; Cp), 4.28 (s, 5H; free Cp), 3.48 (s, 5H; free Cp).  $^{11}\text{B}$  NMR (160.4 MHz,  $\text{CDCl}_3$ , 25 °C)  $\delta = 51.7$  ( $w_{1/2} = 1000$  Hz).  $^{31}\text{P}$  NMR (202.4 MHz,  $\text{CDCl}_3$ , 25 °C)  $\delta = 29.0$ . High-resolution MALDI-MS (+ mode, benzo[ $\alpha$ ]pyrene):  $m/z$  580.0526 ( $[\text{M}]^+$ , 100%, calcd for  $^{12}\text{C}_{32}^{1}\text{H}_{26}^{11}\text{B}^{31}\text{P}^{32}\text{O}^{56}\text{Fe}_2$  580.0514)

**Synthesis of  $\text{Fc}_2\text{BPhPPhAuCl}$ .** To a solution of  $\text{Fc}_2\text{BPhPPh}$  (5 mg) in  $\text{CDCl}_3$  (0.7 mL) was added an equimolar amount of (tht)AuCl. The mixture was stirred for 0.5 h inside the glovebox. All volatile components were removed under high vacuum. The residue was redissolved in 0.7 mL of  $\text{CDCl}_3$  for NMR measurements.  $^1\text{H}$  NMR (499.9 MHz,  $\text{CDCl}_3$ , 25 °C):  $\delta = 7.94$  (br, 2H; BPh), 7.54 (br, 3H; Ph), 7.49 (br, 3H; Ph), 5.26 (nr, 1H; Cp), 5.13 (nr, 1H; Cp), 4.94 (nr, 1H; Cp), 4.92 (nr, 1H; Cp), 4.84 (nr, 2H; Cp), 4.24 (s, 5H; free Cp), 3.44 (s, 5H; free Cp).  $^{11}\text{B}$  NMR (160.4 MHz,  $\text{CDCl}_3$ , 25 °C)  $\delta = 50.8$  ( $w_{1/2} = 1000$  Hz), -6.6 ( $w_{1/2} = 160$  Hz).  $^{31}\text{P}$  NMR (202.4 MHz,  $\text{CDCl}_3$ , 25 °C)  $\delta = 12.9$ . High-resolution MALDI-MS (+ mode, benzo[ $\alpha$ ]pyrene):  $m/z$  795.9961 ( $[\text{M}]^+$ , 100%, calcd for  $^{12}\text{C}_{32}^{1}\text{H}_{26}^{11}\text{B}^{31}\text{P}^{35}\text{Cl}^{56}\text{Fe}_2^{197}\text{Au}$  795.9920)

## 6.5 Supporting Information

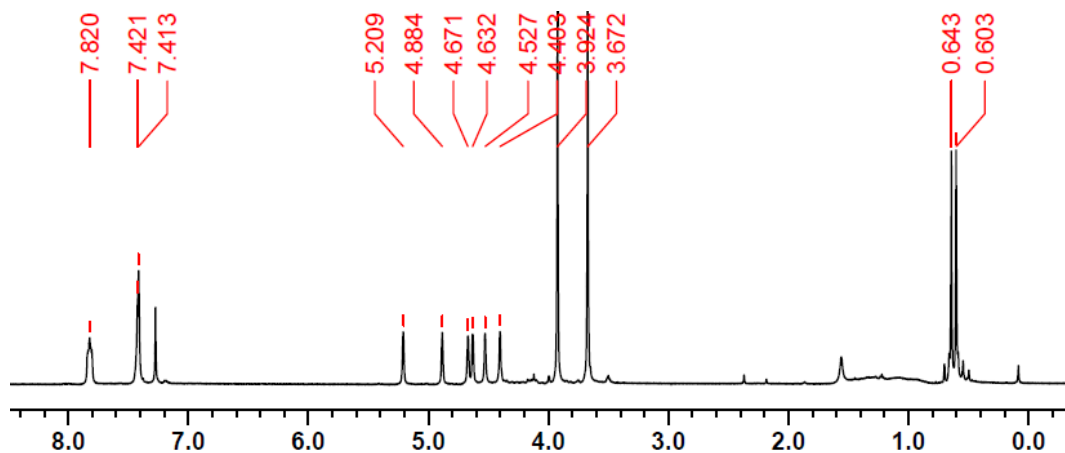


**Figure 6-13a.** <sup>1</sup>H NMR spectrum of **3b-SnP** in CDCl<sub>3</sub>.

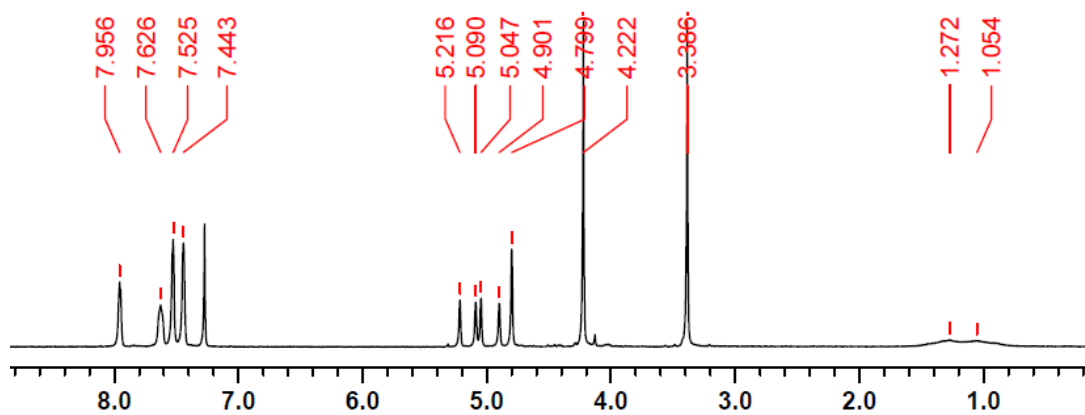


**Figure 6-13b.** <sup>1</sup>H NMR spectrum of **4-BP** in CDCl<sub>3</sub>.

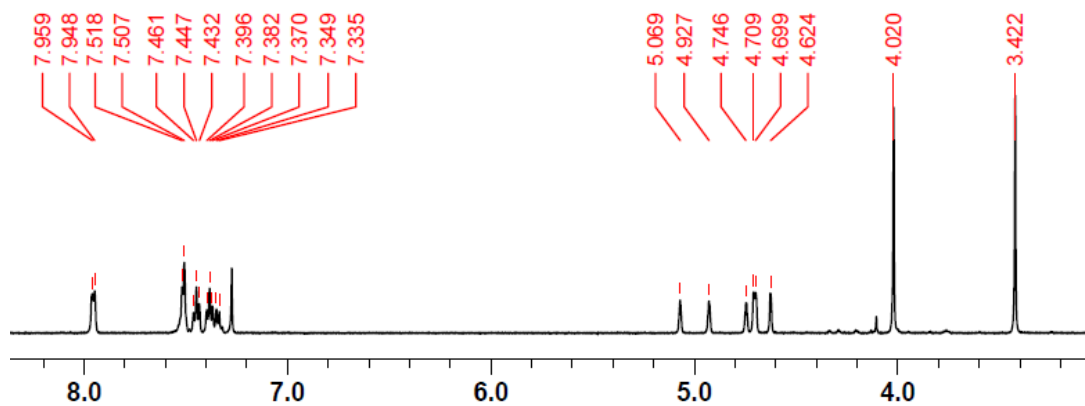


**Figure 6-13c.** <sup>1</sup>H NMR spectrum of **5-BP** in CDCl<sub>3</sub>.

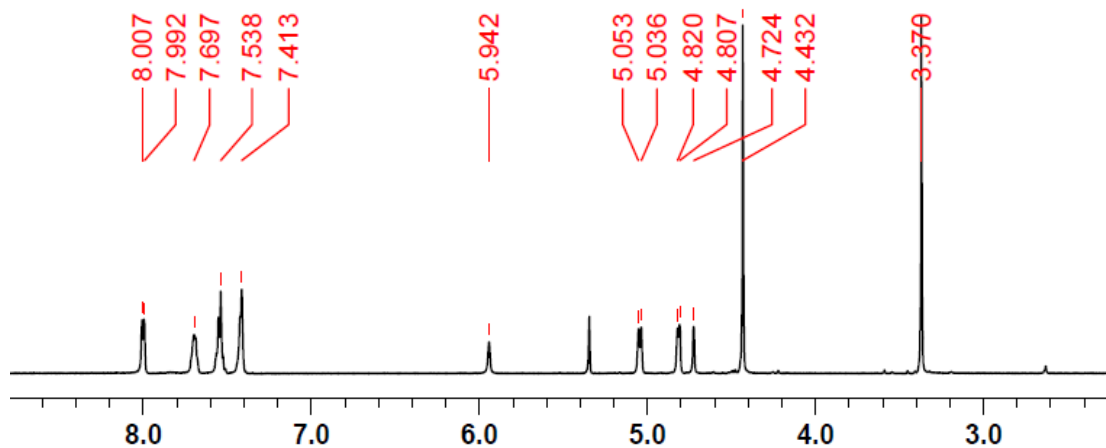


Figure 6-13d.  $^1\text{H}$  NMR spectrum of  $(5\text{-BP})_2\text{Rh}(\text{CO})\text{Cl}$  in  $\text{CD}_2\text{Cl}_2$

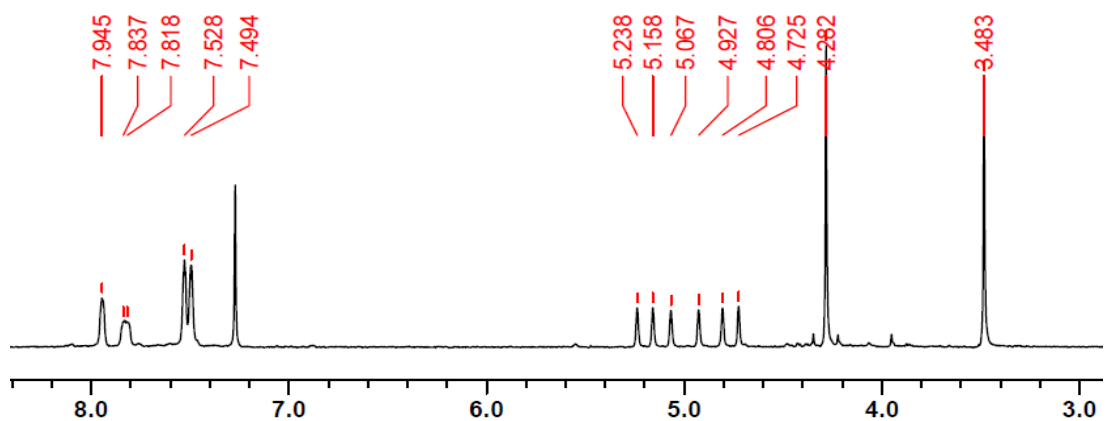


Figure 6-13e.  $^1\text{H}$  NMR spectrum of oxidized **4-BP** in  $\text{CDCl}_3$

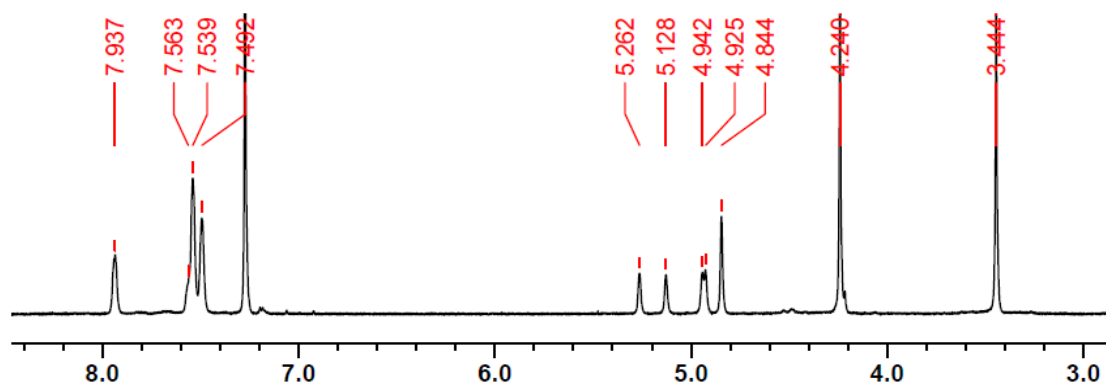
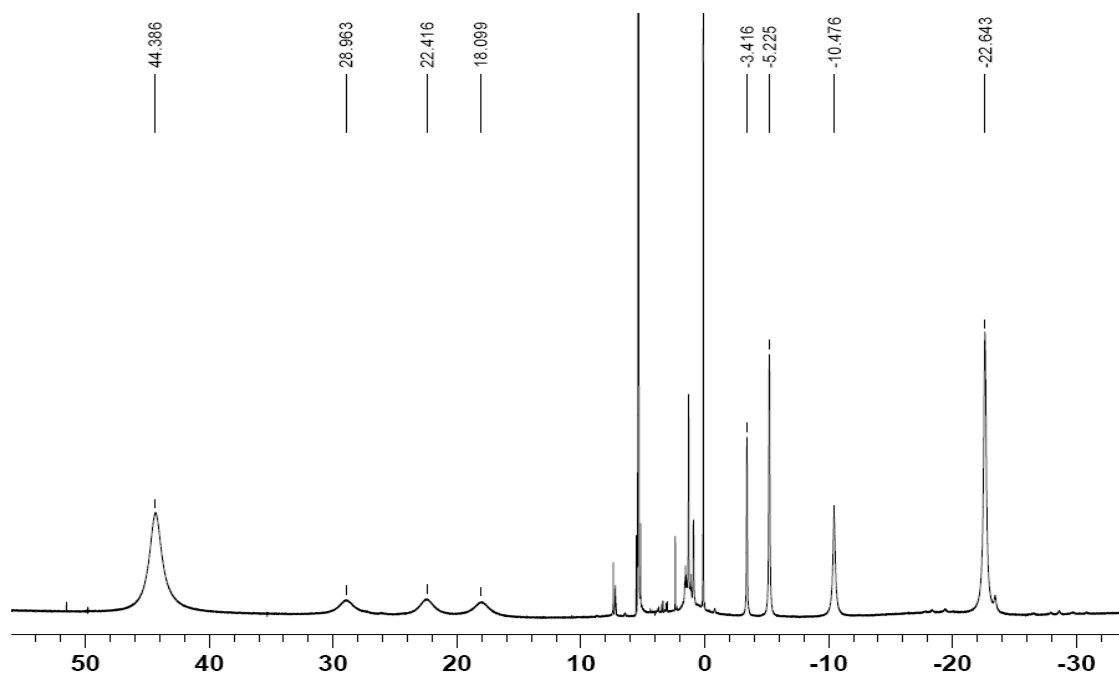
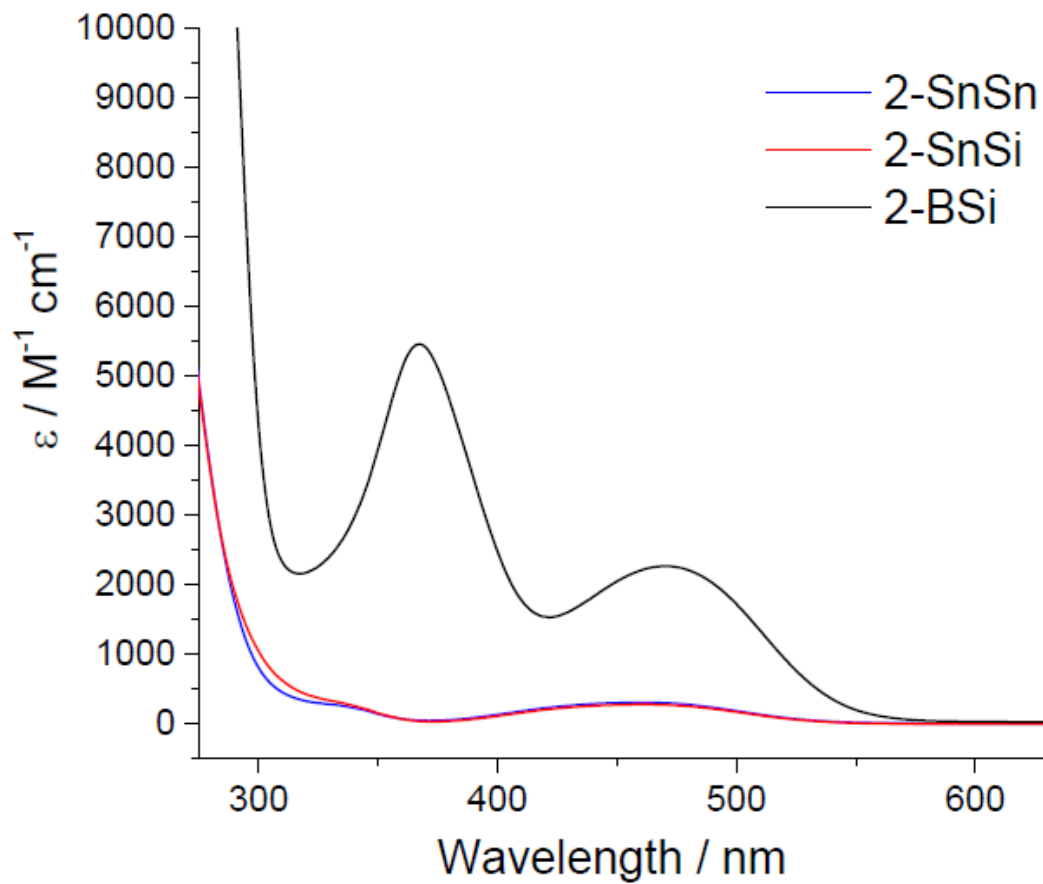


Figure 6-13f.  $^1\text{H}$  NMR spectrum of **4-BP** +  $\text{Au}(\text{tht})\text{Cl}$  in  $\text{CDCl}_3$



**Figure 6-13g.**  $^1\text{H}$  NMR spectrum of doubly oxidized 2-BSi cycle in  $\text{CD}_2\text{Cl}_2$



**Figure 6-14.** UV/Vis absorption spectra of cycles **2-SnSn** (red), **2-SnSi** (blue) and **2-BSi** (black) in  $\text{CH}_2\text{Cl}_2$ .

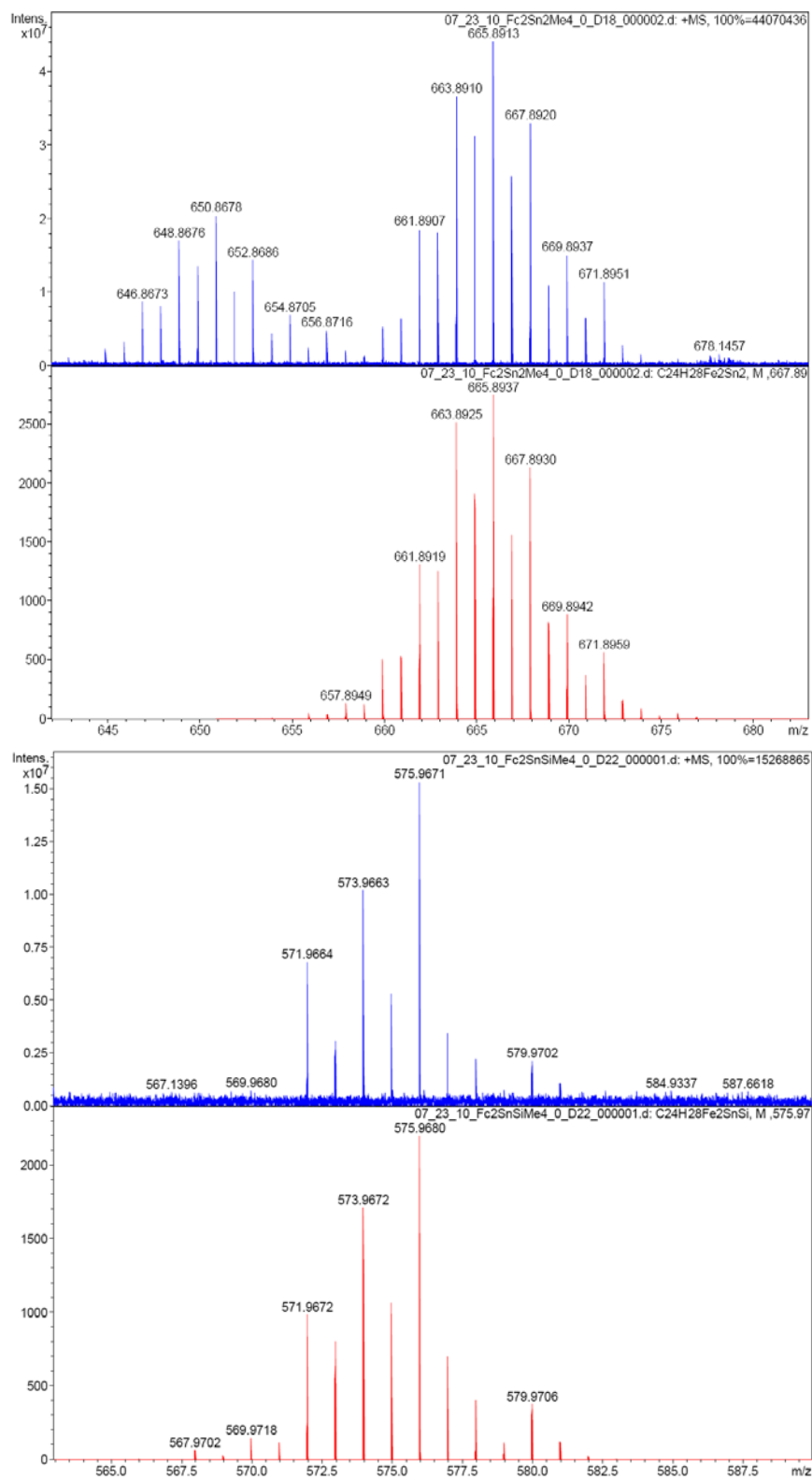


Figure 6-15. Maldi-MS data of compounds 2-SnSn and 2-SnSi.

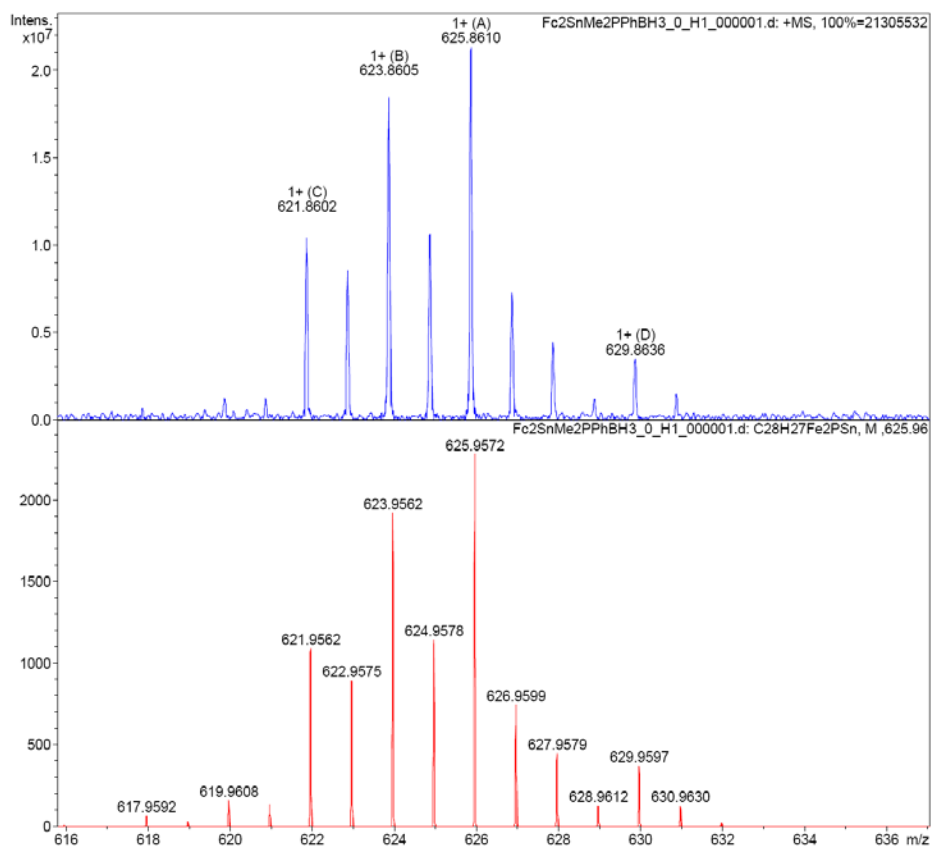


Figure 6-16. Maldi-MS data of compound 3b-SnP.

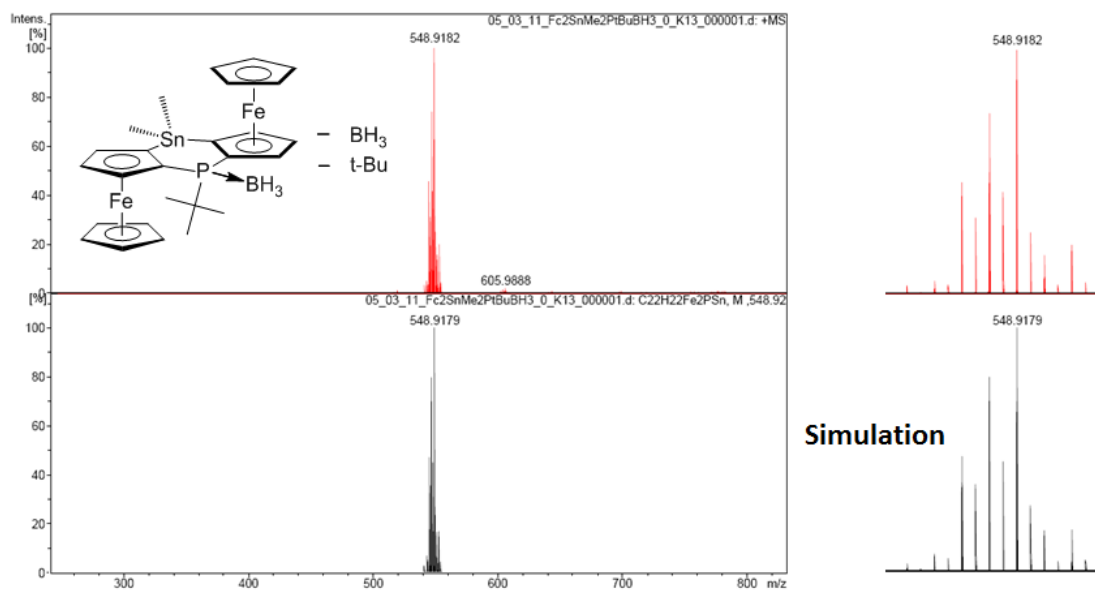
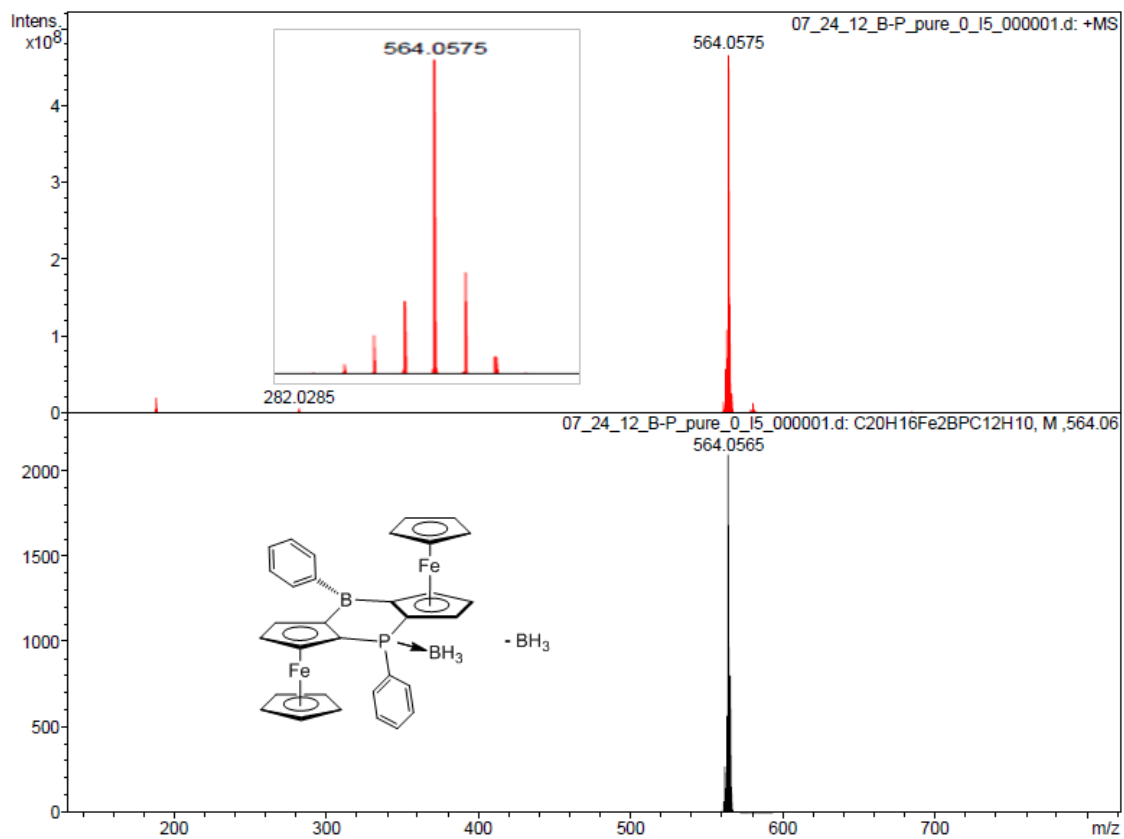


Figure 6-17. Maldi-MS data of compound 3a-SnP.



**Figure 6-18.** Maldi-MS data of compound 4-BP.

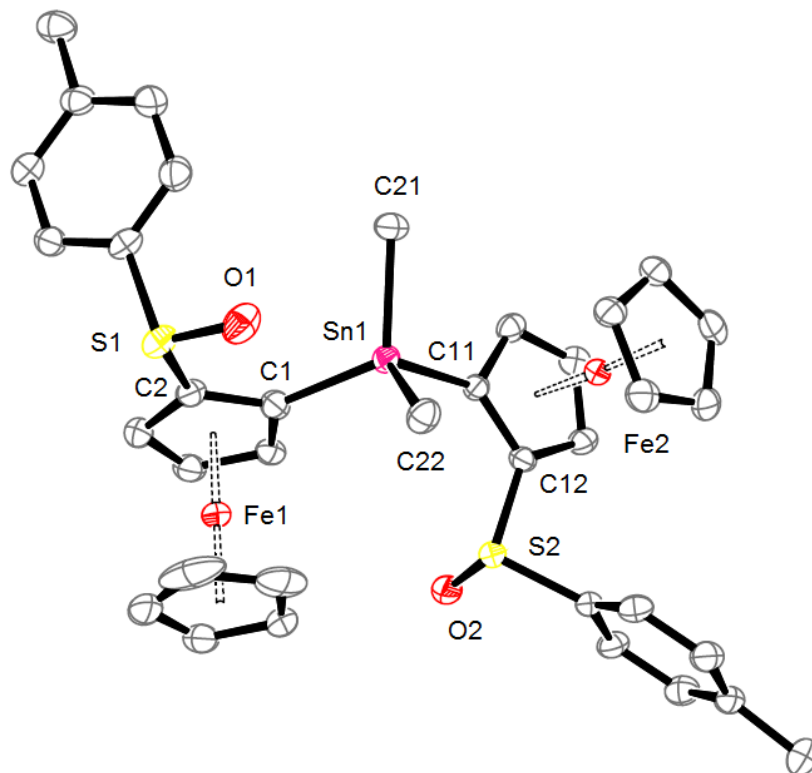
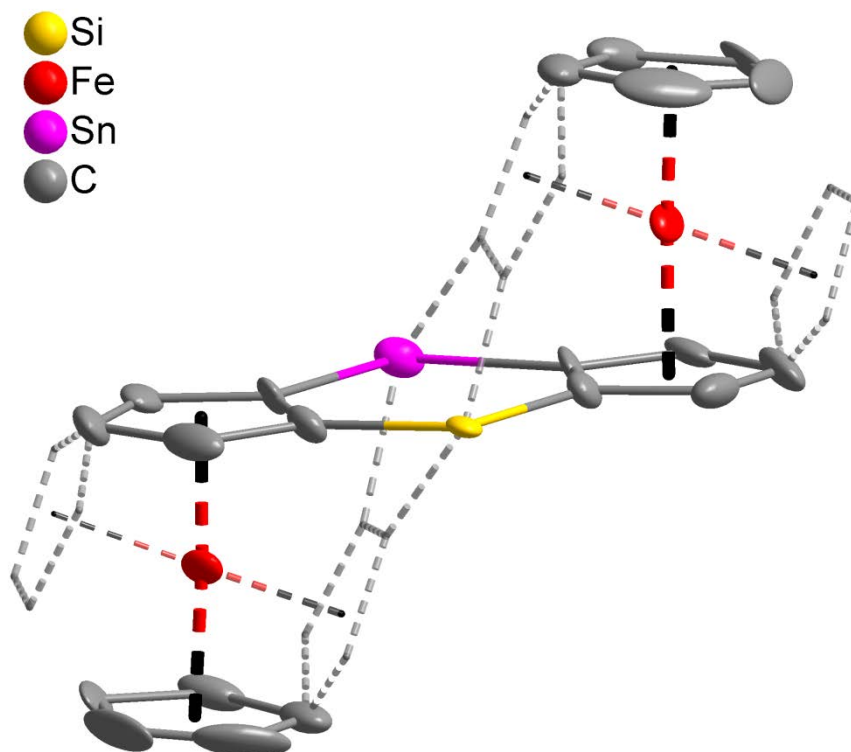
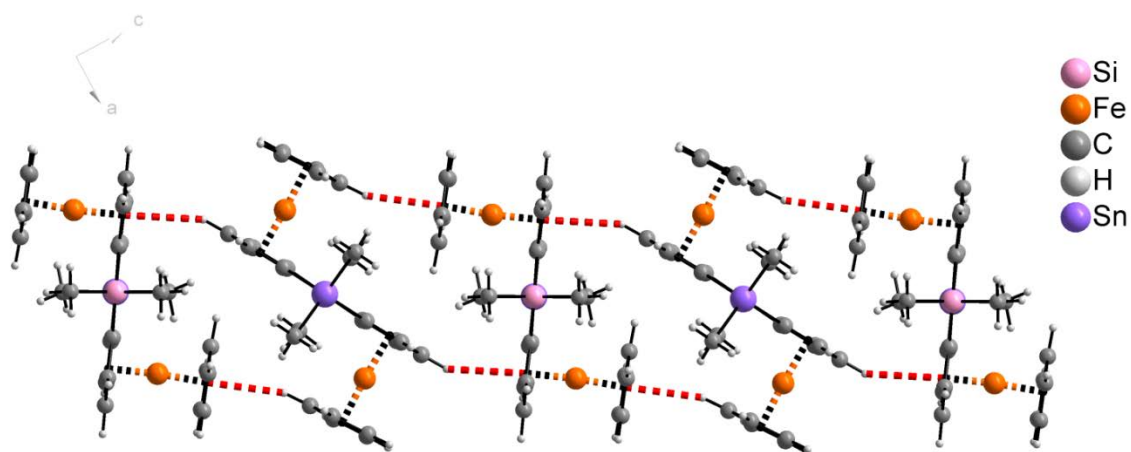


Figure 6-19. Ortep plot of **1-Sn** (50% thermal ellipsoids); H atoms are omitted. Selected distances (Å) and angles (°): Sn1-C22 2.133(4), Sn-C1 2.136(4), Sn1-C21 2.144(4), Sn1-C11 2.169(4), S1-O1 1.499(3), S1-C2 1.769(4), S2-O2 1.501(3), S2-C12 1.758(3), C1-Sn1-C11 104.47(14)



**Figure 6-20a.** During the refinement of the structure for **2-SnSi**, another set of Q peaks, representing the possible orientation of the disordered diferrocene unit, could be found (dashed line, all hydrogens and methyl carbons are omitted for clarity). However, the disorder was not modeled. Constraints such as ISOR and DELU were used to compensate this issue.



**Figure 6-20b.** Supramolecular structure of **2-SnSi**.

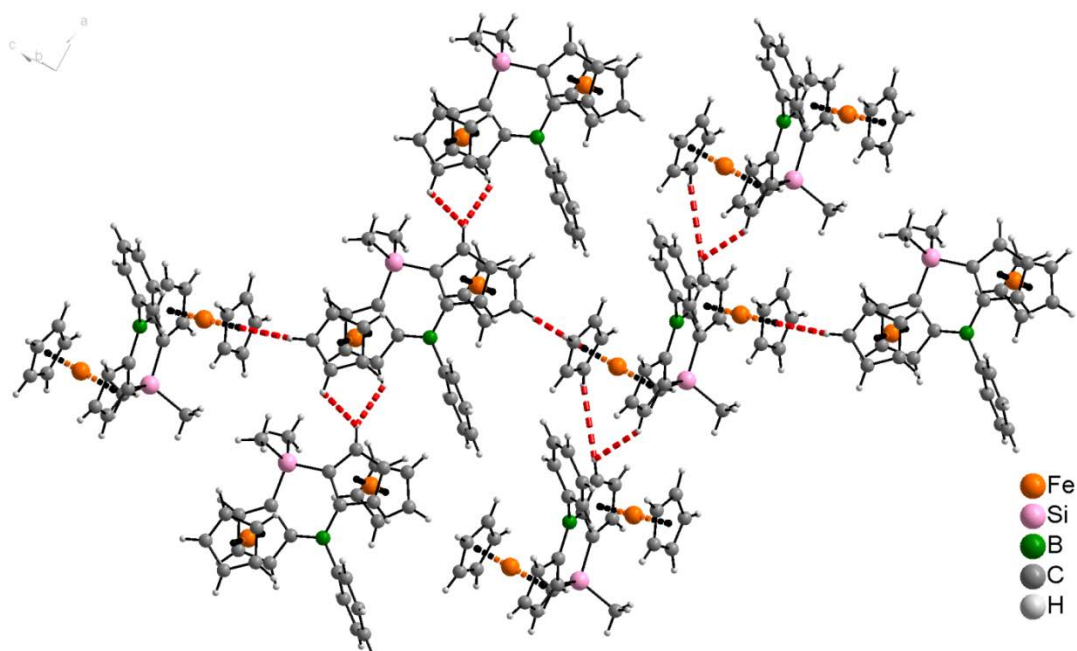


**Figure 6-20c.** Supramolecular structure of 2-BSi.

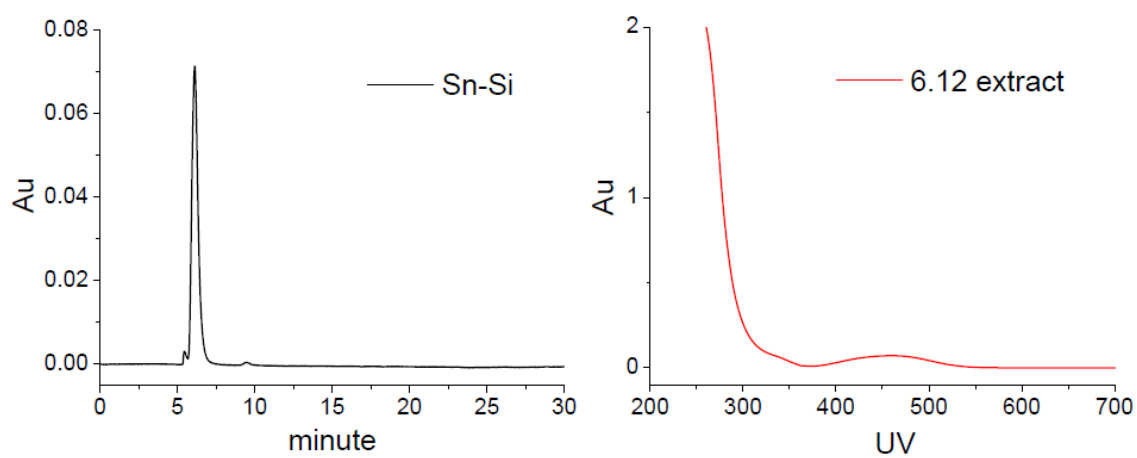


**Figure 6-21a.** Chiral HPLC trace and the corresponding UV-Vis spectrum of 2-SnSi using hexanes/THF (98:2) as eluent.

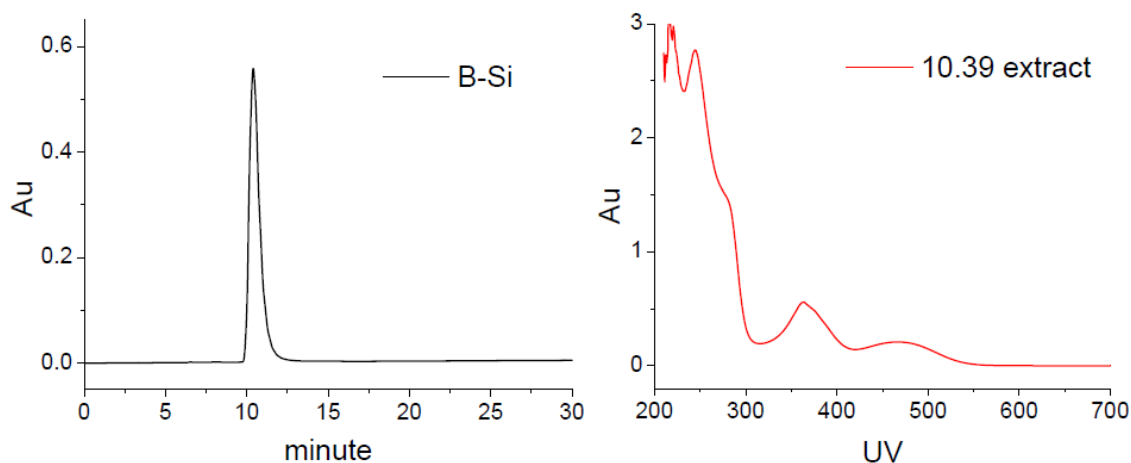


Figure 6-21b. Chiral HPLC trace and the corresponding UV-Vis spectrum of **2-BSi** using hexanes/THF (98:2) as eluent

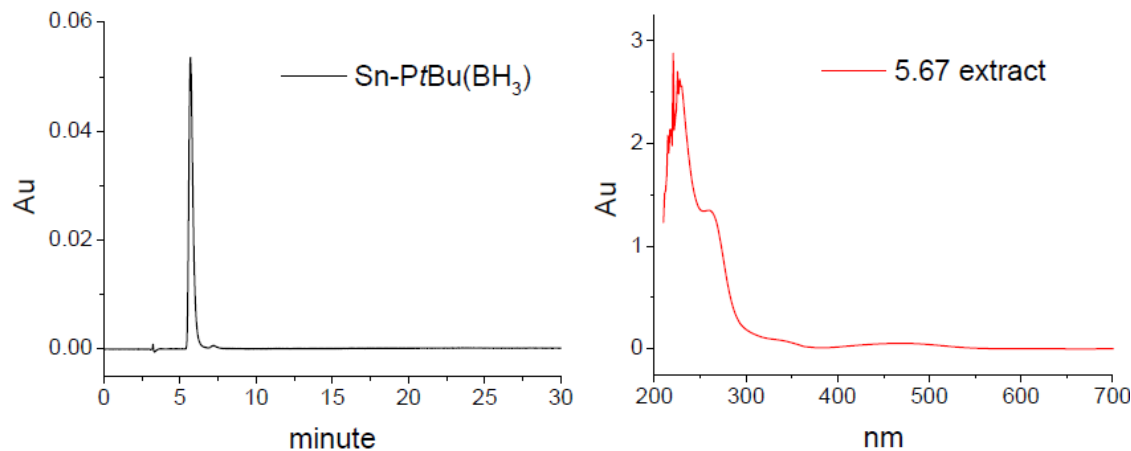


Figure 6-21c. Chiral HPLC trace and the corresponding UV-Vis spectrum of **3a-SnP** using hexanes/THF (90:10) as eluent

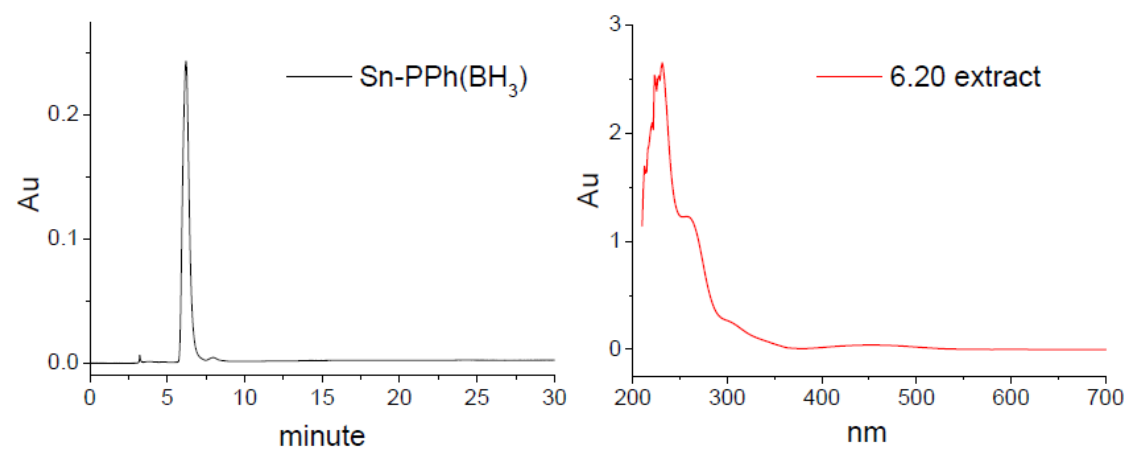
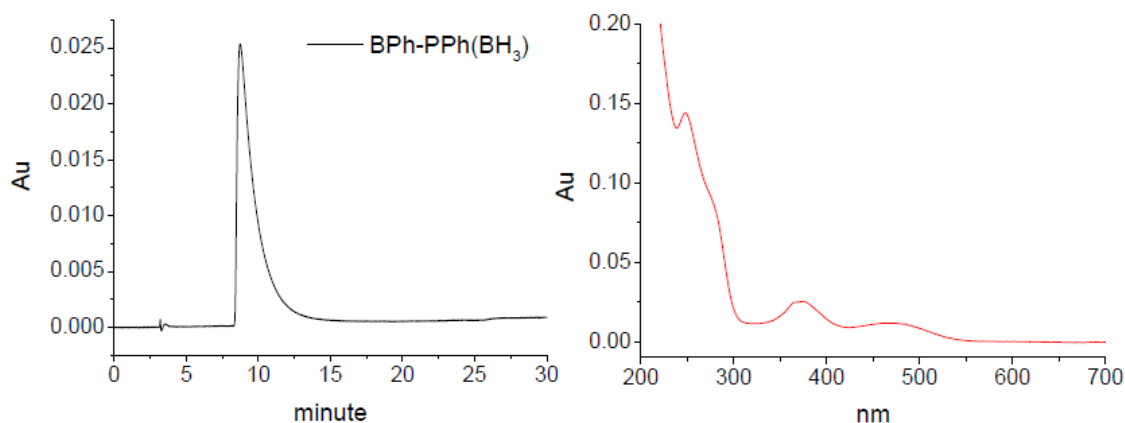


Figure 6-21d. Chiral HPLC trace and the corresponding UV-Vis spectrum of **3b-SnP** using hexanes/THF (90:10) as eluent



**Figure 6-21e.** Chiral HPLC trace and the corresponding UV-Vis spectrum of **4-BP** using hexanes/THF (90:10) as eluent

## 6.6 Notes and References

- (a) Atzkern, H.; Hiermeier, J.; Köhler, F. H.; Steck, A., *J. Organomet. Chem.* **1991**, *408*, 281-296; (b) Fritz, M.; Hiermeier, J.; Hertkorn, N.; Köhler, F. H.; Müller, G.; Reber, G.; Steigelmann, O., *Chemische Berichte* **1991**, *124*, 1531-1539; (c) Atzkern, H.; Bergerat, P.; Beruda, H.; Fritz, M.; Hiermeier, J.; Hudeczek, P.; Kahn, O.; Koehler, F. H.; Paul, M.; Weber, B., *J. Am. Chem. Soc.* **1995**, *117*, 997-1011; (d) Kohler, F. H.; Schell, A.; Weber, B., *J. Organomet. Chem.* **1999**, *575*, 33-38.
- (a) Venkatasubbaiah, K.; Zakharov, L. N.; Kassel, W. S.; Rheingold, A. L.; Jäkle, F., *Angew. Chem. Int. Ed.* **2005**, *44*, 5428-5433; (b) Venkatasubbaiah, K.; Nowik, I.; Herber, R. H.; Jäkle, F., *Chem. Commun.* **2007**, 2154-2156; (c) Venkatasubbaiah, K.; Pakkirisamy, T.; Lalancette, R. A.; Jäkle, F., *Dalton Trans.* **2008**, 4507-4513; (d) Venkatasubbaiah, K.; Doshi, A.; Nowik, I.; Herber, R. H.; Rheingold, A. L.; Jäkle, F., *Chem. Eur. J.* **2008**, *14*, 444-458; (e) Thilagar, P.; Murillo, D.; Chen, J.; Jäkle, F., *Dalton Trans.* **2013**, *42*, 665-670.
- Scheibitz, M.; Winter, R. F.; Bolte, M.; Lerner, H. W.; Wagner, M., *Angew. Chem. Int. Ed.* **2003**, *42*, 924-927.
- Zechel, D. L.; Foucher, D. A.; Pudelski, J. K.; Yap, G. P. A.; Rheingold, A. L.; Manners, I., *J. Chem. Soc. Dalton. Trans.* **1995**, 1893-1899.
- Clearfield, A.; Simmons, C. J.; Withers Jr, H. P.; Seyferth, D., *Inorg. Chim. Acta.* **1983**, *75*, 139-144.
- Utri, G.; Schwarzahans, K. E.; Allmaier, G. M., *Z. Naturforsch. B* **1990**, *45*, 755-762.
- (a) Braunschweig, H.; Clentsmith, G. K. B.; Hess, S.; Kupfer, T.; Radacki, K., *Inorg. Chim. Acta.* **2007**, *360*, 1274-1277; (b) Wrackmeyer, B.; Klimkina, E. V.; Milius, W., *Eur. J. Inorg. Chem.* **2009**, 3155-3162.
- (a) Jutzi, P.; Lenze, N.; Neumann, B.; Stammler, H. G., *Angew. Chem. Int. Ed.* **2001**, *40*, 1424-1427; (b) Althoff, A.; Jutzi, P.; Lenze, N.; Neumann, B.; Stammler, A.;

- Stammler, H. G., *Organometallics* **2002**, *21*, 3018-3022; (c) Althoff, A.; Jutzi, P.; Lenze, N.; Neumann, B.; Stammler, A.; Stammler, H. G., *Organometallics* **2003**, *22*, 2766-2774; (d) Althoff, A.; Eisner, D.; Jutzi, P.; Lenze, N.; Neumann, B.; Schoeller, W. W.; Stammler, H. G., *Chem. Eur. J.* **2006**, *12*, 5471-5480.
9. (a) Agou, T.; Kobayashi, J.; Kawashima, T., *Org. Lett.* **2005**, *7*, 4373-6; (b) Agou, T.; Kobayashi, J.; Kawashima, T., *Inorg. Chem.* **2006**, *45*, 9137-44.
10. Lee, M. H.; Agou, T.; Kobayashi, J.; Kawashima, T.; Gabbai, F. P., *Chem. Commun.* **2007**, 1133-5.
11. Fontaine, F.-G.; Boudreau, J.; Thibault, M.-H., *Eur. J. Inorg. Chem.* **2008**, *2008*, 5431-5431.
12. Bontemps, S.; Bouhadir, G.; Miqueu, K.; Bourissou, D., *J. Am. Chem. Soc.* **2006**, *128*, 12056-12057.
13. (a) Bontemps, S.; Bouhadir, G.; Miqueu, K.; Bourissou, D., *J. Am. Chem. Soc.* **2006**, *128*, 12056-7; (b) Sircoglou, M.; Bontemps, S.; Mercy, M.; Saffon, N.; Takahashi, M.; Bouhadir, G.; Maron, L.; Bourissou, D., *Angew. Chem. Int. Ed.* **2007**, *46*, 8583-8586; (c) Bontemps, S.; Bouhadir, G.; Gu, W.; Mercy, M.; Chen, C. H.; Foxman, B. M.; Maron, L.; Ozerov, O. V.; Bourissou, D., *Angew. Chem. Int. Ed.* **2008**, *47*, 1481-1484; (d) Sircoglou, M.; Bontemps, S.; Bouhadir, G.; Saffon, N.; Miqueu, K.; Gu, W.; Mercy, M.; Chen, C. H.; Foxman, B. M.; Maron, L.; Ozerov, O. V.; Bourissou, D., *J. Am. Chem. Soc.* **2008**, *130*, 16729-16738; (e) Gualco, P.; Lin, T. P.; Sircoglou, M.; Mercy, M.; Ladeira, S.; Bouhadir, G.; Perez, L. M.; Amgoune, A.; Maron, L.; Gabbai, F. P.; Bourissou, D., *Angew. Chem. Int. Ed.* **2009**, *48*, 9892-9895; (f) Sircoglou, M.; Mercy, M.; Saffon, N.; Coppel, Y.; Bouhadir, G.; Maron, L.; Bourissou, D., *Angew. Chem. Int. Ed.* **2009**, *48*, 3454-34547; (g) Bebbington, M. W. P.; Bontemps, S.; Bouhadir, G.; Hanton, M. J.; Tooze, R. P.; van Rensburg, H.; Bourissou, D., *New J. Chem.* **2010**, *34*, 1556-1559; (h) Amgoune, A.; Ladeira, S.; Miqueu, K.; Bourissou, D., *J. Am. Chem. Soc.* **2012**, *134*, 6560-6563.
14. (a) Guillaneux, D.; Kagan, H. B., *J. Org. Chem.* **1995**, *60*, 2502-2505; (b) Riant, O.; Argouarch, G.; Guillaneux, D.; Samuel, O.; Kagan, H. B., *J. Org. Chem.* **1998**, *63*, 3511-3514.
15. Belding, S. R.; Limon-Petersen, J. G.; Dickinson, E. J. F.; Compton, R. G., *Angew. Chem. Int. Ed.* **2010**, *49*, 9242-9245.
16. Gan, K. S.; Hor, T. S. A.; Togni, A.; Hayashi, T., *Ferrocenes: Homogeneous Catalysis, Organic Synthesis, Materials Science*. Wiley-VCH: Weinheim, New York, Basel, Cambridge, Tokyo, 1995; p 93.
17. Roodt, A.; Otto, S.; Steyl, G., *Coor. Chem. Rev.* **2003**, *245*, 121-137.
18. (a) Thomas, J. C.; Peters, J. C. *Inorg. Chem.* **2003**, *42*, 5055-5073. Thomas, J. C.; (b) Peters, J. C. *J. Am. Chem. Soc.* **2003**, *125*, 8870-8888
19. Chen, J.; Lalancette, R. A.; Jäkle, F., *Organometallics* **2013**, *32*, 5843-5851.
20. (a) Krossing, I., *Chem. Eur. J.* **2001**, *7*, 490-502; (b) Reisinger, A.; Trapp, N.; Krossing, I., *Organometallics* **2007**, *26*, 2096-2105.

## Overall Conclusions

We developed a general synthetic method which led to a variety of fluorinated acidic boranes such as **1-Pf** and **2-Pf** via a series of organometallic substitution reactions in Chapter 2. The structures were confirmed by single-crystal X-ray diffraction and the steric effect around the boron center was examined by variable temperature  $^{19}\text{F}$  NMR spectroscopy, suggesting that the naphthylferrocene framework provides a rigid chiral environment for the borane moiety. In related work we pursued the corresponding boronic acid derivative.

In Chapter 3 and 4, we prepared enantiomerically pure lutidylferrocene derivatives by Negishi coupling and subsequent transmetallation reactions. A new stereoselective borylation procedure was introduced by using different transmetallation methods (Sn-B and Hg-B metathesis, respectively) to generate both planar chiral enantiomers from just one enantiomer of the precursor. The ipso-substitution of the mercuriated precursor proceeds as expected. However, the observed directed borylation with chiral inversion in the tin-boron exchange process is unusual and a detailed mechanistic study indicated the formation of a Lewis acid-base complex in the first step and then possibly a reactive borenium cation as an intermediate. The enantiomeric excess for the chiral inversion process is more than 90% by chiral HPLC analysis. The mechanistic studies support the involvement of a borenium cation intermediate as strong electrophile that attacks the *ortho* position of the substituted Cp ring. With the aim to construct the planar chiral FLPs as asymmetric catalysts, electron-deficient pentafluorophenyl (Pf) and bulky mesityl (Mes) groups were introduced to tune the Lewis acidity and steric hindrance at the boron

(**4-Mes** and **5-Pf**). Despite the steric effect a strong B-N bond formed, which is intact even under strongly acidic conditions. A bulky TMS group was then incorporated in the *ortho* position of the pyridine ring to further increase the steric congestion and thus to weaken the B-N interaction (**5-Pf** and **5-Mes**). **5-Pf** formed a labile B-N bond which opened at elevated temperature and activated a water molecule to generate a ring-opened pyridinium borate. In contrast, **5-Mes** adopted an open conformation in which the entire pyridyl group was flipped to release steric repulsion.

In Chapter 5, we described the synthesis and catalytic application of a novel planar chiral borenium cation (**pR**)-**3**<sup>+</sup>. A competition study showed that its Lewis acidity is almost as strong as that of the widely used *tris*(pentafluorophenyl)borane and its affinity towards anions such as Cl<sup>-</sup> is even stronger. The borenium species can not only bind to Lewis basic substrates such as ketones and THF, but also activate the Si-H bond of silanes such as Et<sub>3</sub>SiH. Finally, this unique Lewis acid was tested as a catalyst for the hydrosilylation of ketones with excellent conversion but moderate enantiomeric excess. Further work on optimizing the electronic and steric properties of this novel family of borenium cations is expected to improve the stereo-selectivity.

Last but not least, we established a practical protocol for the synthesis of a number of hetero-atom linked diferrocenes, ranging from group 13 to group 15 elements such as boron, silicon, tin and phosphorus. While the compounds with tricoordinate boron feature a trigonal fragment in the bridge, the others adopt tetrahedral configurations. The successful introduction of planar chirality was supported by single-crystal X-ray crystallography, chiral HPLC and optical rotation measurements. Electrochemical studies reveal that the cycles **2-SnSn**, **2-SnSi** and **2-BSi** undergo 2-step reversible oxidations for

the Fc units. The introduction of boron results in anodic shifts for both of the potentials. For the most interesting system, **5-BP**, the 1<sup>st</sup> quasi-reversible process suggests the possibility to serve as a redox responsive ligand. In the solid state structure of **5-BP**, the tricoordinate phosphorus adopts a pyramidal conformation, indicating very little contribution of its lone pair of electrons to the extended  $\pi$  system. The **5-BP** cycle is a relatively strongly basic ligand as is evident from the  $\nu(\text{CO})$  stretching frequency (1965  $\text{cm}^{-1}$ ) of the corresponding Vaska-type rhodium complex. More interestingly, the binding of  $\text{F}^-$  to the boron shifts the  $\nu(\text{CO})$  to 1937  $\text{cm}^{-1}$ , which is similar to the respective complex with the highly electron-rich alkyl phosphine  $\text{PCy}_3$  complex at  $\nu(\text{CO})$  of 1943  $\text{cm}^{-1}$ .

In conclusion, we have established a practical protocol towards the synthesis of multifunctional planar chiral systems, including Lewis acids, Lewis pairs and ambiphilic ligands. We have already shown our preliminary studies on the hydrosilylation of ketones using the highly Lewis acidic borenium cation derivative. The future efforts on these projects will focus on fine-tuning the steric and electronic effects of this class of catalysts for higher stability and better stereoselectivity. It would be interesting to introduce our chiral Lewis acids and Lewis pairs to the area of FLP chemistry. Moreover, for the ambiphilic species **5-BP**, we expect to trigger the change of the electron donating property by oxidation of the biferrocene backbone and anion binding to the boryl moiety. One interesting aspect would be applying **5-BP** as a responsive ligand to stereoselective transition metal-catalyzed reactions (e.g., rhodium-catalyzed asymmetric hydrogenation).

## List of Publications

1. "Planar Chiral Organoborane Lewis Acids Derived from Naphthylferrocene"  
J. Chen, K. Venkatasubbaiah, T. Pakkirisamy, A. Doshi, A. Yusupov, Y. Patel, R. A. Lalancette and F. Jäkle, *Chem. Eur. J.*, **2010**, *16*, 8861.
2. "Reversible Formation of a Planar Chiral Ferrocenylboroxine and its Supramolecular Structure"  
P. Thilagar, J. Chen, R. A. Lalancette and F. Jäkle, *Organometallics*, **2011**, *30*, 6734.
3. "Synthesis and Supramolecular Assembly of the Bifunctional Borinic Acid [1,2-*fcB(OH)*]<sub>2</sub>"  
P. Thilagar, D. Murillo, J. Chen and F. Jäkle, *Dalton Trans.*, **2013**, *42*, 665.
4. "Synthesis and Lewis acid properties of a ferrocene-based planar-chiral borenium cation"  
J. Chen, R. Lalancette and F. Jäkle, *Chem. Commun.*, **2013**, *49*, 4893.
5. "Stereoselective Ortho Borylation of Pyridylferrocenes"  
J. Chen, R. Lalancette and F. Jäkle, *Organometallics*, **2013**, *32*, 5843.
6. "Organoborane Lewis Pairs Derived from Pyridylferrocene"  
J. Chen, R. Lalancette and F. Jäkle, *Chem. Eur. J.*, **2014**, *accepted*.

## Curriculum Vitae

**Birth:** May 14, 1985, in Zhongshan, Canton, China

**Education:**

09/2008-05/2014 Ph.D., Chemistry, Rutgers University-Newark Campus, U.S.

Advisor: Dr. Frieder Jäkle

09/2004-06/2008 B. Sc., Chemistry, Wuhan University, China

Advisor: Dr. Chuluo Yang

**Honors and Awards:**

2010 Student travel award for 240<sup>th</sup> ACS National Meeting in Boston

2006~2008 Scholarship of Wuhan University